Special Issue Powerskin 2021

Knaack, U.; Klein, T.; Auer, Thomas; Schneider, Jens

DOI
10.7480/jfde.2021.1

Publication date
2021

Document Version
Final published version

Published in
Journal of Facade Design and Engineering

JOURNAL OF FACADE DESIGN & ENGINEERING

VOLUME 9 / NUMBER 1 / 2021

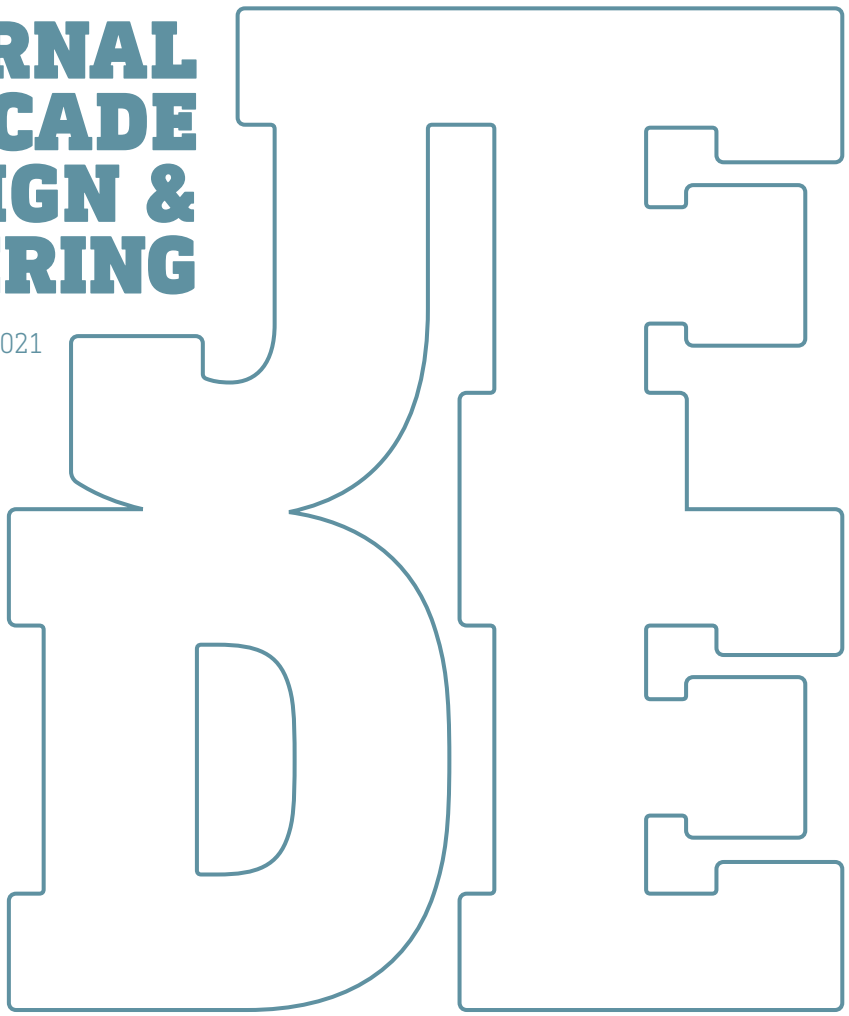

EDITORS IN CHIEF ULRICH KNAACK AND TILLMANN KLEIN
GUEST EDITORS THOMAS AUER AND JENS SCHNEIDER

SUPPORTED BY THE EUROPEAN FACADE NETWORK

SPECIAL ISSUE

POWERSKIN 2021

JFDE Journal of Facade Design and Engineering

JFDE presents new research results and new proven practice of the field of facade design and engineering. The goal is to improve building technologies, as well as process management and architectural design. JFDE is a valuable resource for professionals and academics involved in the design and engineering of building envelopes, including the following disciplines:

– Architecture
– Building Engineering
– Structural design
– Climate design
– Building Services Engineering
– Building Physics
– Design Management
– Facility Management

JFDE will – initially - be directed at the scientific community, but it will also feature papers that focus on the dissemination of science into practice and industrial innovations. In this way, readers explore the interaction between scientific developments, technical considerations and management issues.

Publisher
TU Delft Open
TU Delft / Faculty of Architecture and the Built Environment
Julianalaan 134, 2628 BL Delft, The Netherlands

Contact
Alejandro Prieto
JFDE-BK@tudelft.nl
http://jfde.tudelft.nl/

Policies
Peer Review Process – The papers published in JFDE are double-blind peer reviewed.
Open Access – JFDE provides immediate Open Access (OA) to its content on the principle that making research freely available to the public supports a greater global exchange of knowledge.

Indexation – JFDE is indexed in the Directory of Open Access Journals (DOAJ), Google Scholar, Inspec IET and Scopus.
Publication Ethics – Editors, authors and publisher adopt the guidelines, codes to conduct and best practices developed by the Committee on Publication Ethics (COPE).

Design & layout
Design – Sirene Ontwerpers, Rotterdam
Layout – Nienke Blaauw, TU Delft
Cover image – Louisiana Museum of Modern Art,
Photo by Philipp Vohlidka

ISSN 2213-302X (Print)
ISSN 2213-3038 (Online)
ISBN 978-94-6366-405-9

Submissions
All manuscripts and any supplementary material should be submitted to the Editorial Office (JFDE-BK@TUDelft.nl), through the Open Journal System (OJS) at the following link: http://jfde.tudelft.nl/

Author Guidelines
Detailed guidelines concerning the preparation and submission of manuscripts can be found at the following link:
https://journals.open.tudelft.nl/index.php/jfde/about/submissions

Contents

v **Editorial**

001 **Mono-Material Wood Wall**
Oliver Bucklin, Prof. Achim Menges, Felix Amtsberg, Oliver Krieg, Hans Drexler, Angela Rohr

017 **Effects of Phase Change Materials on Heat Flows Through Double Skin Façades**
Thomas Wüest, Lars O. Grobe, Andreas Luible

031 **Holistic Design Explorations of Building Envelopes Supported by Machine Learning**
Federico Bertagna, Pierluigi D'Acunto, Patrick Ole Ohlbrock, Vahid Moosavi

047 **Potential of Façade-Integrated PVT With Radiant Heating and Cooling Panel Supported by a Thermal Storage for Temperature Stability and Energy Efficiency**
Mohannad Bayoumi

059 **Additive Manufacturing of Thermally Enhanced Lightweight Concrete Wall Elements with Closed Cellular Structures**
Gido Dielemans, David Briels, Fabian Jaugstetter, Klaudius Henke, Kathrin Dörfler

073 **Exploring the Possibility of Using Bioreceptive Concrete in Building Façades**
M. Veeger, A. Prieto, M. Ottelé

087 **Photovoltaic Warm Façades with Phase Change Materials in European Climates**
Christian Popp, Dirk Weiß, Katja Tribulowski, Bernhard Weller

101 **Smart Textile Sun Shading**
Paul-Rouven Denz, Christiane Sauer, Ebba Fransén Waldhör, Maxie Schneider, Puttakhun Vongsingha

117 **A Full Performance Paper House**
Rebecca Bach, Alexander Wolf, Martin Wilfinger, Nihat Kiziltoprak, Ulrich Knaack

131 **Skin Metrics**
Keith Boswell, Stéphane Hoffman, Stephen Selkowitz, Mic Patterson

147 **PAOSS**
Christina Eisenbarth, Walter Haase, Yves Klett, Lucio Blandini, Werner Sobek

Editorial

The PowerSkin conference series is a biennial event organised cooperatively between TU München, TU Darmstadt, and TU Delft, which is already in its third edition, having started in 2017.

The conference aims to address the role of building skins in accomplishing a carbon neutral building stock. The presented papers showcase recent scientific research and developments as well as projects related to building skins from the perspectives of material, technology, and design. Topics such as building operation, embodied energy, energy generation and storage in context of the envelope, energy, and environment are considered.

The building envelope largely determines the energetic performance of the building, plays a significant part in the embodied energy of construction activities, defines the indoor qualities for the user and – quite importantly – defines the appearance of the building in an urban content. So, being central to all these aspects, the building envelope is the focus of research & development, engineering, and design. This is the scope of the PowerSKIN conferences, bringing research, industry, and users together to share and discuss new knowledge in an interdisciplinary environment (albeit an online environment this time around).

The focus of the PowerSKIN Conference 2021 deals with the question of whether simplicity and robustness are in contradiction to good performance or whether they even complement each other. Hence the question *Simplicity vs. Performance?* is tackled throughout the conference from three points of view which define the thematic sessions of the Conference: Energy, Envelope, and Environment. This special issue of the Journal of Façade Design and Engineering dedicated to PowerSKIN 2021 showcases the most prominent and relevant papers of the conference, with the aim of enhancing their visibility for a larger audience.

Ulrich Knaack
Thomas Auer
Jens Schneider

Mono-Material Wood Wall

Digital Fabrication of Performative Wood Envelopes

Oliver Bucklin[1*], Prof. Achim Menges[1], Felix Amtsberg[1], Oliver Krieg[1], Hans Drexler[2], Angela Rohr[2]

* Corresponding author
1 University of Stuttgart, Institute for Computational Design and Construction, Stuttgart, Germany. oliver.bucklin@icd.uni-stuttgart.de
2 Jade University of Applied Sciences, Department of Architecture, Oldenburg Germany

Abstract

The project seeks to create a building envelope that functions as structure, enclosure, and insulation, which is assembled from one solid timber construction element type. Wood has clear environmental benefits when compared to other standard construction materials such as steel and concrete, a good strength-to-weight ratio, relatively high thermal insulation, and low production costs. This research seeks to leverage these characteristics to simultaneously reduce the number of material layers in timber building envelopes while improving the building physics performance. Thus, the environmental impact of buildings can be reduced during planning, construction, operation, and disposal. The project proposes a system that reduces material layers and improves envelope performance by combining contemporary fabrication technologies with traditional woodworking techniques. Design tools should allow for compelling formal opportunities and facilitate fabrication and construction. The system manifests as a free-form, curvilinear log-cabin. Solid timber beams are used to minimise binders and fillers found in composite wood products, and the entire primary construction is achieved with pure wood joinery. CNC machining allows for the precise joining of members to achieve robust, easy-to-assemble, structural and airtight façades. By sawing deep slits into solid timber beams, the resulting air chambers improve thermal insulation values up to 30% compared to comparable solid wood assemblies while also relieving naturally occurring internal stresses. Computational design algorithms generate toolpaths and construction data directly from simple input curves, enabling direct coordination of architects, engineers, and contractors. To evaluate the system, multiple prototypes are fabricated to test constructability, thermal conductance, and airtightness, including a demonstrator building to test full-scale implementation. Laboratory tests and the successful completion of the IBA: Timber Prototype House demonstrate the potential for this renewable material to fulfil the requirements of contemporary building envelopes and open the door for the development of all-wood multi-storey façades.

Keywords

Computational design, timber, digital fabrication, layer-reduced construction, wood, façade, envelope

10.7480/jfde.2021.1.5398

1 INTRODUCTION

1.1 ENVIRONMENTAL BENEFITS OF WOOD

Widespread awareness of anthropogenic global warming has led to the adoption of stricter building energy codes by government regulation agencies as well as increasing consumer demand for sustainable construction solutions. This increasing pressure for environmentally friendly buildings has led to the development of new high-performance materials and pushed architects and contractors to reconsider traditional material solutions such as strawbales, rammed-earth, and log construction. Wood is a strong candidate for wider adoption in contemporary construction due to its environmental merits, good energy performance, low cost, and versatility. Wood is a renewable resource with low energy processing compared to steel and concrete. (Ximenes & Grant, 2013; Skullestad, Bohne, & Lohne, 2016). When the ability of trees to store atmospheric carbon dioxide is considered, solid timber can be tabulated to have a negative carbon footprint (Hill & Dibdiakova, 2016; Rosa, Pizzol, & Schmidt, 2018; González-García, Krowas, Becker, Feijoo, & Moreira, 2013). Tectonic strategies such as beams, trusses, and slabs are translated from standard steel and concrete construction into wood components for structural systems (Skullestad, Bohne, & Lohne, 2016). Wood also has lower thermal conductivity than steel and concrete (ISO 10456), which potentially reduces energy usage for heating and cooling buildings, and a high strength-to-weight ratio that allows for efficient use in structural applications.

With these benefits in mind, this research seeks to develop a building envelope system that achieves modern structural and energy performance requirements with a minimum of non-wood materials.

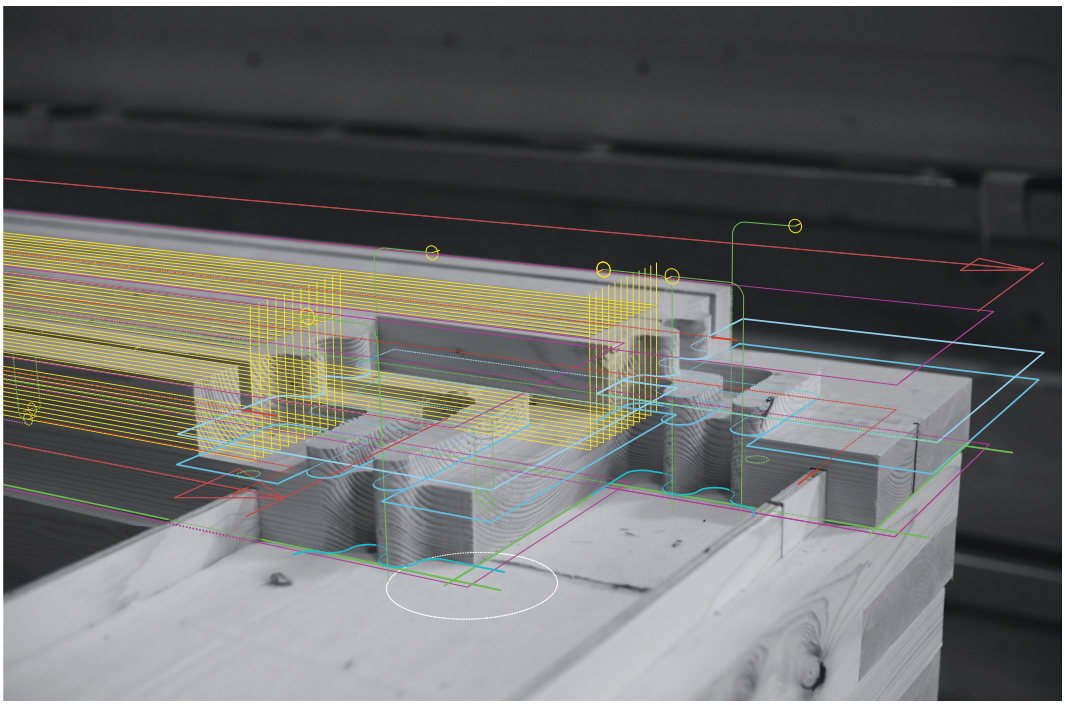

FIG. 1 Solid wood, insulating, airtight, moment frame connection detail with CNC toolpath overlay

1.2 MONO-MATERIAL CONSTRUCTION

Contemporary construction has normalised the continuous addition of subsequent material layers to strive for ever-better energy performance. Adhesives, foams, tapes, and membranes made from synthetic polymers are frequently employed to increase insulation values and reduce air permeation. However, these products require proper installation to function as intended, and performance often suffers from lack of training or discipline from construction workers (Korpi, Vinha, & Kurnitski, 2004; Kalamees, Alev, & Pärnalaas, 2017). Composite wood products require extra energy inputs for binding adhesives, with 8-28% of total energy consumption going to resin production (Puettmann & Wilson, 2005). When dismantling structures for disposal, extraneous materials complicate material separation, impeding recycling. This extends to timber product types, as solid timber has a much higher post-consumer value than composite wood products due to its usefulness in subsequent construction projects and furniture making, and produces less damaging pollution when it is incinerated for energy production (Erlandsson & Sundqvist, 2014).

Mono-material construction offers a strategy for simplifying building assemblies by using a single material that can be functionally graded and geometrically manipulated to achieve performance that is on par with composite systems. Einfach Bauen is a research project being undertaken at the Technical University of Munich, which explores mono-material construction strategies in both concrete and wood, where material density is varied to achieve different thermal and structural performance characteristics; for example, aerated concrete is used to improve insulation values. To similar ends, their wood system embeds air chambers into the construction to reduce density and increase thermal resistance. However, it relies on glued and pressed layers of planks, essentially creating composite panels (Nagler, Jarmer, Niemann, & Cruel, 2018).

The traditional precedent for solid timber construction is the Log House. Log construction uses minimally processed tree trunks, often left round or milled only on one side, which are notched at the ends and stacked to create solid wall sections. They suffer several shortcomings: the wood grain is perpendicular to principal loading creating an inefficient structure (Ross & USDA Forest Service, 2010); the joints are often cut by hand and suffer air leakage (Alev, Uus, Teder, Miljan, & Kalamees, 2014; Alev, Uus, & Kalamees, 2017); and they don't usually have added insulation layers, meaning thermal insulation relies on a thick wall section to achieve comfortable interior temperatures (Roos, Eklund, & Baylon, 1993). Log construction demonstrates a strategy for building architectural envelopes with a linear material by using a system of wood joinery and is the starting point for the development presented in this paper.

1.3 CAD/CAM INTEGRATION

Automation has entered nearly every industry to increase production speed and reduce labour costs. The timber construction industry developed automation strategies to fabricate standard components and joinery details precisely and quickly but expanded to include differentiated components for free-form architectural geometries (Schwinn, 2016). These developments have been enabled by advancements in Computer Aided Design (CAD) and Computer Aided Machining (CAM). The integration of these tools allows a holistic approach to design and construction that involves all project partners.

2 METHODOLOGY

The research follows a project at the Münster School of Applied Science called Timber Prototype I. That project used a system of horizontally oriented stacked beams, sawn longitudinally with deep slits (Fig. 2) to create air chambers within the wall section that improve thermal insulation. This research seeks to improve the energy performance of TimberPrototype I while reducing extraneous material layers, expanding the formal capabilities of the system, and creating an integrated design and fabrication system.

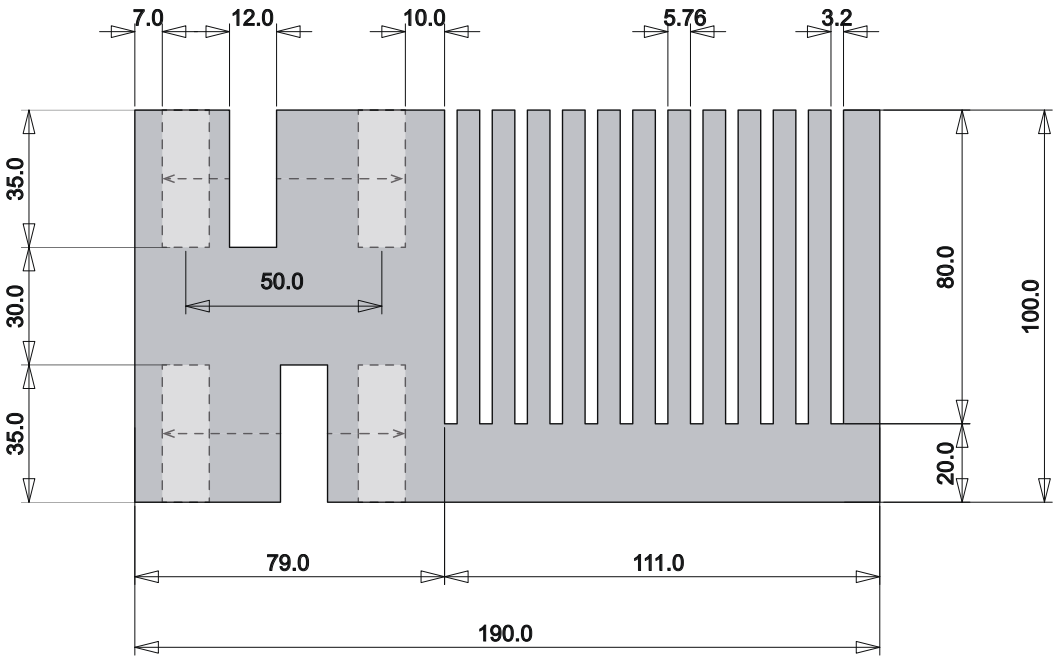

FIG. 2 Timber profile dimensions

2.1 TIMBER ELEMENT PROFILE

The research uses a 100 × 200mm spruce beam as the base material. The cross-section profile is subdivided into three distinct functional sections: insulation, structure, and enclosure (Fig. 3). The deep slits sawn into the construction elements of Timber Prototype I are utilised to generate a section of lower thermal conductivity and alleviate internal stresses that cause large-dimension timbers to crack and warp over time. These slits consist of 80mm deep slits sawn with a 3.2mm wide circular saw blade. The remaining 20mm of section profile acts as a structural member, allowing efficient bearing of axial and horizontally spanning loads. Finally, a section milled with longitudinal slits provides material required for airtight enclosure and geometrical variation.

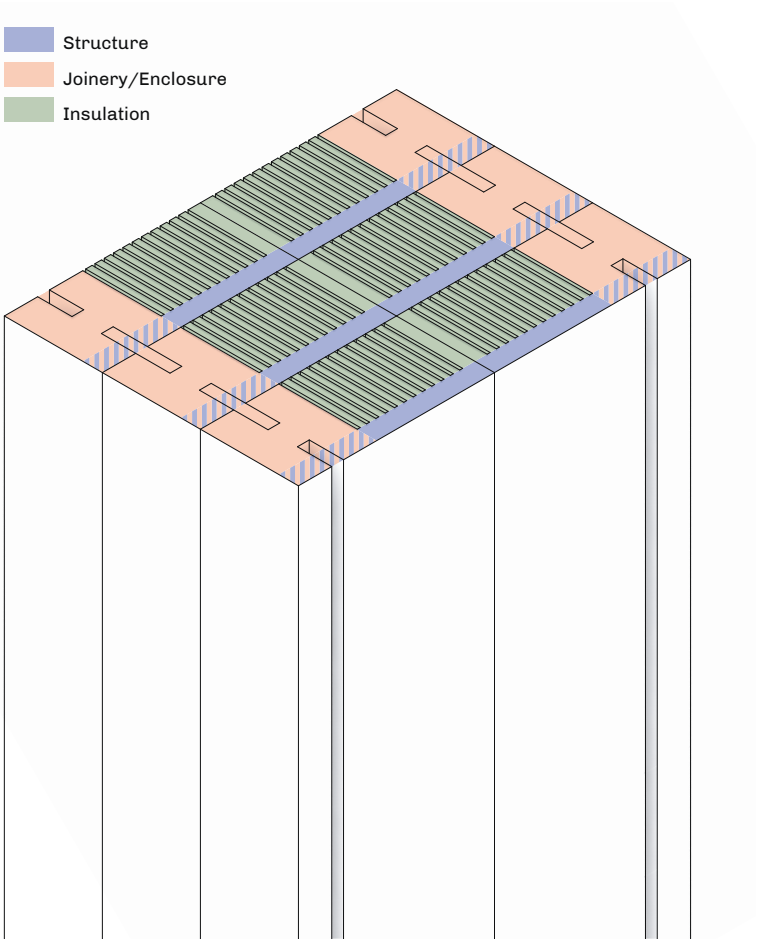

FIG. 3 Timber profile functional zones

2.2 ELEMENT CONNECTIONS

The construction elements connect using three different joinery techniques (Fig. 4). To create a thick wall section with adequate rigidity and thermal resistance, two construction elements are joined with a dovetail key to create a two-layer, 400mm deep wall section. At each end, the elements are finished with a lap joint with interlocking milled features that stiffen the joint to create a rigid moment frame and are oriented perpendicular to airflow through the envelope to reduce air permeation. Eight elements are joined into a single, rigid, trapezoidal frame. In contrast to the vertical stacking of horizontal elements found in traditional log construction and Timber Prototype I, these frames are vertically oriented in order to align the wood fibre with the principal structural forces for optimal use of the material. The frames are joined with a spline joint that uses a plywood plank to generate an airtight barrier, and which is pinned with beechwood dowels to bind the frames and minimise movement.

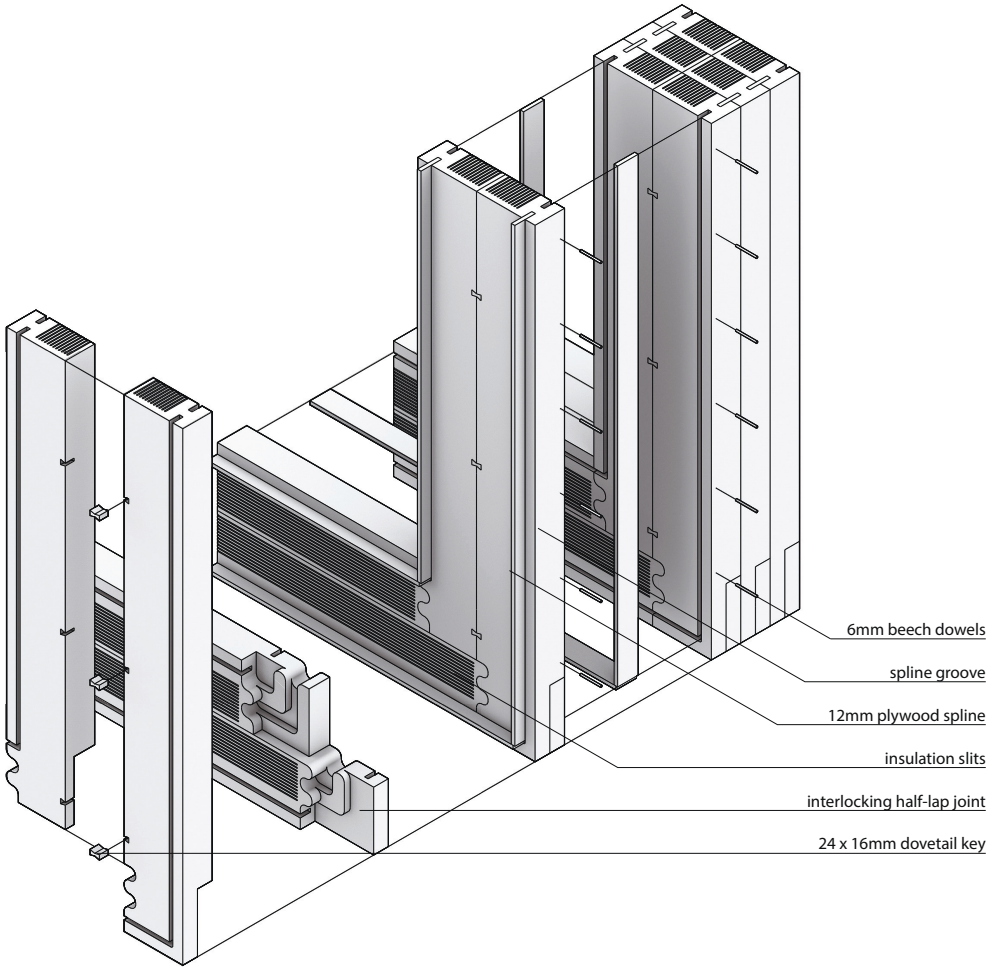

FIG. 4 Wood joinery assembly details

2.3 CONSTRUCTION SYSTEM

The construction system is developed to comprise factory prefabricated modules that are transported to site and assembled by crane. Individual modules are assembled flat and then tipped up to their final vertical orientation. They are then wrapped with a waterproof membrane to protect against rain and then a façade of wood planks is screwed onto the exterior. The modules are dimensioned for highway transport and assembly by crane. Assembly of modules is intended to utilise the same spline connection that joins the preassembled frames. Doors and windows are also aligned and mounted using the same spline joint.

2.4 CAD/CAM INTEGRATION

In traditional log construction, each layer bears upon the layer below, necessitating a near-vertical wall. However, orienting the trapezoidal frames vertically presents an interesting design opportunity. Each frame supports the spanning beams of the roof with efficient, vertical wood grain. This allows the subtle offset of subsequent frames to generate non-orthogonal and curving walls.

By changing the lengths of timber beams and the angles of joints that connect them, the walls can form three-dimensional curved surfaces.

This research develops a method for creating freeform building envelopes by systematising this formal flexibility through custom computational scripts that automatically produce detail variations based on simple user input. CAD software allows architects to rapidly design and evaluate buildings. To design with the system, a user manipulates curves in the three-dimensional CAD software Rhinceros3D. Custom C# scripts for the plugin Grasshopper were developed by the researchers which convert these curves into a complex model with layers of building information (Fig. 5). The script begins by creating intersection points at regular intervals along the curves. By connecting these points, lines are generated that correlate to the timber beams of the envelope. The scripts generate a broad array of model geometry and data relating to the building and the fabrication thereof:

- Solid geometries are generated to rapidly evaluate the quality of proposed forms and spaces.
- Frame geometry is evaluated to ensure that structural capacity will not be exceeded.
- Connection details are evaluated to ensure that the components can be assembled.
- Building metrics such as floor space, internal volume, and material quantities are output for cost analysis.
- Construction sequences can be tested virtually to ensure fit and feasibility.
- Machine Code instructions are generated to drive CAM milling.

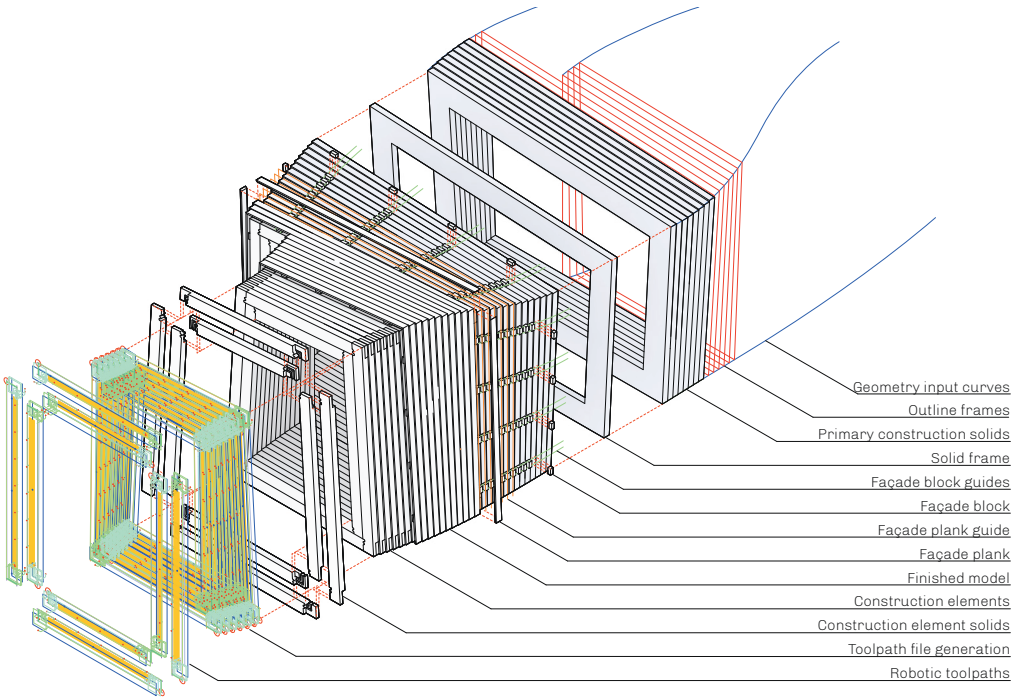

FIG. 5 CAD/CAM integrated digital model

The various outputs are accessible to project partners including building physicists, structural engineers, and contractors. Structural analyses were an important aspect of early system development. Building codes informed wood connections to ensure proposed parametric joints

would remain within acceptable dimensions. Strength values for these joints were inserted into bending moment analyses of the trapezoidal frames. These yielded structural capacities of individual frames which were integrated into the CAD/CAM model as geometric limits. Thus, the model would avoid design options where walls or roof exceeded certain angles or span lengths. By ensuring that each individual frame could bear its own weight, the designer was given free rein to design within that range without worrying about the building's global structural system. The custom software that integrates CAD and CAM processes permits the subtle yet precise variation in detail planning and fabrication that allows the high-fidelity realisation of the complex, global design geometry. The submillimetre precision of modern Computer Numeric Control (CNC) milling machines gives the added benefits of accurate planar surfaces and tight-fitting joints, which are necessary to improve airtightness by minimising gaps between construction elements and to generate stiff moment connections for the trapezoidal frames.

3 EXPERIMENT/RESEARCH

To verify all aspects of the Mono-Material Wood Wall system, small- and large-scale tests were constructed. Small test panels were used in laboratory building physics measurements. A large-scale construction mock-up was fabricated to test the CAD/CAM workflow and assembly processes, and a full-scale demonstrator building was constructed to test industrial implementation.

Test panels and the construction mock-up were fabricated using a 8kW milling spindle end effector on a KUKA KR125-2 6-Axis industrial robotic arm. The demonstrator components were produced in a factory on a Homag BOF 311_5 5-axis CNC mill with 9kW spindle and automatic tool changer. Insulation slits were sawn with a 250mm circular saw blade resulting in 3.2mm wide air chambers. Dovetail connections were milled with a 30°, 16mm wide dovetail endmill. Spline grooves were milled with a 12mm end mill and lap joints with a 20mm end mill. Additionally, demonstrator components used a variety of surfacing tools for planing.

3.1 TEST PANELS

Approximately 32 linear metres of timber beam were milled for laboratory tests. These each had twelve, 80mm deep insulation slits and one spline groove on each of the larger faces. Some of the beams were milled with dovetail grooves to bind interior and exterior layers. These elements were assembled into two test panels for thermal and airtightness measurements.

3.2 THERMAL CONDUCTION

The research seeks to measure the reduction of thermal conduction across the building envelope. This is initially done through the tabulations outlined in ISO 6946. Those values are compared to a wall section of solid wood and to the wall section of Timber Prototype I. Then, a 200mm thick test panel consisting of nine, 900mm long construction element profiles was tested for thermal conductivity in a Hot-Box test per DIN EN 12664:2001-05 (Fig. 6).

3.3 AIRTIGHTNESS

A 900×1200mm double layer airtightness test panel was tested in a blower-door test in a laboratory setting to estimate the airtightness of the envelope and to identify problem areas that should be addressed. This measurement gave a value in cubic metres per square metre of façade per hour, which could be applied to a proposed building design to determine Air Changes per Hour (ACH), the typical airtightness unit for evaluating entire structures. This panel consisted of beam elements whose exterior profiles were not milled to precise dimensions and arrived from the lumber supplier with up to 5mm of dimensional variation.

Once constructed, the research demonstrator was also fitted with a blower-door device and tested for air tightness (Fig. 7). This value was given in ACH and is extrapolated to leakage per surface area and leakage per linear metre of joint for comparison to other systems. All demonstrator elements were fully milled on each side to achieve submillimetre dimensional tolerances.

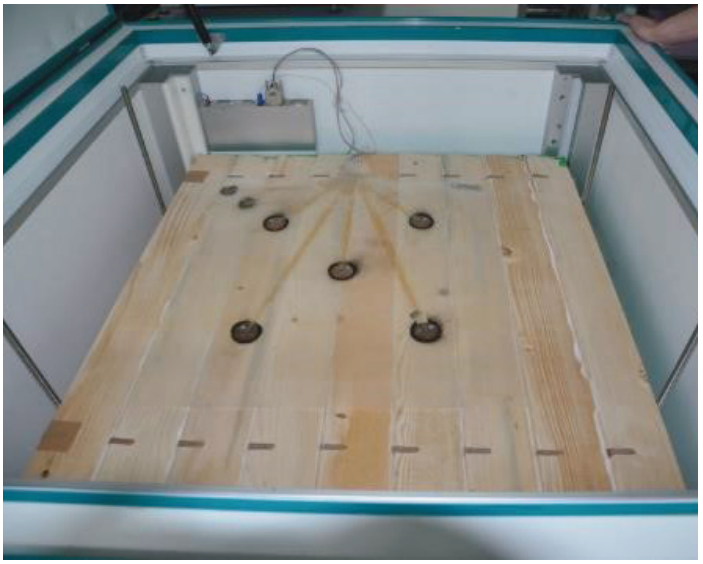

FIG. 6 Hot Box thermal conductivity test

FIG. 7 IBA: Timber Prototype House blower-door test

3.4 CONSTRUCTION MOCK-UP

24 complete elements including end joint details were fabricated on the KUKA robot to test fabrication and assembly. This was an early version of the corner joint detail which relied on an inserted block in the corners and a series of wooden dowels which pinned the lap joints to create rigidity. These joints lacked the interlocking channels of the final corner lap joint. From those elements, a 3.2×2.5×0.3m (H×W×D) section consisting of three layers of frames was assembled. This process highlighted issues in the production and assembly of components and informed changes that were implemented in the final version of the system.

3.5 DEMONSTRATOR

A full-scale demonstrator, called the IBA: Timber Prototype House, was designed and built to test industrial implementation. The primary construction of the 6×5×3.5m(L×W×H) structure consists of 464 milled elements. The elements were assembled into six modules that were clad with a waterproof membrane and rain screen façade before being transported to a site in Apolda, Germany, where they were assembled into the final structure. The design is meant to show the expressive flexibility of the system and is capped with two large picture windows and custom operable glazed doors. The demonstrator was designed as a micro-house, and can be fitted with a prefabricated utility box that contains the essential systems for a residential unit (Fig 8).

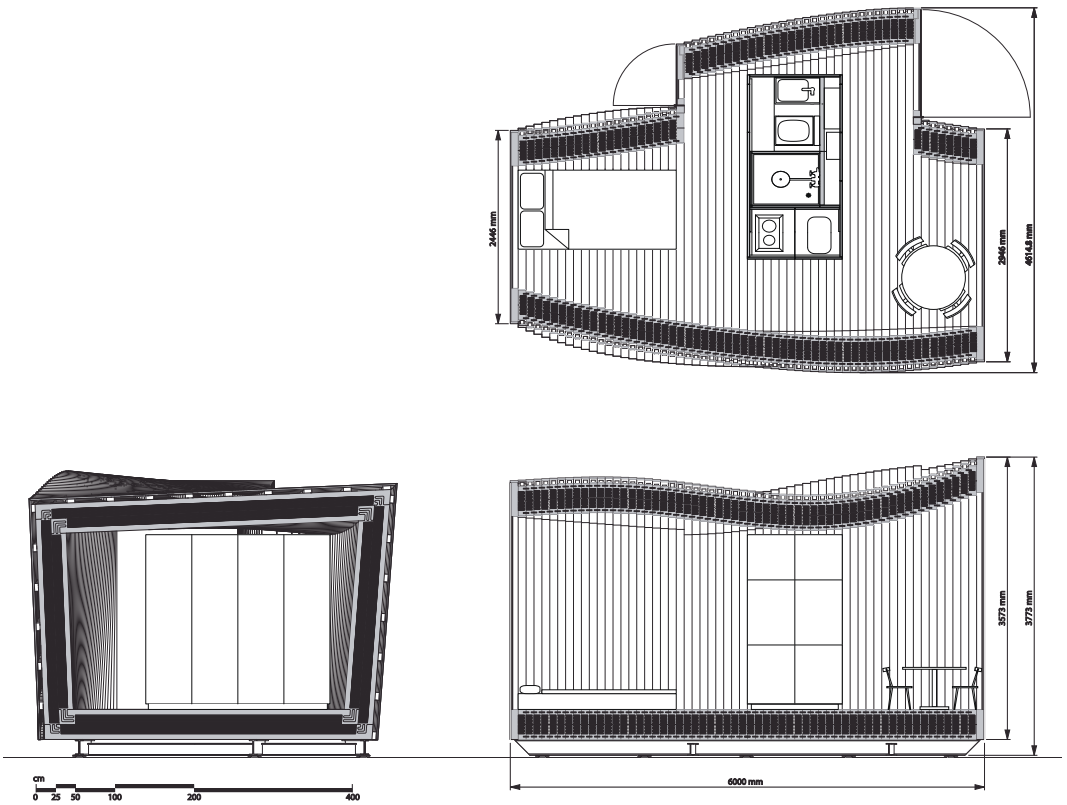

FIG. 8 Plan and Sections of IBA: Timber Prototype House

4 RESULTS

4.1 THERMAL CONDUCTANCE

Calculations of thermal conductance demonstrated a significant improvement in thermal insulation due to sawn air chambers. Compared to a solid timber wall section of the same thickness, which would have a thermal conductance of 0.285 W/ m^2·K, the Mono-Material Wood Wall would have a conductance of 0.230 W/ m^2·K, a nearly 24% improvement. Hot-Box tests demonstrated even better performance, with a conductivity of λ =0.0846 W/m·K at 10˚C. At a wall thickness of 400mm, that would result in conductance value of 0.20W/ m^2·K per (ISO 6946).

4.2 AIRTIGHTNESS

The initial laboratory test of airtightness test had very high permeability of q50 = 13.3 m^3/m^2h. By taping off the ends of the insulation slits, this value was brought down to a reasonable q50 = 2.1 m^3/m^2h. This result demonstrated the need to fully enclose the insulations slits, and in subsequent component configurations, the slits ended short of the corner, leaving a solid section of wood for the corner joint. This elucidated the need to minimise gaps between components and led to the decision to fully plane all sides of the components.

These improvements seem to have been effective as demonstrated in the IBA: Timber Prototype House. The Blower-Door test of the finished structure demonstrated an average permeability of 2.7 ACH. From this value, the performance of the Mono-Material Wood Wall itself can be estimated to be 1.22m^3/m^2·h. However, anemometer tests identified areas of significant leakage at the gaps between modules and where windows and doors were installed, so the permeability of the preassembled envelope would be lower.

4.3 CONSTRUCTION MOCK-UP

The construction mock-up informed refinements to the system. It proved the basic functionality of the CAD/CAM integration script which could directly output machine-readable code. It demonstrated assembly feasibility and a strong formal expression. The fabrication of the 24 components took approximately one hour each, as mounting the material and changing milling tools was done manually. Beams were mounted on a rotating external axis to extend the KUKA industrial robot's reach to mill 3.5m components, allowing milling on 3 sides of the beam without manually flipping it (Fig. 9).

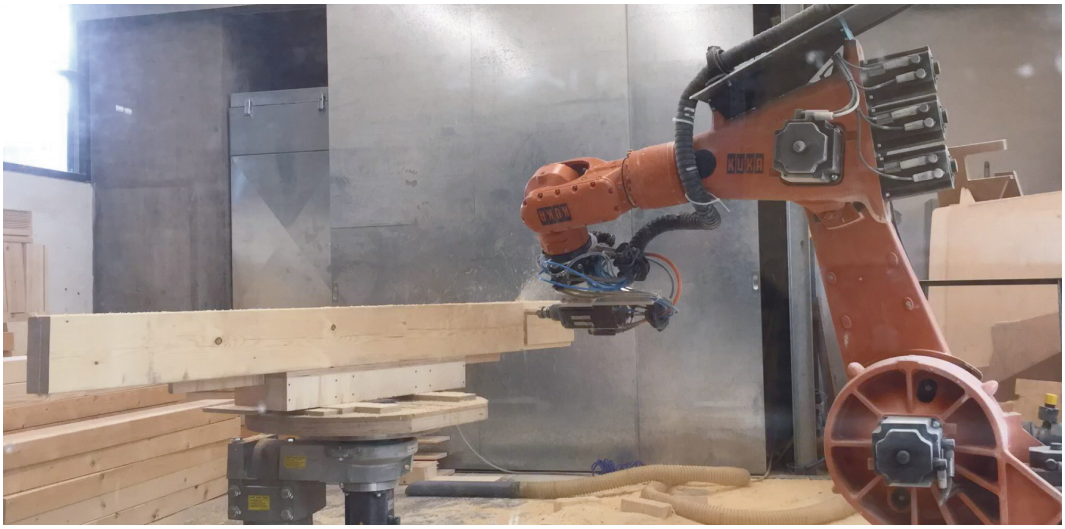

FIG. 9 Robotic milling of construction mock-up component

The external axis, loose tolerances in the robotic arm, and varying material quality led to the imprecise fit of components. The tolerances aggregated to create gaps of up to 10mm, which would have a detrimental effect on airtightness and led to the decision to fully plane all sides of the components in the demonstrator.

4.4 DEMONSTRATOR

Despite being kiln-dried and factory planed, the timber beams had up to 5mm of variation from their nominal dimensions and displayed significant warping and twisting. Therefore, oversized lumber was ordered and milled to precise final dimensions. Each face of the element had to be fully surfaced during milling and each component was flipped twice during milling.

Due to the depth of the insulation chambers, each was sawn in two passes of 40mm deep to reduce torque CNC mill's spindle and linear axis. Thus, most of the machining time was spent sawing the insulation slits. Milling times ranged from 20-30 minutes, depending on component length and, including loading and unloading material, production lasted 30-40 minutes per element.

Each component was milled with a numeric code that allowed rapid identification and straightforward assembly sequencing (Figs. 10-11). A single worker could assemble a frame of eight construction elements in 30-40 minutes. Other processes, such as wrapping the finished modules in waterproof membrane and installing the rainscreen façade planks, took a significant amount of time, but the main bottleneck was still the CNC milling. Accounting for this, one work shift per day assembling modules could keep up with two shifts per day of mill operation.

FIG. 10 CNC milled corner lap joint detail

FIG. 11 Assembled corner lap joint detail

The demonstrator was assembled in the factory into six finished modules averaging 1m deep (Fig. 12). The modules were loaded onto deep-bed trailers and transported to site (Fig. 13). In two days, the modules were placed on a lightweight steel foundation frame and mated together (Fig. 14). The spline connection used for component assembly was the planned method for connecting finished modules, but due to their weight and resulting friction, it was not possible to generate enough force to press the splines into the grooves between modules. Ultimately, short sections of planks were used to align modules during mating. This led to visible gaps between modules, which were areas of higher leakage during the airtightness test of the finished demonstrator. The same intended connection between the primary construction and the window frames and door jambs were not feasible and installers had to rely on smaller blocking for alignment and large screws and adhesives for structural mounting.

FIG. 12 completed modules in factory

FIG. 13 transport of modules

FIG. 14 onsite assembly

5 CONCLUSIONS

The validity of the integrated design and fabrication process was demonstrated by the successful completion of the IBA: Timber Prototype House (Fig. 15). The simple design, assembly, and construction processes resulted in a fully enclosed mini house that showcases the formal flexibility and building physics performance in a full-scale, inhabitable structure.

FIG. 15 Completed IBA: Timber Prototype House Demonstrator

5.1 CAD/CAM INTEGRATION

The custom computational scripts developed for the Mono-Material Wood Wall proved to be instrumental in the successful realization of the demonstrator. Dozens of designs were proposed and evaluated to suit the needs of the client, with a variety of proposed spatial configurations and formal expressions. The digital model was used to plan every stage of fabrication and assembly, including element production, module assembly, transport, and façade installation. Subcontractors were able to use the model to plan fabrication and installation of windows and doors using the spline connections for alignment.

If the Mono-Material Wood Wall is to be adopted as a method for widespread implementation, the scripts would need to be expanded into more robust programs with a simpler user interface, better error detection, and broader utilisation cases. More rigorous integration with structural engineering software, coupled with thorough benchmarking of joint strengths could expand the range of potential forms the envelope could take. Adding more joint types could allow for new architectural spaces, including internal spatial subdivision or changing the orientation of the frames. Similarly, new milling steps could be introduced that would create voids for plumbing, electrical and HVAC installations within the envelope. Functionalities could be added that facilitate fabrication on a wider range of machines.

5.2 FABRICATION AND ASSEMBLY

The very intensive milling process is the greatest hurdle to overcome in the wider adoption of the Mono-Material Wood Wall. There are several proposals to address this issue. The most time intensive machining step, sawing the insulation slits, could be shortened by mounting multiple circular saw blades on a single axle with a much more powerful spindle and material feed. This could be done on a standalone machine, such as an adapted planer with material feeder, or integrated into an industrial wood joinery centre. The latter would have the additional benefit of integrated material handling, which would nearly eliminate both time and physical labour required for loading and unloading material onto the CNC milling bed. Because fully planed beams are then milled again to achieve the necessary precision for the system's joints, overall material savings could be found by sourcing rough sawn timber or even round logs.

5.3 BUILDING PHYSICS

The performance of the Mono-Material Wood Wall was shown to be an improvement over previous solid-timber systems. To continue to make improvements, more in-depth tests should be undertaken to isolate variables and identify specific details that can be further improved. Assembly of completed modules will also require thorough investigation. Joint details between frames were out of scope of the research. However, an effective method for mating the 2-3 tonne pieces that results in an airtight seal will be crucial.

5.4 OUTLOOK

The research is currently in further development to expand the system to a multi-storey façade system. This inherently presents new challenges to create different self-supporting structural systems, to plan the logistics of transport and installation, and to generate new details to attach to other novel and pre-existing building systems. While these new challenges must be addressed, researchers are also returning to the initial aims of the project by continuing to reduce the extraneous material layers in the envelope to achieve a true Mono-Material envelope.

Acknowledgements

The authors acknowledge the support of the Forschungsinitiative Zukunft Bau, Bundesinstitut für Bau-, Stadt- und Raumforschung (BBSR) as part of the project "Baukonstruktionen aus Massiv-Holz (SWD-10.08.18.7-15.59)" lead by ICD University of Stuttgart in collaboration with Jade Hochschule and IBA Thüringen. In addition, Oliver Bucklin and Achim Menges acknowledge the partial support of the Deutsche Forschungsgemeinschaft (DFG, German Research Foundation) under Germany´s Excellence Strategy – EXC 2120/1 – 390831618.

Special thanks to Tobias Haag, Dr. Martina Doehler-Behzadi, and Elisa Wrobel of IBA Thüringen, Victor Rodriguez of the University of Stuttgart: ICD, Geronimo Bunjy, Ganna Bulavintseva, Marie Deilmann of Jade Hochschule: Oldenburg, Manfred Weid of Ackermann GmbH, and our industrial partners: Thüringer Forst, Rettenmeier Holz, Ackermann GmbH, Uni-Holzbau, Serge Ferarri GmBh, Wider Holz, MFPA

References

Alev, Ü., Uus., A, Teder, M., Miljan, M-J., & Kalamees, T. (2014). Air leakage and hygrothermal performance of an internally insulated log house. In J. Arfvidsson, L-E. Harderup, A. Kumlin, and B. Rosencrantz (Eds.). *NSB 2014-10th Nordic Symposium on Building Physics - Full Papers*. Lund: Building Physics, LTH, Lund University, pp. 55–62.

Alev, Ü., Uus, A., & Kalamees, T. (2017). Airtightness improvement solutions for log wall joints. *Energy Procedia 132*, pp. 861–866. doi: 10.1016/j.egypro.2017.09.678.

ISO 6946: 2017. *Building components and building elements – Thermal resistance and thermal transmittance – Calculation methods* (ISO 6946:2017).

ISO 10456, 2007 + Cor. 1:2009. *Building materials and products – Hygrothermal properties – Tabulated design values and procedures for determining declared and design thermal values* (ISO 10456:2007 + Cor. 1:2009).

Erlandsson, M., Sundqvist, J-O. (2014). *Environmental consequences of different recycling alternatives for wood waste*. Retrieved from https://www.ivl.se/download/18.343dc99d14e8bb0f58b76a7/1445517707516/B2182.pdf, checked on 11/18/2019.

González-García, S., Krowas, I., Becker, G., Feijoo, G., & Moreira, M. T. (2013). Cradle-to-gate life cycle inventory and environmental performance of Douglas-fir roundwood production in Germany. *Journal of Cleaner Production* 54, pp. 244–252. doi: 10.1016/j.jclepro.2013.05.012.

Hill, C. A. S., & Dibdiakova, J. (2016): The environmental impact of wood compared to other building materials. In International Wood Products Journal 7 (4), pp. 215–219. doi: 10.1080/20426445.2016.1190166.

Kalamees, T., Alev, Ü., & Pärnalaas, M. (2017): Air leakage levels in timber frame building envelope joints. *Building and Environment,* 116, pp. 121–129. doi: 10.1016/j.buildenv.2017.02.011.

Korpi, M., Vinha, J., & Kurnitski, J. (Eds.) (2004). Airtightness of Timber-Framed Houses with Different Structural Solutions. *Buildings Conference*, December. Oak Ridge National Laboratory: Building Technologies Program. Retrieved from https://web.ornl.gov/sci/buildings/conf-archive/2004%20B9%20papers/070_Korpi.pdf.

Nagler, F., Jarmer, T., Niemann, A., & Cruel, A. (2018). *Einfach Bauen. Ganzheitliche Strategien für energieeffizientes, einfaches Bauen – Untersuchung der Wechselwirkung von Raum, Technik, Material und Konstruktion. Endbericht für das Forschungsvorhaben [Simply Building. Holistic strategies for energy-efficient, simple building - investigating the interaction of space, technology, materials and construction. Final report for the research project].* With the assistance of Thomas Auer, Laura Franke, Hermann Kaufmann, Stefan Winter, Stephan Ott, Marco Krechel, Christoph Gehlen, , Charlotte Thiel. Technische Universität München: Lehrstuhl für Entwerfen und Konstruieren. Munich, Germany. Retrieved from https://www.einfach-bauen.net/wp-content/uploads/2019/04/einfach-bauen-schlussbericht.pdf.

Puettmann, M. & Wilson, J. (2005). Life-cycle analysis of wood products: Cradle-to-gate LCI of residential wood building materials. *Wood and Fiber Science Journal, 37*, pp. 18–29.

Roos, C., Eklund, K., & Baylon, D. (1993). *The Thermal Performance and Air Leakage Characteristics of Six Log Homes in Idaho.*. US Bonneville Power Administration. United States. doi: 10.2172/10103110

de Rosa, M, Pizzol, M., Schmidt, J. (2018). How methodological choices affect LCA climate impact results: the case of structural timber. *International Journal of Life Cycle Assessment,* 23 (1), pp. 147–158. doi: 10.1007/s11367-017-1312-0.

Ross RJ (ed) (2010) Wood Handbook: Wood as an Engineering Material. General Technical Report FPL-GTR-190. U.S. Dept. of Agriculture, Forest Service, Forest Products Laboratory,

Madison, W.I, & Schwinn, T. (2016). Manufacturing Perspectives. Tobias Schwinn in conversation with Holzbau Amann and Müllerblaustein. In A. Menges, T. Schwinn, and O. D. Krieg (Eds.). *Advancing wood architecture. A computational approach*. London: Routledge.

Skullestad, J.L., Bohne, R.A., & Lohne, J. (2016). High-rise Timber Buildings as a Climate Change Mitigation Measure – A Comparative LCA of Structural System Alternatives. *Energy Procedia 96,* pp. 112–123. doi: 10.1016/j.egypro.2016.09.112.

Ximenes, F.A. & Grant, T. (2013). Quantifying the greenhouse benefits of the use of wood products in two popular house designs in Sydney, Australia. *International Journal of Life Cycle Assessment,* 18 (4), pp. 891–908. doi: 10.1007/s11367-012-0533-5.

Effects of Phase Change Materials on Heat Flows Through Double Skin Façades

Thomas Wüest [1*], Lars O. Grobe [2], Andreas Luible [2]

* Corresponding author
1 Lucerne University of Applied Sciences and Arts, Institute of Civil Engineering IBI, Switzerland, thomas.wueest@hslu.ch
2 Lucerne University of Applied Sciences and Arts, Institute of Civil Engineering IBI, Switzerland

Abstract

The potential of exemplary organic and inorganic Phase Change Materials (PCMs) as façade integrated storage is tested. The impact of two PCMs on heat flows is assessed in comparison with water and concrete. The simulation-study employs a transient Modelica simulation model of a test cell featuring the Solar Energy Balanced Façade (SEBF). It is shown that, when compared to water, PCMs of identical volume change the seasonal energy balance in winter and summer by only ± 4%. Other than water, the PCMs maintain this effect even if the storage volume decreases. Due to spatial constraints, this can support the integration of thermal storage in façade design considerably. Preliminary results indicate that designing thermal storage in façades with PCMs must not only consider the latent heat storage capacity, but also take into account the combined effects of latent heat capacity, melting point, conductivity, and dead load. The application of PCMs promises to foster the integration of the technology of SEBF into façades, but the necessary deliberate selection of, and design with, PCMs requires further research.

Keywords

thermal storage, passive solar façade, trombe wall, phase change materials, solar energy balanced façade

10.7480/jfde.2021.1.5408

1 INTRODUCTION

Façades greatly affect energy demand and the level of comfort that can be achieved in a building. Both targets are addressed by a novel hybrid façade system, that integrates a controlled solar-thermal collector and storage into the transparent and opaque zones of double-skin-façades (DSF). The adaptive seasonal and daily management of solar gains of the Solar Energy Balanced Façade (SEBF) (Wüest & Luible, 2018) improves the energy balance through the passive use of solar energy. The SEBF reduces the transparent façade area, and instead introduces an opaque parapet which functions as thermal storage and mitigates daily energy flux variations. The second skin structure protects shading devices that are essential for the efficient and reliable management of solar gains absorbed by the thermal absorber, and admitted through the transparent areas.

The SEBF employs the functional principles of the Trombe Wall (TW) (Hu, He, Ji, & Zhang, 2017). TWs are passive solar façade systems, which store and redistribute heat. A typical TW combines a solid wall, acting as thermal storage, with external glazing to exploit the greenhouse effect to form a solar collector. Openings, often equipped with fans, allow for an air exchange between the attached space and the cavity of the TW. Several studies suggest that TWs have a high potential to reduce energy demand in buildings, e.g. by 50% (Quesada, Rousse, Dutil, Badache, & Hallé, 2012) and up to 69.7% (Zhang et al., 2020). The main drawbacks of TWs are i) the massive structure, ii) poor insulation, and iii) unbalanced performance for winter and summer (Hu, He, Ji, & Zhang, 2017). A lightweight, ventilated TW element (Lohmann & Santos, 2020) showed up to 27% savings on heating energy demand; summer conditions were not considered.

A thermal simulation model of the SEBF, including an approximation of vertical heat flows between the opaque and transparent areas, has been developed in Modelica. Modelica is an object orientated, equation-based language that can describe physical systems in various domains (Wetter, 2009). It supports transient thermal modelling and allows it to be combined with a customised control strategy for seasonal adaptive solar gain management. The model was validated against measurements on a test cell installation (Wüest, Grobe, & Luible, 2020).

The SEBF aims to turn the fundamental overheating susceptibility of DSFs (Manz & Frank, 2005; Balocco, 2002) into a means to improve the energy balance of buildings without active heat exchange. It aims to passively reduce heat losses in winter, and to control solar heat gains in summer. Preliminary studies (Wüest & Luible, 2018; Wüest & Luible, 2019) confirmed the fundamental design of the SEBF, and demonstrated the suitability of concrete and water as materials for the thermal storage. Nevertheless, both materials are difficult to integrate into lightweight façades. Concrete has a high dead load. Water implies the risk of leakage and freezing.

Latent heat storage techniques lend themselves as an alternative to these problematic materials (Biswas, 2016; Vukadinović, Radosavljević, & Đorđević, 2020). This research compares the performance of a SEBF element with thermal storage employing either water, concrete, or a set of Phase Change Materials (PCMs) by studying annual simulations under identical conditions.

2 MODEL DEVELOPMENT

For this study, the storage tank, made of a high absorbing aluminium tank within the DSF cavity, was simulated with different materials (gelled water, concrete, and two PCMs). In line with previous studies, all simulations were conducted in the Modelica modelling environment and were performed at intervals of one minute.

2.1 THE SOLAR ENERGY BALANCED FAÇADE

One-dimensional heat transfer elements from the Modelica standard library, e.g. Modelica. Thermal package, and its HeatTransfer sub-package were employed The SEBF was modelled as two one-dimensional heat flows through its transparent (A) and opaque (B) areas. These fluxes were coupled via a vertical heat exchange element (C1) within the air cavity (see Fig. 1). This approach has been validated experimentally (Wüest, Grobe, & Luible, 2020)

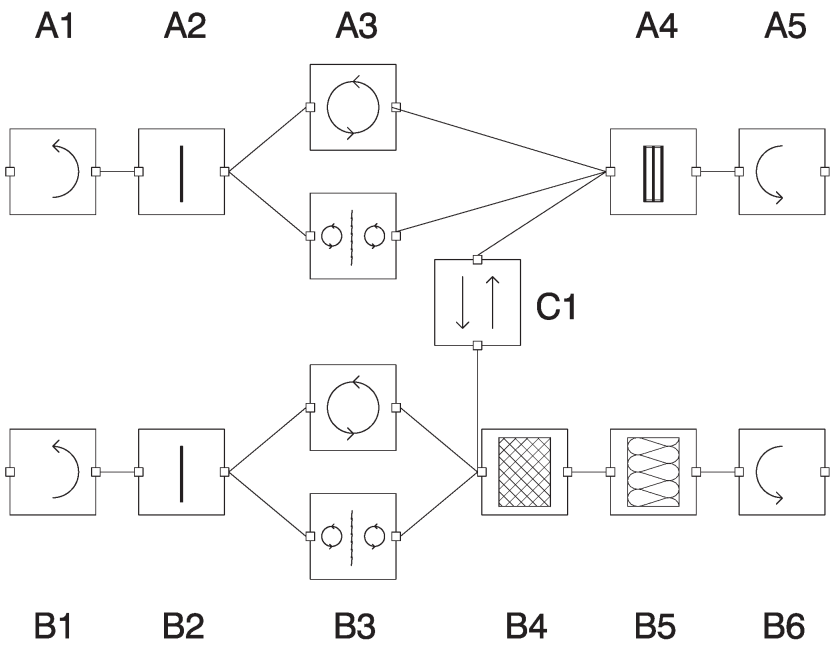

FIG. 1 Modelica model scheme for the four main components of the SEBF system

The modelling of convective heat flows on surfaces (external and internal) and through cavities was based on EN 15099. To simulate unsteady (transient) heat transfer, material layers were divided into *n* equidistant conductors, and *n+1* masses. Each conductor represents *1/n* of the layer thickness. The *n+1* masses represent the surfaces with two times *1/(2n)* of the total material layer mass and *n-1* times core masses of *1/n* of total material layer mass between the conductors (Wüest & Luible, 2019). This approach was applied with $n = 6$ to model the stack of storage materials and insulation forming the parapet. Glass panes and venetian blinds were simplified with $n = 2$ and only one centred mass. Air gap models A3 and B3 stand for the two different states without and with shading. The corresponding heat fluxes were modelled by one in the unshaded, and two convective and radiative conduction elements in the shaded case (acc. ISO 15099 section 8.3.2.2 and 8.4.3.1).

The elements in Fig. 1 are: external Solar Heat Transfer Coefficient (SHTC, A1 and B1), external glass pane (A2, B2), air gap with shading (A3 and B3 independent from each other), Triple Glazing Unit (TGU, A4), storage mass (B4), insulation (B5), internal SHTC (A5, B6), and vertical bi-directional heat flow element (C1).

2.2 HEAT CAPACITY OF PHASE CHANGE MATERIALS (PCMS)

Modelling PCMs in building simulation is challenging. The Modelica standard library is not designed for dynamic heat flow elements. Consequently, modelling heat transfer through PCMs with its irregularity (reflected by the heat storage capacity parameter), meant that the standard mass element had to be modified. The varying enthalpy due to the phase transition is described by a continuous temperature-dependent function (Halimov, Lauster, & Müller, 2019). For this research, the heat capacity during the melting and freezing process was approximated by a standard distribution. It was centred at the melting point $\mu = T_{melt}$. The standard variation σ was set to 1/6 of the melting range ΔT_{melt} (to include 99.73% of latent capacity within the melting range ΔT_{melt}). Its integral was scaled by the latent heat storage capacity (c_{lat}). Adding the sensible specific heat capacity (c_{sens}) leads to the dependent heat storage capacity ($c_{(T)}$) as described in Formula 1.

$$c_{(T)} = c_{sens} + c_{lat} \cdot \frac{1}{\sqrt{2 \cdot \pi \cdot \left(\frac{\Delta T_{melt}}{6}\right)^2}} \cdot e^{-\frac{(T - T_{melt})^2}{2 \cdot \left(\frac{\Delta T_{melt}}{6}\right)^2}} \qquad (1)$$

From the innumerable variants of PCMs, two exemplary storage materials from Rubitherm were used: high density salt-water PCM (SP29Eu) and organic PCM (RT25HC) as shown in Table 1. Fig. 2a illustrates the temperature dependent heat storage capacities ($c_{(T)}$), and Fig. 2 b and c the heat storages per kg and L respectively. It is evident that the two PCMs differ mostly by density, which accounts for the greater heat capacity per volume of SP29Eu.

In this research, only the effects of latent heat storage of PCMs were taken into account.
The influence of varying heat conductivities in solid and liquid states, as well as volume effects, were neglected. The thermal conductivity within the storage material layer is of minor influence and would lead to extended simulation time. A refined model taking account of varying heat conductivity could be realised in parallel to the described model.

TABLE 1 Exemplary PCMs evaluated in this research, source: https://www.rubitherm.eu/en/productCategories.html

PCM ID	PCM	MELTING POINT T_{MELT} [°C]	MELTING RANGE ΔT_{MELT} [K]	SENSIBLE SPECIFIC HEAT CAPACITY C_{SENS} [KJKG^{-1}K^{-1}]	LATENT HEAT STORAGE CAPACITY C_{LAT} [KJKG^{-1}]	DENSITY (SOLID) ρ [KGM^{-3}]
$PCM_{A(30/3)}$	SP29Eu	30	3	2'000	170'000	1525
$PCM_{B(25/5)}$	RT25HC	25	5	2'000	200'000	825

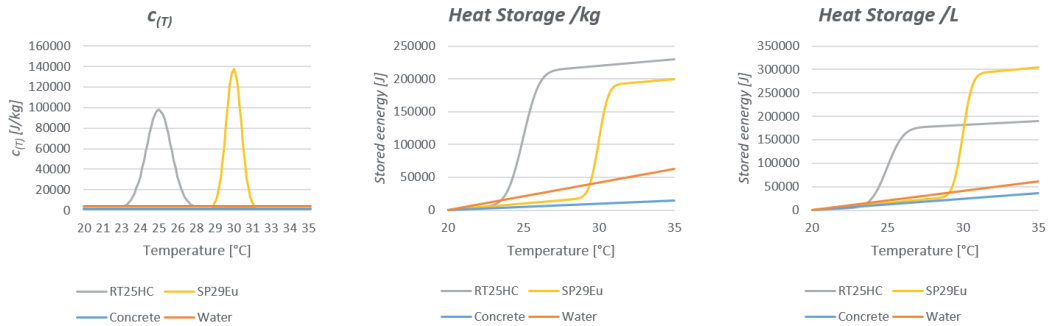

FIG. 2 Sensible and latent heat storage of PCM, concrete and water according Table 1 as a) function of temperature according to Formula 1, b) heat storage per kg, and c) heat storage per litre

3 EXPERIMENT

3.1 CONFIGURATION OF THE SOLAR ENERGY BALANCED FAÇADE AND EVALUATED STORAGE MATERIALS

The simulations only consider one SEBF element, 1.35 m x 2.9 m. The SEBF was configured so that its external layer is an 8 mm thick single pane of glazing (τ = 0.823, ρ = 0.076). The inner layer is horizontally divided into a parapet area of 1.5 m^2, and a transparent area covered by the TGU of 1.9 m^2. The depth of the cavity was set to about 150 mm in front of the TGU, and 100 mm in front of the storage. The shading was implemented by means of highly reflective Venetian blinds (ρ = 0.75).

The thermal storage tank consists of two 3 mm aluminium sheets with 20 mm or 40 mm of filling material (Table 2). The external surface of the tank has low reflectance and is highly absorbent (ρ = 0.25). The properties of the evaluated PCMs (PCM_A and PCM_B) were derived from the products reported in Table 1. They differ in terms of density, conductivity, and latent heat capacity.

TABLE 2 Relevant properties of the evaluated storage materials

MATERIAL	THICKNESS T [MM]	DENSITY ρ [KGM^{-3}]	CONDUCTIVITY Λ [$WM^{-1}K^{-1}$]	SPECIFIC HEAT CAPACITY C_{SENS} [JKG-1K-1]	LATENT HEAT CAPACITY C_{LAT} [JKG-1]	THERMAL EFFUSIVITY B [$JK^{-1}M^{-2}S^{-1/2}$]
Water Gel	20 /40	981	0.35	4'183	-	1198
Air	20 /40	Var.	Var.	-	-	-
Concrete	20 /40	2400	2.1	1'000	-	2245
PCM A	20 /40	1525	0.5	2'000	170'000	1235
PCM B	20 /40	825	0.2	2'000	200'000	575

3.2 VARIATIONS OF STORAGE MATERIALS

The selection of the PCMs is challenging due to the wide range of properties of available materials and products, which by no means is represented by the selection of the two PCMs (Table 1). The selection of the two PCMs is rather regarded as an example by which to evaluate the effect two different types—organic and high density—on the performance of the SEBF's thermal storage.

The effectivity of PCMs is mainly defined by their melting temperatures. To activate the latent heat storage, variants of the PCM types were chosen with melting points low enough to be reached on cold and sunny winter days, but high enough to be discharged on summer nights. In the simulation experiment, each of PCM_A and PCM_B was evaluated assuming three different melting points: 25°C, 30°C, and 35°C.

In the following passages, PCM types (A or B) and their variants (defined by T_{melt} and ΔT_{melt}) are indicated as subscripts. A PCM of type A with T_{melt} = 35°C and ΔT_{melt} = 5 K would therefore be referred to as $PCM_{A(35/5)}$.

The simulations assume an initial maximum depth of the storage material of 40 mm. This is motivated by the identical geometric configuration of the SEBF evaluated in a precedent study, the results of which shall be compared to Wüest, Grobe, and Luible (2020). In addition, the effect of decreasing the thickness by of 50% to = 20 mm was analysed.

Water and concrete were modelled as reported by Table 2. In parallel with the previous research, all results were compared to the case of an empty storage tank (material "air"). This allows the effects of the thermal mass of the storage to be isolated from those of other solar-optical mechanisms.

3.2.1 Shading Control

To make use of solar gains in cold periods but prevent overheating during warmer periods, a customised control of the shading devices in the transparent and opaque zones was employed. The control enters three predefined modes based on the mean average external temperature over the last 24 hours T_{24} (Wüest, Grobe, & Luible, 2020). If T_{24} is lower than 12°C, the system is in heating mode and maximises solar gains. If T_{24} is higher than 15°C, the SEBF is in cooling mode and minimises gains. The range between 12° and 15° activates 'free floating' mode, avoiding gains through the storage, and moderating direct gains through the TGU. The set points of the modes are listed in Table 3. In all three modes, night-time losses are controlled by application of a threshold of 25 W/m2 to monitored global vertical irradiance E_v.

TABLE 3 Global irradiance set points for shading control

RESPONSE	HEATING MODE $T_{24} \leq 12°C$	FREE FLOAT MODE $12°C < T_{24} < 15°C$	COOLING MODE $15°C \leq T_{24}$
Close shading of TGU	if $E_v > 350$ W/m²	if $E_v > 350$ W/m²	if $E_v > 150$ W/m²
Close shading of TGU at night	always	always	never
Close shading of storage	if $E_v < 25$ W/m²	if $E_v > 25$ W/m²	if $E_v > 25$ W/m²
Close shading of storage at night	always	never	never

3.3 BOUNDARY CONDITIONS

In all simulations, internal air temperature was set to 22°C. Influences of occupancy were not considered. The outdoor conditions were given by a standard design year for Zürich (CH) on an hourly basis from Meteonorm (Meteotest AG, 2018). All parameters, such as temperature, wind speed, façade irradiance, and sun position were interpolated linearly from hourly values.

3.4 EVALUATION VARIABLES

The effect of varying storage materials was evaluated by four variables that were solved by the simulation:

- the maximum surface temperature of the storage tank,
- the energy balance of the SEBF element for each season,
- short-term effects such over the course of the day, and
- the dead load introduced into the façade by the storage material.

The maximum surface temperature of the storage tank was expected to be the warmest point within the SEBF element. Because of its non-ventilated DSF structure, the façade tends to overheat (Manz & Frank, 2005). Therefore, the maximum temperature within the element acts as an indicator for thermal loads on the SEBF's component. High temperatures could, for example, accelerate ageing processes or lead to fogging (outgazing of plasticisers and condensation on the glass surface).

Effects on the energy balance, as the primary design target of the SEBFs, were evaluated as the key output of the simulation. Therefore, the heat flow at the inner façade surface is regarded to evaluate the needed heating or cooling demand in the interior. To reduce complexity, the thermal balance of an SEBF element was evaluated seasonally for winter (January, February, December), spring (March, April, May), summer (June, July, August), and autumn (September, October, November). To evaluate the intended delay of passive solar gains, as the secondary design target, one winter and one summer day were analysed in detail.

The dead load imposed by building materials significantly affects the structural design of curtain walls. Traditionally, the weight of glass accounts for the largest proportion of the dead load on façade elements. A typical TGU for façade applications consists of about 21 mm glass (comprising three panes of 8 mm, 5 mm and 8 mm), corresponding to a dead load of 57 kg/m^2. This is the reference for the storage tank, where 29 kg/m^2 is contributed by the containing aluminium sheets (~10 mm) and insulation (70 mm) alone.

4 RESULTS

4.1 TEMPERATURES

Table 3 shows that the shading control is effective in that the storage tank only receives solar irradiance when the external 24-hour mean temperature T_{24} is below 12°. Since this effectively blocks irradiance on hot days in summer, the maximum surface temperatures of the storage occur

only from September until April. In summertime (June – August), they rarely surpass 40°C for the 40 mm tank, while the storage of reduced thickness of 20 mm reaches 47°C, and the empty (air-filled) tank 53°C. Fig 3 distils these findings by showing only the daily maximum temperatures T_{max} on the storage tank in its 40 mm, 20 mm, and air configurations.

The maximum temperatures for the entire year are summarised in Fig. 4. All configurations, except of air, reach higher temperatures when the thickness of storage material is reduced. The air element reaches the highest temperatures, up to 88°C, whereas the 40 mm water element, as proposed in the initial design of the SEBF, is significantly cooler at approximately 63°C. The variants of PCM_B with a thickness of 40 mm achieve similar results to 40 mm of water. With PCM_A, the maximum temperatures are significantly lower. Even the 20 mm configurations of $PCM_{A(30/3)}$ and $PCM_{A(35/3)}$ are at the same level as a water-filled tank of twice the volume.

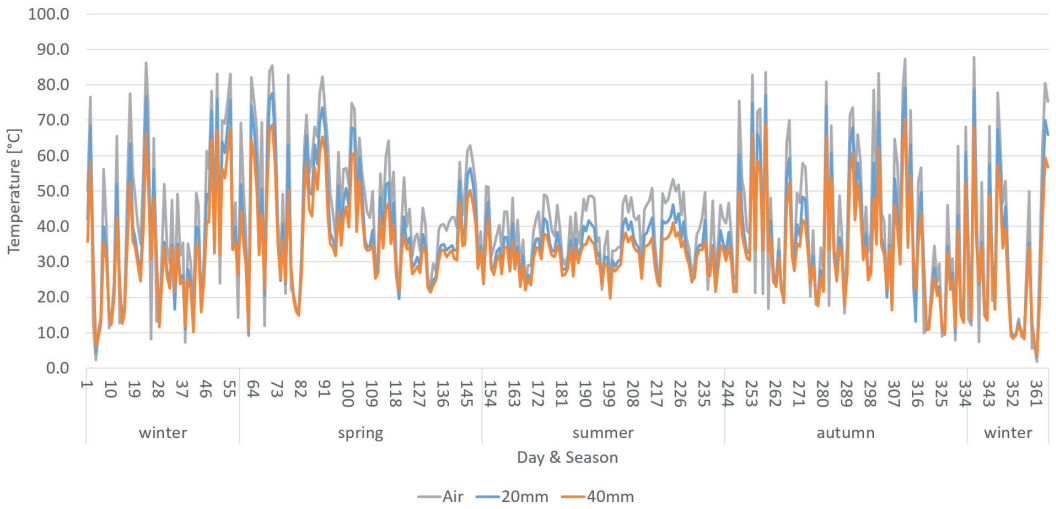

FIG. 3 Maximum tank surface temperature Tmax of 40 mm, 20 mm and air configurations, in °C

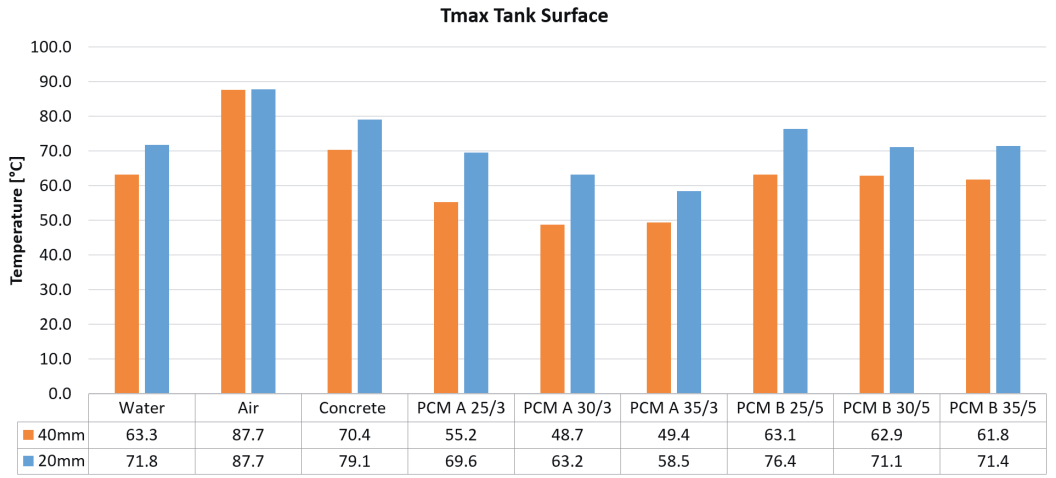

	Water	Air	Concrete	PCM A 25/3	PCM A 30/3	PCM A 35/3	PCM B 25/5	PCM B 30/5	PCM B 35/5
40mm	63.3	87.7	70.4	55.2	48.7	49.4	63.1	62.9	61.8
20mm	71.8	87.7	79.1	69.6	63.2	58.5	76.4	71.1	71.4

FIG. 4 Maximum annual tank surface Temperatures Tmax for all storage material configurations, in °C

4.2 ENERGY BALANCE FOR EACH SEASON

The energy balance at the internal façade surface for each season due to heat conduction for all storage variants is summarised in Table 4. In addition, the direct solar heat gains are reported, which are identical for all elements. All configurations achieve similar results, especially in winter and summer. Higher differences occur at intermediate climate conditions in spring and autumn.

TABLE 4 Energy balance for each element and season in [kWh]

		WATER	AIR	CON-CRETE	PCM A 25/3	PCM A 30/3	PCM A 35/3	PCM B 25/5	PCM B 30/5	PCM B 35/5	DIR. SOL. GAIN
40 mm	**Winter**	-29.0	-32.2	-29.6	-29.3	-29.1	-28.6	-30.3	-30.1	-30.2	28.8
	Spring	5.8	2.5	5.3	5.63	6.1	6.7	5.00	5.2	5.2	52.9
	Summer	13.6	15.5	13.6	13.0	13.4	13.6	13.4	13.6	14.0	35.8
	Autumn	-4.1	-5.6	-4.4	-4.5	-4.0	-3.9	-4.9	-5.02	-4.7	37.7
20 mm	**Winter**	-30.2	-32.3	-31.5	-29.4	-29.8	-29.20	-30.6	-30.8	-30.7	
	Spring	4.9	2.3	3.7	5.7	6.1	6.27	5.2	5.0	4.8	
	Summer	13.9	15.4	14.3	13.0	13.5	13.9	13.5	13.7	14.2	
	Autumn	-4.7	-5.8	-5.4	-4.8	-4.3	-4.2	-5.01	-5.2	-5.0	

Table 5 shows the percentage deviation relative to the 40 mm water tank for winter and summer periods. As reported by Table 4, only the empty tank leads to significantly higher heat losses and gains (11% to 14%).

TABLE 5 Energy balance for each element an season in [kWh]

		WATER	AIR	CON-CRETE	PCM A 25/3	PCM A 30/3	PCM A 35/3	PCM B 25/5	PCM B 30/5	PCM B 35/5
40 mm	**Winter**	0%	11%	2%	1%	0%	-1%	4%	4%	4%
	Summer	0%	14%	0%	-4%	-2%	0%	-2%	0%	3%
20 mm	**Winter**	4%	11%	9%	1%	3%	1%	5%	6%	6%
	Summer	2%	13%	5%	-5%	-1%	2%	-1%	0%	4%

4.3 SHORT-TERM ENERGY BALANCE

The short-term energy balance is presented for two sample days each for both winter (Fig. 7) and summer (Fig. 8). The corresponding exterior conditions are illustrated by Fig. 5 and Fig. 6. The two days in February represent the coldest two-day period (nights below -7°C), whereas the two days in July represent the warmest two-day period (peak 32.7°C).

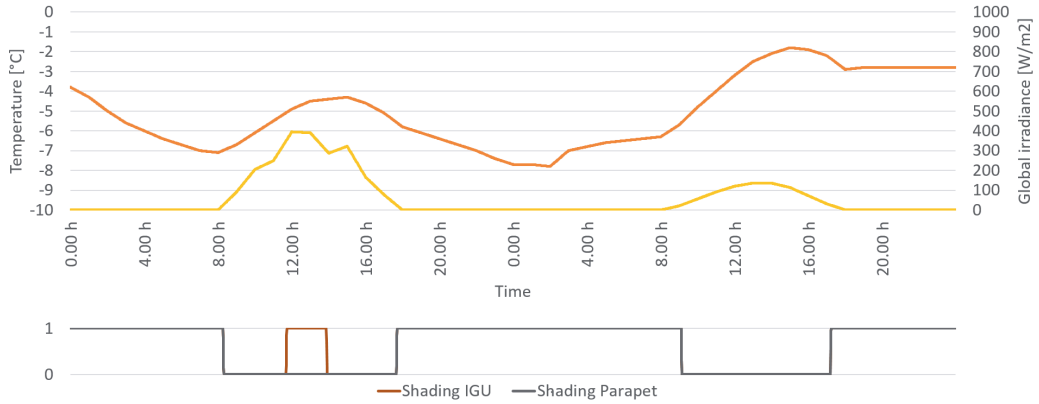

FIG. 5 External conditions (air temperature, solar irradiance façade) 9th – 10th February according Meteonorm

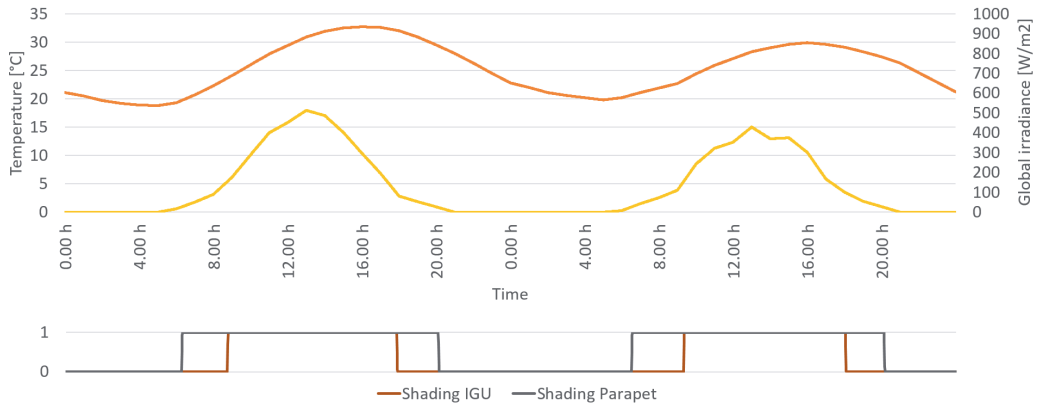

FIG. 6 External conditions (air temperature, solar irradiance façade) 24th – 25th July according Meteonorm

Both Fig. 7 and Fig. 8 confirm the short-term behaviours of what Table 4 and Table 5 indicate as seasonal effects: all storage variants act very similarly. Heat is mostly stored and released within 24 hours. Therefore, only 40 mm water and 40 mm air variants were highlighted within the figures. A first analysis of those graphs reveals the following main findings:

- All parapet heat flows are slightly undulated and close to zero,
- all TGU heat flows are extremely volatile, because they react immediately to solar irradiance,
- higher solar irradiance increases the differences in heat flows,
- due to the low temperature and solar irradiance in winter (9th -10th February), the storage is almost ineffective, leading to nearly identical heat flows through all configurations, and
- the effects of PCMs are reflected by plateaus of constant heat flow in summer at values decreasing with melting temperature, e.g. 2 W, 4 W, and 7 W for melting temperatures of 25°C, 30°C, and 35°C => 7 W respectively.

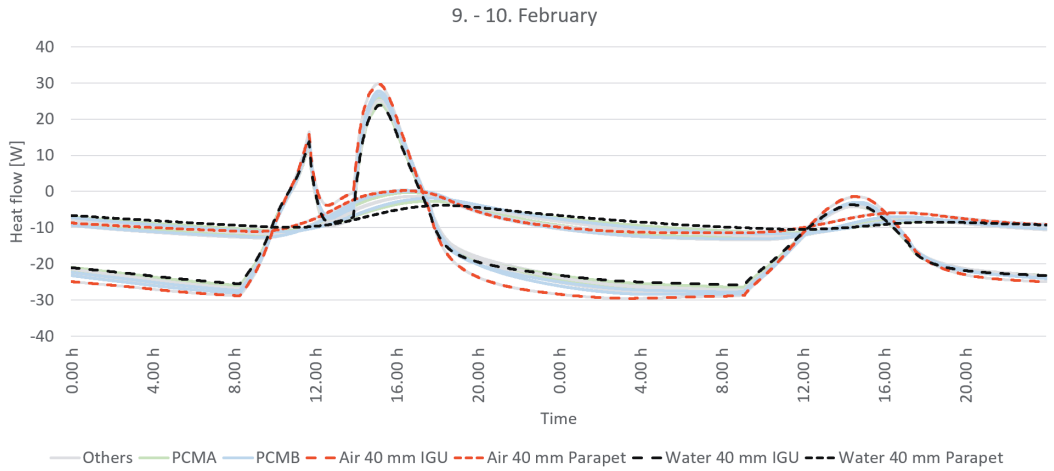

FIG. 7 Two-day period winter (9th – 10th February) heat flows

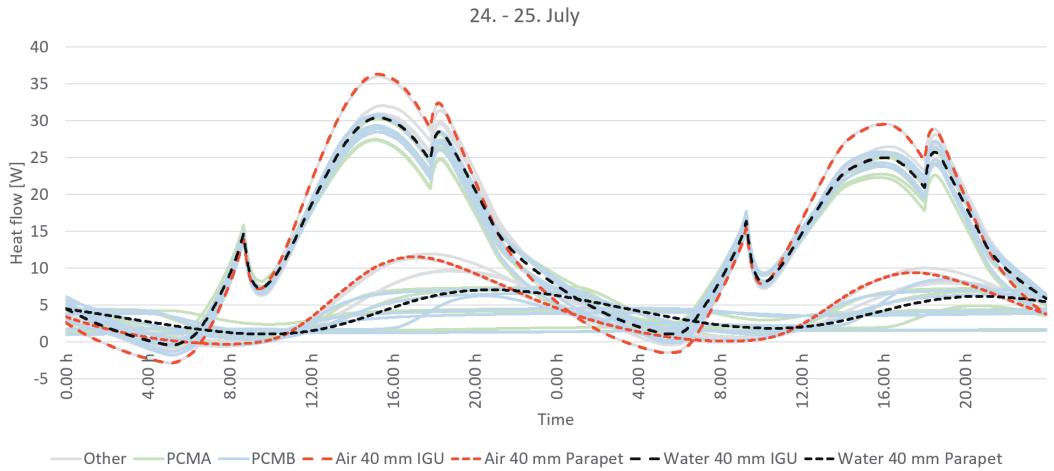

FIG. 8 Two-day period summer (24th – 25th July) heat flows

4.4 DEAD LOAD

The effect of the evaluated storage materials on the dead load of the SEBF is evaluated in comparison to a transparent parapet comprising a TGU with a typical glass mass (21 mm) of 57 kg m^{-2}.
The additional mass of 29 kg m^{-2} is taken into account for the supporting structure required for the storage tank (aluminium and insulation). Table 6 reports the dead load per unit area corresponding to the evaluated storage materials compared to a TGU.

TABLE 6 Storage materials dead load

MATERIAL	THICKNESS T [MM]	DENSITY ρ [KGM^{-3}]	MASS M [KGM^{-2}]	ADDITIONAL TANK MASS M_{TANK} [KGM^{-2}]	TOTAL MASS M_{TOT} [KGM^{-2}]	TO REFERENCE TGU (57 KGM^{-2}) [KGM^{-2}]
Water Gel	20	981	19.6	29	48.6	-8.4
	40	981	39.2	29	68.2	+11.2
Concrete	20	2400	48.0	29	77	+20
	40	2400	96.0	29	125	+68
PCM A	20	1525	30.5	29	59.5	+2.5
	40	1525	61	29	90	+33
PCM B	20	825	16.5	29	45.5	-11.5
	40	825	33.0	29	62	+5

5 CONCLUSIONS

As expected, with increasing thermal mass the tank surface temperature and therefore the overheating risk decrease. The tested high density PCM (PCM_A) limited the maximum temperatures on the storage tank, indicating the potential to limit the risk of overheating and thermal stress on façade components. Concrete and PCM_B had adverse effects. With all evaluated storage materials, surface temperatures covered a wide range from approximately 0°C to 70°C. Under such extreme fluctuations, the beneficial effects of the latent heat storage capacity of PCMs are not fully leveraged due to its low sensitivity. It has to be noted that some PCMs might become in stable at the high temperatures that can occur within a non-ventilated DSF, e.g. up to 76.4°C in the studied configurations.

The differences in overserved effects on seasonal and short-term energy balances by the tested storage materials were low. This holds true even with significantly different sensitive and latent heat storage capacities. This can be explained by effects of the thermal effusivity *b*, which is a measure of a material's ability to exchange and store thermal energy. Regarding the formula of thermal effusivity , a high influence of thermal conductivity appears. Compared to water gel, concrete, for example, has a 42% lower volumetric heat capacity (ρ*c), but almost twice its thermal effusivity. Consequently, concrete has a lower heat capacity but higher exploitation. For PCM_A and PCM_B, effusivity differs by a factor of approximately 2 due to their significantly different conductivities (see Table 2).

The particularly high dead load introduced into the SEBF by concrete as a storage material based on high density is problematic. This drove the motivation to rely on water, with its outstanding specific heat capacity, in the first implementations of the SEBF, although the integration of a liquid into a façade element was expected to be challenging. The dead load introduced by PCM_A due to its high density seems to be a problem at first glance. On further observation, Table 6 shows that 20 mm PCM_A is competitive against 40 mm water gel and, therefore, a good option to reduce weight and enhance thermal performance. The dead load of PCM_B in 40 mm is not problematic, but, due to its low thermal effusivity *b,* the volume is poorly exploited.

In this comparison, the PCM_A of 20 mm shows the highest potential for the application in terms of dead load and thermal effects. To sum up, the application of PCM as thermal storage material within non-ventilated DSFs is possible and justified. Nevertheless, the results of this research indicate that the main benefit of PCMs is not their effects on energy balance, but rather space and weight saving within the construction when compared to other storage materials. The choice should be carried out carefully and not just be based on sensitive and latent storage capacity. Density and conductivity (thermal effusivity) could decide between success and failure in a particular application. As mentioned, PCM_A seems promising for this application. However, further investigation on the right combination of its properties (λ, ρ, c_{sens}, c_{lat}) for a DSF storage application could further improve thermal and structural aspects.

For future development of the SEBF or similar elements, two conclusions are made: a) PCM could enhance thermal performance, but non-PCM materials could also contribute to improved energy balance; and b) the choice of a suitable PCM needs an in-depth evaluation to find the right material. Furthermore, besides the criteria in this work, other criteria as processability, availability, durability, price and so on should be considered.

Acknowledgements

The authors gratefully acknowledge the funding provided by the Swiss National Science Foundation (SNF), Grant No. IZCNZ0-174562).

References

Balocco, C. (2002). A simple model to study ventilated façades energy performance. *Energy and Buildings, 34*, pp. 469-475. https://doi.org/10.1016/S0378-7788(01)00130-X

Biswas, D. (2016). Nano-based phase change materials for building energy efficiency*. *Start-Up Creation*, pp. 183-211. https://doi.org/10.1016/B978-0-08-100546-0.00009-1

Halimov, A., Lauster, M., & Müller, D. (2019). Validation and integration of a latent heat storage model into building envelopes of a high-order building model for Modelica library AixLib. *Energy and Buildings, 202,* p. 109336. https://doi.org/10.1016/j.enbuild.2019.109336.

Hu, Z., He, W., Ji, J., & Zhang, S. (2017). A review on the application of Trombe wall system in buildings. *Renewable and Sustainable Energy Reviews,* 70, pp. 976-987. https://doi.org/10.1016/j.rser.2016.12.003

ISO 15099. (2003). *Thermal performance of windows, doors and shading devices - detailed calculations.* Geneva: ISO copyright office.

Lohmann, V., & Santos, P. (2020). Trombe wall thermal behaviour and energy efficiency of a light steel frame compartment: Experimental and numerical assessments. *Energies,* 13, p. 2744. https://www.mdpi.com/1996-1073/13/11/2744

Manz, H., & Frank, T. (2005). Thermal simulation of buildings with double-skin façades. *Energy and Buildings, 37*, pp. 1114-1121. https://doi.org/10.1016/j.enbuild.2005.06.014

Meteotest AG. (2018). *Meteonorm V7.3.3*. Bern Switzerland.

Quesada, G., Rousse, D., Dutil, Y., Badache, M., & Hallé, S. (2012). A comprehensive review of solar façades. Opaque solar façades. *Reviews, Renewable and Sustainable Energy,* 16, pp. 2820-2832. https://doi.org/10.1016/j.rser.2012.01.078

Vukadinović, A., Radosavljević, J., & Đorđević, A. (2020). Energy performance impact of using phase-change materials in thermal storage walls of detached residential buildings with a sunspace. *Solar Energy,* 206, pp. 228-244. https://doi.org/10.1016/j.solener.2020.06.008

Wetter, M. (2009). Modelica-based modelling and simulation to support research and development in building energy and control systems. *Journal of Building Performance Simulation,* pp. 143-161. https://doi.org/10.1080/19401490902818259

Wüest, T., & Luible A. (2019). Trombe curtain wall façade. *PowerSkin Conference Proceedings,* p. 313. Retrieved from https://books.bk.tudelft.nl/index.php/press/catalog/view/isbn_9789463661256/786/679-3

Wüest, T., & Luible, A. (2018). Solar Energy Balanced Façade. Façade 2018 - Adaptive! *Proceedings of the COST Action TU1403 Adaptive Façades Network Final Conference,* pp. 183-194.

Wüest, T., Grobe, L. O., & Luible, A. (2020). An Innovative Façade Element with Controlled Solar-Thermal Collector and Storage. *Sustainability,* 12, p. 5281. https://doi.org/10.3390/su12135281

Zhang, L., Hou, Y., Lui, Z., Du, J., Xu, L., Zhang, G., & Shi, L. (2020). Trombe wall for a residential building in Sichuan-Tibet alpine valley – A case study. *Renewable Energy,* 156, pp. 31-46. https://doi.org/10.1016/j.renene.2020.04.067

Holistic Design Explorations of Building Envelopes Supported by Machine Learning

Federico Bertagna[1*], Pierluigi D'Acunto[2], Patrick Ole Ohlbrock[1], Vahid Moosavi[3]

* Corresponding Author
1 ETH Zurich, Institute of Technology in Architecture, Chair of Structural Design, Zurich (Switzerland). bertagna@arch.ethz.ch
2 Technical University of Munich, Department of Architecture, Munich (Germany)
3 ETH Zurich, Institute of Technology in Architecture, Chair of Digital Architectonics, Zurich (Switzerland)

Abstract

The design of building envelopes requires a negotiation between qualitative and quantitative aspects belonging to different disciplines, such as architecture, structural design, and building physics. In contrast to hierarchical linear approaches in which various design aspects are considered and conceived sequentially, holistic frameworks allow such aspects to be taken into consideration simultaneously. However, these multi-disciplinary approaches often lead to the formulation of complex high-dimensional design spaces of solutions that are generally not easy to handle manually. Computational optimisation techniques may offer a solution to this problem; however, they mainly focus on quantitative aspects, not always guaranteeing the flexibility and interactive responsiveness designers need in the early design stage. The use of intuitive geometry-based generative tools, in combination with machine learning algorithms, is a way to overcome the issues that arise when dealing with multi-dimensional design spaces without necessarily replacing the designer with the machine. The presented research follows a human-centred design framework in which the machine assists the human designer in generating, evaluating, and clustering large sets of design options. Through a case study, this paper suggests ways of making use of interactive tools that do not overlook the performance criteria or personal preferences of the designer while preserving the simplicity and flexibility needed in the early design stage.

Keywords

holistic design approach, building envelopes, graphic statics, conceptual structural design, machine learning, simplicity and performance

10.7480/jfde.2021.1.5423

1 INTRODUCTION

1.1 BUILDING ENVELOPES AND THE ILL-DEFINED NATURE OF DESIGN

The building envelope is the main interface between the outdoors and the interior spaces of a building. The design of building envelopes is an excellent example of a multi-disciplinary process in which both qualitative and quantitative aspects must be addressed simultaneously. Conflicting parameters belonging to diverse fields – such as architecture, structural design, and building physics – strongly influence the performance and the outcome of the design, thus making the building envelope a dominant system among all the subsystems in a building (Lang, 2013). Because of the number of aspects involved, it is crucial to operate in a holistic way in order to have effective coordination between these aspects throughout the entire design process, and especially in the conceptual phase. Designers have to find suitable trade-offs based on a cognitively complex process of synthesis between objective and subjective evaluations. Digital tools offer adequate support to designers in dealing with such a complexity. However, their implementation within the design process is not always straightforward. Indeed, computers typically require a precise numerical formulation and univocal objectives (Harding & Olsen, 2018), elements that are both generally in conflict with the ill-defined nature of the design process itself (Rittel & Webber, 1973).

1.2 HOLISTIC DESIGN OF BUILDING ENVELOPES

When dealing with the design of building envelopes, designers have the opportunity to explore different levels of integration between disciplines (Rush, 1986) and investigate the influence of each aspect, starting from the early design stage. Definition of the architectural space, load-bearing capacity, and mitigation of external climate conditions are all aspects that can become an integral part of the building envelope. Despite the lack of a univocal definition (Rush, 1986), the term *holistic* – or *integrated* – *design* refers here to an approach based on mutual relationships between the different aspects involved in the design process.

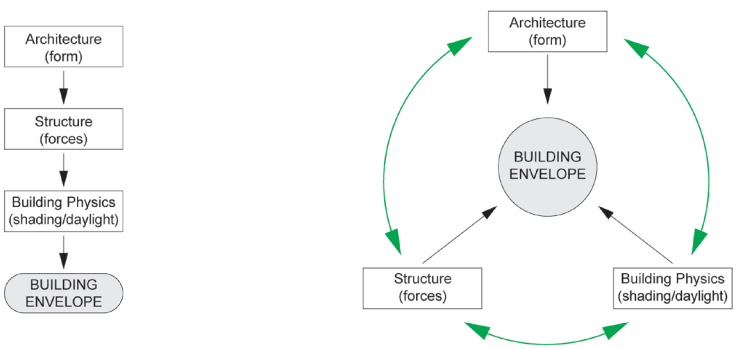

FIG. 1 Schematic workflow of a possible sequential linear approach (left) and a holistic approach (right) for the design of building envelopes

The present research is based on the assumption that the lack of such relationships often leads to a linear design process (Fig. 1, left) where the outcome is conceived just as a sum of the different parts (Saint, 2007), and which frequently entails the non-optimal use of material resources (Nervi,

1965). Conversely, the ability to operate through holistic approaches (Fig. 1, right) would foster an interdisciplinary discourse that, in addition to widening the range of possible design options, ultimately allows for more conscious use of the available resources in the final built constructions. This paper aims to investigate the latter strategy, regarding geometry as the mediator between architectural qualities, structural and sun-shading performance of the building envelope. Specifically, the research focuses on the interplay between the form of the building envelope, the inner forces within its load-bearing structure, and its performance in terms of solar protection and daylight modulation.

1.3 DIGITAL DESIGN FRAMEWORKS IN ARCHITECTURE AND ENGINEERING

A design framework can be generally characterised as a process that is composed of different individual operations (Brown, Jusiega, Mueller, 2020). Fig. 2 schematically shows three characteristic frameworks that represent an adaptation of the work of Oxman (2006) and Wortmann (2018). The main features of these three different frameworks will be briefly described in the following paragraph.

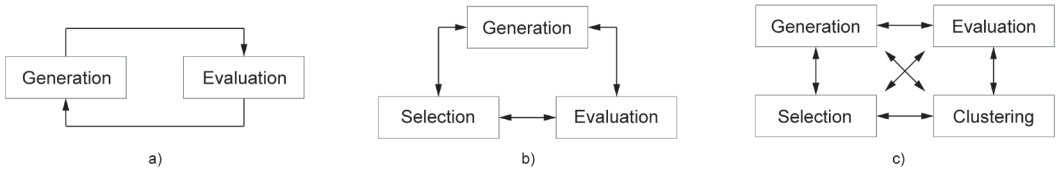

FIG. 2 Three design frameworks, with their different operations and relationships highlighted

One typical design approach is to first *generate* design options and then *evaluate* them with respect to a set of criteria. Designers can repeat this sequence, meaning that they can generate new options according to the results of the evaluation in a trial-and-error fashion (Fig. 2a). Thanks to the introduction of digital parametric tools, designers can now automatically generate a vast number of alternative options with minimal computational effort. However, this generation is often not directly guided by any performance criteria. Hence, such a problem-oriented approach is often time-consuming and not very efficient when dealing with multi-dimensional design spaces that involve a high number of design parameters. One possible way to address this challenge is to make use of optimisation techniques such as multi-objective optimisation (MOO). These techniques allow the *evaluation* step in searching for the best performing options to be simplified. More precisely, in the case of multi-objective optimisation, they support guided explorations of the design space, providing sub-optimal options (Brown & Mueller, 2017; Turrin, Von Buelow, & Stouffs, 2011; Yang Ren, Turrin, Sariyildiz, & Sun, 2018), from which the designer has to make a *selection* (Fig. 2b). Although very powerful in solving well-defined problems, optimisation techniques do not always offer the flexibility and the responsiveness necessary in early, ill-defined design stages. In this context, the major challenge is that all design objectives must be explicitly formulated before they are even known (Harding & Olsen, 2018), thus making the inclusion of qualitative aspects rather complex to achieve. The introduction of an intermediate *clustering* step enables the systematic integration of such qualitative considerations (Fig. 2c). For example, clustering algorithms based on machine learning can provide additional support by automatically organising large sets of diverse design options according to similarities pertaining to specific criteria (Wortmann & Schroepfer, 2019).

In combination with filtering functions, these algorithms offer the possibility to manage vast, multi-dimensional design options and eventually allow designers to negotiate quantitative and qualitative aspects according to personal preferences (Harding & Olsen, 2018; Fuhrimann, Moosavi, Ohlbrock, & D'Acunto, 2018; Saldana Ochoa, Ohlbrock, D'Acunto, & Moosavi, 2020). Following this approach, the designer is prevented from being overwhelmed (Brown & Mueller, 2017) by examining all the options individually and at the same time is not forced to focus exclusively on quantitative aspects. In line with the approach of Saldana Ochoa et al. (2020), the present research also implements a design process that includes *generation*, *evaluation*, *clustering*, and *selection* steps with the scope of considering both quantitative performance criteria and qualitative preferences of the designer while preserving the simplicity and flexibility needed in the early design stage.

1.4 OBJECTIVES AND CONTENT OF THE PAPER

This research aims to support an effective design workflow for the multi-disciplinary design of building envelopes, with a particular focus on the conceptual design phase. Thanks to its holistic nature, the proposed approach fosters new design possibilities and opens up new perspectives for the conscious use of the available resources. Following a geometry-based approach in which the form of the building envelope is simultaneously informed by aspects related to architecture, structure, and solar control, a set of user-defined performance criteria are taken into consideration without necessarily overlooking the qualitative aspects involved in the design.

The paper is structured as follows. Section 2 outlines the methods that form the basis of the research, introducing the applied geometry-based approach, the digital tools involved, and the metrics considered. Section 3 illustrates the advantages of the proposed framework through a case study in which several non-standard design options for a load-bearing façade are investigated and discussed. Finally, Section 4 outlines the conclusions and presents an outlook on future work.

2 METHODOLOGY

2.1 GEOMETRY-BASED DESIGN APPROACH

Geometry plays a crucial role in the generation of architectural space. This dependency from geometry persists in other fields, thus making geometry a common ground where aspects belonging to diverse fields meet. For example, in structural design, geometry plays a key role in defining the overall behaviour of a structure. Equilibrium-based methods such as graphic statics (Culmann, 1866; Maxwell, 1864; Cremona, 1872) and their contemporary digital implementations have proved to be powerful tools for the generation of structures (Van Mele, Rippmann, Lachauer, & Block, 2012; Rippmann, Lachauer, & Block, 2012; Beghini, Carrion, Beghini, Mazurek, & Baker, 2014; D'Acunto et al., 2019; Konstantatou, D'Acunto, & McRobie, 2019; Ohlbrock & D'Acunto, 2020). Unlike analytical methods, which are generally implemented through quantitative numerical approaches, geometry-based methods provide significant support since the conceptual stages of the design, when a visual understanding of forces is essential in order to generate creative design options (Schwartz, 2012; Kotnik & D'Acunto, 2013). Geometry has a relevant role also in the phase of evaluation of given design options. Digital tools for structural and energy analysis can now provide very accurate calculations on high resolution models. However, this often comes at the price of long computation time, and

it requires a consistent effort for the creation of the models. Since such accuracy usually is not needed in the early stage of the design, material-independent geometry-based approaches represent a suitable simplification for conceptual design tasks and are therefore the base for the present research. Detailed models that take into account material properties can be then included in the design process at a later stage.

2.2 TOOLS, PARAMETERS AND METRICS USED IN THE DESIGN PROCESS

Fig. 3 gives an overview of the various tools that are part of the proposed design framework for the conceptual design of building envelopes. Drawing from the approach presented by Saldana Ochoa et al. (2020), the proposed framework consists of four main steps: *generation*, *evaluation*, *clustering*, and *selection*. The whole framework is developed using the CAD platform Rhinoceros (www.rhino3d.com, accessed 20/11/2020) and the Grasshopper visual scripting environment (www.grasshopper3d.com, accessed 20/11/2020).

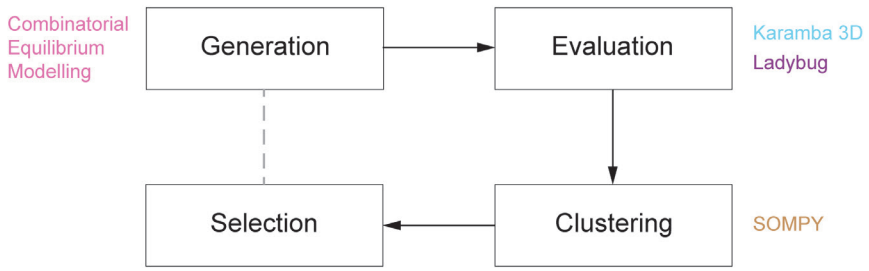

FIG. 3 Different tools integrated into the proposed framework for the conceptual design of building envelopes

The *generation* of design options is addressed through the Combinatorial Equilibrium Modelling (CEM) (Ohlbrock & D'Acunto, 2020). The CEM is a digital form-finding tool grounded in vector-based 3d graphic statics (D'Acunto et al., 2019), and it is used in this work to quickly generate a broad set of form diagrams in static equilibrium as pin-jointed frameworks that represent the structures of load-bearing building envelopes. Within the CEM, the edges of the form diagrams are subdivided into two distinct categories: the *trail edges* that connect each node with a (topologically) direct load transfer to the closest support; the *deviation edges* that connect nodes on different trail edges. Moreover, the user can directly assign a set of metric values to the edges, and specifically the *trail lengths* – i.e. the lengths of the trail edges – and the *deviation force magnitudes* – i.e. the force magnitudes of the deviation edges (Ohlbrock & D'Acunto, 2020). After the definition of the topology of the structure and the dominant load case, which in this case are kept constant, the CEM is able to generate different form diagrams as alternative *design options*. This step is performed considering various user-defined combinations of tension and compression forces in the edges of the form diagrams and metric values assignments for the *trail lengths* and the *deviation force magnitudes*.

Interpreting the form diagrams generated via the CEM as framed structures, various additional performance metrics are then assessed (*evaluation)* for each design option. The Finite Element Analysis (FEA) tool Karamba3D (Preisinger, 2013) is used to evaluate the linear-elastic response of the framed structures under lateral loads in terms of axial and bending deformation energies. The evaluation of environmental criteria such as solar radiation and daylight availability is performed using Ladybug Tools (Roudsari, Pak, & Smith, 2013).

Table 1 shows all the parameters and metrics that are used to describe each design option (form diagram and related framed structure). Note that Load Case 1 [LC1] refers to the vertical loads considered in the generation of the form diagram and Load Case 2 [LC2] to additional unitary horizontal forces taken into account in the FEA. For each generated design option, its geometric characteristics and related performance values, evaluated using the parameters and metrics of Table 1, are recorded into an indexed multi-dimensional vector $D_k = \{d_{k,1},..., d_{k,n}\}$. The latter is stored in a dataset, which constitutes a numerical description of the *design space*.

TABLE 1 List of parameters and metrics used to characterize each design option

SOURCE	PARAMETER/METRIC	LABEL	DESCRIPTION	UNITS
CEM	node position	posXY	position of the nodes (x_i, y_i) in the form diagram	[m]
	edge (trail/deviation) length	edgeLen	length of trail and deviation edges in the form diagram	[m]
	edge (trail/deviation) magnitude	edgeMag	magnitude of axial forces within trail and deviation edges in the form diagram	[kN]
	edge load path [LC1]	edgeLP	product of the length l_i of each edge of the form diagram by the axial force f_i acting in it	[kNm]
	total load path [LC1]	totLP	sum of the products of the length l_i of each edge of the form diagram by the absolute value of the axial force f_i acting in it	[kNm]
	max/min force [LC1]	forMax, forMin	maximum and minimum axial forces within the edges in the form diagram	[kN]
Karamba3D	total mass	totMass	total mass of the structural members of the framed structure	[kg]
	axial deformation energy [LC2]	defAxial	sum of the products of axial forces of the framed structure by the corresponding displacements parallel to their direction	[Nm]
	bending deformation energy [LC2]	defBend	sum of the products of bending forces of the framed structure by the corresponding displacements parallel to their direction	[Nm]
Ladybug	solar radiation reduction	SRR	reduction in percentage of the total amount of solar radiation on a test point without shading elements (SR_i) and with shading elements (SR_s)	[%]
	daylight factor	DF	ratio between the illuminance at an indoor test point (E) and the illuminance at an outdoor test point (E_0)	[%]

Hard quantitative filtering criteria can be then implemented to eliminate the relatively worst-performing sub-set of the design space. After this filtering process, Self-Organizing Maps (Kohonen, 1982) are used for *clustering* the design space. Self-Organising Maps (SOMs) can be regarded as a specific class of unsupervised artificial neural network, which allows for data dimensionality reduction without the loss of non-linear associations between the data (Harding, 2016). Based on user-defined clustering criteria, the SOM algorithm maps the data from a high-dimensional space

onto a lower-dimensional one, without losing the topological features of the high-dimensional space. That is, the design options are clustered in the low-dimensional space based on the distance of their corresponding data points in the high-dimensional space. In this way, it is possible to conveniently represent a multi-dimensional design space onto a 2D map, in which each node N_j (x_{j1}, x_{j2}) of the map has an associated multi-dimensional vector $W_j = \{w_{j,1},..., w_{j,n}\}$ or Best Matching Unit (BMU). In fact, each node of the map contains a cluster of design options that are similar with respect to the defined clustering criteria. The SOM thus provides the designer with a quick overview of the design space. The algorithm used in this work is implemented within the Python environment using SOMPY (Moosavi, 2014).

Eventually, in the *selection* step of the design process, the designer can easily navigate within the SOM and select the preferred design options considering both quantitative and qualitative criteria. If necessary, design options can be filtered out according to quantitative criteria in order to reduce the size of the design space further.

3 CASE STUDY

This section outlines an application of the proposed framework for the design of load-bearing and shading façades based on the *FAU Building* designed in 1964 by the Italian architect Enrico Tedeschi (1910-1978) for the campus of the Architecture Faculty of Mendoza, Argentina (Fig. 4).

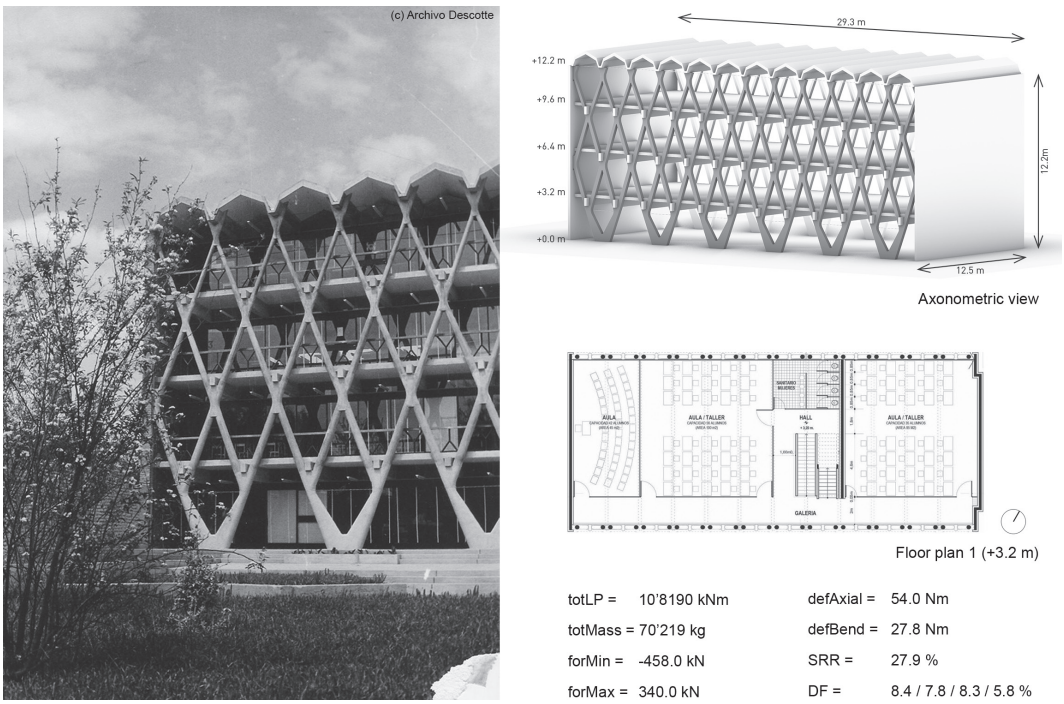

FIG. 4 FAU Building (1964), arch. Enrico Tedeschi, Mendoza (Argentina)

This building was chosen as a case study as its façades are not only load-bearing, but they also provide solar protection to the glazed surfaces and create a unique architectural motif for the building. It is, therefore, a relevant example of a holistic design approach, in which aspects related to architecture, structure, and solar control are considered at the same time. The façades on the long side of the FAU Building are planar diagrids made of reinforced concrete elements with a hollow circular cross-section that support a series of post-tensioned concrete beams spanning 12.5 metres across the façades (Codina, 2013). Thanks to these reticular façades, the architect could achieve column-free spaces and solve the question of horizontal stability at the same time, a peculiar feature considering the high seismicity of the zone. A critical aspect of the design was the control of natural lighting. In this case, the objective of the architect was to obtain diffuse lateral lighting, avoiding glare and overheating issues due to direct solar radiation on the glazed surfaces.

3.1 GENERATION AND EVALUATION OF THE DESIGN OPTIONS

Taking the FAU Building as a reference, various alternative design options for its façade were explored following the proposed design framework, based on the same design objectives that led to the realisation of the FAU Building.

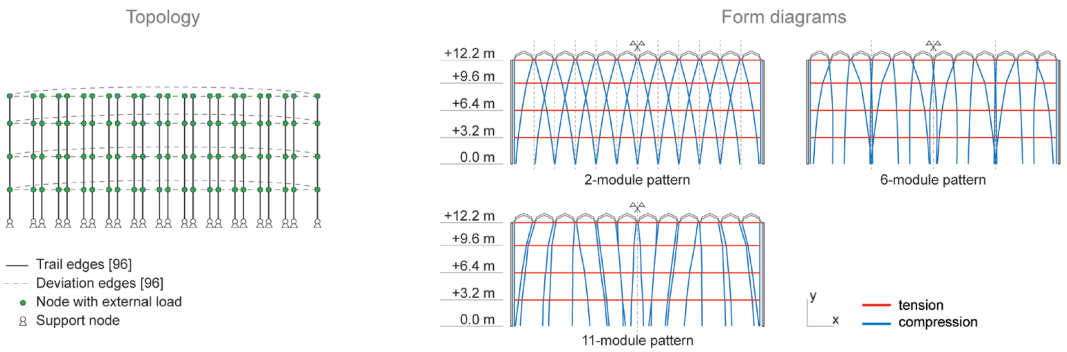

FIG. 5 Generation of various form diagrams (right) via the CEM. The topology (left), the floor heights and the load-case are kept constant, and only the distribution of deviation force magnitudes (devMag) is varied

Fig. 5 (left) shows the topology of the structure that was used as a base for the entire generative process via the CEM. The topology consists of 120 vertices, which are connected through 96 trail edges and 96 deviation edges. The 96 values of the deviation force magnitudes (*devMag*) were randomly generated following linear, parabolic, and sinusoidal distributions. These distinct force distributions were then applied to groups of two, six, or eleven neighbouring edges, keeping the central axis of the form diagram as an axis of symmetry. The values of the trail lengths (*trailLen*) were controlled by the given floor heights and the necessity to ensure that all the nodes of the form diagram belonging to the same floor were horizontally aligned. External forces [LC1] were applied to the nodes of the form diagram according to their corresponding tributary area and assuming a 10 kN/m^2 distributed load on the floor slabs (5 kN/m^2 dead load + 5 kN/m^2 live load). Fig. 5 (right) shows three exemplary form diagrams that resulted from this generative set-up in which only the 96 deviation force magnitudes (*devMag*) were automatically varied (Fig. 6a).

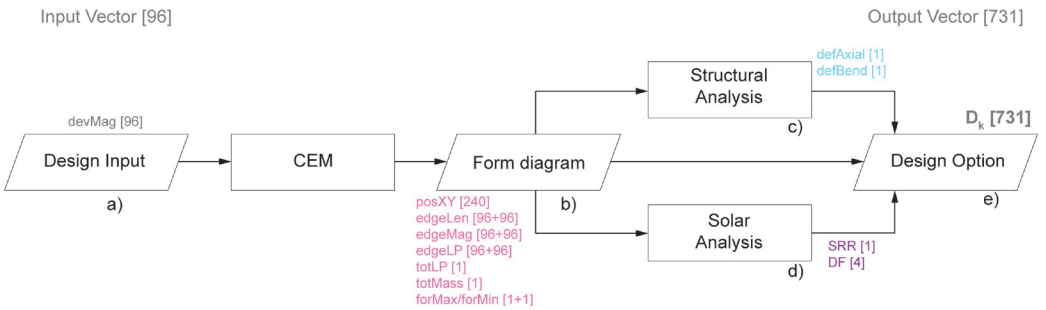

FIG. 6 Flowchart of the generation and evaluation steps showing the parameters involved, their labels (Table 1) and the number of items for each parameter (in square brackets)

Each of the form diagrams was subsequently interpreted as a framed structure and then analysed in relation to structural (Fig. 6b, c) and sun-shading performance (Fig. 6d) using the CEM, Karamba, and Ladybug. These analyses were carried out in order to evaluate the quantitative metrics introduced in Table 1. In particular, the total mass *totMass* of each design option was calculated considering hollow circular cross-sections in reinforced concrete (C20/25) for the façade elements, dimensioned according to the axial forces they had to withstand. The evaluation of the axial and bending deformation energies – *defAxial* and *defBend*, respectively – was performed with respect to a load case [LC2] where unitary horizontal forces were applied to the framed structure in addition to the vertical forces of load case 1 [LC1]. The solar radiation reduction *SRR* was calculated on a vertical test grid corresponding to the glazed surface of the façade, with a resolution of 0.5 x 0.5 m and an analysis period of one year. Four daylight factors *DF(0-3)* were evaluated considering four horizontal test grids, with a resolution of 1.0 m by 1.0 m, located at the four floors, at a height of 0.9 m above the floor planes. Each generated design option (form diagram and corresponding framed structure) and its performance was then numerically described using a 731-dimensional indexed vector $D_k = \{d_{k,1}, ..., d_{k,731}\}$ (96 input and 635 output) (Fig. 6e). Using a 10-core 2.5 GHz CPU, the generation and evaluation of each design option required 15 seconds, on average. By taking advantage of parallel computing, it was possible to generate and evaluate 20'144 design options in about 20 hours.

3.2 QUANTITATIVE FILTERING AND CLUSTERING OF THE DESIGN OPTIONS

In order to describe the peculiarities of the design options synthetically, the higher-order statistics (mean, variance, skewness, kurtosis) (Farid, 2002) of the following parameters were additionally calculated: position of the nodes *posXY*, edge length *edgeLen*, edge force magnitude *edgeMag*, edge load path *edgeLP*. Before proceeding with the clustering of the generated design options, hard filters were introduced to eliminate those design options that did not meet specific performance levels. The filtering criteria and their sequence of application can be defined by the user based on the task at hand. Within the analysed case study, the following filters were applied: total load path *totLP* (90^{th} percentile, 18'129 options kept), maximum edge force *forMax* (90^{th} percentile, 15'944 options kept), minimum edge force *forMin* (90^{th} percentile, 14'349 options kept), and solar radiation reduction *SRR* (90^{th} percentile, 12'758 options kept). That is, from the initial set of 20'144 design options, 12'758 were kept after the filtering process.

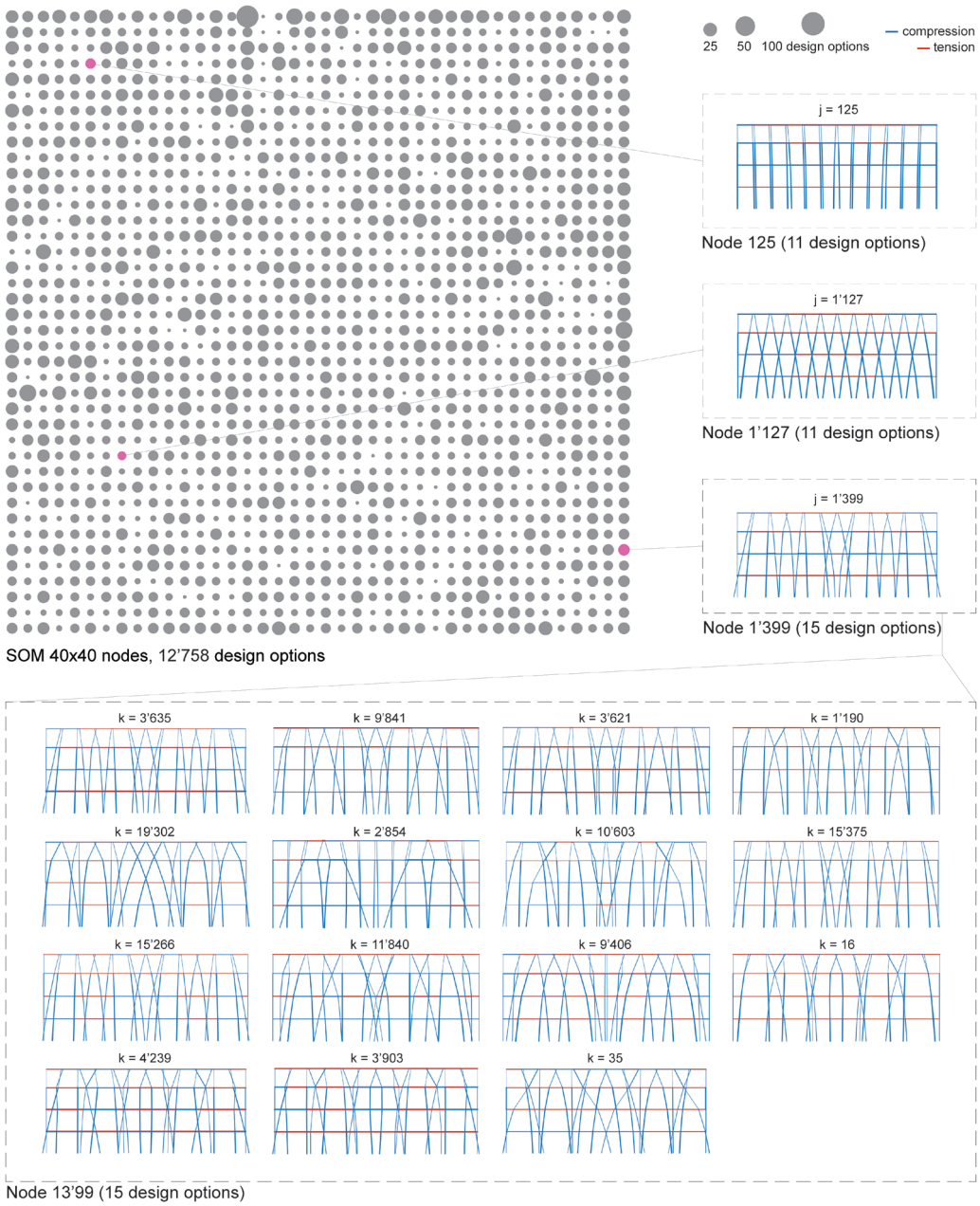

FIG. 7 Using the SOM algorithm, the generated and filtered design options (12'758) are clustered onto a 40x40 map (top left). Each node Nj of the map (grey circle) contains several design options, the size of the circle being proportional to the number of design options contained in that node. Representative design options for three nodes of the grid (N125, N1127, N1399) are shown (top right). The designer can easily navigate within the design space and select any of the nodes to explore further the entire set of design options contained therein. For example, N1399 (bottom) includes 15 similar design options, each one identified with its corresponding index k and the associated 731-dimensional vector Dk.

After the filtering process, the remaining design options were clustered onto a 40 x 40 map using the SOM algorithm (Fig. 7). The clustering was performed taking into account the following parameters: total mass *totMass*, maximum edge force *forMax*, minimum edge force *forMin*, axial deformation energy *defAxial*, bending energy *defBend*, solar radiation reduction *SRR*, and higher order statistics of edge load path *edgeLP*, position of nodes *posXY*, and daylight factors per floor *DF*.

3.3 SELECTION OF THE FINAL PREFERRED OPTIONS

Thanks to the SOM, the designer can navigate a complex multi-dimensional design space, having a clear overview of the relationship between the different design options with respect to qualitative and quantitative criteria. If necessary, the designer can also re-iterate the process investigating a different clustering strategy, introducing new filters for the quantitative evaluation, or generating a new pool of design options informed by the outcome of the first iteration. Within the analysed case study, additional filters were applied to the SOM (Fig. 7) to narrow down the design space further and proceed with the selection of three final design options. Considering the distribution maps of Fig. 8, in the first case, only those design options whose total mass *totMass* was less than the 5th percentile and the mean value of daylight factor *DF_mean* was greater than the 90th percentile were considered. These filters accounted for 14 nodes in the SOM (Fig. 9). Out of this subset, node N_{61} (j = 61), containing 20 design options, was chosen. Among these design options, the one with index k = 16'562 was eventually selected as *Option A*.

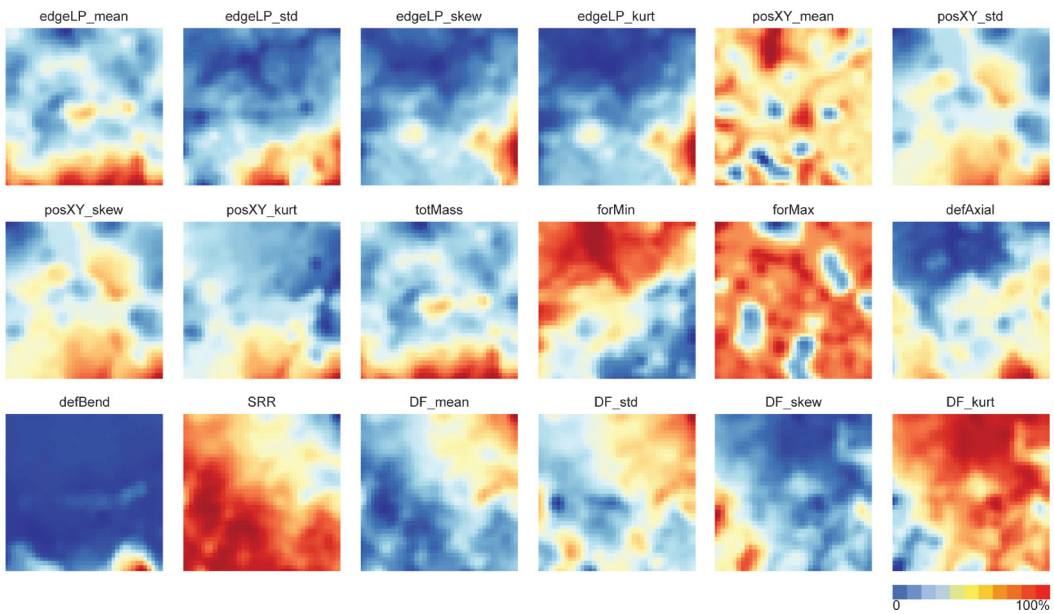

FIG. 8 Distribution maps of the 18 parameters used for the SOM. Values are normalised in the range 0-100%.

Following a similar procedure, *Option B* (j = 969; k = 19'117) was selected among the design options with a standard deviation value of daylight factor *DF_std* lower than the 10th percentile and maximum force magnitude *forMax* lower than the 5th percentile. Finally, *Option C* (j = 1'213; k = 1'041) was selected among the design options with a solar radiation reduction *SRR* higher than the 95th percentile and a standard deviation value of the position of the nodes *posXY* higher than the 70th percentile.

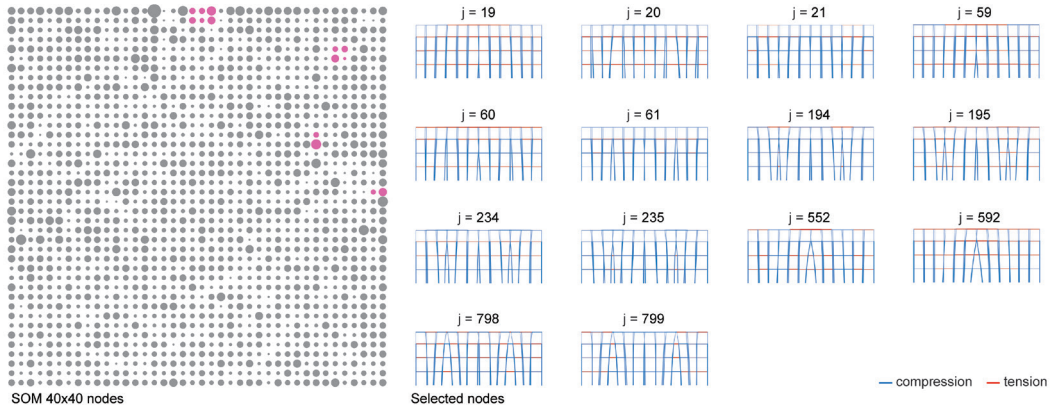

FIG. 9 Selection procedure for Option A (j = 61; k = 16'562). Representative design options (right) for the 14 nodes retained from the 40 x 40 SOM (left) after the application of hard filters on the total mass totMass (5th percentile) and the mean value of daylight factor DF_mean (90th percentile).

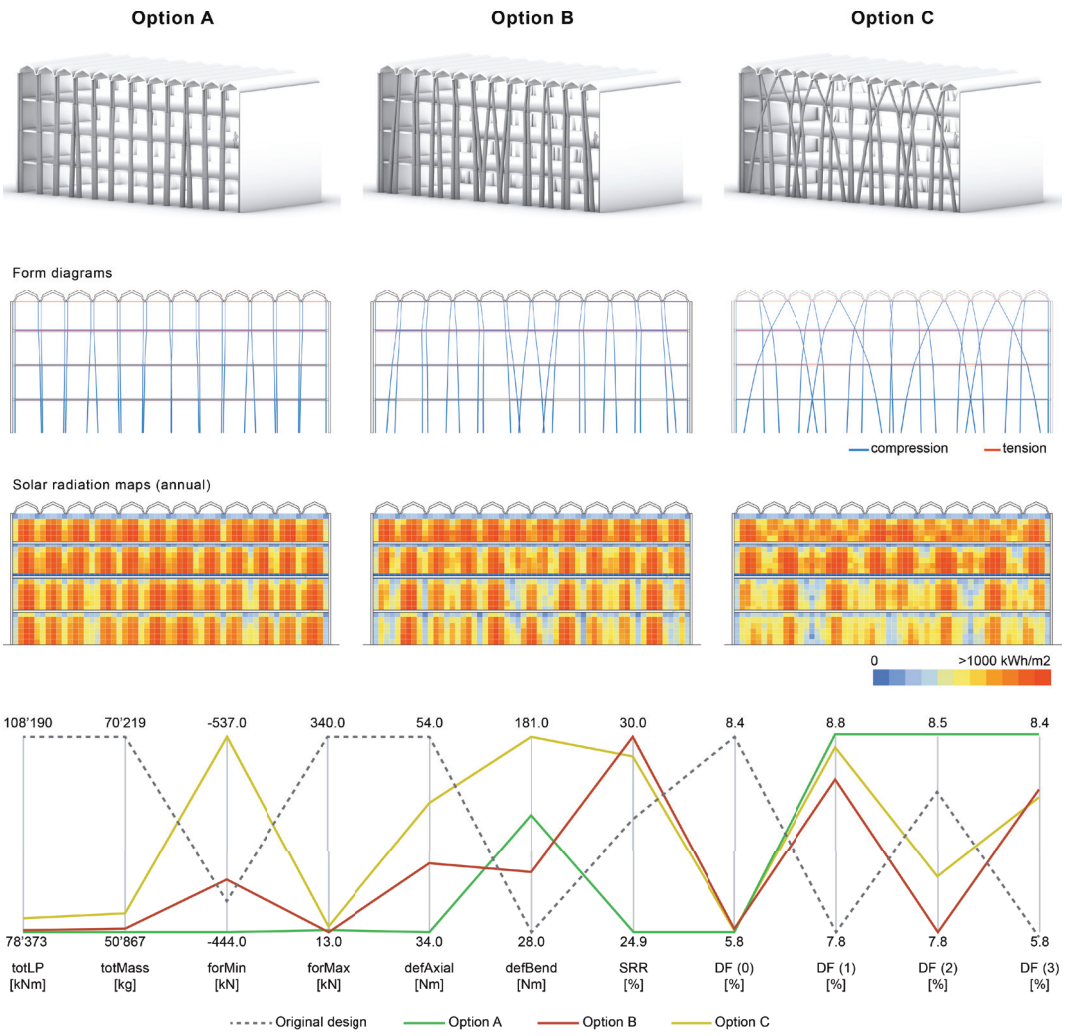

FIG. 10 Axonometric views, structural diagrams, and solar radiation maps for 3 options extracted from the dataset

3.4 DISCUSSION

The parallel coordinates plot in Fig. 10 shows the structural and sun-shading performance metrics of the three selected design options in comparison to the original design of the FAU Building by Enrico Tedeschi. Although illustrating very diverse geometries and patterns, all the selected design options are characterised by similar values for the total load path *totLP* and its correlated total mass *totMass* (Fig. 10), which are lower than those of the original design. These differences can be mainly explained with the high maximum axial forces *forMax* that is needed to redirect the accumulated vertical forces at the height of the first floor in the original design. Since the original design defines an overall triangulated structure, the bending deformation energy *defBend* is smaller than the one calculated for the selected design options, which strongly rely on the bending capacity for resisting lateral loads. Among the selected design options, *Option B* and *Option C* show a better performance for the solar radiation reduction *SRR* in comparison to *Option A* and the original design. As expected, when it comes to the daylight factor on different floors, the opposite can be observed.

The presented design exploration considered the FAU building as a reference case study. Several global and local geometric parameters used for the generation of the façades were intentionally made compliant with the original design. Indeed, introducing additional geometric parameters such as, for example, three-dimensionality of the façade geometries, variable overhang of the floor slabs and roof, and adjustable cross-section geometries of the façade elements, could potentially widen the design space and possibly lead to the generation of entirely new design options. For instance, the cross-sections of the façade elements could be materialised into different shapes, thus introducing further local variations among the design options. Fig. 11 shows a possible application of such a principle, taking *Option C* as a reference. The geometry of the façades in *Option C1* and *Option C2* are based on the form diagram of *Option C,* but their edges are materialised into façade elements with rectangular cross-sections instead of the circular hollow cross-sections of the original design. While neglecting local instability problems, the façade elements of *Option C1* and *Option C2* are dimensioned to withstand the same axial forces of *Option C* – i.e. same cross-section areas. As a result, these three options have the same values for total load path *totLP*, total mass *totMass,* and maximum and minimum internal forces *forMax/forMin*. In particular, the façade elements in *Option C1* are thin walls perpendicular to the plane of the façade. While its width is kept constant, its thickness is adjusted proportionally to the axial force it has to resist. The cross-section of the façade elements in *Option C2* follows a similar rule, although in this case, the elements are parallel to the plane of the façade. The parallel coordinates plot in Fig. 11 shows that varying these local parameters has an impact not only on the visual appearance of the design options but also on their sun-shading performances in terms of solar radiation reduction *SRR* and daylight factor *DF*. This parallel coordinates plot further visualises the relationships between the different considered metrics and informs the negotiation process that is, in any case, necessary in multi-disciplinary design.

4 CONCLUSIONS AND FUTURE WORK

Despite allowing full control over the design process, manual design explorations often show severe limitations due to the restricted evaluation capabilities of the designer when dealing with vast, multi-dimensional design spaces. With the aim to couple the advantages of traditional interactive manual explorations with the power of contemporary computational approaches, this paper presented a holistic framework for the conceptual design of building envelopes that integrates aspects related to architecture, structural design, and building physics.

The proposed framework relies on a geometry-based tool (Combinatorial Equilibrium Modelling - CEM) for the generation of design options as structures in static equilibrium, tools for the evaluation of the structural (Karamba3d) and solar (Ladybug) performances of these options, and machine learning (Self-Organising Map - SOM) for clustering the design space. These tools facilitate the designer in the selection process, which is informed by sets of quantitative performance criteria and takes into consideration the designer's subjective preferences at the same time. The machine eventually becomes a precious support through which the designer can easily generate, evaluate, cluster, and finally select one or more suitable design options.

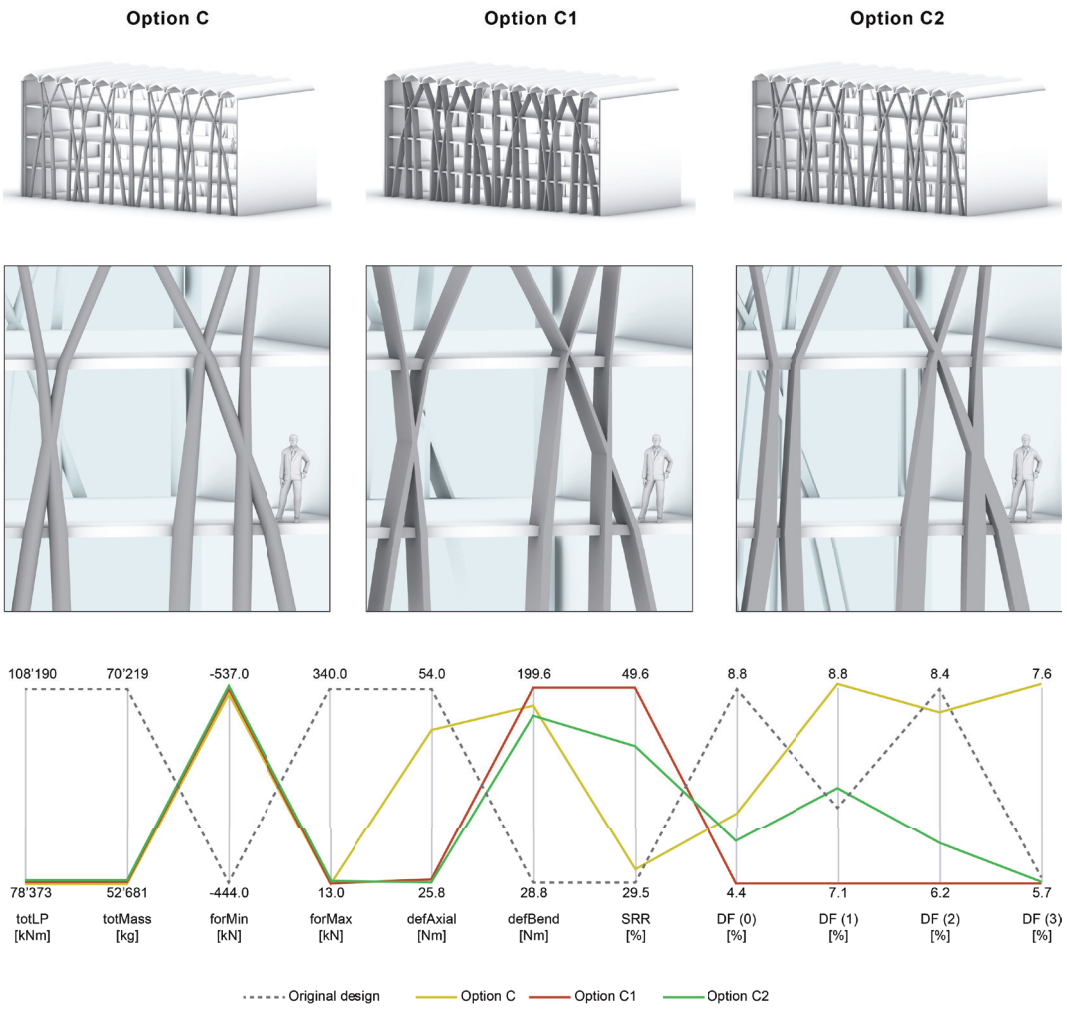

FIG. 11 Three different materialisations of the same form diagram. While keeping constant values for the cross-section areas, rectangular cross-sections with different proportions (Option C1 and C2) are compared to the circular hollow sections of Option C.

The illustrated case study demonstrated the application of the proposed design framework to the design of alternative solutions for an existing building façade. This example was developed by running the different steps of the proposed design process in a sequence. Future work will explore the opportunity of using the set of design options selected by the designer to inform the re-generation of new design options, potentially through supervised machine learning algorithms

for classification (Saldana Ochoa et al., 2020). Besides, in the proposed generative step carried out using the CEM, the topology of the structure was kept constant. A computational implementation that is topologically flexible would allow the number of possible design options to be significantly enhanced, thus fostering the diversity and openness needed in the early design stage without overlooking performance criteria or personal preferences of the designer. Future developments of this research will thus investigate possibilities to compare and cluster design options with different topologies. Moreover, further applications and extensions of the design framework to different case studies and building typologies will be investigated as well as the combination with other relevant design aspects.

When dealing with building energy simulations, long computation times may represent a significant limitation for workflows that benefit from the interactivity in the early design phase. In the presented case study, this issue was solved by reducing the number of aspects evaluated and by keeping the overall resolution of the simulation on a moderate level. A possible approach to reduce computation time could be the implementation of surrogate modelling, which has already been applied to building energy simulation in the early design stage in several research projects (Ritter, Schubert, Geyer, Borrmann, & Petzold,., 2014; Wortmann, Costa, Nannicini, & Schroepfer, 2015). Alternatively, geometry-based solar design tools (Olgyay & Olgyay, 1957; Lechner, 2014) – similarly to graphic statics in the field of structural design – could represent a possible alternative research direction. Interpreting sun rays as vectors that interact with the building envelope, simplified solar radiation and daylight availability studies could be embedded into a fully geometrical generative tool that possibly allows for real-time design explorations. The designer would mostly interact with a limited number of parameters, such as the angle and intensity of sun rays and the geometry of the building itself. Indeed, being able to integrate environmental parameters as early as the generative phase of the design process would greatly enhance the variability of the design space.

Acknowledgements

The authors would like to thank the student Roberto Gharib (ETH Zurich – DBAUG), whose master's thesis has provided useful insights for the development of the present research.

References

Beghini, L.L., Carrion, J., Beghini, A., Mazurek, A., & Baker, W.F. (2014). Structural optimisation using graphic statics. *Structural and Multidisciplinary Optimization*, 49(3): pp.351–366.

Brown, N., & Mueller, C. (2017). Designing with data: Moving beyond the design space catalog. In T. Nagakura, S. Tibbits, & C. Mueller (Eds.). *ACADIA 2017 Disciplines and Disruption: Proceedings of the 37th Annual Conference for the Association for Computer Aided Design in Architecture* pp. 154–163.

Brown, N., Jusiega, V., & Mueller, C. (2020). Implementing data-driven parametric building design with a flexible toolbox. *Automation in Construction*, 118: pp.1-16.

Codina, L. (2013). *La estructura como instrumento de una idea [The structure as a tool for an idea].* Buenos Aires: 1:100 Ediciones

Cremona, L. (1872). *Le figure reciproche nella statica grafica [Reciprocal figures in graphic statics].* Milano: Tipografia Bernardoni.

Culmann, C. (1866). *Die Graphische Statik [Graphic statics].* Zurich: Von Meyer & Zeller.

D'Acunto, P., Jasienski, J. P., Ohlbrock, P. O., Fivet, C., Schwartz, J., & Zastavni, D. (2019). Vector-based 3D graphic statics. *International Journal of Solids and Structures*, 167, 58–70.

Farid, H. (2002). Detecting hidden messages using higher-order statistical models. In *Proceedings of the international conference on image processing*, Rochester, NY, 22–25 September 2002

Fuhrimann, L., Moosavi, V., Ohlbrock, P. O., & D'Acunto, P. (2018). *Data-Driven Design: Exploring new Structural Forms using Machine Learning and Graphic Statics.* Retrieved from http://arxiv.org/abs/1809.08660

Harding, J. (2016). Dimensionality reduction for parametric design exploration. In S. Adriaenssens, F. Gramazio, M. Kohler, A. Menges, & M. Pauly (Eds.), *AAG 2016,* pp.274–287.

Harding, J., & Brandt-Olsen, C. (2018). Biomorpher: Interactive evolution for parametric design. *International Journal of Architectural Computing*, 16(2), pp.144–163.

Kohonen, T. (1982). Self-organised formation of topologically correct feature maps. *Biological Cybernetics*; 43(1): pp.59–69

Konstantatou, M., D'Acunto, P., & McRobie, A. (2018). Polarities in structural analysis and design: n-dimensional graphic statics and structural transformations, *International Journal of Solids and Structures*, 152–153, pp. 272-293.

Kotnik, T. & D'Acunto, P. (2013). Operative Diagramatology: Structural Folding for Architectural Design, in C. Gengnagel, A. Kilian, J. Nembrini, F. Scheurer (Eds.). *Rethinking Prototyping: Proceedings of Design Modelling Symposium 2013*, Universität der Künste Berlin, pp. 193–203.

Lang, W. (2013). Is it all "just" a façade? *Detail - Building Skins,* 29–45.

Lechner, N. (2014). *Heating, Cooling, Lighting: Sustainable Design Methods for Architects*. New Jersey: Wiley.

Maxwell, J.C. (1864). On reciprocal figures, frames and diagrams of forces. *Philosophical Magazine 27*, 250–261.

Moosavi, V. (2014). Computing With Contextual Numbers. *Journal of Machine Learning Research*. Retrieved from https://arxiv.org/abs/1408.0889

Nervi, P. L. (1956). *Structures*. New York: F. W. Dodge Corp.

Ohlbrock, P. O., & D'Acunto, P. (2020). A Computer-Aided Approach to Equilibrium Design Based on Graphic Statics and Combinatorial Variations. *CAD Computer Aided Design*, 121.

Olgyay, A., & Olgyay, V. (1957). Solar Control & Shading Devices. New Jersey: Princeton University Press.

Oxman, R. (2006). Theory and design in the first digital age. *Design Studies*; 27(3): 229–265.

Preisinger C. (2013). Linking Structure and Parametric Geometry. *Architectural Design*; 83(2): 110–113.

Rippmann, M., Lachauer, L., & Block, P. (2012). Interactive vault design. *International Journal of Space Structures*; 27(4), 219–230.

Rittel, H., & Webber, M. (1973). Dilemmas in a general theory of planning. *Policy Sciences*; 4: 155–169.

Ritter, F., Schubert, G., Geyer, P., Borrmann, A., & Petzold, F. (2014). Design decision support - Real-time energy simulation in the early design stages. *Proceedings of the 31st International Conference on Computing in Civil and Building Engineering, USA,* 2023–2031.

Roudsari, M.S., Pak, M., & Smith, A. (2013). Ladybug: a parametric environmental plugin for grasshopper to help designers create an environmentally-conscious design. *Proceedings of the 13th international IBPSA Conference, Chambéry, France, 3128–3135.*

Rush, R. D. (1986). *The building systems integration handbook.* New Jersey: Wiley.

Saint, A. (2007). *Architect and Engineer. A Study in Sibling and Rivalry*. New Haven: Yale University Press.

Saldana Ochoa, K., Ohlbrock, P. O., D'Acunto, P., & Moosavi, V. (2020). Beyond Typologies, Beyond Optimization. *International Journal of Architectural Computing*, 1-25.

Schwartz, J. (2012). Structural Theory and Structural Design. In Flury, A. (Ed.) *Cooperation*. Basel: Birkhäuser.

Turrin, M., Von Buelow, P., & Stouffs, R. (2011). Design explorations of performance driven geometry in architectural design using parametric modeling and genetic algorithms. *Advanced Engineering Informatics*. 25(4), 656-675.

Van Mele T, Rippmann M, Lachauer L, & Block P. (2012). Geometry-based understanding of structures. *Journal of the International Association for Shell and Spatial Structures*; 53(2): 285–95.

Wortmann, T. (2018). *Efficient, Visual , and Interactive Architectural Design Optimization with Model-based Methods* (Doctoral Dissertation). Singapore University of Technology and Design.

Wortmann, T., & Schroepfer, T. (2019). From optimisation to performance-informed design. *Simulation Series*, 51(8).

Wortmann, T., Costa, A., Nannicini, G., & Schroepfer, T. (2015). Advantages of surrogate models for architectural design optimisation. *Artificial Intelligence for Engineering Design, Analysis and Manufacturing: AIEDAM, 29(4),* 471–481.

Yang, D., Ren, S., Turrin, M., Sariyildiz, S., & Sun, Y. (2018). Multi-disciplinary and multi-objective optimisation problem re-formulation in computational design exploration. *Automation in Construction*, 92, 242–269.

Potential of Façade-Integrated PVT With Radiant Heating and Cooling Panel Supported by a Thermal Storage for Temperature Stability and Energy Efficiency

Mohannad Bayoumi

Faculty of Architecture and Planning, King Abdulaziz University, Saudi Arabia

Abstract

Hybrid photovoltaic/thermal (PVT) systems combine electric and thermal energy generation and provide noiseless operation and space-saving features. As the efficiency of photovoltaic (PV) panels increases at low surface temperatures, this paper suggests combining the PVT panel with a radiant cooling and heating panel in one system. A thermal storage tank fluidly connects the heat-exchanging pipes at the back of the PVT system and radiant panel. The upper portion of the tank feeds the radiant panel and the lower portion of the tank is connected to the PVT system. The proposed device is expected to function in connection with a heat pump that feeds the thermal storage. Using the dynamic thermal simulation software Polysun, the performance of the proposed façade-integrated device was investigated while considering the surface temperatures and energy production in the moderate climatic condition of the city of Munich. The results indicate a substantial impact on the efficiency of the PV module with an increase of up to 35% in the electricity production of the PV due to the lowered surface temperature. The obtained results contribute to façade-supported cooling/heating and electricity generation through the novel coupling and integration of PV, PVT, and radiant cooling elements.

Keywords

Photovoltaic/thermal systems, radiant cooling, building-integrated photovoltaic, façade, solar cooling

10.7480/jfde.2021.1.5442

1 INTRODUCTION

Façade-integrated energy generation essentially contributes to the increase in the energy efficiency of buildings. In such an unconventional local energy generation approach, remarkable savings are achieved through the reduced efforts and losses in the transportation and conversion processes. In building-integrated photovoltaics, photovoltaic (PV) cells absorb a significant portion of the irradiated energy. This results in a significant increase in the surface temperature of the PV panel. The increased cell temperature substantially reduces the overall module efficiency. The output performance of the PV decreases by 0.4-0.5% for each degree increase in the cell temperature (Natarajan, Mallick, Katz, & Weingaertner, 2011). This is calculated in comparison with the standard test conditions (STC), where 25°C and 1000 W/m^2 are set as the standard values of ambient temperature and solar irradiance (G), respectively. Furthermore, according to experiments, the STC parameters do not represent the real operating conditions of PV panels (Razak et al., 2016). In an investigation by Radziemska (2003), the increase in surface temperature led to a power deterioration of 0.65% per kelvin. Obviously, in hot climates, this effect is more severe owing to the relatively higher ambient temperatures.

Despite low ambient temperatures in moderate climates, the absorbed solar irradiance leads to remarkable losses as it also increases the cell temperature (Huld & Gracia Amillo, 2015). This effect is particularly noticeable in façade-integrated PV module, for example, a south-oriented vertical PV module in Europe. Another important factor that affects the module efficiency is wind velocity, which is associated with convective heat transport. Huld and Gracia Amillo (2015) claimed that despite the clear impact of this factor, ambient temperature and solar irradiance are still the two primary parameters that affect the efficiency. This is particularly true in the case of crystalline silicon-based cells. Obviously, the geographical location performs a role in the intensity of either factor and results in a fluctuation in module efficiency ranging from -15% to +5% (Huld & Gracia Amillo, 2015). Moreover, the surface cooling of the PV has an inverse effect and increases the electricity production efficacy (Pathak, Pearce, & Harrison, 2012). Therefore, associating cooling with façade-integrated energy provides the potential for a further increase in efficiency. This indicates a deviation from the fact that high cooling loads often occur during times of high solar irradiation.

PV cells can be cooled by attaching pipes that circulate a fluid at the back of the PV absorber. This combination of two systems is called hybrid PV/thermal (PVT) technology (Zhang, Zhao, Smith, Xu, & Yu, 2012). The fluid in the pipes absorbs the thermal energy from the heated surface and delivers it to another point for uses such as potable water heating. Depending on the design of the system, water is usually used as a refrigerant owing to its higher thermal capacity. Moreover, the generated thermal energy can also be used for other applications such as potable water, air, and room heating. Kern and Russell (1978) were the first to present this technology in 1978.

Basically, a PVT system includes the functions of both a PV panel and a solar collector. Besides the increased space efficiency, it offers lesser installations and more cost reductions. According to a study by Charalambous, Maidment, Kalogirou, and Yiakoumetti (2007), a PVT system can produce more energy per unit area than a pair of PV panels and a solar collector located next to each other. Generally, the generated heat in the PV surface that is absorbed by the fluid is of low quality for domestic hot water uses or room heating. Therefore, several PVT domestic hot water generation systems are equipped with auxiliary heaters connected to the heat exchanger at the top of the hot water storage tank to compensate for the thermal energy deficit (Aste, Del Pero, & Leonforte, 2012). Furthermore, heat can be used for cooling energy generation. Prieto, Knaack, Auer, and Klein (2017) discussed the potential of façade-integrated PVT systems for solar-assisted cooling based on the

principles of solar cooling addressed by Henning (Henning and International Energy Agency, 2004). However, these approaches are limited by the outlet temperature of the fluid that comes out of the PVT system, as significantly high temperatures in the range of 90-110 °C are often required for the operation of the absorption or adsorption chiller. This issue is beyond the scope of this paper.

Radiant cooling and heating systems have garnered significant interest owing to their potential to achieve high thermal comfort, low energy demand, noiseless operation, and space-saving features. In these systems, water pipes are attached to the back of a radiating panel. The circulating chilled water is delivered through the pipe and it cools down or heats up the panel, which eventually exchanges heat with other surfaces primarily through radiation or convection (Rhee & Kim, 2015; Stetiu, 1999). The radiating panels can be integrated into floors, ceilings, walls, or any room surface. However, the surface temperature of the panel must remain above the dewpoint temperature of the air in the room to avoid condensation on the surface. Several studies explored different methods to eliminate the risk of condensation, which often occurs in the cooling scenario (Bayoumi, 2018b; Hindrichs & Daniels, 2007; Hong, Yan, D'Oca, & Chen, 2017; Seo, Song, & Lee, 2014; Song & Kato, 2004; Vangtook & Chirarattananon, 2007; Zhang & Niu, 2003).

The potential of combining façade-integrated radiant cooling and the PVT system in one device was investigated (Bayoumi, 2018a). The cooling water is supplied by a chiller to the radiant panel; the return water is supplied to the PVT system and the return water of the PVT is supplied back to the chiller. The simulation results of this investigation concluded that in the selected warm climate, an increase of 35% in power conversion efficiency was achieved when compared to a conventional PV system. In another study, a detailed calculation of the heat transfer process was presented in association with thermal comfort simulations in several locations (Bayoumi, 2020). The results indicated a substantial impact of thermal comfort as well as energy generation efficiency. In both studies, the simulated façade device is attached to a heat pump or chiller that supplies the radiant cooling panel surface with cold water. Further, a pipe links the return of the radiant cooling surface with the supply of the PVT element. This helps to cool down the surface of the PVT element using relatively cool water that has already cooled the radiant cooling surface. Both studies were limited to the room cooling process, which recommends further exploration of the potential for developing such devices for both purposes, i.e., room cooling and heating.

The potential of a façade-integrated solar heater with thermal storage was discussed by Pugsley, Zacharopoulos, Mondol, & Smyth (2020). It primarily focused on the domestic use of warm water. The results indicate significant potential for increasing the efficiency of the heat generation process as well as the utilisation factor. This is primarily owing to the potential for overnight water storage. However, the potential for radiant heating for room climatisation was not considered in the proposed solution.

The present research suggests a combination of a façade-integrated PVT panel with a radiant cooling/heating panel and thermal storage located between both panels. The thermal storage is connected to a heat pump and supplies both panels with water. The analysis includes the impact of thermal storage on increasing the efficiency of the system through the reduced energy demand of the heat pump.

2 METHODS

The basic components of the proposed façade-integrated system are a PVT panel, 150 l thermal storage, radiant heating and cooling panel, and heat pump that can be attached to the system. The characteristics of the heat pump are outside the scope of this proposal. As illustrated in Fig. 1, while the PVT is located on the external side, the radiating surface faces the interior space and the thermal storage is located between both panels. The inlet and outlet points that connect the system with the heat pump are located on the side of the thermal storage. This implies that thermal storage is the distributor of the hot and cold water to the panels. The system was modelled using Polysun to assess the performance and functionality of the proposed system.

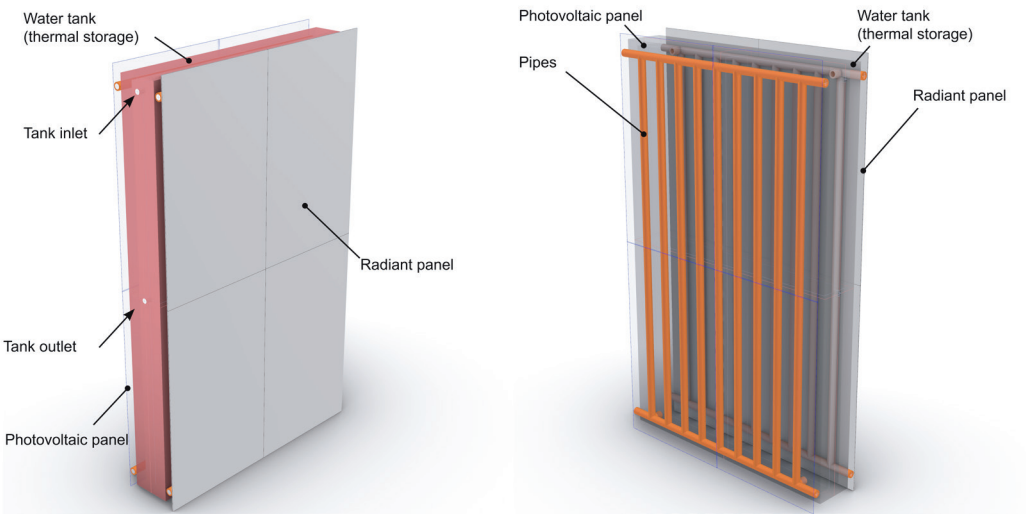

FIG. 1 Left: Axonometric drawing showing the radiant heating/cooling panel from inside; Right: External view showing the pipes attached to the back of the photovoltaic/thermal (PVT) panel. A high level of transparency has been set to the PVT panel for illustrative purpose

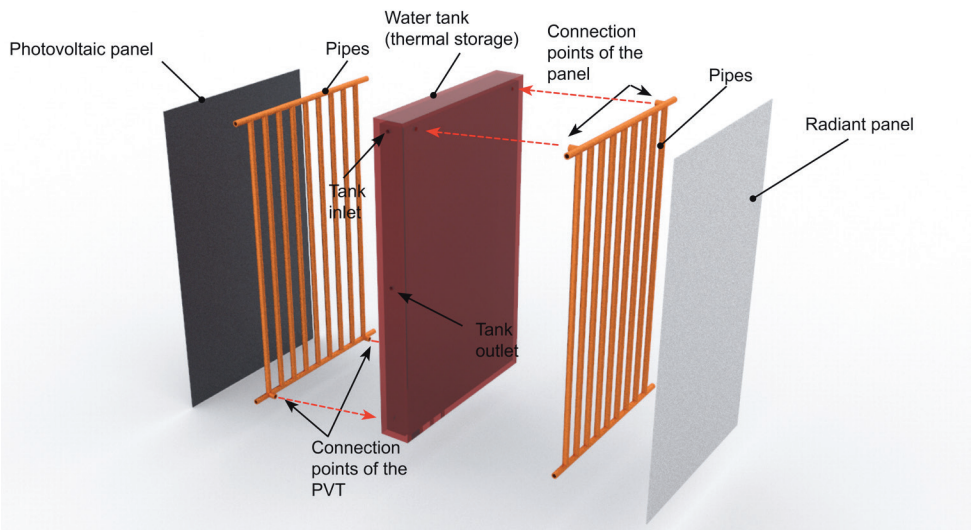

FIG. 2 Exploded axonometric drawing of the system

The exploded axonometric drawing in Fig. 2 illustrates the basic relationships between the components. It can be observed that the radiant panel is connected to the thermal storage through supply and return connections located in the upper part. In the lower part, the supply and return connections transfer relatively cold water to the PVT system. In this approach, the thermal storage works as a water exchange medium between the three elements: PVT, radiant panel, and heat exchanger. Further, this concept benefits from the temperature stratification that occurs during thermal storage. Thus, cold water always goes to the PVT element and the output warm water goes to the radiant panel in winter. In summer, the cooling is not significantly affected because the radiant cooling panel operates at temperatures in the range of 18-24 °C, which is one of the advantages of a so-called high-temperature cooler.

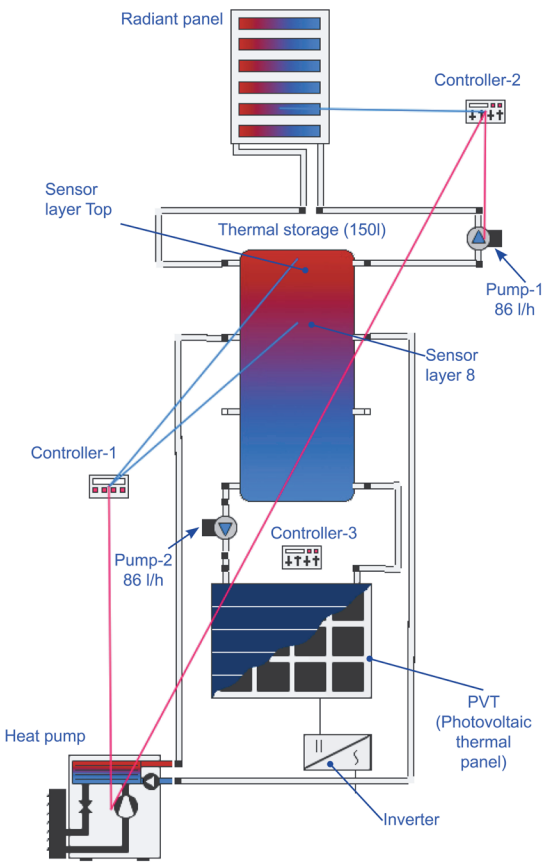

Controller-1		
Cut-in tank temperature	[°C]	20
Cut-off tank temperature	[°C]	20
Maximum tank temperature	[°C]	22
Control inputs		
Layer temperature sensor on	[-]	Storage tank: Layer 8
Layer temperature sensor off	[-]	Storage tank: Top Layer
Control outputs		
On/Off heating device	[%]	Heat pump: On/Off
Controller-2		
Control inputs		
Sensor input-1	[°C]	Radiant cooling temperature
Sensor input-2	[°C]	Average outdoor temperature
Control outputs		
Pump-1	[%]	On/Off
Heat pump	[W]	Conrolled power heat generator
Operating status		
If Sensor input-1 (i1>23)	then	Pump-1 -> off
If Sensor input-1 (i1>23)	then	Heat pump -> off
If Sensor input-2 (i2>20)	then	Pump-1 -> on
If Sensor input-2 (i2>20)	then	Heat pump-> 100 W
If Sensor input-1 (i1<20)	then	Pump-1 -> on
If Sensor input-1 (i1<20)	then	Heat pump -> 100 W
Controller-3		
Control inputs		
Sensor input-1	[°C]	PVT panel temperature
Control outputs		
Pump-2	[%]	On/Off
Operating status		
If Sensor input-1 (i1>22)	then	Pump-1 -> on
If Sensor input-2 (i2<20)	then	Pump-1 -> off

FIG. 3 Left: Layout of the simulated system; Right: Parameters of the controllers

The image on the left in Fig. 3 illustrates an overview of the simulated model using Polysun. It can be observed that the system includes two main pumps attached to each panel in addition to the primary heat pump. The pumps are operated by output signals from a set of controllers that read input signals from the surface temperatures of the radiant and PVT panels. In addition, the water temperature on different layers of the tank sends input signals to Controller-1. The table on the right of the figure lists the protocols and operation statuses of the three controllers. The simulation was performed for 8760 h and covers the four seasons of the year. According to the schematic diagram, the height of the water supply and return in each component, including the thermal storage, is

crucial as it affects the thermal quality of the water. The listed configuration is the result of different arrangements and indicates the optimum outcome. The system includes a DC/AC inverter attached to the PVT system. However, the efficiency of the inverter is not considered in the context of this study, and the analyses were primarily limited to the DC output. The proposed system has been filed for patenting (US patent application number: 16999129).

TABLE 1 Specifications of the photovoltaic/thermal module

ELECTRICAL DATA [1]			
Typical power	(Pn)	[Wp]	245
Open circuit voltage	(VOC)	[V]	
Maximum power voltage	(Vpm)	[V]	
Short circuit current	(Isc)	[A]	8.74
Maximum power current	(Ipm)	[A]	8.17
Module efficiency	(η)	[%]	15.5
Maximum system voltage		[V DC]	1000
Reverse current load	(Ir)	[A]	15
Temperature coefficient - Pn	(Υ)	[%/°C]	-0.43
Temperature coefficient - VPm	(β)	[%/°C]	-0.34
Temperature coefficient - Ipm	(α)	[%/°C]	0.065
[1] STC condition: irradiance = 1000 W/m^2, cell temperature = 25 °C			
THERMAL DATA - IN THE CASE OF PVT			
Aperture area		[m^2]	1.59
Thermal efficiency [2]	(η_0)	[%]	56
Nominal thermal power [3]		[W]	888
Volume flow rate		[l/m]	1.5-2.5
Flow losses		[mmH_2O]	400-900
Fluid volume		[l]	0.9
Coefficient α1 [2]		[-]	9.12
Coefficient α2 [2]		[-]	0
Effective thermal capacity		[kJ Kg^{-1} K^{-1}]	20
IAM K0 at 50 °C			
[2] Based on aperture area			
[3] PV OFF conditions referred to (Tm-Ta) = 0			
SPECIFICATION			
Cells		[-]	60 poly-Si
Thickness		[mm]	156
Electrical connectors		[-]	MC4
Hydraulic connector		["]	1/2 female
Dimensions		[mm]	1638 x 982 x 41
Weight		[kg]	27

For the purpose of testing the practicality of the presented invention, a location that requires heating and cooling was selected. Consequently, Munich, Germany, was selected as the standpoint for the simulations. An orientation to the south with an inclination of 90° was selected. The assessment focused on the surface temperatures of both the PVT system and radiating panel corresponding to external factors such as outdoor temperature and irradiance into the PVT module. One of the advantages of radiant heating systems is to provide heating with a relatively low surface temperature and thus less heating power. For this to work effectively, the temperature of the room surfaces should be homogeneous and within the human comfort zone. Besides air tightness, this requires well insulated walls, floors, and ceilings, as well as effective radiant heating elements. In this study, the surface temperature was set to around 21°C. The quality of the room surfaces and their insulation properties, which obviously affect the room temperature, were out of the scope of this paper. More focus was given to the surface temperature of a single radiant heating/cooling element. Obviously, more elements may be needed in a room depending on its heating load.

The radiating panel comprises an aluminium sheet with a thermal conductivity of approximately 202 W/m.K and specific heat capacity (Cp) of 871 J/kg.K. Further, the selected size of the radiating panel is similar to the PVT module, which is 1 m × 1.65 m. The pipes of both panels are of the same size, and the water mass flowrate is also identical across the components of the system. However, the water mass flowrate to/from the heat pump and the storage tank can be varied according to the heating or cooling demand of the system. Table 1 lists the specifications of the PVT module.

3 RESULTS AND DISCUSSION

An overview of the simulation results is shown in Fig. 4. The average data over the course of one year are presented. The preliminary axis depicts the temperatures in degrees Celsius and the secondary axis depicts the energy in watts. The light grey curve indicates the PVT DC electric energy production in watts and the black curve indicates the thermal energy exchange between the heat pump and the thermal storage in watts. The outdoor temperature is indicated by the yellow curve. The light blue curve depicts the surface temperature of the radiating panel that achieves the cooling and heating functions of the room. While the PVT panel temperature is indicated by the dark blue curve, the pink curve indicates the surface temperature of a typical PV panel under the same conditions. From the first glimpse, it can be noted that in summer, a difference of approximately 12 K is achievable between the surface temperature of the PV and the PVT panels. This suggests that the proposed system has succeeded in significantly cooling down the surface temperature.

From the figure, it can be observed that the temperature of the radiating element is stable at approximately 21 °C and varies within a small range of 1-1.5 K. This reflects the impact of thermal storage on stabilising the temperature of the radiating panel. Another advantage of the relatively cool water at the bottom of the tank is that the surface temperature of the PVT panel in summer is significantly lower than the outdoor temperature. In winter, the panel temperature is maintained above 0 °C when the outside temperature is below 0 °C to avoid the requirement for antifreeze solutions. However, this aspect can be further optimised using controlling schemes.

From the results of other simulations, it can be noted that the surface temperature of a conventional PV panel reaches 52.8 °C in the selected location. In the proposed system, the maximum surface temperature reached 37 °C. This difference has significant advantages for energy production and performance enhancement. As described earlier, for every 1 K increase in the surface temperature of

the PV panel above 25 °C, a reduction of 0.5% in the performance is expected. From the diagram, it is also clear that the PVT DC electric energy production increases in winter, spring, and autumn, when the altitude of the sun is relatively low. During these seasons, the radiating panel presents a surface temperature that is reliable for maintaining the mean radiant temperature of the room within the comfort range. The generated electric energy can be used to operate the electric-driven heat pump.

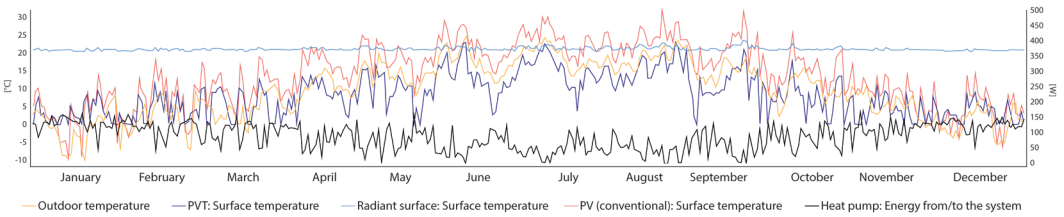

FIG. 4 General overview on the system performance over the course of one year

Fig. 5 illustrates a comparison of the simulation results for the energy production in DC between a conventional PV system and the proposed PVT system. The brown and orange curves represent the energy production using the PV and PVT systems, respectively. Generally, higher electricity production is expected in autumn, winter, and spring owing to the low altitude of the sun on the south façade. It is notable that a substantial increase in production efficiency can be achieved using the PVT system. This is primarily owing to the cooling effect and the reduction in surface temperature caused by the integrated thermal storage tank. Further, the difference in electricity production reaches to more than 35%.

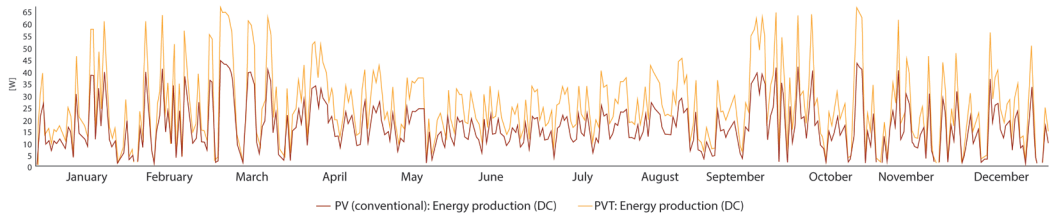

FIG. 5 Comparison in energy production in DC

A detailed observation during a high-temperature summer period in the first two weeks of July is shown in Fig. 6. It is important to notice the effect of ambient temperature on the surface temperature of the conventional PV and proposed PVT systems. The right axis presents the solar irradiance into the module area. A remarkable temperature increase was observed in the first case that exceeds the outdoor temperature by approximately 40%. Conversely, the PVT system presents a reduced module surface temperature in most of the cases, which reaches up to 10% of the outdoor temperature. The surface temperature of the radiant cooling/heating panel is stable and marginally affected by the outdoor temperature. It moderately varies between 20 and 24 °C. However, there is a clear indication that the surface temperature of the PV module is significantly affected by the solar irradiance into the module area. It is notable that both curves are in correlation.

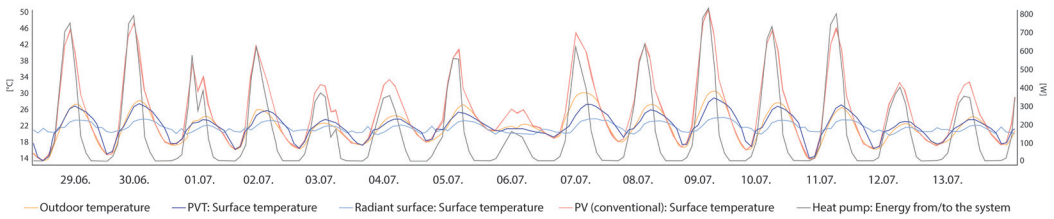

FIG. 6 Detailed observation during a high-temperature summer period

In winter, another detailed observation was performed around the beginning of February and the results are shown in Fig. 7. A significant increase in the surface temperature of the conventional PV system is evident from the figure. As noted in the previous figure, unlike the conventional PV module, the surface temperature of the PVT system is less likely to be affected by solar irradiance. The surface temperature of the radiant cooling/heating panel is nearly stable at 20 °C despite the extreme drop in temperature that reaches up to -12 °C.

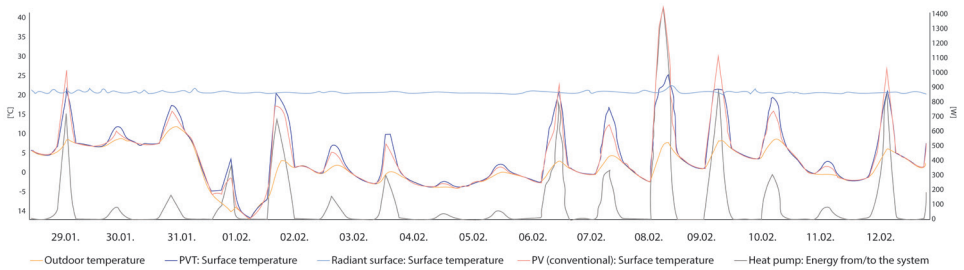

FIG. 7 Detailed observation during a low-temperature winter period

To provide a validation for the increased efficiency of the proposed and simulated system over conventional ones, two comparisons have been made against existing systems whose live statistical data are available online. Both PV systems are located in Munich. The characteristics of each system are outlined in Table 2.

TABLE 2 Table 2 Framework of the reference systems

SYSTEM NUMBER	[-]	1	2
System name	[-]	dahoam (pvoutput.org, 2020a)	GB53 (pvoutput.org, 2020b)
System size	[kW]	4.176	4.5
Number of panels	[-]	16	20
Panel capacity	[Wp]	260	225
Inverter	[-]	Samil SolarLake 4500 TL-D	SMA Sunnyboy 3600 TL
Maximum efficiency (inverter)	[%]	97.6	97
Orientation	[-]	South	South West
Tilt	[°]	37	42

Using the simulation software PolySun, comparisons have been made between the proposed system and each of the reference systems. Therefore, in each simulation the framework of the proposed system has been modified to match the reference case. These modifications were essentially applied to the panel capacity, inverter efficiency, orientation, and tilt angle. The comparisons shown in Fig. 8 and Fig. 9 depict the difference in the accumulated monthly AC output of the PV panels (primary axis) and the associated increase/decrease in module efficiency (secondary axis).

The diagram in Fig. 8 presents an overall increase in the PV output of the proposed system over the reference system-1. It is clear that in the cold months remarkable increases in efficiency can be noticed. This is basically attributed to the decreased surface temperature of the panels. This is notable as the radiant panels are used for heating and the upper part of the thermal storage supplies it with relatively warm water. Therefore, the water coming out of the thermal storage and moving at the back of the panel doesn't seem to negatively affect the efficiency of the module. Further, a slight decrease in the output in February can be seen. This exception maybe attributed to the statistically collected climate data that are embedded in the simulation software and may have different data regarding the irradiance and cloudiness of the site in comparison to the real readings from the system. This obviously affects the simulated output. Moreover, thanks to the proposed an increase in efficiency of up to 31% can be noted.

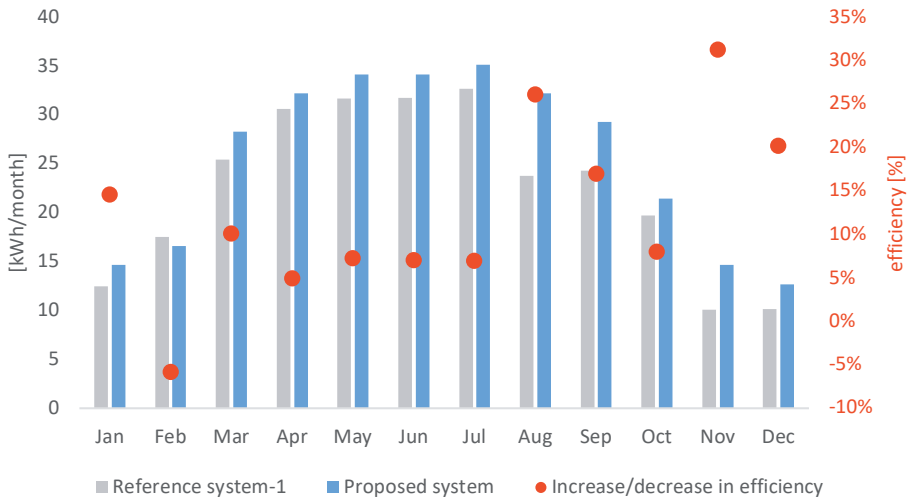

FIG. 8 Comparison between the proposed system and the reference system-1

A more remarkable increase in efficiency is noted in Fig. 9, where the efficiency of the proposed system has improved by 47% over the reference case. Generally, the electrical output of the PV panel has substantially increased over the course of the 12 months. This is of particular interest in summer as, despite the increased ambient temperature, the cooled water from the thermal storage helped reduce the surface temperature and thus increase the module efficiency. However, the increased module efficiency and thus PV output are amongst the advantages of the proposed system that combines radiant cooling, radiant eating, thermal storage, and energy generation with an increased efficiency in one façade-integrated device.

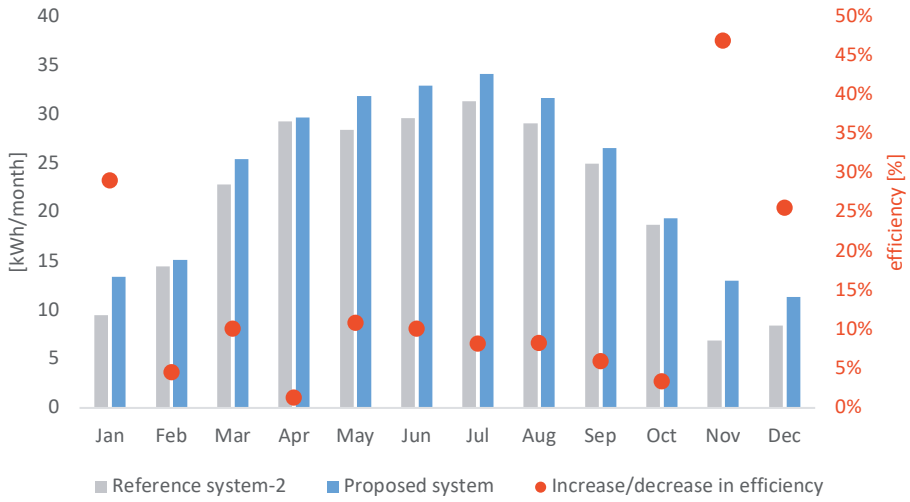

FIG. 9 Comparison between the proposed system and the reference system-2

4 CONCLUSION

This paper has presented the potential of a façade-integrated device where the PVT panel is located on the external side and the radiant cooling/heating surface faces an interior space; moreover, a thermal storage tank is located between the panels. Both elements are connected through thermal storage. A comparison with conventionally free integrated PVs was included. The results indicate the high potential of the proposed system over the conventional PV system in terms of reduction in surface temperature and increase in electricity production efficiency. As high cooling loads coincide with high façade irradiance, the proposed solution has practical applications for an integrated building envelope system. The system also helps save space as it combines energy generation with radiant cooling/heating and integrates this into the building envelope. The impact of the thermal storage was clear in stabilising the surface temperatures and eliminating the correlation between the solar irradiance and the surface temperature. Furthermore, the cooling or heating energy can be directly generated using a heat pump that is connected to the thermal storage. The proposed system can be developed in different sizes and depths and can be incorporated into walls, roofs, or inclined surfaces at any angle. Multiple elements can be connected in series to achieve higher cooling and heating loads.

Key advantages:

- A year-long solution in locations where heating and cooling are required.
- The integration of thermal storage reduces overheating.
- Increased efficiency for electricity, cooling, and heating.
- A shorter reaction time owing to thermal storage.
- Supply of heating energy during both the day and night.
- Good façade insulation owing to the various layers of materials, including the thermally insulated storage tank.
- No requirement for antifreeze as the thermal storage can supply warm water to the PVT element when required.

— The entire system is a wall element that can be sized flexibly. The thickness of the system can vary, and the water tank can also have variable thicknesses.
— A larger system can also include potable water production.

Further research and development can be conducted to convert the panel to a window element that is operable to allow fresh air intake during periods of pleasant temperature. Instead of cooling pipes, capillary tubes can be attached to the surfaces to achieve higher performance and a slimmer design.

References

Aste, N., Del Pero, C., & Leonforte, F. (2012). Optimization of solar thermal fraction in PVT systems. *Energy Procedia*, 30, 8–18. Retrieved from https://doi.org/10.1016/j.egypro.2012.11.003

Bayoumi, M. (2018a). Façade-integrated PVT with radiant cooling panels for increased energy and space efficiency. In *13th Conference on Advanced Building Skins* (pp. 749–758). Bern: Advanced Building Skins GmbH.

Bayoumi, M. (2018b). Method to Integrate Radiant Cooling with Hybrid Ventilation to Improve Energy Efficiency and Avoid Condensation in Hot, Humid Environments. *Buildings*, 8(5), 69. Retrieved from https://doi.org/10.3390/buildings8050069

Bayoumi, M. (2020). Extending the Efficiency of Facade-Integrated PVT through Coupling with Radiant Cooling. *Journal of Civil Engineering Inter Disciplinaries*, 1(2), 5–16.

Henning, H.-M., & International Energy Agency. Solar Heating and Cooling Programme. (2004). *Solar-assisted air-conditioning in buildings : a handbook for planners*. Wien ; New York: Springer.

Hindrichs, D. U., & Daniels, K. (2007). *Plusminus 20°/40° latitude : sustainable building design in tropical and subtropical regions*. Stuttgart ; London: Edition A. Menges.

Hong, T., Yan, D., D'Oca, S., & Chen, C. (2017). Ten questions concerning occupant behavior in buildings: The big picture. *Building and Environment*, 114, 518–530. Retrieved 1 April 2017 from https://doi.org/10.1016/j.buildenv.2016.12.006

Huld, T., & Gracia Amillo, A. M. (2015). Estimating PV module performance over large geographical regions: The role of irradiance, air temperature, wind speed and solar spectrum. *Energies*, 8(6), 5159–5181. Retrieved from https://doi.org/10.3390/en8065159

Natarajan, S. K., Mallick, T. K., Katz, M., & Weingaertner, S. (2011). Numerical investigations of solar cell temperature for photovoltaic concentrator system with and without passive cooling arrangements. *International Journal of Thermal Sciences*. Retrieved from https://doi.org/10.1016/j.ijthermalsci.2011.06.014

Pathak, M. J. M., Pearce, J. M., & Harrison, S. J. (2012). Effects on amorphous silicon photovoltaic performance from high-temperature annealing pulses in photovoltaic thermal hybrid devices. *Solar Energy Materials and Solar Cells*, 100, 199–203. Retrieved from https://doi.org/10.1016/j.solmat.2012.01.015

Prieto, A., Knaack, U., Auer, T., & Klein, T. (2017). SOLAR COOLFACADES Framework for the integration of solar cooling technologies in the building envelope. *Energy*. Retrieved from https://doi.org/10.1016/j.energy.2017.04.141

Pugsley, A., Zacharopoulos, A., Mondol, J. D., & Smyth, M. (2020). BIPV/T facades – A new opportunity for integrated collector-storage solar water heaters? Part 2: Physical realisation and laboratory testing. *Solar Energy*, 206(February), 751–769. Retrieved from https://doi.org/10.1016/j.solener.2020.05.098

pvoutput.org. (2020a). PVOutput-dahoam 4.176kW. Retrieved 18 November 2020, from https://pvoutput.org/display.jsp?sid=31109

pvoutput.org. (2020b). PVOutput-GB53 4.500kW. Retrieved 18 November 2020, from https://pvoutput.org/display.jsp?sid=75152

Razak, A., Irwan, Y., Leow, W. Z., Irwanto, M., Safwati, I., & Zhafarina, M. (2016). Investigation of the Effect Temperature on Photovoltaic (PV) Panel Output Performance. *International Journal on Advanced Science, Engineering and Information Technology*, 6(5), 682. Retrieved from https://doi.org/10.18517/ijaseit.6.5.938

Rhee, K.-N., & Kim, K. W. (2015). A 50 year review of basic and applied research in radiant heating and cooling systems for the built environment. *Building and Environment*, 91, 166–190. Retrieved 20 June 2017 from https://doi.org/10.1016/j.buildenv.2015.03.040

Seo, J.-M., Song, D., & Lee, K. H. (2014). Possibility of coupling outdoor air cooling and radiant floor cooling under hot and humid climate conditions. *Energy and Buildings*, 81, 219–226. Retrieved 11 July 2014 from https://doi.org/10.1016/j.enbuild.2014.06.023

Song, D., & Kato, S. (2004). Radiational panel cooling system with continuous natural cross ventilation for hot and humid regions, 36, 1273–1280. Retrieved from https://doi.org/10.1016/j.enbuild.2003.07.004

Stetiu, C. (1999). Energy and peak power savings potential of radiant cooling systems in US commercial buildings. *Energy and Buildings*, 30(2), 127–138. Retrieved from https://doi.org/https://doi.org/10.1016/S0378-7788(98)00080-2

Vangtook, P., & Chirarattananon, S. (2007). Application of radiant cooling as a passive cooling option in hot humid climate. *Building and Environment*, 42(2), 543–556. Retrieved from https://doi.org/10.1016/j.buildenv.2005.09.014

Zhang, L. Z., & Niu, J. L. (2003). Indoor humidity behaviors associated with decoupled cooling in hot and humid climates. *Building and Environment*, 38(1), 99–107. Retrieved from https://doi.org/10.1016/S0360-1323(02)00018-5

Zhang, X., Zhao, X., Smith, S., Xu, J., & Yu, X. (2012). Review of R&D progress and practical application of the solar photovoltaic/thermal (PV/T) technologies. *Renewable and Sustainable Energy Reviews*, 16(1), 599–617. Retrieved from https://doi.org/10.1016/j.rser.2011.08.026

Additive Manufacturing of Thermally Enhanced Lightweight Concrete Wall Elements with Closed Cellular Structures

Gido Dielemans[1*], David Briels[2], Fabian Jaugstetter[1], Klaudius Henke[3], Kathrin Dörfler[1]

* Corresponding author
1 TT Professorship Digital Fabrication, Department of Architecture, Technical University of Munich, Munich, Germany, gido.dielemans@tum.de
2 Chair of Building Technology and Climate Responsive Design, Department of Architecture, Technical University of Munich, Munich, Germany
3 Chair of Timber Structures and Building Construction, Department of Civil, Geo and Environmental Engineering, Technical University of Munich, Munich, Germany

Abstract

Building envelopes incorporate a multitude of functions, such as structure, room enclosure, insulation, and aesthetic appeal, typically resulting in multi-material layered constructions. With the technology of additive manufacturing, geometrical freedom can instead be utilised to integrate functional requirements into mono-material building components. In this research, the additive manufacturing method of lightweight concrete extrusion and its potential for thermal performance via geometric customisation is explored. It investigates whether the insulating performance of wall components can be increased through the creation of closed cellular structures, and further, whether these performance features can be functionally graded by locally adapting the geometric properties. A design tool for closed-cell wall geometries is created, which integrates lightweight concrete extrusion related fabrication constraints and takes into account thermal and structural performance considerations. Through the simulation of heat transfer, generated wall geometries are analysed for their thermal performance. By calculating the layer cycle times and determining the overhang during extrusion, the structural capacity during printing is validated. Finally, experimental manufacturing of 1:1 scale architectural prototypes is executed to test the feasibility of the concept.

Keywords

Additive manufacturing, lightweight concrete extrusion, computational design, thermal performance, functionally graded materials

10.7480/jfde.2021.1.5418

1 INTRODUCTION

Computer-aided design has enabled architects and engineers to construct a formal language with unprecedented geometric complexity and attention to detail. Additive Manufacturing (AM) methods in construction such as 3D Concrete Printing (3DCP) are the response to this paradigm shift as a method with which complex designs can be materialised. In extrusion-based 3DCP, fresh concrete is deposited layer by layer, shaping concrete without formwork and placing the material only where desired. In view of the large ecological footprint of the construction sector, recent research has increasingly investigated how this new technology redefines architectural design-to-realisation strategies and enables the production of material-effective structures through structural optimisation and geometric customisation (Agustí-Juan & Habert, 2017). While research has made remarkable technological advances, the construction of fully functional spaces with AM technology applied to building envelopes requires architects and engineers to also consider climatic performance features. At this time, constructions produced utilising 3DCP are still rather modest in terms of integrating aspects of human comfort and ensuring a suitable indoor climate when compared to most traditional fabrication alternatives.

In this paper, building components are integrated with climatic performance functions through exploration of geometric freedom provided by 3DCP. It investigates whether the geometric properties of closed cellular geometries of lightweight concrete can increase the insulating performance of mono-material wall components (see Fig. 1), and further, whether these performance features can be functionally graded by locally adapting the geometric properties. It then investigates whether such mono-material building components can present a viable alternative to conventional layered multi-material constructions for fulfilling thermal functions. The experimental methodology of this research enabled the realisation of two prototypes, which provided essential insights into the feasibility of the concept.

FIG. 1 Close-up of a concrete cellular structure manufactured using extrusion-based 3DCP (Jaugstetter, 2020).

2 STATE OF THE ART

Recent research has brought forward a few approaches in achieving increased climatic performance with building components manufactured using AM methods. Closely related to conventional layered construction, one method applies insulating material to the outside of an additively manufactured structural concrete element. This was shown in the Office of the Future in Dubai (Dubai Future Foundation, n.d.) and the structural wall of the multi-storey house at Kamp C in Westerlo (Van Der Putten et al., 2020). The filling of cavities in the 3DCP structural system with insulation is a second approach, which has been applied to the case study of the Nyborg Studio (Bos, Wolfs, Ahmed, & Salet, 2019), and the insulated wall of the multi-storey house at Kamp C in Westerlo (Van Der Putten et al., 2020). A reverse approach using additively manufactured geometries of insulating material as lost formwork for the casting of concrete has been researched with the Digital Construction Platform by the Mediated Matter Group at MIT (Keating, Leland, Cai, & Oxman, 2017). Additionally, a house dubbed *Yhnova* was constructed using a similar technique called Batiprint3D as part of the Nantes Digital Week (Furet, Poullain, & Garnier, 2019). Besides the addition of insulation materials, other approaches are being developed that alter the material composition of concrete with the aim of increasing thermal insulation capacity, and reducing component weight and material usage. The research direction of foamed concrete for AM has most recently been explored at the TU Dresden (Markin, Ivanova, Fataei, Reißig, & Mechtcherine, 2020) and the Polytechnic of Turin (Falliano et al., 2020), where reduced material density was achieved by creating regular air cavities in the concrete while material strength and rheological properties are maintained. Another approach of material research for AM with thermal insulation in mind is through the use of lightweight aggregates in the concrete mixture (Henke, Talke, & Matthäus, 2020).

While research has proven the thermal capacity of building components to increase by adding insulating materials or by altering the material composition, one potential method for functional enhancement is the geometric manipulation of a mono-material building component. This can be done through an optimisation process, iteratively improving structural and thermal performances by altering the cross-sectional shape of the building component (Vantyghem, Steeman, De Corte, & Boel, 2020). More elaborate graded materials can be created by enclosing air in the geometry of the object, inspired by natural occurring meso-materials like wood, coral and cancellous bone (Vantyghem, Steeman, De Corte, & Boel , 2017). Due to the internal geometry of the structure, these materials benefit from high strength capacity, light weight, improved thermal conductivity, and electrical resistance. Applying this geometrical philosophy to the macro scale has the potential to improve thermal and structural characteristics, but results in complex geometries that can only be created with advanced manufacturing processes. With the potential for complex geometries in 3DCP, this research further explores geometrical design with the aim to achieve higher thermal performance.

3 METHODOLOGY

In order to fundamentally address the topic of thermal improvement of building components with concrete AM, this research is carried out at the interface between architecture, climate responsive design, and materials science. By creating a computational design tool, possible shapes of closed-cell geometries are investigated for their potential as thermal insulator, enabled by 3DCP of lightweight concrete (Henke et al. 2020). In continuation, the modelling of a continuous extrusion print path of the cellular geometry according to associated manufacturing constraints is explored.

The geometric results are then thermally evaluated in simulation, and experimentally validated for production feasibility through prototype manufacturing.

3.1 DESIGN PRINCIPLE

Cellular structures can be divided into open-cell and closed-cell typologies. Open-cell structures in concrete extrusion practice are often applied for stabilisation and material reduction; additionally, these cells can be filled with insulating material. While open-cell typologies such as honeycomb or simple zigzag patterns are the most common internal designs, AM technology also allows for three-dimensional internal design, where volumes are enclosed in the structure.

To tessellate internal space entirely, only five three-dimensional geometric solids are suitable to be arrayed: the cube, prism, rhombic dodecahedron, elongated dodecahedron, and truncated octahedron (see Fig. 2). While all these shapes can tessellate space, a high volume to a low surface area is advantageous for limiting heat losses through conduction. With its 14 faces, the truncated octahedron is the shape that adapts most closely to the ideal ratio of a sphere, and was thus chosen as the basis for geometrically modelling the closed cell structures of this research.

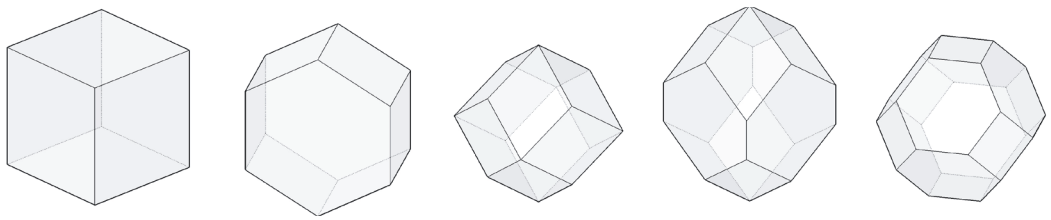

FIG. 2 The five main space-filling polyhedra. From left to right: Cube, Prism, Rhombic Dodecahedron, Elongated Dodecahedron, and the chosen Truncated Octahedron (Jaugstetter, 2020).

In this research enclosed air volumes are constructed using support-free 3DCP, applied at the building scale. Creating closed cells, with an encapsulated volume that holds air, is not possible in all AM technologies. Particle bed solutions, for instance, would result in the particulates being trapped inside the structure (Weger et al., 2020). The unique thermal properties of closed-cell typologies are evidenced by closed-cell foams, which have the lowest thermal conductivity of any conventional non-vacuum insulation (Gibson & Ashby, 2014).

3.2 DESIGN TOOL

To design and evaluate closed-cell geometries that integrate the production constraints of 3DCP, a design tool was created in Rhino (McNeel & Associates, n.d.) and Grasshopper, supplemented with specially developed Python scripts (see Fig. 3). A wall element was chosen as a use-case to examine the enhancement strategy. Two guide surfaces are defined to shape the outer boundaries of the element, defining parameters such as width, height, and length of the component. An attractor point can be placed in the wall element to vary the density of the cells inside the wall, for example, to locally increase the loadbearing behaviour of the wall, or satisfy design-related decisions. The cell size can be changed in width, depth, and height to affect structural and thermal performance, for which the user is guided by a performance feedback.

The context of this feedback is constructed from process parameters in the design tool, like layer height, filament width, ideal layer cycle time, and maximum overhangs.

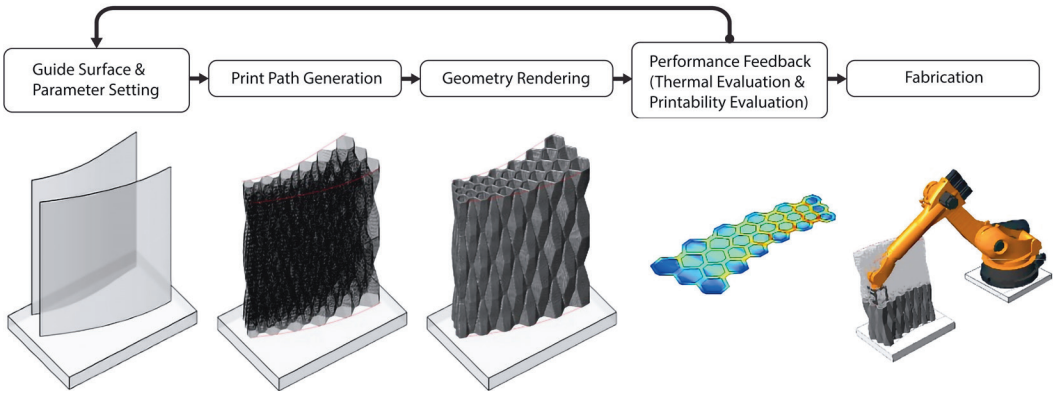

FIG. 3 Overview of the proposed parametric design tool, which integrates the modelling of the closed-cell geometry and the associated print path according to the given boundary surfaces, the rendering of the resulting geometry, and the evaluation possibilities of defined performance criteria for the generated geometry (Jaugstetter, 2020).

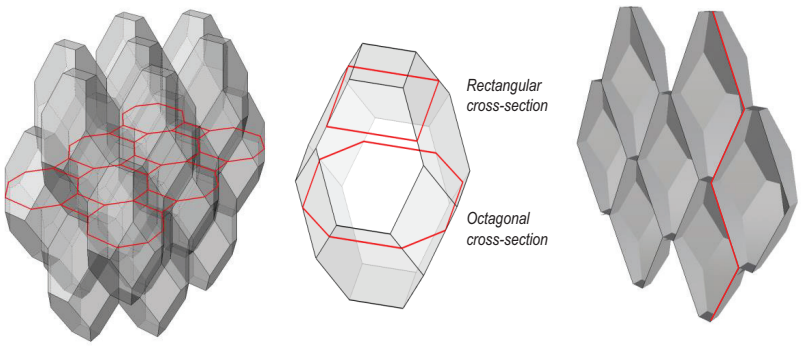

FIG. 4 Truncated octahedron geometry with rectangular and octagonal path slices (Jaugstetter, 2020)

The chosen cell geometry of a truncated octahedron has two cross-section types within the slicing procedure, an octagonal and a rectangular section (see Fig. 4). Over the height of the cell the path length follows a periodic trend, with the shortest rectangular paths at either end.

To manufacture an array of these cells, a print path is modelled as a sequence of incremental vectors describing the geometry of half a cell (see Fig. 5), which is inspired by turtle graphics (Goldman, Schaefer, & Ju 2004). To evaluate the change of cross-sectional geometry and print path length, a function has been defined describing the behaviour:

$$f(x) = \pm \frac{a}{\pi} \sin^{-1}\left(\cos\left(\pi \frac{x-p}{p}\right)\right) + \frac{a}{2} \qquad (1)$$

The first derivative of the previous function defines the point at which sectional geometry changes:

$$f'(x) = \frac{a}{\pi}\sin^{-1}\left(\cos\left(\pi\frac{x-2p}{2p}\right)\right) + \frac{a}{2} \qquad (2)$$

To make this approach valid for freeform elements, the cellular structure needs to adapt by reorientating the sequence and varying the width and depth of the cell. This adaptation is done by evaluating points on the centreline of the structure, where the angle, tangent, and normal of the point on the curve represent the reorientation angle, width, and depth respectively (Fig. 6). The height of the cell is remained fixed in accordance with process parameters, like layer height and maximum overhangs.

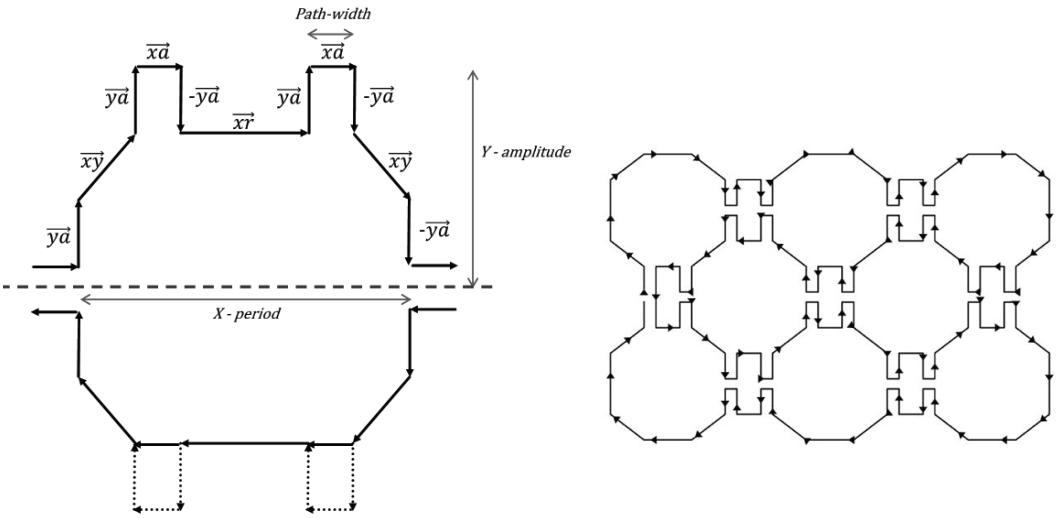

FIG. 5 Print path geometry, built from vector sequencing (Jaugstetter, 2020)

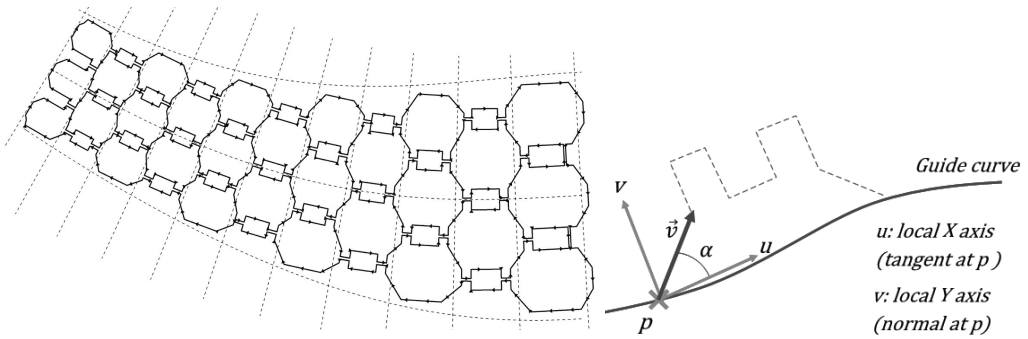

FIG. 6 Vector sequence according to a guide curve: $\vec{v}$: vector of vector sequence, α : reference angle, p : reference point (left), and applying the system to two boundary surfaces (right) (Jaugstetter, 2020)

3.3 PERFORMANCE FEEDBACK

3.3.1 Thermal Performance

The thermal conductivity of cellular structures comprises conduction through the solid and gas as well as convection and radiation within the cells (Gibson & Ashby, 2014). Air is an insulator with low thermal conductivity when in a rested state; in a moving state, however, heat transfer is accelerated as a result of convection (Bankvall, 1972). Convection can be reduced by encapsulating air in cells, limiting buoyancy-driven natural convection, with decreasing sizes of encapsulating volumes having reduced natural convection (Gibson & Ashby, 2014). For closed-cell foams it was found that convection can be neglected at a maximum cell size of 10 mm (Gibson & Ashby, 2014). Opposite to convection, conduction increases with decreasing air layer thickness. Considering the combined heat transfer, a study by Bekkouche et al. (2013) described an ideal air layer thickness of 40 to 60 mm for a cavity wall under given assumptions (see Fig. 7).

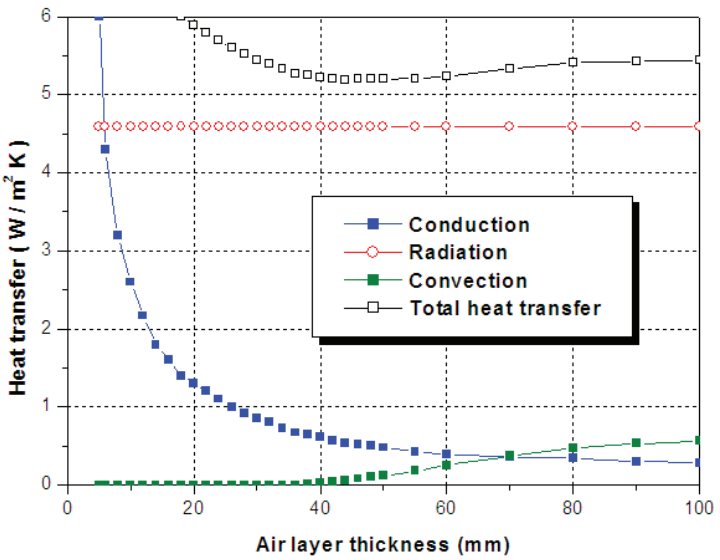

FIG. 7 Estimated heat transfer in a closed air cavity bounded by ordinary materials e = 0.9 (Bekkouche et al., 2013)

By directly implementing LBNL THERM 7.4 into the design tool through the Grasshopper plugin Ladybug (Roudsari & Pak, 2013), the thermal performance of the cellular structure is analysed by performing heat flux simulations of horizontal cross-sections of the geometry. The calculations are based on two-dimensional simulations, where three types of heat transfer are included. Conduction and radiation are both modelled explicitly with the Finite Element Method (FEM) and a view-factor calculation, whereas convection is estimated through correlations and heat transfer coefficients (Huizenga et al., 1999). Three-dimensional heat transfer is not taken into account, assuming that the main heat flow is directed horizontally due to the temperature differences between indoors and outdoors. Furthermore, the influence of buoyancy driven natural convection within the closed cells is simplified by using film coefficients and neglecting the cell height. By using this simplified, automated, integral simulation process, the thermal performance of each layer can be assessed to derive a mean U-value for the whole element.

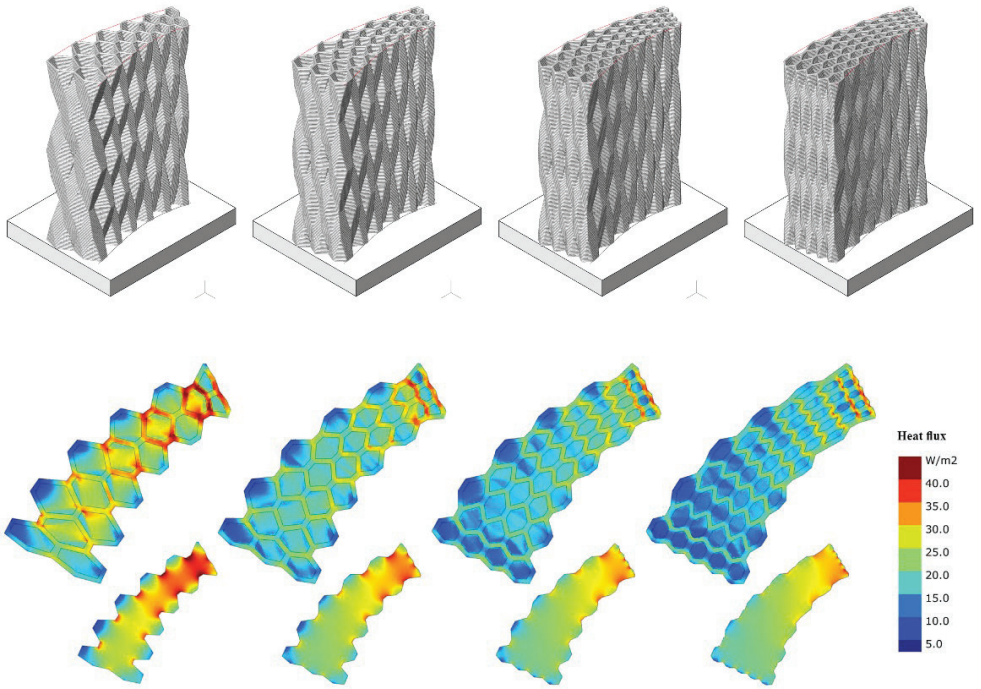

FIG. 8 Design variations of a wall element with increasing cell count in y-direction; visualisation of simulated heat flux for one exemplary layer each with and without internal cellular structure (Jaugstetter, 2020; adapted by David Briels).

TABLE 1 Geometrical properties of design variations of a wall element, as shown in Fig. 8, and results for thermal assessment.

CELL COUNT (Y)	1 / 2	2 / 3	3 / 4	4 / 5
Max cell size (y)	199 mm	129 mm	87 mm	65 mm
Wall thickness	150 – 450 mm	190 – 460 mm	220 – 460 mm	230 – 460 mm
air/solid-ratio	1,54	1,36	1,11	0,86
U-Value$_{tot}$ (cell)	0,71 W/m^{2}K	0,63 W/m^{2}K	0,61 W/m^{2}K	0,57 W/m^{2}K
U-Value$_{proj}$ (cell)	1,07 W/m^{2}K	0,80 W/m^{2}K	0,71 W/m^{2}K	0,64 W/m^{2}K
U-Value$_{proj}$ (solid)	1,28 W/m^{2}K	1,11 W/m^{2}K	1,05 W/m^{2}K	1,01 W/m^{2}K

A study of four design variations (see Fig. 8) uses a decreasing cell size from 200 to 65 mm and a cell count increasing from two to five. The thermal performance is visualised by a simulated heat flux and quantified by calculated U-values for one exemplary layer respectively. The areas with a heat flux of 25 W/m^2 or higher (yellowish to red) are visibly reduced, decreasing the calculated U-Value$_{tot}$ (from 0.71 W/m^{2}K to 0.57 W/m^{2}K (see Table 1). Due to higher geometrical resolution, the size of cells and thickness variation is reduced, while the amount of surface undulations and the size of the heat transferring surface is increased. This is indicated by an increase of the minimum wall thickness from 150 to 230 mm (see Table 1) and boundary line length in cross-sections, which are used for the calculation of the U-Value$_{tot}$. Projecting the boundary line on the guide surface results in a U-Value$_{proj}$ for the heat transfer through the wall element, allowing an improved comparability between variants. Comparing the calculated U-Value$_{proj}$ (cell) of the elements with cellular structure to the same geometries without air cavities (solid) a thermal enhancement of 16 to 37 % is evidenced for these four design variations. The increased thermal performance of the design variations can partially be attributed to the internal cellular structure, specifically to the reduced cell size resulting in lower convective heat transfer and the wall geometry resulting from the arrangement of cells.

At the same time, the air to solid ratio is decreasing, which implies an increase in heat conduction through solids, though the tipping point for the total heat transfer seems to not yet have been reached (compare Fig. 7).

3.3.2 Printability

The main constraint on 3DCP remains its buildability, specifically of free-standing and unsupported complex geometries requiring the concrete filament to cantilever. Cantilevering geometries can be categorised in terms of local and global inclinations, where local inclination is the result of cantilevering parts of the undistorted, often internal, geometry. Global inclination is the cantilevering geometry resultant of distortion of the overall geometrical design. The overhang is then defined as the eccentricity of the filament compared to the underlying layer, by calculating the projected distance between the two print paths. Short path segments are expected to be less critical despite having large overhangs; to account for this a segment length threshold is introduced with a value equal to the filament width.

The factor of time plays a large role for 3DCP, as viscosity increases over time to a degree where it can no longer be extruded (Buswell, Leal de Silva, Jones, & Dirrenberger, 2018). This is reflected in the design and print path generation as layer cycle time, with a lower limit being the buildability and the upper limit being defined by the bond strength between layers. To maintain geometric freedom and ensure manufacturability the path length is allowed to deviate in accordance with these limits, while the tool velocity is kept constant.

An estimated print duration is calculated based on the total print path length, where a correction factor based on directional changes is introduced to account for inevitable acceleration and deceleration of the robot (see Equation 3).

$$t_{layer} = \frac{l}{v_{robot}} + f \qquad (3)$$

3.4 PARTITIONING

The layer cycle time significantly influences the concrete extrusion process, with layer adhesion deteriorating for longer print paths (Wangler et al., 2016). No matter whether the elements are prefabricated or printed in-situ, their size is limited as a result of layer adhesion. For off-site printed elements, the size of these elements is additionally limited by transportation. Hence, a geometrical joint following the logic of the cellular structure is conceptualised, creating an interlocking connection between multiple elements. The convex and concave areas of the cells form either female or male joints, expected to be beneficial for force transmission and minimising thermal loss. To ensure the precise fit of the joint, shrinkage and interpolated print path geometry need to be controlled. In this research, joints are designed with tolerance on the print path to compensate for the discrepancy between the digital and real geometry. A wall design of two elements with their joint solution is shown in Fig. 9.

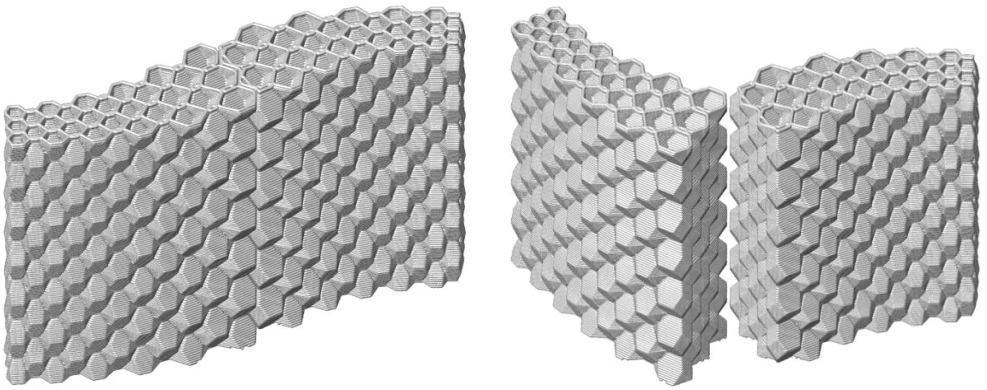

FIG. 9 Wall design composed of two elements joined together with cell-like joints (Jaugstetter, 2020)

4 EXPERIMENTAL RESULTS AND VALIDATION

4.1 MANUFACTURING PROCEDURE

For the placement of concrete filament, a KUKA KR150 L110 6-axis robot provided by the Chair of Building Realisation and Robotics at the Technical University of Munich has been used. The robot can reach a distance of 3500 mm with a maximum payload of 110 kg at the end effector and is mounted on a 7 m rail, which is implemented as a linear 7th axis. The robot was equipped with a custom end-effector, which includes a quick-change system for interchanging nozzles (Henke et al., 2018). Since live communication between design environment and robot was not possible due to the architecture of the controller, a translation was made from the print path to machine instructions with the Grasshopper plugin KUKA-PRC (Association for Robots in Architecture, 2020). The material that was used for the demonstrator objects is a lightweight aggregate concrete, using cement, water, and expanded glass granulate (Matthäus et al., 2020), resulting in a low density concrete of 300 – 800 kg/m^3 that has a relatively high pressure resistance of 1.4 – 1.8 N/mm^2. The concrete was batch-fed to a Knauf PFT Swing L FC-400V concrete pump with a feed-rate of 3.5-10.0 l/min, conveying the material through a 10-metre hose with 25 millimetre diameter.

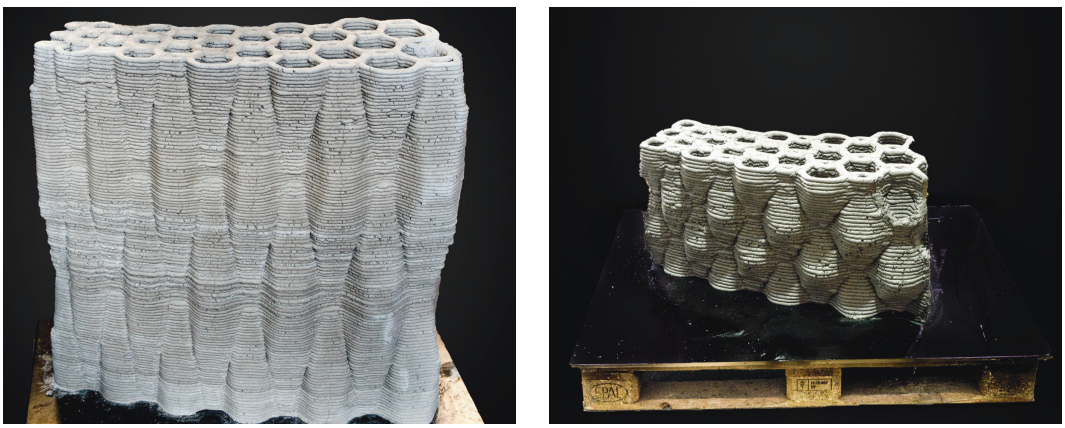

FIG. 10 3D printed demonstrator A with cell height of 740 mm (left) and demonstrator B with cell height 370 mm (right) (Jaugstetter, 2020)

Two demonstrator objects have been printed with the cellular geometry to validate the design tool for printability. These demonstrator objects will be referred to as 'A' and 'B', both designed to fit on a single pallet with dimensions of 1200 x 800 mm for ease of transportation (see Fig. 10). Demonstrator A has a cell height of 740 mm as defined by a maximum overhang of 4 mm, demonstrator B has a reduced cell height of 370 mm with 6.2 mm as maximum overhang to assess the stability of the cellular structure (see Table 1 for main characteristics of the designed demonstrator objects). For the demonstrator objects a nozzle of 22 mm diameter was used, which caused clearly visible filaments but removed the need for orienting the nozzle tangential to the printing path (Henke et al., 2020).

TABLE 2 Summary of characteristics of demonstrator objects in design phase (Jaugstetter, 2020)

	DEMONSTRATOR A	DEMONSTRATOR B
Base dimensions	1200 x 800 mm	1200 x 800 mm
Element height	1040 mm	1040 mm
Layers	116 layers at 9 mm	116 layers at 9 mm
Cell height	740 mm	244 mm
Maximum overhang per layer	4.1 mm	6.2 mm
Thickness	240 – 450 mm	240 – 450 mm
Cell diameter	340 – 870 mm	340 – 870 mm
Total print path length	1666.4 m	1666.2 m
Estimated weight	427 kg	427 kg

4.2 PRINTABILITY

To ensure bonding of the print path within a horizontal layer, an alteration to the digital geometry was made by partially overlapping the path. For a filament width of 22 mm, a distance between the centreline of two paths of 5 mm has been observed to ensure appropriate bonding between horizontal extrusions. Secondly, a layer cycle time correction factor has been derived from predicted times and cycle times as measured during the manufacturing process. With a correction factor of f_{robot} = 0.033 [s/°] an average deviation of 1.3 % between predicted and measured cycle time was be calculated (see Table 2).

TABLE 3 Comparison of predicted and measured layer cycle times (Jaugstetter, 2020)

LAYER	PREDICTED CYCLE TIME (S)	MEASURED CYCLE TIME (S)	DEVIATION
5	59.9 s	62 s	3.4 %
35	65.5 s	64 s	2.3 %
50	69.1 s	70 s	1.3 %
7-81	Ø 70.4 s	Ø 71.3 s	Ø 1.3 %

5 CONCLUSION

5.1 DESIGN TOOL AND FABRICATION

This research has shown the extrusion-based additive manufacturing with lightweight concrete to be capable of creating structures with enclosed cells. With the implementation of such cellular structures to a wall geometry, functionally enhancing the material for improved thermal performance has been achieved. Combined with a new design language, this customised geometry for a mono-material building component can thus represent a viable alternative to the conventional multi-material layered constructions.

However, limitations are still present with the lightweight concrete extrusion in a matter of achievable cell sizes and design freedom. The collapse of the outermost cells of the second demonstrator object has suggested that neighbouring cells can structurally support each other, allowing for steeper overhangs to be created inside than at the border (Bos et al., 2016).

The integration of fabrication constraints into a fabrication-aware design tool provides a possible solution for creating complex geometries customised for the manufacturing method, e.g., ensuring print path continuity across layers without compromising build time by preventing manufacturing interruptions. Print path continuity for manufacturing in construction may become obsolete with advances in the field, though in terms of build time it will likely remain advantageous as retractions and travel are not required (Jin, He, Fu, Gan, & Lin, 2014).

The implementation of a prognosis on manufacturing data in the design tool provides direct feedback to the user for refinement of the design in terms of resulting printability, material cost, and time. This integration allows for the creation of complex geometry with increased ease of use, allowing for more designers to interact with the digital manufacturing technology in construction. In turn, this could improve the distribution of digital concrete manufacturing, as currently a lack of experts in the field of complex design and machinery limits the adoptability (Buswell et al., 2018).

5.2 THERMAL PERFORMANCE

An ideal air layer thickness for the reduction of heat flux in a cavity wall was determined by Bekkouche et al. (2013), as between 40 and 60 mm, and, according to Gibson et al. (2014), at a cell size of 10 mm or lower, convection within closed cells can be neglected. Concrete extrusion with filament widths of around 20 mm limit the possibilities to create foam-like cellular structures without a decrease of the air to solid ratio, in which density causes the filament to act as a thermal bridge. This proportion is currently restricted by the low print resolution of the manufacturing process. This print resolution cannot be increased as smaller filament widths would substantially slow down the build rate, inhibiting either the printability or buildability of the material. In addition, the arrangement of the cells and the resulting wall geometry, as well as surface area, influence the thermal behaviour.

By using the integrated workflow for performance feedback within the design process, the thermal performance can be optimised. In the example case of four design variations (see Fig. 8) the reduction of cell size (in y direction) from 199 mm to 65 mm led to a substantial improvement of the $U\text{-}Value_{proj}$ by 40 % even though the air to solid ratio dropped from 1.54 to 0.86. Comparing the elements with cellular structure to the same geometries without air cavities a thermal enhancement

of 16 to 37 % is evidenced for these four design variations. This is based on a two-dimensional representation of the cellular geometry, where conduction and radiation are explicitly modelled in a finite element model and with a view-factor calculation whereas convective heat transfer is calculated based on heat transfer coefficients (Huizenga et al., 1999). Irregularities as a result of meshing of several complex layers have been seen to lead to anomalies in the simulation results, reducing the total number of useable thermally assessed layers. No measurements were taken from the manufactured demonstrators, while only scarce literature of digital manufactured concrete elements tested for thermal conductivity exists.

5.3 OUTLOOK

With the further development of 3DCP technology with the goal of achieving higher resolution and advances in eccentrically layering of filament, more complex geometries with smaller air cavities could be designed and manufactured that allow for further improvement in thermal performance. By now the estimated $U\text{-}Value_{proj}$ of the design variations up to 0.64 W/m2K still does not reach the common standard values for external walls, for example compared to the reference value of 0.28 W/m^2K in the German Energy Conservation Regulation (*EnEV*, 2007). However, this paper shows that with further improvements it seems feasible to thermally enhance mono-material lightweight concrete wall elements by adding and optimising an internal cellular structure to fulfil these requirements. To ensure buildability, the design tool could be extended to contain advanced structural feedback, preventing the element from collapse during the manufacturing process.

The thermal heat flux simulations should be extended by simulating the three-dimensional heat flow through the element and especially checking the influence of the buoyancy-driven natural convection within the closed cells. The theoretical assessment of the thermal performance via simulations should be tested and validated through heat flux measurements on the prototypes. In addition, filled cell geometries with porous materials could be simulated and researched in terms of their thermal behaviour as an application for particle bed processes, which provide higher print resolutions and thus the possibility to create more foam-like cellular structures.

Acknowledgements

Experimental work was executed by the Chair of Timber Structures and Building Construction and the Chair of Material Science and Testing at the Technical University of Munich in the course of the project "Additive Manufacturing of Multifunctional, Monolithic Wall Elements by Extrusion of Lightweight Concrete" funded by the innovation program "Zukunft Bau" of the Federal Ministry of Interior, Building and Community, Federal Republic of Germany. The research presented in this paper is being conducted as part of the collaborative research centre 'Additive Manufacturing in Construction - The Challenge of Large Scale,' funded by the Deutsche Forschungsgemeinschaft (DFG, German Research Foundation) - project number 414265976 - TRR 277, within the projects B05 and C03.

References

Agustí-Juan, I., & Habert, G. (2017). Environmental design guidelines for digital fabrication. *Journal of Cleaner Production*, *142*, 2780–2791. https://doi.org/10.1016/j.jclepro.2016.10.190

Association for Robots in Architecture. (2020). *KUKA|prc*. https://www.robotsinarchitecture.org/kukaprc

Bankvall, C. (1972). *Natural convective heat transfer in insulated structures*. https://portal.research.lu.se/ws/files/4596708/8227870.pdf

Bekkouche, S. M.A., Cherier M. K., Hamdani, M., Benamrane, N., Benouaz, T., & Yaiche, M. R. (2013). Thermal resistances of air in cavity walls and their effect upon the thermal insulation performance. *International Journal of Energy and Environment*, *4*(3), 459–466. http://www.ijee.ieefoundation.org/vol4/issue3/IJEE_11_v4n3.pdf

Bos, F., Wolfs, R., Ahmed, Z., & Salet, T. (2016). Additive manufacturing of concrete in construction: potentials and challenges of 3D concrete printing. *Virtual and Physical Prototyping*, *11*(3), 209–225. https://doi.org/10.1080/17452759.2016.1209867

Bos, F., Wolfs, R., Ahmed, Z., & Salet, T. (2019). Large scale testing of digitally fabricated concrete (DFC) elements. In *RILEM Bookseries* (Vol. 19, pp. 129–147). Springer Netherlands. https://doi.org/10.1007/978-3-319-99519-9_12

Buswell, R. A., Leal de Silva, W. R., Jones, S. Z., & Dirrenberger, J. (2018). 3D printing using concrete extrusion: A roadmap for research. In *Cement and Concrete Research* (Vol. 112, pp. 37–49). Elsevier Ltd. https://doi.org/10.1016/j.cemconres.2018.05.006

Dubai Future Foundation. (n.d.). *Office of the Future*. Retrieved September 4, 2020, from https://www.dubaifuture.gov.ae/our-initiatives/office-of-the-future/

EnEV. (2007). https://www.gesetze-im-internet.de/enev_2007/BJNR151900007.html

Falliano, D., Crupi, G., De Domenico, D., Ricciardi, G., Restuccia, L., Ferro, G., & Gugliandolo, E. (2020). Investigation on the Rheological Behavior of Lightweight Foamed Concrete for 3D Printing Applications. In *RILEM Bookseries* (Vol. 28, pp. 246–254). Springer. https://doi.org/10.1007/978-3-030-49916-7_25

Furet, B., Poullain, P., & Garnier, S. (2019). 3D printing for construction based on a complex wall of polymer-foam and concrete. In *Additive Manufacturing* (Vol. 28, pp. 58–64). Elsevier B.V. https://doi.org/10.1016/j.addma.2019.04.002

Gibson, L. J., & Ashby, M. F. (2014). Thermal, electrical and acoustic properties of foams. In *Cellular Solids: Structure and Properties, Second Edition* (pp. 283–308). Cambridge University Press. https://doi.org/10.1017/CBO9781139878326

Goldman, R., Schaefer, S., & Ju, T. (2004). Turtle geometry in computer graphics and computer-aided design. *CAD Computer Aided Design*, *36*(14), 1471–1482. https://doi.org/10.1016/j.cad.2003.10.005

Henke, K., Talke, D., & Matthäus, C. (2020). *Additive Manufacturing by Extrusion of Lightweight Concrete - Strand Geometry, Nozzle Design and Layer Layout* (pp. 906–915). https://doi.org/10.1007/978-3-030-49916-7_88

Huizenga, C., Arasteh, D., Finlayson, E., Mitchell, R., Griffith, B., & Curcija, D. (1999). *THERM 2.0: a building component model for steady-state two-dimensional heat transfer*. https://escholarship.org/uc/item/66n7n302

Jaugstetter, F. (2020). *Design Tool for Extrusion Based Additive Manufacturing of Functionally Enhanced Lightweight Concrete Wall Elements with Internal Cellular Structures*. Technische Universität München.

Jin, Y. an, He, Y., Fu, J. zhong, Gan, W. feng, & Lin, Z. wei. (2014). Optimization of tool-path generation for material extrusion-based additive manufacturing technology. *Additive Manufacturing*, *1*, 32–47. https://doi.org/10.1016/j.addma.2014.08.004

Keating, S. J., Leland, J. C., Cai, L., & Oxman, N. (2017). Toward site-specific and self-sufficient robotic fabrication on architectural scales. *Science Robotics*, *2*(5). https://doi.org/10.1126/scirobotics.aam8986

Markin, V., Ivanova, I., Fataei, S., Reißig, S., & Mechtcherine, V. (2020). Investigation on Structural Build-Up of 3D Printable Foam Concrete. In *RILEM Bookseries* (Vol. 28, pp. 301–311). Springer. https://doi.org/10.1007/978-3-030-49916-7_31

Matthäus, C., Back, D., Weger, D., Kränkel, T., Scheydt, J., & Gehlen, C. (2020). *Effect of Cement Type and Limestone Powder Content on Extrudability of Lightweight Concrete* (pp. 312–322). https://doi.org/10.1007/978-3-030-49916-7_32

McNeel & Associates. (n.d.). *Rhinonoceros (Rhino) Version 6.0*. Retrieved September 4, 2020, from https://www.rhino3d.com/

Roudsari, M. S., & Pak, M. (2013). *LADYBUG: A PARAMETRIC ENVIRONMENTAL PLUGIN FOR GRASSHOPPER TO HELP DESIGNERS CREATE AN ENVIRONMENTALLY-CONSCIOUS DESIGN*.

Van Der Putten, J., Van Olmen, A., Aerts, M., Ascione, E., Beneens, J., Blaakmeer, J., De Schutter, G., & Van Tittelboom, K. (2020). 3D Concrete Printing on Site: A Novel Way of Building Houses? In *RILEM Bookseries* (Vol. 28, pp. 712–719). Springer. https://doi.org/10.1007/978-3-030-49916-7_71

Vantyghem, G., Steeman, M., De Corte, W., & Boel, V. (2017). Design of cellular materials and meso-structures with improved structural and thermal performances. *Proceedings of the 12th World Congress of Structural and Multidisciplinary Optimisation*. http://hdl.handle.net/1854/LU-8524436

Vantyghem, G., Steeman, M., De Corte, W., & Boel, V. (2020). Design Optimization for 3D Concrete Printing: Improving Structural and Thermal Performances. In *RILEM Bookseries* (Vol. 28, pp. 720–727). Springer. https://doi.org/10.1007/978-3-030-49916-7_72

Wangler, T., Lloret, E., Reiter, L., Hack, N., Gramazio, F., Kohler, M., Bernhard, M., Dillenburger, B., Buchli, J., Roussel, N., & Flatt, R. (2016). Digital Concrete: Opportunities and Challenges. *RILEM Technical Letters*, *1*, 67. https://doi.org/10.21809/rilemtechlett.2016.16

Weger, D., Kim, H., Talke, D., Henke, K., Kränkel, T., & Gehlen, C. (2020). *Lightweight Concrete 3D Printing by Selective Cement Activation – Investigation of Thermal Conductivity, Strength and Water Distribution* (pp. 162–171). https://doi.org/10.1007/978-3-030-49916-7_17

Exploring the Possibility of Using Bioreceptive Concrete in Building Façades

M. Veeger[1*], A. Prieto[1], M. Ottelé[2]

* Corresponding author

1 TU Delft, Faculty of Architecture and the Built Environment, Department of Architectural Engineering and Technology, maxveeger@hotmail.com

2 TU Delft, Faculty of Civil Engineering and Geosciences, Department of Materials, Mechanics, Management & Design (3Md)

Abstract

A bioreceptive material allows for biological content (biofilms) to grow on it, without necessarily affecting the material itself. If a bioreceptive concrete could therefore be integrated into a building façade, it could lead to green façades that do not need additional technical systems. As part of previous research by the authors, a promising bioreceptive concrete mixture was formulated. The aim of this research is to develop this concept by using the previously developed mixture to create a bioreceptive concrete façade panel prototype, made using commonly available materials, that can direct where the biological growth takes place. The latter is done by combining the bioreceptive concrete with a non-bioreceptive (UHPC-based) concrete in the same panel, through a two-stage pouring process. A biofilm was developed on this prototype panel and results show that full coverage of the bioreceptive parts of the panel can be achieved within two weeks under optimal growing conditions and biological growth can be directed. However, exterior survivability is an issue for now. The concept of bioreceptive façades therefore shows promise, yet further investigation into improving exterior survivability is necessary, while further research into the underlying ecology, material, economics, and climate effects is also necessary.

Keywords

Bioreceptivity, biofilm, concrete façade panel

10.7480/jfde.2021.1.5527

1 INTRODUCTION

Increased urbanisation and the associated loss of green spaces, in combination with climate change, are leading to a range of problems in our cities, including but not limited to a loss in biodiversity, heat stress, increased air pollution, and more, bringing with them concerns for ecological and public physical and mental health (Beatley & Newman, 2013; Kleerekoper, van Esch, & Salcedo, 2012; Lai & Cheng, 2010; McKinney, 2008). In a bid to increase the amount of green in our cities, the use of green roofs and façades has become more common. These have been found to play a positive role in reducing building surface temperatures, capturing airborne pollutants, increasing biodiversity, and sequestering carbon (Charoenkit & Yiemwattana, 2017; Kleerekoper et al., 2012; Perini & Rosasco, 2013). However, at the same time, green roofs and façades incur additional costs both in construction and maintenance, while they also put higher structural demands on the buildings they are attached to (Li & Yeung, 2014; Perini & Rosasco, 2013).

Recently, a new typology of green building envelope has been proposed, based on the principle of bioreceptivity. Bioreceptivity is a term originally coined by Guillitte (1995), which he defined as: "the aptitude of a material to be colonised by one or several groups of living organisms without necessarily undergoing any biodeterioration" (p.216). If a material with a high bioreceptivity were applied on a building surface, a green surface could therefore be achieved. The biological growths that develop on these surfaces are called biofilms and consist of bacteria, algae, fungi, lichen, and mosses. These biofilms can survive under virtually all natural environmental conditions, provided the substrate they grow on is suitable (Gorbushina, 2007; Pentecost & Whitton, 2012). Therefore, they can theoretically be placed anywhere on a building envelope. At the same time, similar to regular green façades, they can affect the building surface temperature, digest some airborne pollutants, and sequester carbon through calcite precipitation (Freystein, Salisch, & Reisser, 2008; Mayaud, Viles, & Coombes, 2014; Zhang & Klapper, 2010). They do all this while not requiring additional technical systems or maintenance, thereby opening up the possibility of creating green building envelopes with reduced costs and embedded energy.

The main challenge in the creation of bioreceptive concrete façades lies in the material itself. Based on existing literature, the main requirements for biological growth appear to be a substrate pH below 10, sufficient surface roughness to protect the biofilm from environmental influences, high water absorbing capacity and retention within the substrate, and the presence of nutrients within the substrate, in particular phosphorus (Guillitte & Dreessen, 1995; Jones & Bennett, 2017; Miller et al., 2010; Prieto & Silva, 2005; Tiano, Accolla, & Tomaselli, 1995; Vázquez-Nión, Silva, & Prieto, 2018; Wiktor, De Leo, Guyonnet, Grosseau, & Garcia-Diaz, 2009; Grosseau, Guyonnet, & Garcia-Diaz, 2010). If these requirements can be met using common materials and methods, it could then form the basis for a bioreceptive concrete mixture that can be used on a large scale in building façades.

In previous research conducted by the authors, the underlying ecology of the colonisation of stony substrates by biofilms was used to develop and test several bioreceptive concrete mixtures (Veeger, Prieto & Ottelé, 2021). This resulted in the formulation of a concrete mixture that was found to be highly bioreceptive (see Table 1). The blast furnace slag cement was used to lower the concrete pH (although a pH lower than 10 was not found to be necessary), crushed expanded clay (CEC), and a high water cement factor (wcf) were used in combination with a low overall cement content to improve the porosity and thereby water absorption of the concrete, and bone ash was added to provide the biofilm with phosphorus.

TABLE 1 Bioreceptive concrete mixture as formulated in previous research by the authors (Veeger et al., 2021)

CONSTITUENTS	BIORECEPTIVE CONCRETE
Cement	300kg/m^3 OPC cement (62.5% slag)
Aggregate	578 kg/m^3 Argex AG4/8 (crushed expanded clay) / 762 kg/m^3 sand (0-4mm)
Water	150kg/m^3 (wcf 0.50)
Mineral admixture	30kg/m^3 Bone ash
Plasticiser	None

However, whilst this gives us a suitable bioreceptive substrate, it needs further development to be used in a building façade. In its current form, growth is uncontrolled and takes place on the entire surface, which is not always preferable. Also, due to its high porosity, this mixture is expected to have a reduced compressive strength and increased susceptibility to freeze-thaw damage (McCarthy & Dyer, 2019; Paine, 2019). Additionally, its high susceptibility to carbonation, whilst positive for the biological growth, reduces the pH of the concrete, removing the passive protection layer that is usually present around steel rebar, making it susceptible to corrosion (Mindness, 2019). Based on this, the use of the formulated bioreceptive concrete mixture cannot be recommended in structural or otherwise critical applications.

As such, in this research we investigate how bioreceptive concrete can be used to create a bioreceptive façade panel that can control where biological growth takes place. A panel system was chosen as this decouples the exterior part of the façade from the load-bearing structure, eliminating one of the constraints of bioreceptive concrete and allowing for more design flexibility. This research will include the materialisation, design, production, and the testing of the façade panel prototype.

2 METHODOLOGY

This paper starts with the creation of a façade panel design and its production methods. For the façade panel, two criteria were observed. First of all, the façade panel is preferably produced using existing methods and common construction materials. To make the façade panel economically and practically feasible the use of exotic construction methods and materials should be minimised, as these would drive up the cost and complexity of the design significantly. Secondly, the façade panel should be able to direct biological growth. The usability and design flexibility of this panel would be increased if it were possible to direct where biological growth occurs.

Once the design and production methods were finalised, these were used to create two prototype panels, the exact production of which will be discussed later on in this paper. After creation, these panels were tested to ascertain whether they were in fact bioreceptive and able to direct biological growth.

This testing was done by producing two prototypes of these façade applications. These were then inoculated with the same liquid biofilm that was used in our previous research (Veeger et al., 2021). This biofilm was originally sourced from an existing biofilm growing on an exterior concrete structure of the Faculty of Architecture, TU Delft. It was originally kept in a BG-11 liquid growth medium under optimal growing conditions (room temperature, ~90% humidity, 12h day/night cycle with a light intensity of 40 µmol m-2s-1; (see Veeger et al. (2021) for full test set-up).

However, after the initial experiment the BG-11 stock was depleted, therefore a solution of 10mL liquid NPK fertiliser (1:1 water diluted 7-2-7 NPK fertilizer with added trace minerals and humic acid) and 450mL distilled water was used instead. During this period, every three weeks 50mL of the old liquid biofilm was added to a new water and liquid fertiliser solution, to avoid cell senescence. Per prototype, 350mL of this liquid biofilm was added, which is a higher relative amount than used in our previous research and should therefore show faster results.

After inoculation, the prototypes where kept in a distilled water bath, with the water line just below the concrete surface, under the same optimal growing conditions as described above. They were kept there until almost full coverage of the panel surface was achieved, after which they were kept outside for a period of 1 week. As our previous research had already found some type of additional nursery was likely needed once placed outside, the surface of the panels was wetted twice daily during this period to avoid extended desiccation of the biofilm. Growth progression was recorded throughout the experiment.

3 PANEL DESIGN

3.1 DIRECTING BIOLOGICAL GROWTH

The most obvious way to direct biological growth is to make some parts of the façade panel hospitable and other parts of the panel inhospitable to biological growth. In previous research conducted by the authors it was found that the bioreceptive concrete substrate needs a high water-absorbing capacity, and must provide nutrients and shelter the biofilm from environmental stressors in order for it to be bioreceptive (Veeger et al., 2021). In this same research, it was also shown that when these conditions are met, concrete does indeed become bioreceptive, whereas a concrete substrate that does not meet these criteria shows very little to no biological growth. The question therefore becomes how to achieve the optimal conditions for bioreceptivity in some parts of the panel, whilst creating the opposite conditions on other parts of the panel.

One of the most essential inputs for photosynthesis is light. Therefore, changing lighting conditions on the concrete surface might at first glance seem a relatively straightforward way to achieve differing conditions for the micro-organisms, thereby influencing bioreceptivity. In theory, one could, for example, create a bioreceptive part of the panel which is exposed to the sun and shades the non-bioreceptive part of the panel, thereby limiting growth due to a lack of photosynthetically active radiation (PAR; the part of the solar spectrum used for photosynthesis) from the sunlight. However, in practice, light is hardly ever the factor that stops biological growth from occurring. In fact, from field observations it has been found that micro-organisms that occurred in full sunlight in the tropics, under PAR radiation levels of 2,000 µmol $m^{-2}s^{-1}$, were also found in cave thresholds where the PAR levels were as low as 0.4 µmol $m^{-2}s^{-1}$ (Pentecost & Whitton, 2012). As such, it seems unlikely that restricting the access the micro-organisms have to light by shading certain parts of the panel, will have a significant impact on the bioreceptivity of these areas.

Restricting the nutrients in certain parts of the panel is the next possible option. In nature, nitrogen and phosphorus are often limiting factors for biological growth, with the latter being especially limiting in the growth of biofilms on stony materials (Johansson, Johansson, Giesler, & Palmqvist, 2011; Mostert & Grobbelaar, 1987; Pentecost & Whitton, 2012). As such, it is expected that limiting access to these nutrients will severely limit biological growth. However, while restricting the nutrients that are available within the substrate in certain parts of the panel is possible up to a point, it is likely not enough to create a severe enough nutrient limitation. This is because limiting the nutrient input from the surrounding environment (i.e. the air) is not always possible. Heterotrophic organisms in the biofilm (organisms using organic molecules as nutrients) are highly dependent on the nutrients that are available on the concrete surface and organic atmospheric particles, as they cannot extract inorganic nutrients from the air (Gorbushina, 2007). As such, limiting the organic nutrients that are available on the surface should severely inhibit their growth. This means that the substrate should contain no nutrients, but also that there should be little to no organic material from the air that gets attached to the substrate, as this is their main nutrient input. This can be done by creating a smooth surface, with as few attachment points for this organic material to settle as possible. This has an added advantage in that it also limits the attachment points and refuges for the micro-organisms themselves.

Nonetheless, heterotrophic organisms are only part of the total biofilm. Autotrophic organisms such as algae and cyanobacteria do not need organic material as their nutrient input and can instead get most nutrients from the air. Of the two elements that were identified earlier, nitrogen and phosphorus, nitrogen is usually not a limiting factor. This is due to the ability of several organisms within biofilms to fix N_2 from the air, making phosphorus the element that is usually in limited supply, due to it not being an aerosol (Pentecost & Whitton, 2012). Restricting the amount of phosphorus in the substrate can therefore limit growth up to a point, however, previous research has shown that whilst not adding phosphorus to the substrate can slow biological growth, it does still take place (Veeger et al., 2020). The other elements these autotrophic organisms need - carbon, hydrogen, nitrogen, oxygen, and sulphur - are readily available in the air and therefore cannot be limited on the substrate surface. As such, limiting nutrient access will need to be combined with other measures.

The most promising measure is to limit the access to water. As all biofilm organisms need water, restricting their access to it in part of the panel could severely limit growth in that part. In fact, in previous research conducted by the authors, water was proposed to be the main driver for the differences between different bioreceptive concrete mixtures (Veeger et al., 2021). Limiting this access is also relatively straightforward. If the porosity is kept very low, not only is the total water absorption of the concrete reduced, but the movement of water to the surface is also very restricted. In previous research it was also shown that if a surface is not treated with a surface retarder, water transport into the substrate is also severely reduced, thereby further restricting water access.

It is therefore suggested that using a combination of a smooth surface texture, and a concrete with low porosity and phosphorus content could make part of the panel inhospitable to biological growth. This is corroborated by previous research, where it was found that the reference samples, with their low porosity and no phosphorus content, showed very little to no biological growth, especially when no surface retarder was used. If this concrete is then combined in a panel where the other part uses a highly bioreceptive concrete, it should be possible to direct growth and achieve partial biofilm coverage of the panel.

TABLE 2 Overview of proposed measures to direct biological growth and their expected impact

PROPOSED MEASURES	EXPECTED IMPACT
Restricting PAR radiation	Extremely limited due to high range of acceptable PAR levels for organisms
Restricting nutrients	Limited due to nutrient input from the atmosphere, although it could limit growth of heterotrophic organisms
Restricting access to water	High based on previous research and easy implementation of water restrictions

3.2 CONCRETE MIXTURES

Both a bioreceptive and non-bioreceptive concrete have to combined in the panel to be able to direct biological growth. For the bioreceptive concrete, the mixture that was tested in previous research conducted by the authors will be used (Veeger et al., 2021). The non-bioreceptive concrete mixture needs to be one that has the exact opposite properties from this mixture. As determined in the previous paragraph, this means that it should have a low porosity and a smooth surface. A concrete mixture with these properties is already being used in the concrete industry, under the name of ultra high-performance concrete (UHPC).

Developed to increase the strength and durability of concrete, its properties should make it highly effective as a concrete that inhibits biological growth. Due to a combination of pozzolanic mineral fillers, high cement content, and a very low water/cement factor (made possible through the use of a superplasticiser) UHP concrete has a very low porosity, low water permeability and high carbonation resistance (Wang et al., 2015). As such, it has the ideal properties to form the non-bioreceptive part of the panel, as access to water should be severely restricted and its high carbonation resistance makes it so that the pore structure will remain stable over time, thereby ensuring that water access will remain low on this concrete throughout its lifetime.

We will therefore use an existing UHPC mixture employed by our company partner, Byldis, with one small adjustment. Most UHPC mixtures (including the one used by Byldis) use fibres to increase the tensile strength of the concrete (Shi et al., 2015). However, as high tensile strength is not a necessity for this application, this ingredient will be omitted to simplify the mixture and keep costs down. This leads to the two concrete mixtures in Table 3.

TABLE 3 Concrete mixtures used for the creation of the prototype panels

CONSTITUENTS	BIORECEPTIVE CONCRETE	UHPC CONCRETE
Cement	300 kg/m^3 OPC cement (62.5% slag)	700 kg/m^3 OPC cement
Aggregate	578 kg/m^3 Argex AG4/8 (CEC) 762 kg/m^3 sand (0-4mm)	Crushed gravel (4-11mm) Sand (0-4mm) 50:50 ratio
Water	150 kg/m^3 (wcf 0.50)	189 kg/m^3 (wcf 0.27)
Mineral admixture	30 kg/m^3 Bone ash	25 kg/m^3 silica fume 115 kg/m^3 limestone powder
Plasticiser	None	Yes (including additives)

3.3 PANEL STRUCTURE

In order to create a panel that is partially covered by a biofilm, these two types of concrete have to be combined within the same panel. However, if this is achieved by using the two types of concrete over the full depth of the panel, not only is the length of the joint minimal, reducing the bonding strength between the two types of concrete (exacerbated by the joint shape), but it also limits the amount of water that can be stored within the panel (see also Figure 1; option 1). Especially considering the latter, it would be better to use the bioreceptive concrete for a larger part of the panel, and only using the non-bioreceptive concrete on that part of the surface where biological growth is not desired (see also Figure 1; option 2). This way a large amount of storage capacity for water is provided in the form of the pores within the bioreceptive concrete, and joint length increased.

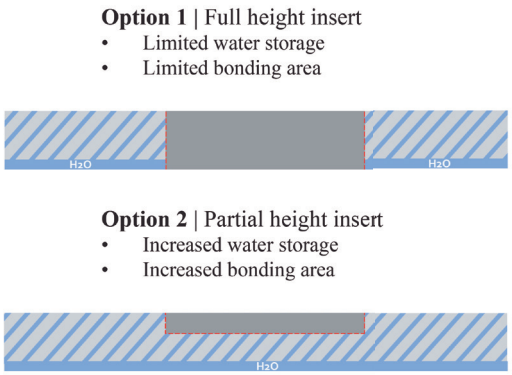

FIG. 1 Sectional overview of different insert options

This water can only reach the surface on the bioreceptive part of the panel, as the UHPC severely limits the transport of water to the non-bioreceptive parts of the panel. Combined with a smooth surface for the non-bioreceptive part of the panel, biological growth should be sufficiently hampered. On the bioreceptive part, on the other hand, water transport to the surface is already higher due to the used concrete and can be further improved by using a surface retarder on this part. This also increases the surface area, and nutrient and microorganism entrapment on this part of the panel. One more thing to consider is the aggregate on the surface of the washed concrete. In previous research it was shown that if the surface consists of a CEC aggregate, the complete panel will become covered with a biofilm, due to the CEC's inherent bioreceptivity (Veeger et al., 2021). The regular limestone aggregate, on the other hand, remained free of growth on the aggregate itself, giving a different visual appearance to the concrete. As such, changing just the aggregate on the surface of the panel can change the visual appearance of the bioreceptive part of the panel. Also, as long as the interior part of the panel consists of the CEC aggregate, the hydraulic properties will not be influenced extensively. Changing the surface aggregate therefore increases the range of visual options available for the panel. This leads to the final design as depicted in Figure 2.

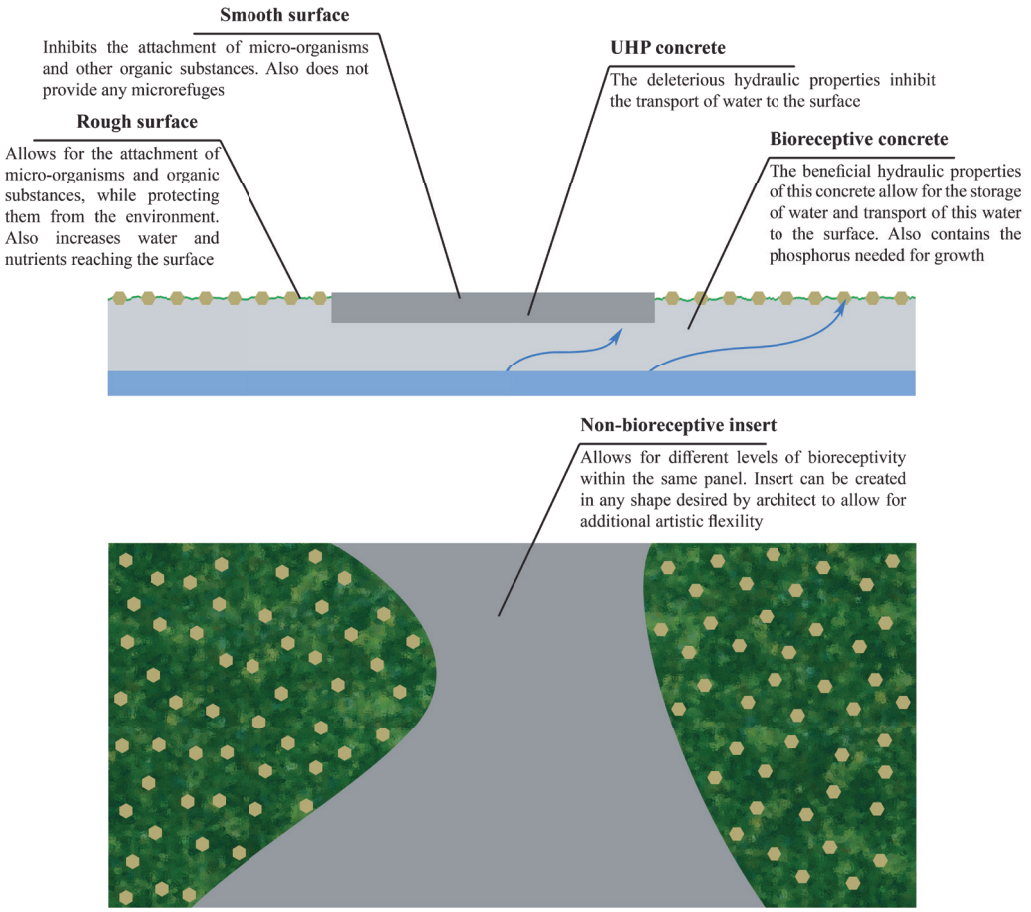

FIG. 2 Overview of the final panel design

3.4 PANEL PRODUCTION

The first step is to create the UHPC insert, which can later be embedded into the panel by pouring the bioreceptive concrete over it (similar to the way prefab brick façades are made). The UHPC insert can either be created in a separate mould, which has the size and shape that is required, or it can be created in the panel mould itself. By placing tempex or similar inserts the mould for the UHPC insert can be created within the larger mould. This also reduces the risk of breaking the insert, which is relatively thin and therefore could be fragile. By adding extra aggregate to the surface of the UHPC insert after pouring, the total surface area to which the bioreceptive concrete can bond in the next step is increased, as such increasing the total bonding strength.

The UHPC is then removed from its own mould and placed in the panel mould (in case a separate mould is used), or the tempex inserts are removed (in case the UHPC inset is made inside the panel mould). Next, the bottom of the panel mould is prepared. As this will become the exterior surface of the panel, this is where the surface retarder is applied in the area around the UHPC insert. If a surface aggregate other than CEC is preferred, this aggregate is added to the bottom of the mould as well. In this way, the panel itself will have the CEC aggregate that is present within the bioreceptive concrete mixture, whereas the aggregate that is visible on the surface is the one that is placed on the bottom of the mould. The surface appearance thus can be easily changed, without changing the bioreceptive concrete mixture.

After this, the bioreceptive concrete can be poured into the mould. When it has hardened, the panel can be demoulded and the unhardened cement on the surface of the bioreceptive part of the concrete can be washed away, revealing the aggregate. After some initial carbonation (28 days in our prototypes' case), the biofilm can be applied to the panel and initial biofilm growth can take place. A graphical overview of the production process can be found in Figure 3.

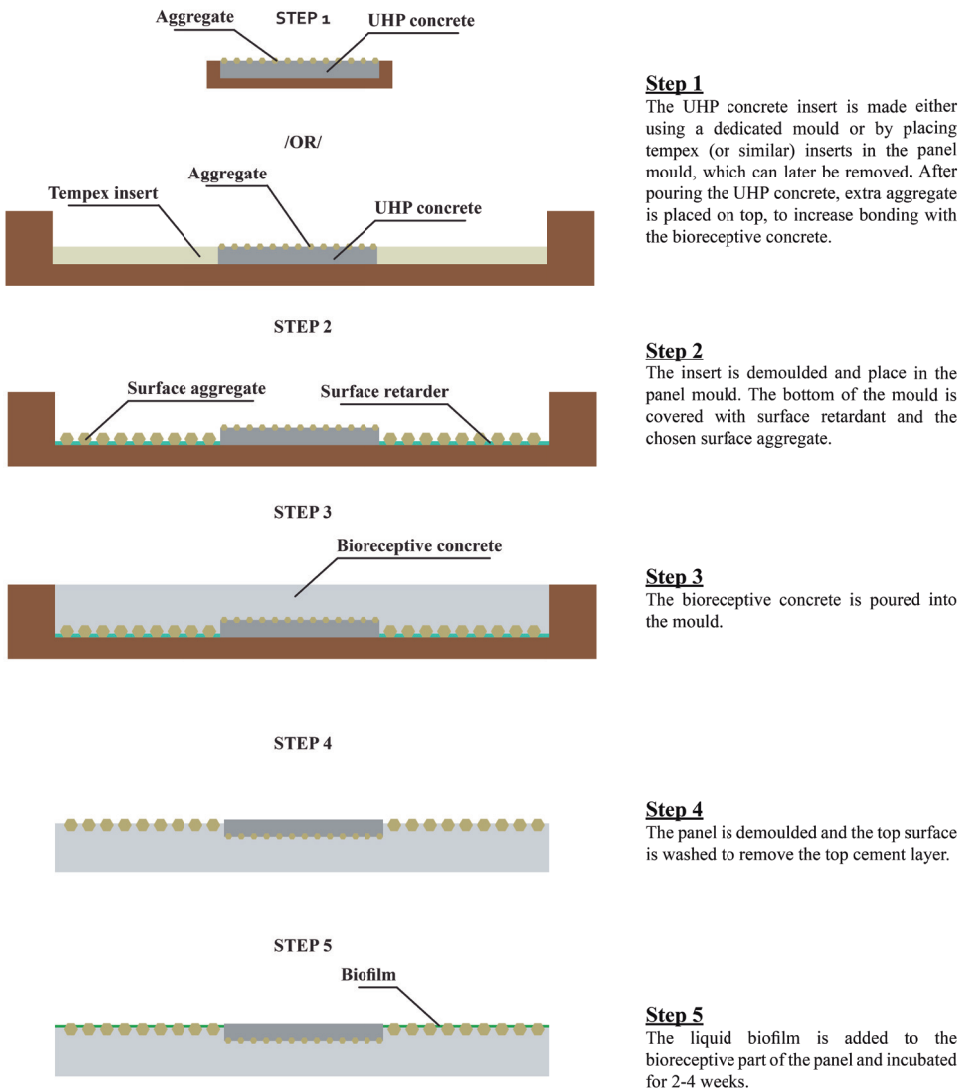

FIG. 3 Graphical overview of the panel production process

4 PANEL TESTING

4.1 RESULTS AND DISCUSSION

As a proof of concept, two prototype façade panels were made, one with CEC as a surface aggregate and one with limestone as an added surface aggregate. The production process is as discussed before (see also Fig. 3) and can be seen in Fig. 4. The mixtures used can be found in Table 3.

After inoculation these panels were kept under the same growing conditions as described in the methodology. It was found that after only 2 weeks under these conditions, the bioreceptive areas of the panels were almost fully covered (see Fig. 5). This shorter time to full colonisation as compared to the samples in our previous research, which were not yet fully covered after a period of 8 weeks, can likely be explained by the higher concentration of biofilm used for the inoculation of the panel and the higher surface area allowing for more refuges for the biofilm, acting as sources of biological growth.

It can also be seen that while the bioreceptive parts of the panel are fully covered, the non-bioreceptive part remains free from growth. Although this does not prove that this will remain so in the long-term, it does prove that the panel has the ability to direct growth, at least in the short-term.

The panels were then placed outside for a period of 1 week, to see how the biofilm responded to external conditions. During this period, the panels were placed on an exposed roof surface (height circa 12 metres). The surface was wetted twice daily, as discussed in the methodology. However, the rapid change in environmental conditions still proved too sudden and harsh for the biofilms, resulting in a significant deterioration of the biofilm (see Fig. 6).

Whilst the testing of the prototype panels under optimal growing conditions shows their ability to harbour and direct biological growth, the period spent outside shows that additional steps are necessary to make it a viable façade product. However, as the used biofilm was originally harvested from a biofilm growing under similar circumstances as those experienced by the panels on the exposed rooftop, this deterioration in the biofilm under exterior conditions cannot be caused by the fact that the organisms are inherently unable to grow under these exterior conditions, as they have done so before. There is also some evidence of a small recovery of the biofilm after 5 months, suggesting that the biofilm can grow under these conditions. Instead it likely has to do with the so-called 'lag-phase' microbial and algal organisms experience when a sudden change in environmental conditions takes place. This lag-phase is the period during which the biofilms cells adjust themselves to their new environment and no growth can take place, the duration of which is dependent on several factors, amongst which are the amount of change between environments, the type of cells, and the growth stage of the microbial cells (Swinnen, Bernaerts, Dens, Geeraerd, & Van Impe, 2004). This lag effect was also seen when the initial biofilm was harvested and added to a liquid growth medium, where it took a few days for exponential growth to start as the biofilm adjusted to its new environment. Based on this, if the environmental changes can be made to be more incremental, survivability of the biofilm will likely be higher, as it reduces the duration of this lag-phase.

FIG. 4 Overview of the production process of the prototype panels. (1) UHPC concrete is poured into the mould using tempex inserts. (2) Aggregate is added to the top of the UHPC. (3) Tempex inserts are removed. (4) Surface retarder and surface aggregate are added to the bottom of the mould. (5) Bioreceptive concrete is added on to the mould. (6) The panel is demoulded and washed. (7) Final prototype panels.

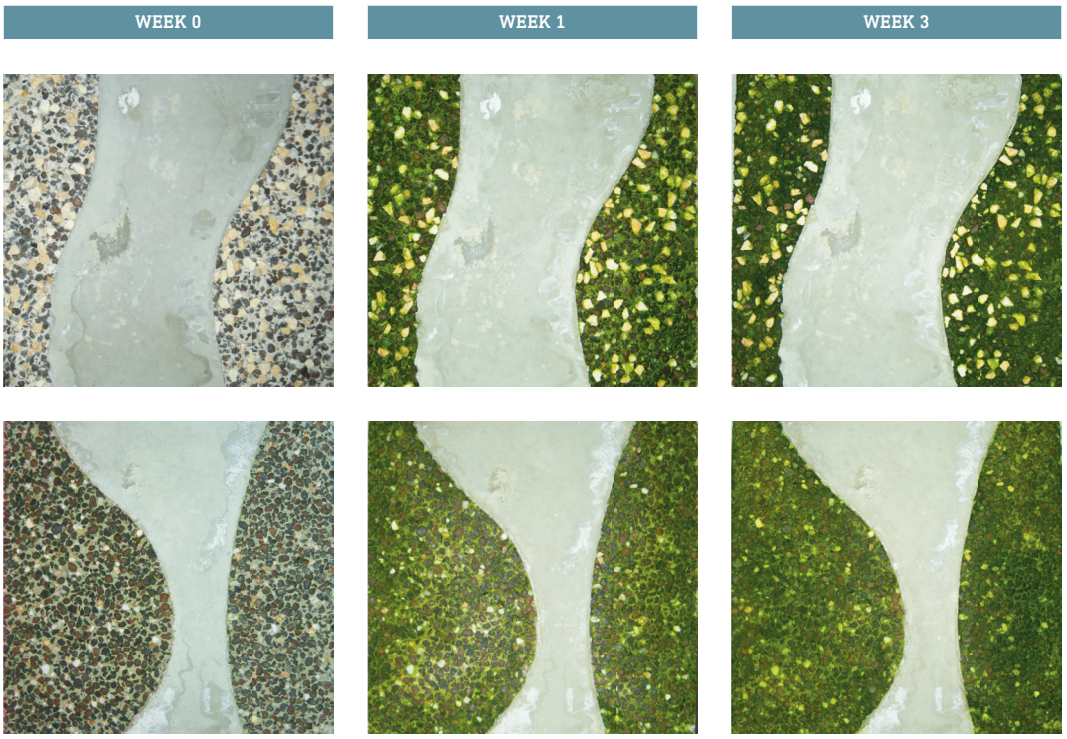

FIG. 5 Biofilm growth progression during the period under optimal growing conditions

FIG. 6 Photos taken at the start of the exterior part of the experiment, and after 1 week outside and 5 months outside

Something that plays a compounding factor in the poor survival is likely the lack of extracellular polymeric substances (EPS) in the biofilm. EPS are polymers produced by organisms in the biofilm and one of their functions is to mediate environmental extremes, thereby creating a more stable microclimate for the biofilm (Wolfaardt, Lawrence & Korber, 1999). However, under optimal growing conditions, such as those used to initially develop the biofilm on the prototypes, EPS will not be produced, as its energy requirements do not outweigh the benefits under those conditions (Wolfaardt, Lawrence, & Korber, 1999). Therefore the incremental environmental changes discussed in the previous paragraph could also stimulate the productions of EPS, as under suboptimal conditions the benefits of EPS production will start outweighing the associated costs.

5 CONCLUSION

The aim of this research was to investigate how bioreceptive concrete could be used within a building façade. In order to achieve this, a design was formulated, combining bioreceptive and non-bioreceptive, UHPC-based concrete within the same panel. This allows for biological growth to be directed, allowing for more design flexibility. This was also shown as a proof-of-concept in a prototype panel using the proposed design and production guidelines, resulting in a bioreceptive façade panel using commonly available construction materials. Based on the results from the growth tests it can be concluded that these prototypes can form the basis for a bioreceptive concrete façade application. And that the concept of bioreceptive façades may provide an alternative to contemporary green façades.

Not only that, the resulting growth shows that biological growth can be directed by combing bioreceptive and UHPC concrete within the same panel. The results also show that the necessary time for biofilm's initial development is relatively short and can be achieved within two weeks if sufficient biofilm material is applied at the start of the nursery period. However, whilst initial biofilm development is rapid and relatively straightforward, the short period under exterior conditions shows that further research is necessary.

The authors suggest that this future research encompasses three different aspects:

- **Ecology**
  This would include the development of a proper nursing regime in order to increase outdoor survivability, directing the type of growth that occurs on the panel (e.g. algae or moss) and finding the best organisms to use for the colonisation of the panels

- **Material**
  This would include optimising the mixture and topology, as well as possible ways of upscaling the production

- **Economy and secondary effects**
  This would include determining whether or not bioreceptive façades can compete with contemporary green façades in terms of costs and beneficial secondary effects, such as the reduction of the UHI effect and air pollution

Acknowledgements

We would like to thank Byldis B.V. and in particular Ellen van Genechten, Koen Spijkers, and Gerard Brood for helping us with the production of the prototypes used within this research.

References

Beatley, T., & Newman, P. (2013). Biophilic Cities Are Sustainable. *Sustainability, 5*(8), 3328-3345.

Charoenkit, S., & Yiemwattana, S. (2017). Role of specific plant characteristics on thermal and carbon sequestration properties of living walls in tropical climate. *Building and Environment, 115*, 67-79.

Freystein, K., Salisch, M., & Reisser, W. (2008). Algal biofilms on tree bark to monitor airborne. *Biologica, 63*(6), 866-872.

Gorbushina, A. A. (2007). Life on the rocks. *Environmental Microbiology, 9*(7), 1613-1631.

Guillitte, O. (1995). Bioreceptivity: a new concept for building ecology. *Science of the Total Environment, 167*(1-3), 215-220.

Guillitte, O. & Dreessen, R. (1995). Laboratory chamber studies and petrographical analysis as bioreceptivity assessment tools of building materials. *Science of the Total Environment, 167*(1-3), 365-374.

Johansson, O., Johansson, O., Giesler, R., & Palmqvist, K. (2011). Lichen responses to nitrogen and phosphorus additions can be explained by the different symbiont responses. *New Phytologist, 191*(3), 795-805. doi:10.1111/j.1469-8137.2011.03739.x

Jones, A. A., & Bennett, P. C. (2017). Mineral ecology: Surface specific colonization and geochemical drivers of Biofilm accumulation, composition, and phenology. *Frontiers in Microbiology, 8*(491).

Kleerekoper, L., Van Esch, M., & Salcedo, T. B. (2012). How to make a city climate-proof, addressing the urban heat island effect. *Resources, Conservation and Recycling, 64*, 30-38.

Lai, L., & Cheng, W. (2010). Urban Heat Island and Air Pollution—An Emerging Role for Hospital Respiratory Admissions in an Urban Area. *Journal of Environmental Health, 72*(6), 32-36.

Li, W., & Yeung, K. (2014). A comprehensive study of green roof performance from environmental perspective. *International Journal of Sustainable Built Environment, 3*(1), 127-134.

Mayaud, J. R., Viles, H. A., & Coombes, M. A. (2014). Exploring the influence of biofilm on short-term expansion and contraction of supratidal rock: An example from the Mediterranean. *Earth Surface Processes and Landforms, 39*(10), 1404-1412.

McCarthy, M. J., & Dyer, T. D. (2019). Pozzolanas and Pozzolanic Materials. In P. Hewlett, & M. Liska, *Lea's chemistry of cement and concrete* (5th ed., pp. 363-467). Oxford: Elsevier.

McKinney, M. L. (2008). Effects of urbanization on species richness: A review of plants and animals. *Urban Ecosystems, 11*(2), 161-176.

Miller, A. Z., Leal, N., Laiz, L., Rogeiro-Candelera, M. A., Silva, R. J., Dionisio, A., . . . Saiz-Jimenez, C. (2010). Primary bioreceptivity of limestones used in southern European monuments. In B. J. Smith, M. Gomez-Heras, H. A. Víles, & C. J, *Limestone in the Built Environment: Present-day Challenges for the Preservation of the Past* (pp. 79-92). London: Geological Society.

Mindness, S. (2019). Resistance of Concrete to Destructive Agencies. In P. Hewlett, & M. Liska, *Lea's chemistry of cement and concrete* (5 ed., pp. 251-283). Oxford: Elsevier.

Mostert, E. S., & Grobbelaar, J. (1987). The influence of nitrogen and phosphorus on algal growth and quality in outdoor mass algal cultures. *Biomass, 13*(4), 219-233. doi:10.1016/0144-4565(87)90061-8

Paine, K. A. (2019). Physicochemical and Mechanical Properties of Portland Cements. In P. Hewlett, & M. Liska, *Lea's chemistry of cement and concrete* (5 ed., pp. 285-339). Oxford: Elsevier.

Pentecost, A., & Whitton, B. A. (2012). Subaerial Cyanobacteria. In B. A. Whitton, *Ecology of Cyanobacteria II* (pp. 291-316). Dordrecht: Springer.

Perini, K., & Rosasco, P. (2013). Cost-benefit analysis for green façades and living wall systems. *Building and Environment, 70*, 110-121.

Prieto, B., & Silva, B. (2005). Estimation of the potential bioreceptivity of granitic rocks from their intrinsic properties. *International Biodeterioration & Biodegradation, 56*(4), 206-215.

Shi, C., Wu, Z., Xiao, J., Wang, D., Huang, Z., & Fang, Z. (2015). A review on ultra high performance concrete: Part I. Raw materials and mixture design. *Construction and Building Materials, 101*, 741-751.

Swinnen, I. A., Bernaerts, K., Dens, E. J., Geeraerd, A. H., & Van Impe, J. F. (2004). Predictive modelling of the microbial lag phase: A review. *nternational Journal of Food Microbiology, 94*(2), 137-159.

Tiano, P., Accolla, P., & Tomaselli, L. (1995). Phototrophic biodeteriogens on lithoid surfaces: An ecological study. *Microbial Ecology, 29*(3), 299-309.

Vázquez-Níon, D., Silva, B., & Prieto, B. (2018). Influence of the properties of granitic rocks on their bioreceptivity to subaerial phototrophic biofilms. *Science of the Total Environment, 610-611*, 44-54.

Veeger, M., Prieto, A., & Ottelé, M. (2021). Making bioreceptive concrete: formulation and testing of bioreceptive concrete mixtures. *Manuscript under review*.

Wang, D., Shi, C., Wu, Z., Xiao, J., Huang, Z., & Fang, Z. (2015). A review on ultra high performance concrete: Part II. Hydration, microstructure and properties. *Construction and Building Materials, 96*, 368-377.

Wiktor, V., De Leo, F. U., Guyonnet, R., Grosseau, P., & Garcia-Diaz, E. (2009). Accelerated laboratory test to study fungal biodeterioration of cementitious matrix. *International Biodeterioration & Biodegradation, 63*(8), 1061-1065.

Wiktor, V., Grosseau, P., Guyonnet, R., & Garcia-Diaz, E. L. (2010). Accelerated weathering of cementitious matrix for the development of an accelerated laboratory test of biodeterioration. *Materials and Structures, 44*(3), 623-640.

Wolfaardt, M., Lawrence, J. R., & Korber, D. R. (1999). Function of EPS. In J. Wingender, T. R. Neu, & H. Flemming, *Microbial Extracellular Polymeric Substances: Characterization, Structure and Function* (pp. 171-200). Berlin: Springer Science & Business Media.

Zhang, T., & Klapper, I. (2010). Mathematical model of biofilm induced calcite precipitation. *Water Science and Technology, 61*(11), 2957-2964.

Photovoltaic Warm Façades with Phase Change Materials in European Climates

Christian Popp[1*], Dirk Weiß[2], Katja Tribulowski[2], Bernhard Weller[1]

* Corresponding author
1 Technische Universität Dresden, Institute of Building Construction, Dresden, Germany, christian.popp1@tu-dresden.de
2 Technische Universität Dresden, Institute of Building Climatology, Dresden, Germany

Abstract

Since façade-integrated photovoltaic (PV) modules heat up greatly, which reduces the efficiency of the PV, façade panels with PV and phase change materials (PCM) were developed. PCMs absorb a significant amount of thermal energy during the phase transition from solid to liquid, while maintaining a specific melting temperature. This cools down the PV and increases the electrical yield. Numerical studies on PV-PCM warm façades without rear-ventilation have so far been missing. Therefore, a thermal and an electrical simulation model for PV-PCM warm façades were developed and validated. They were then used to analyse the yield increase of two PCM-types and -quantities in PV warm façades facing east, south, and west in Athens, Potsdam, and Helsinki. An annual yield increase of 1.2% to 8.5% for monocrystalline PV modules was determined. The maximum monthly yield increase is 8.0% in Helsinki, 11.4% in Potsdam, and 11.3% in Athens. The study shows that a case-specific selection of the appropriate type and quantity of PCM is necessary. Using the models, a design tool for PV-PCM warm façades will be developed. It will be validated with real monitoring data from PV-PCM façade test rigs at the Technische Universität Dresden and the National Technical University of Athens.

Keywords

Building-integrated photovoltaics, efficiency increase, phase change materials, thermal simulation, yield simulation

10.7480/jfde.2021.1.5513

1 INTRODUCTION

1.1 PHOTOVOLTAIC FAÇADES

As buildings account for nearly 40% of the total energy consumption in Europe, new buildings built from 2021 onwards need to be nearly-zero energy buildings (NZEBs) within the European Union. These NZEBs are energy efficient buildings sourcing locally renewable energies to reduce the energy consumption of the existing building stock (European Commission, 2016).

Building-integrated photovoltaic (BIPV) is an excellent method to achieve this, as it provides renewable energy on-site. Fath (2018) determined a theoretical photovoltaic (PV) potential of 37,700 km^2 of usable building surfaces with sufficient irradiation for BIPV applications for 2015 in Germany – 65% (24,505 km^2) of these areas are façade surfaces. Considering the irradiation, current PV technologies, and plant efficiencies, a theoretical electrical potential of 2,923 TWh can be generated with the whole BIPV potential; 44% (1,286 TWh) of this can be generated through façade applications (Fath, 2018). This theoretically available PV façade potential would be enough to feed the total electricity demand of Germany in 2019, which amounts to 575 TWh (Wilke, 2020), twice. However, the actual number of BIPV applications in façades these days is still low. In 2017, the share of BIPV applications in the total number of PV installations in Europe was estimated to be 2% (Ullrich, 2018).

This low proportion is probably due to some of the disadvantages of using PV on façades. In addition to the lower irradiation compared to inclined PV modules, possible shading situations, and higher reflection losses, the thermal coupling to the building is a decisive factor that must be taken into account when planning façade integrated PV systems (Decker, Grimmig, Mencke & Stellbogen, 1998). Regarding the thermal coupling to the building, one can differentiate between *warm façades* and *cold façades*, which differ in the location and thermal coupling of their outermost layer of the façade (Engin et al., 2016). Accordingly, rear-ventilated façades or double skin façades are called *cold façades*, since the façade cladding is ventilated and thermally decoupled. Wall constructions with thermal insulation composite systems, mullion-transom, or unitized façades are considered *warm façades*, since the façade cladding is in contact with the "warm" interior of the building (Engin et al., 2016; Krippner et al., 2016).

According to Weller, Hemmerle, Jakubetz, and Unnewehr (2009), freely mounted PV modules heat up to 22 K above the ambient temperature. Due to the temperature-dependent performance decrease of photovoltaics, the annual yield of these systems is decreased by 2.0% compared to a PV system running permanently under optimal conditions. For good ventilated *cold façades* temperatures of up to 35 K above the ambient temperature are reached, whereby the annual electrical yield is decreased by 6.0%. The constructional integration of PV modules into the opaque areas of *warm façades* like mullion-transom or unitized façades leads to module temperatures of up to 55 K above the ambient temperature due to missing rear-ventilation. These high temperatures lead to a reduction of the annual electrical yield by 10.5%. Because of this, PV integration into mullion-transom or unitized façades is usually considered unfavourable, even though it comes with constructional benefits: The glasses are supported on all sides linearly, the junction box and cables are hidden in the construction, and regular grid dimensions of mullion-transom façades can lead to more cost-efficiency by series production of the PV façade panels (Weller et al., 2009).

1.2 PHOTOVOLTAIC FAÇADES WITH PHASE CHANGE MATERIALS

One way to reduce the temperature of PV in façades and to increase the electrical yield is to combine the PV modules with phase change materials (PCM). The PCMs absorb a lot of energy during the phase transition from solid to liquid while maintaining their melting temperature and thereby keeping the PV cool and the electrical efficiency high. When the environment cools down and the PCM reaches the freezing temperature, it solidifies and recrystallizes again while transferring the thermal energy to the environment (Horn, Seeger, Scheuring & Weller, 2017).

The integration of PV and PCM in the façade is not a novelty. Giuseppina, Brano, Cellura, Franzitta, and Milone (2012); and Huang, Eames, and Norton (2004) analysed the combination of PV and PCM and developed thermal numerical models, which were validated through comparison with experiments. These models provided the possibility to reproduce the melting process and the thermodynamic behaviour of PCMs. A 1D transient model based on the enthalpy method is presented and validated by Elarga, Goia, and Benini (2017) to analyse the thermal behaviour of a ventilated PV-PCM double skin façade. Depending on the ventilation strategy in the double skin façade, it showed a positive effect of the PCM on the cooling and heating loads. Other similar façade constructions with rear-ventilated PV-PCM systems are analysed numerically and with experimental studies. Aelenei, Pereira, Gonçalves, and Athienitis (2014) combined a PV module with a PCM gypsum board and a ventilation gap between both components to pre-heat the air for space heating. Čurpek and Cekon (2020) analysed a similar system, in which aluminium PCM containers are attached to the rear side of the PV modules and the ventilation gap follows after the PCM containers. Wieprzkowicz, Knera and Heim (2015) presented a numerical study on four organic PCMs in a system with an identical ventilation situation but the PCMs are encapsulated in aluminium honeycomb structures. They concluded that dynamic climate data, location, and orientation of the PV-PCM system are decisive for the right choice of the specific melting temperature and thereby for the choice of a specific type of PCM. Čurpek and Cekon (2020) also point out that there are still difficulties in choosing the right type of PCM depending on the location.

The main research interest focuses on rear-ventilated PV-PCM façades (*cold façades*), which use PCMs both to condition the air for heating buildings and to increase the PV yield. For one of these systems, Wieprzkowicz et al. (2015) determine an average annual PV yield increase of 0.25% by the PCM. The reason for this low yield increase could be the already favourable temperature conditions of PV in rear-ventilated systems, as mentioned in section 1.1. A greater effect of the PCMs and a higher yield increase can be achieved by adding PCM in PV *warm façades*. Here, the basic system reaches higher temperatures, which reduces the annual electrical yield by 10.5% (Weller et al., 2009). These bigger losses provide more potential to be compensated by the PCM. A mullion-transom façade system combining PV modules with encapsulated PCM was developed and monitored by Horn et al. (2017). The monitoring from March to October showed an efficiency increase of 3.4% for thin-film cadmium telluride (CdTe) PV modules. For crystalline PV modules the increase is expected twice as high. Further studies on the influence of PCMs on the PV yield increase of *warm façades* and more information about the location-specific selection of the right type and quantity of PCM are missing. New findings could help to enhance the number of PV façade applications.

This paper addresses the achievable yield increase and its façade-specific influencing factors of PV-PCM *warm façades* without ventilation. PCM capsules are mounted on the rear side of the PV modules, followed by insulation. In this paper, a dynamic thermal simulation model and a PV yield simulation model are presented to analyse the temperature behaviour and the electrical yield of these PV-PCM *warm façades*.

The models are validated and used for a study on the efficiency increase of two types of PCMs in PV-PCM *warm façades*. Different European climates, different façade orientations, and two different PCM quantities are analysed.

2 METHODS

2.1 PCM MATERIAL MODEL FOR THERMAL SIMULATION SOFTWARE

Different PCMs vary in their melting points. Fig. 1 shows the increase of enthalpy of four PCMs, melting at 31 °C (SP31), 26 °C (SP26E), 21 °C (SP21EK) and 15 °C (SP15) on the left. On the right monitoring results from a recently installed PV-PCM test rig at *Technische Universität Dresden* (*TU Dresden*) are shown. The effect of two different PCMs, SP26EK and SP31 (melting at 26 °C resp. 31 °C), on the temperature of the PV modules is visible. The melting point of the PCMs defines the temperature stage where the enthalpy increases and the cooling is usable.

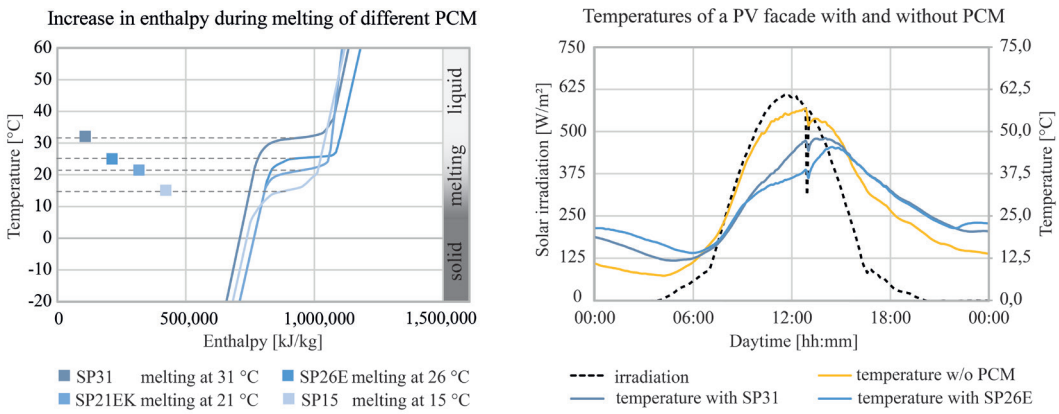

FIG. 1 Increase of enthalpy during melting of different PCMs (left) and the cooling effect of this enthalpy increase on the temperatures of a PV façade system, monitored at a test rig at TU Dresden (right).

To analyse the thermal behaviour of PCMs, a dynamic enthalpy model for the integration into the thermal simulation software *DELPHIN* was developed. The model works with the following basic assumptions and physical equations:

- The change in the internal energy of a body is proportional to the change in temperature and to the mass of the body, which usually remains constant. It is described by the specific heat capacity c_p $[J/(kg \cdot K)]$.
- The internal energy U depends on the mass m, the specific heat capacity c_p and the temperature T. It is described with the equation (1):

$$U = m \cdot c_p \cdot T \qquad (1)$$

— The change of the internal energy by change of temperature is described with the equation (2):

$$\Delta U = m \cdot c_p \cdot \Delta T \tag{2}$$

— In order to change the state of aggregation, energy must be added or withdrawn. The energy required for this depends on the material (specific melting/boiling energy E_m or E_b [*kJ/kg*]) and the mass of the body.
— The change in internal energy that is required for a change in the state of aggregation is described by (3):

$$\Delta U_{phase\ change} = m \cdot E_{m/b} \tag{3}$$

— This must be added to the internal energy if a change of the state of aggregation has occurred (4):

$$U = m \cdot c_p \cdot \Delta T + \Delta U_{phase\ change} \tag{4}$$

In order to model the abrupt change of the internal energy during the transition of the state of aggregation of PCMs, the function of the specific heat capacity of a standard material was virtually changed. An offset for the phase change was implemented in the function, which normally depends linearly on the temperature. This offset reproduces the change in the internal energy of the PCMs during melting resp. solidification, as shown in Fig. 1 (left). To create this function, the thermal characteristics given on the PCM data sheets of the suppliers are fed into the PCM material model. The course of the internal energy of the PCMs is determined gradually. According to equation (1) the inner energy at absolute zero point is zero. From this point on, the course of the internal energy is calculated for the different states of aggregation, with their temperature-specific material parameters. The internal energy of the preceding temperature stages is increased by the internal energy of the following temperature stages (5):

$$U_{(n+1)} = m \cdot c_{p,n+1} \cdot (T_{(n+1)} - T_{(n)}) + U_n \tag{5}$$

Besides typical material parameters, like density, specific heat capacity, and thermal conductivity, the function for the thermal storage behaviour is implemented in a material file of the thermal simulation software. The function replaces the generally given material parameters during the transition of the state of aggregation. Thus, the enthalpy function as shown in Fig. 1 (left) is reproduced in the model.

2.2 ELECTRICAL YIELD CALCULATION

The electrical yield calculation is based on the one-diode model. To model the dynamic relationship between the current and voltage of PV modules, the voltage-current characteristic curve needs to be determined. The manufacturer's data sheets provide three points on this characteristic curve (short-circuit current, open-circuit voltage and maximum power point). A system of equations, according to Dobos (2012), is used to determine the missing parameters for calculating the dynamic values of current and voltage. The dynamic current-voltage curve can then be fully mapped and the electrical PV power can be calculated for each time step, depending on temperature and irradiation (Dobos, 2012; Hansen, 2015).

The module temperature and the irradiation on the surface of the PV module are determined using the thermal simulation software, which uses data from climate files (e.g. epw-files).

3 STUDY ON PV-PCM WARM FAÇADES IN EUROPEAN CLIMATES

3.1 METHODOLOGY

To analyse the effect of different PCMs and their quantities on the electrical output of differently located and oriented PV *warm façades,* the developed PCM material model, the thermal simulation software *DELPHIN*, and the one-diode model were used. Fig. 2 (left) shows the main components of the PV-PCM *warm façade* and the simplified simulation model. The capsule contains fins for higher thermal contact surface to the PCM. The mullion resp. transom is not modelled, as prior studies determined its influence on the results is less than 0.5% and in doing so, the simulation time was reduced significantly. The electrical yield calculations consider a PV module with 60 cells of monocrystalline silicon (aleo Solar SL19 270). The material data of the analysed PCMs is shown in Table 1.

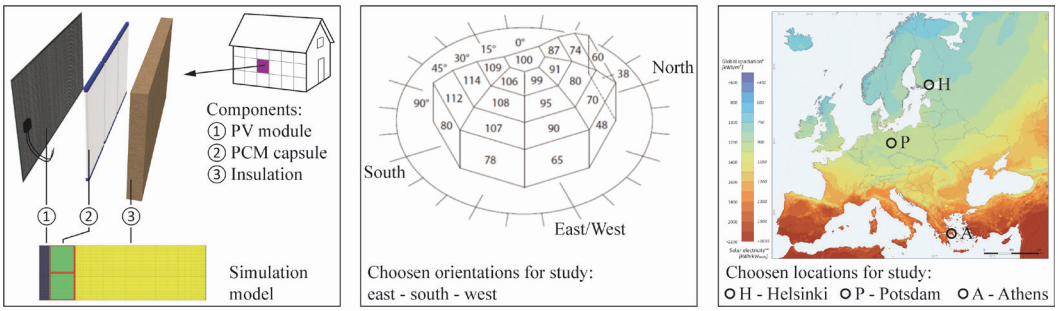

Main components of PV-PCM facade and thermal simulation model

Intensity of solar radiation depending on orientation

Global irradiation for different locations © European Union, 2012 - PVGIS

FIG. 2 Schematic layout of the PV-PCM façade and influence of the orientation and location on the solar irradiation

The proper functionality of all three models was tested first. The thermal simulation and the material model were compared to real test results. For the electrical tool, a comparison to a commercial PV planning software (*PV*SOL*) was carried out. In a second step, yield simulations with long-term average climate data were carried out for two types of PCM (SP21EK and SP31 from the company *Rubitherm GmbH*) in east-, south-, and west-facing PV-PCM *warm façades* for Helsinki, Potsdam, and Athens, as shown in Fig. 2 (centre and right). The thickness of the PCM capsules was increased from 10 mm to 20 mm in a third step for both PCMs and all orientations and locations.

TABLE 1 PCM parameters of the simulations

PCM	SP21EK	SP31	
melting range	22 - 23	31 - 33	[°C]
density	1,3 - 1,35	1,4 - 1,5	[kg/l]
thermal conductivity	~ 0.5	~0.5	[W/(m K)]
specific heat storage capacity	2	2	[kJ/(kg K)]
heat storage capacity during phase change	170 (at 13 °C to 28 °C)	210 (at 23 °C to 38 °C)	[kJ/kg]
thickness PCM	10, 20	10, 20	[mm]

3.2 VALIDATION OF THERMAL SIMULATION MODEL

First, a simulation model of a PV mullion-transom façade without PCM was developed and compared to real monitoring values from a PV façade without PCM at a test rig at TU Dresden. In the simulation model, the real climate data gathered from the monitoring were implemented. Fig. 3 shows the temperature curves of the simulation and the monitoring for January, May, and August. The comparison of the temperature curves shows a good correspondence, especially in the months with high irradiation (spring to summer). The higher deviations in January are probably caused by the albedo. This was assumed constantly at 0.2 in the simulation, but is variable in reality and can increase to values of 0.8 in case of snow. The total annual average deviation between simulation and monitoring is 2.66 K. This is considered to be sufficiently low for further analyses.

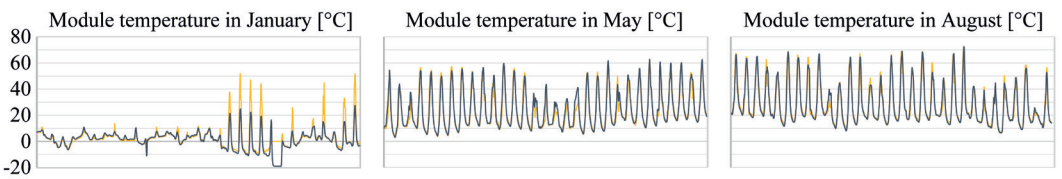

FIG. 3 Temperature curves of simulation and monitoring for January, May, and August

3.3 VALIDATION OF THE PCM MATERIAL MODEL

For the validation of the PCM material model, a quality test from production control of the PCM supplier and developer was simulated. During this *three-layer calorimeter test*, a chilled PCM sample is put into an insulated box, which is placed in a heat cabinet. The heat cabinet runs a temperature curve depending on the melting point of the PCM. The temperature in the middle of the

PCM sample is recorded. Fig. 4 shows the setup of the test schematically (left) and proves that the simulation model can reproduce the temperature curve of the real test properly (right). The short-term "sub cooling" of the PCM, which is indicated by a local minimum before solidification, after approximately 1000 minutes at SP21EK and 1600 minutes at SP31, is not reproduced by the PCM model. The reason for this is found in an asymmetry between the melting and the solidification process of PCMs in reality. This hysteresis is not implemented in the model, because the model assumes a symmetrical course for the melting and the solidification process. However, the relevant melting process, which happens when the solar energy is converted into electricity by the PV, is reproduced properly. Therefore, the PCM material models are considered sufficiently accurate for the analysis of the PV yield.

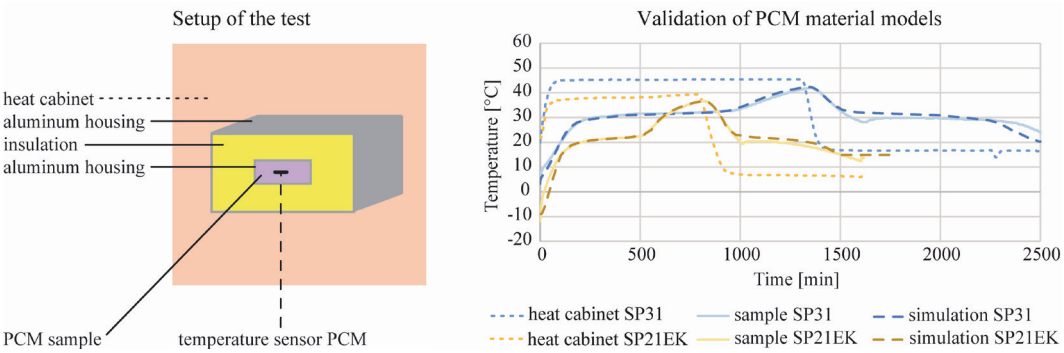

FIG. 4 Schematic sketch of production control test (left) and temperature curves of simulation and real tests for validation of PCM material models of SP31 and SP21EK (right)

3.4 VERIFICATION OF THE ELECTRICAL YIELD CALCULATION TOOL

The electrical yield calculation (hereafter called "PV-Tool") was verified by comparing it to commercial state-of-the-art PV planning software. The input parameters, boundary conditions, and analysed systems were identical. To cover different environmental influences, the simulations were carried out for monocrystalline PV systems in *warm façades* without PCM in Helsinki, Potsdam, and Athens, each with east, south, and west orientations. Fig. 5 shows the monthly deviation (left) and the total annual deviation (right) between the PV-Tool and the commercial software for all locations and orientations. During the months with high irradiation (April to October), the simulations show a good match with low deviations between -7% to +9%. The maximum deviation within one single month appears in Helsinki in December with -25%. For Potsdam and Helsinki, the maximum deviation is in the winter months, when the irradiation is low. Over the whole year, only small deviations between the simulations exist. The deviations are below 1% in Potsdam, below 2% in Helsinki, and below 4% in Athens.

A validation based on real measured data will help to better evaluate the accuracy of the electrical yield calculation model. A sensitivity analysis with focus on situations with low radiation, a high percentage of diffuse radiation, and high reflections can help to make an assessment of possible weak points.

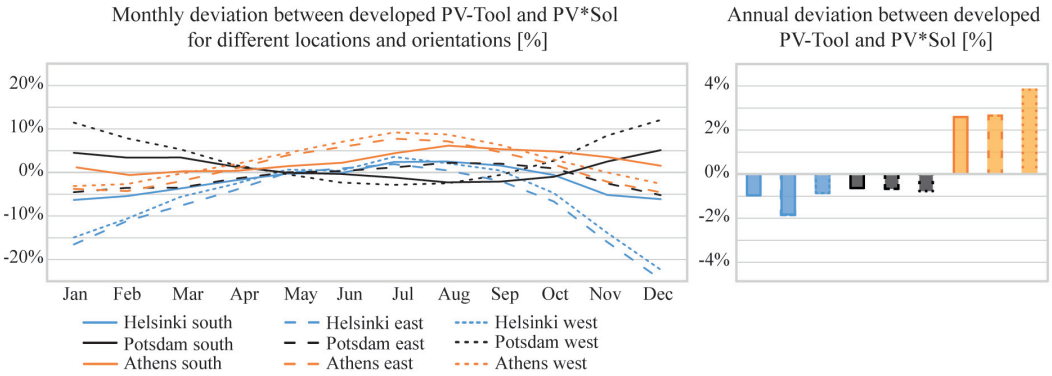

FIG. 5 Monthly (left) and total (right) deviation between electrical yield calculation model and PV planning software

3.5 ELECTRICAL YIELD HELSINKI

Helsinki is located at 60 degrees latitude and reaches a maximum sun elevation angle of 53.3° in summer. This means that the reflection losses are low in summer and only visible in the results of the south façade in June. All orientations have their yield maximum and the maximum efficiency increase by the PCMs in summer. At this time of the year, the south façade in Helsinki reaches higher yields than the façades in Potsdam and Athens. In the winter months, the yield is barely increased because the melting temperature of the PCMs investigated is rarely reached. Overall, the annual yield on the east and south façade is comparable to that of Potsdam. Fig. 6 shows the electrical output and its increase through the analysed PCMs in 10 mm and 20 mm thick capsules for east, south, and west façades.

The yield increase of the PCMs reaches a minimum of 0.1% with 10 mm of SP31 in December on the east façade and a maximum of 8.0% with 20 mm of SP21EK in August on the south façade. From November to February, the two PCMs achieve additional yields over 1.0% only on the south façade. On the west façade, this is only possible with 20 mm of SP21EK. All other variants show low additional yields below 1.0% in this time. The average additional yield between November and February for 20 mm of SP21EK is 0.7% (east), 2.6% (south), and 1.1% (west). In these variants, 20 mm of SP31 achieve 0.5% (east), 1.8% (south), and 0.9% (west). During the period of high irradiation, from March to October, the SP21EK in 20 mm capsules achieves additional yields of 3.5% (east), 6.6% (south), and 4.7% (west), while the SP31 produces 1.7% (east), 3.8% (south), and 2.7% (west).

Thus, depending on the orientation, the SP31 achieves about half of the yield increase in summer and about one fifth to one third of the yield increase in winter, compared to the SP21EK. It is also found that the 10 mm of SP21EK achieves a higher annual yield than the doubled quantity of 20 mm of SP31 at all orientations. Due to the lower melting point of the SP21EK, the cooling effect starts earlier, in all orientations in the summer months. Doubling the PCM capsule thickness to 20 mm leads to a further yield increase from 33% to 51%, depending on the orientation of the façades. A PCM with a melting point below SP21EK or between SP21EK and SP31 might achieve a higher increase. Since the albedo was constant during the simulation, higher irradiation values on the façade could occur in reality in winter. As a result, the PV output in winter and its increase due to the PCM could also be slightly higher.

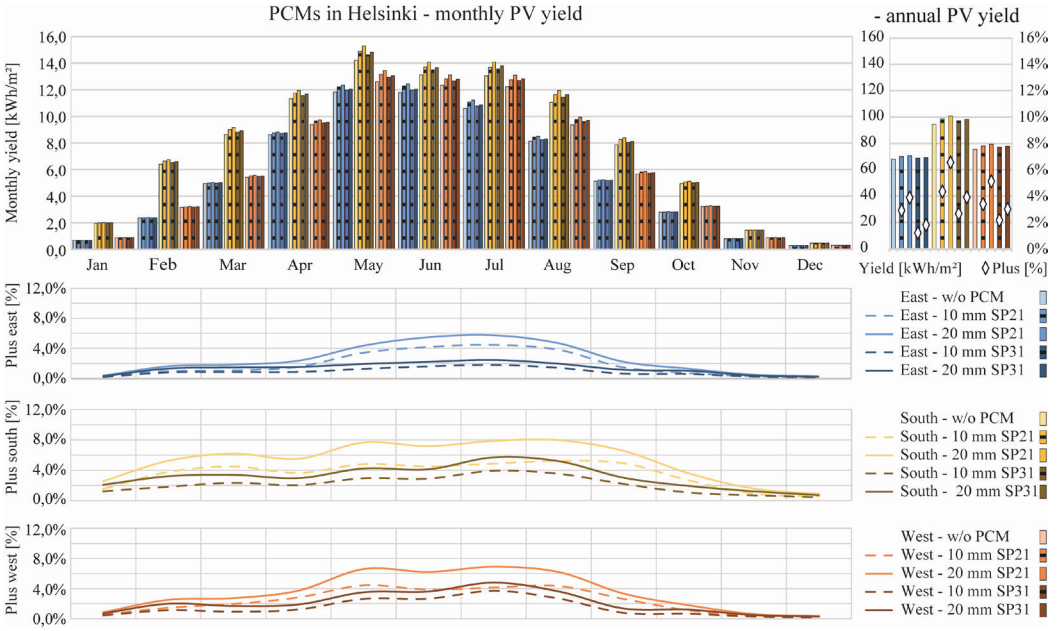

FIG. 6 Monthly electrical output of a PV warm façade without and with PCM in Helsinki (top - left), absolute and relative annual PV yield (top - right) and monthly yield increase for all three orientations and both PCMs (bottom)

3.6 ELECTRICAL YIELD POTSDAM

Potsdam is located at 52 degrees latitude and reaches a maximum sun elevation angle of 62.0° in summer. This results in higher reflection losses on the south façade in summer compared to Helsinki. The east and west façades are not affected by this and reach their maximum in summer. The minimum yield increase by the PCMs in Potsdam is 0.3% with 10 mm of SP31 in east orientation in December. A maximum increase of 11.4% is reached with 20 mm of SP21EK in September on the west façade. Fig. 7 shows the results for the analysed PCMs, capsule dimensions, and orientations.

With both PCMs, an efficiency increase is possible even in the winter months. The average additional yield between November and February for 20 mm of SP21EK is 1.0% (east), 5.6% (south) and 3.0% (west). For these variants, 20 mm of SP31 achieve 0.8% (east), 3.6% (south), and 2.2% (west). During the time with higher irradiation, from March to October, the SP21EK in 20 mm capsules achieves additional yields of 4.4% (east), 8.7% (south), and 9.1% (west), while the SP31 gains 2.5% (east), 6.0% (south), and 7.6% (west) extra yield in this period.

Thus, depending on the orientation, the SP31 in Potsdam achieves 17% to 43% less efficiency increase in summer and 20% to 35% less efficiency increase in winter than the SP21EK. Only on the west façade in June, July, and August, the yield increase of the SP31 is, at 6%, slightly higher than that of the SP21EK. As the SP21EK melts earlier than the SP31 during the course of a day in summer, less cooling potential is available when the sun shines on the west façade in the afternoon. Nevertheless, all variants show that the SP21EK achieves a significantly higher annual yield increase than the SP31. Again, the melting point at 21 °C, and thus the cooling effect of the SP21EK, can be used more often throughout the year. On the east façade, the annual yield of 10 mm of SP21EK is higher than the yield of the doubled amount of 20 mm of SP31. On the south façade, 10 mm of SP21EK and 20 mm of SP31 reach almost the same yield. Only on the west façade, the 20 mm of SP31 produces significantly more yield than 10 mm of SP21EK. In Potsdam, a doubling of the

PCM capsule from 10 mm to 20 mm leads to a further yield increase of 26% to 63% depending on the façade orientation. PCMs with a melting point between the two PCMs could be analysed for further potential.

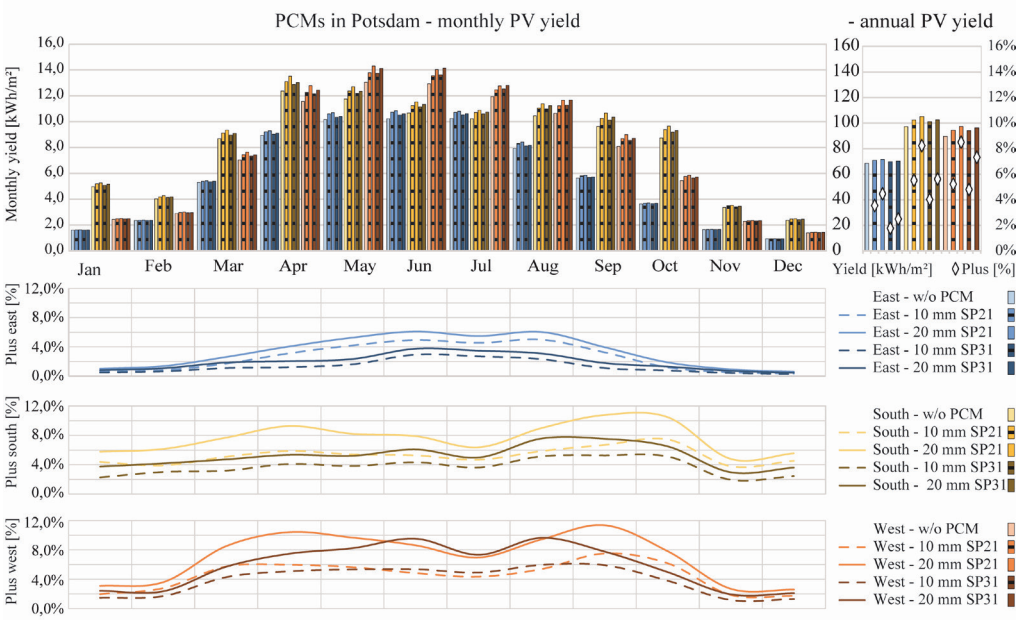

FIG. 7 Monthly electrical output of a PV warm façade without and with PCM in Potsdam (top - left), absolute and relative annual PV yield (top - right), and monthly yield increase for all three orientations and both PCMs (bottom)

3.7 ELECTRICAL YIELD ATHENS

Athens is located at 37 degrees latitude and reaches a sun elevation angle of 45° as early as March. The angle increases to a maximum sun elevation angle of 75.5° in June. As early as April, yield losses due to reflection losses on the south façade become apparent, which continue until August. The east and west façades reach their typical maximum in summer. Fig. 8 shows the output and its increase in Athens for the analysed PCMs, capsule dimensions, and orientations.

Both PCMs generate additional yields throughout the year. The lowest efficiency increase of the PCM in Athens is 0.9% with 10 mm of SP31 in the east orientation in December, while the maximum efficiency increase of 11.3% is achieved with 20 mm of SP31 in September on the south façade. The additional yield of 20 mm SP21EK from October to May averages at 5.1% (east), 9.6% (south), and 6.8% (west) and is higher than for 20 mm of SP31 with 2.7% (east), 6.6% (south), and 4.4% (west). Depending on the orientation, the SP31 thus achieves 31% to 47% less efficiency increase than the SP21EK in these months. From June to September, however, the SP31 is more productive in all façade orientations. Here, 20 mm of SP21EK achieves an average yield increase of 4.7% (east), 4.1% (south), and 4.4% (west) and 20 mm of SP31 achieves 8.2% (east), 8.9% (south), and 10.2% (west). This means that the SP21EK achieves 43% to 57% less yield increase than the SP31 in these months. In the summer months, temperatures in Athens are so high that the SP21EK melts too early in the course of the day or cannot recrystallize completely during night. Therefore, SP21EK in summer in Athens only reaches a lower cooling and a lower additional output. This can be

seen in all façade orientations between May and October. A similar phenomenon can be observed with 10 mm SP31, especially in the south and west orientation. Doubling the quantity of SP31 to 20 mm helps to reach sufficient enthalpy capacity to achieve a significantly higher efficiency increase between May and September.

For Athens, it can be concluded from the results that SP21EK and SP31 lead to comparable efficiency increase. On the east and south façades, the additional yield of SP21EK in the cooler phase of the year is equal to the additional yield of SP31 in the warmer phase of the year. On the west façade, SP31 has a significant increase in additional yield of 0.9 (for 10 mm) and 1.4 (for 20 mm) percentage points compared to SP21. Doubling the PCM capsule thickness leads to a further yield increase of 32% to 61% in Athens, depending on the orientation. Further potential can probably be achieved by a PCM with a melting point somewhere between the two PCMs investigated.

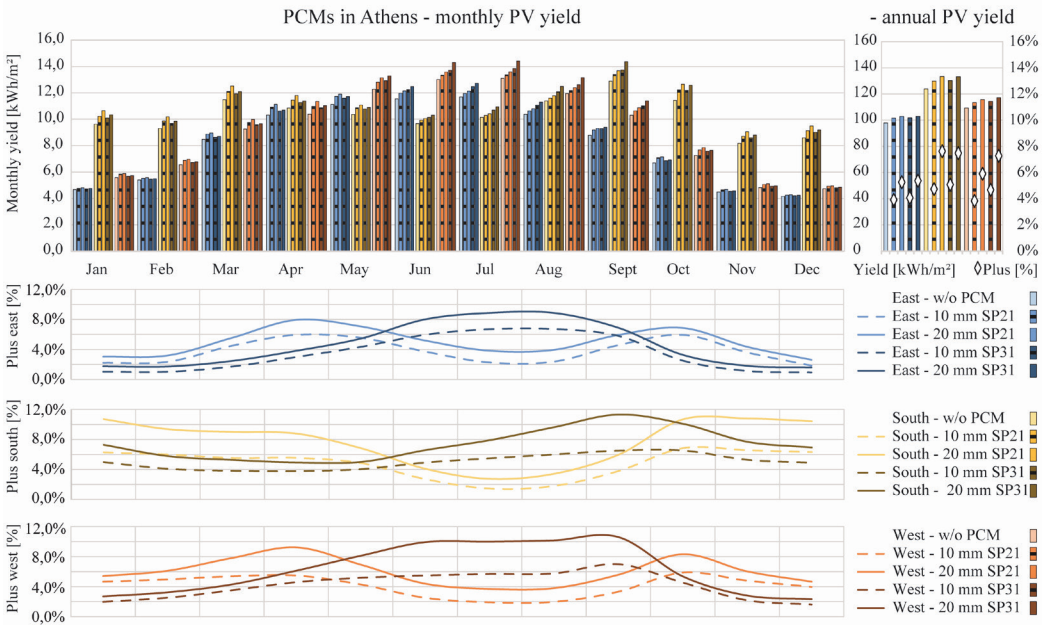

FIG. 8 Monthly electrical output of a PV warm façade without and with PCM in Athens (top - left), absolute and relative annual PV yield (top - right), and monthly yield increase for all three orientations and both PCMs (bottom.

4 DISCUSSION

The study shows that the combination of the analysed PCMs and monocrystalline PV modules in east-, south-, and west-oriented façades in Helsinki, Potsdam, and Athens leads to an annual yield increase of 1.2% to 8.5%. In the moderate climates (Helsinki and Potsdam), SP21EK proved to be more productive. In Helsinki, the SP21EK performed better than the SP31, regardless of the orientation of the façade. All year round, the most productive combination is 20 mm of the SP21EK on the south façade, achieving a yield increase of 6.6%. In Potsdam, the SP21EK is more productive than the SP31 and reaches a maximum annual yield increase of 8.5% with 20 mm capsules on the west façade. In the Mediterranean climate, the higher melting point of SP31 achieves comparable or even higher results than the SP21EK. In Athens, it was found that the optimal type of PCM changes over the course of the year and depends on the orientation and quantity of PCM. Throughout the

year, 20 mm of SP21EK achieves the highest additional yield of 7.6% on the south façade. At 7.5%, 20 mm of SP31 reaches almost the same amount in this orientation. The SP21EK achieves the highest increase in spring and autumn while the SP31 is more productive in summer. Utilising this, it becomes possible to selectively support the yield increase in a certain phase of the year, when the electricity demand is higher (e.g. spring and autumn).

For all orientations in Helsinki and for the east and south orientations in Potsdam, it was found that 10 mm of SP21EK reaches higher yields than the double amount (20 mm) of SP31. According to this, by choosing the right PCM, the required quantity can be greatly reduced. Results also show that doubling the quantity of PCM from 10 mm to 20 mm results in a further yield increase between 26% and 63% for the analysed variants. An increase in the quantity of PCM will therefore increase the costs proportionally, but the yield will only increase on a diminishing scale. Since the cost of the PCMs and the reachable additional yield are crucial decision factors for the realisation of PV-PCM *warm façades*, location and orientation dependent dimensioning is necessary. The analysis of further PCMs will also offer additional possibilities for yield increase.

5 CONCLUSION AND PROSPECT

This work focuses on the integration of PCMs in PV *warm façades*. The achievable yield increase of these systems depending on location, orientation, and PCM type and quantity was analysed for the first time. It was shown that PV-PCM *warm façades* achieve a significantly higher average annual PV yield increase (e.g. 8.5% in Potsdam, south oriented), compared to rear-ventilated PV-PCM façades (0.25% (Wieprzkowicz et al., 2015)). This makes the use of PCMs in PV *warm façades* attractive. Simulation models were developed and validated. A numerical study with these models showed that the location and orientation strongly influence the optimal melting range and thus the required PCM type and quantity. Productive PCM melting ranges can be derived for the analysed locations. Melting ranges around 20 °C to 25 °C for Helsinki and Potsdam and 25 °C to 30 °C for Athens seem promising. By adjusting the melting range, the maximal yield increase could also be achieved in spring and autumn to create a more homogeneous energy production over the course of the year.

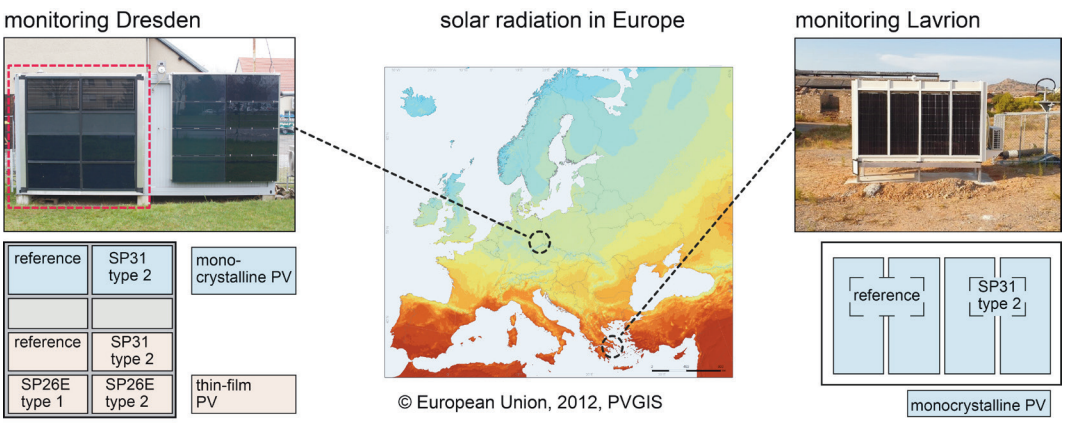

FIG. 9 Monitoring test rigs with PV-PCM warm façades in Dresden and Lavrion for the validation of the PV-PCM design tool

For the effective and economical use of PV-PCM *warm façades*, a case-specific dimensioning is required to reduce the quantity of PCM. For this purpose, a design tool will be developed that can take into account different orientations, locations, PCM types and quantities, PV modules, and insulation thicknesses. The design tool will be based on the simulation models and calculation methods described in this paper. In order to achieve a validation of the whole design tool, free field measurements on PV-PCM façade test rigs will be used. For this purpose, two monitoring test rigs with different PV technologies, different PCM types and capsule types have been installed. One is located at *TU Dresden* and the second on a property of the *School of Mining and Metallurgical Engineering* of the *National Technical University of Athens* (NTUA) in Lavrion, Greece, as shown in Fig. 9.

Acknowledgements

This work originated from the research project PV-Tool – Development of a simulation tool for dimensioning of modular energy producing façade systems with phase change materials, funded within the scope of the Central Innovation Program for SMEs (German: Zentrales Innovationsprogramm Mittelstand, ZIM) of the Federal Ministry of Economic Affairs and Energy (grant number: ZF4123720HF8). The authors are grateful to all project partners for their excellent cooperation. The authors would like to thank Dimitris Mantelis from the NTUA for the excellent and collegial cooperation.

References

Aelenei, L., Pereira, R., Gonçalves, H., & Athienitis, A. (2014). Thermal Performance of a Hybrid BIPV-PCM: Modeling, Design and Experimental Investigation. *Energy Procedia, 48*. https://doi.org/10.1016/j.egypro.2014.02.056.

Čurpek, J., & Cekon, M. (2020). Climate response of a BiPV façade system enhanced with latent PCM-based thermal energy storage. *Renewable Energy*. https://doi.org/10.1016/j.renene.2020.01.070.

Decker, B., Grimmig, B., Mencke, D., & Stellbogen, D. (1998). Besonderheiten bei der Projektierung von Photovoltaikfassadenanlagen [Special requirements for the planning of photovoltaic façade systems]. *Forschungsverbund Sonnenenergie - "Themen 97/98," Solare Gebäudetechniken*, 95-103.

Dobos, A. (2012). An Improved Coefficient Calculator for the California Energy Commission 6 Parameter Photovoltaic Module Model. *Journal of Solar Energy Engineering, 134*. https://doi.org/10.1115/1.4005759.

Elarga, H., Goia, F., & Benini, E. (2017). PV-PCM integration in glazed buildings. Numerical study through MATLAB/TRNSYS linked model. *Building Simulation Applications 2017, 3*.

Engin, B., Brandau, K., Flohr, S., Horn, S., Roos, M., Vaupel, G., & Bernhard, W. (2016). Photovoltaik Fassaden: Leitfaden zur Planung [Photovoltaic façades: planning guide]. *DAW SE und GWT-TUD GmbH*.

European Commission. (2016). *Commission Recommendation (EU) 2016/1318 - Of 29 July 2016 - On guidelines for the promotion of nearly zero-energy buildings and best practices to ensure that, by 2020, all new buildings are nearly zero-energy buildings. 12*.

Fath, K. (2018). Technical and economic potential for photovoltaic systems on buildings. (Doctoral dissertation). *KIT Scientific Publishing, Band 25_Produktion und Energie*. https://doi.org/10.5445/KSP/1000081498.

Giuseppina, C., Lo Brano, V., Cellura, M., Franzitta, V., & Milone, D. (2012). A finite difference model of a PV-PCM system. *Energy Procedia, 30*, 198-206. https://doi.org/10.1016/j.egypro.2012.11.024.

Hansen, C. (2015). Parameter Estimation for Single Diode Models of Photovoltaic Modules. *Sandia Report SAND2015-2065*. https://doi.org/10.13140/RG.2.1.4336.7842.

Horn, S., Seeger, J., Scheuring, L., & Weller, B. (2017). Fassade mit temperaturregulierenden Photovoltaik-Paneelen - Ergebnisse aus einem ersten Praxistest [Façade with temperature-regulating photovoltaic panels - results from a first field test]. *ce/papers*, 1(1), 240-253. https://doi.org/10.1002/cepa.25.

Huang, M. J., Eames, P. C., & Norton, B. (2004). Thermal regulation of building-integrated photovoltaics using phase change materials. *International Journal of Heat and Mass Transfer*, 47, 2715-2733. https://doi.org/10.1016/j.ijheatmasstransfer.2003.11.015.

Krippner, P. D. R., Becker, P. D. G., Maslaton, P. D. M., Maurer, D. C., Seltmann, T., Kuhn, T. E., Kämpfen, B., Reinberg, G. W., Haselhuhn, R., & Hemmerle, C. (2016). Gebäudeintegrierte Solartechnik: Photovoltaik und Solarthermie - Schlüsseltechnologien für das zukunftsfähige Bauen: Energieversorgung als Gestaltungsaufgabe [Building-Integrated Solar Technology: Architectural Design with Photovoltaics and Solar Thermal Energy] (1. Edition). *Institut für internationale Architektur-Dokumentation GmbH & Co. KG, DETAIL*.

Ullrich, S. (2018, October 16). Der Mehrpreis schreckt ab [The additional price deters]. *photovoltaik*, 10-2018, 10-13.

Weller, B., Hemmerle, C., Jakubetz, S., & Unnewehr, S. (2009). Detail Praxis: Photovoltaik: Technik, Gestaltung, Konstruktion [Photovoltaics: Technology, Architecture, Installation] (1. Edition). *Institut für internationale Architektur-Dokumentation GmbH & Co. KG, DETAIL*.

Wieprzkowicz, A., Knera, D., & Heim, D. (2015). Effect of Transition Temperature on Efficiency of PV/PCM Panels. *Energy Procedia, 78,* 1684-1689. https://doi.org/10.1016/j.egypro.2015.11.257.

Wilke, S. (2020, March 16). Stromerzeugung erneuerbar und konventionell [Renewable and conventional power generation]. *Umweltbundesamt*. https://www.umweltbundesamt.de/daten/energie/stromerzeugung-erneuerbar-konventionell.

Smart Textile Sun Shading

Development of Functional ADAPTEX Prototypes

Paul-Rouven Denz[1*], Christiane Sauer[2], Ebba Fransén Waldhör[2], Maxie Schneider[2], Puttakhun Vongsingha[1]

* Corresponding author

1 Priedemann Facade-Lab, Germany/Delft University of Technology, Architecture and the Built Environment, Netherlands, paul.denz@priedemann.net

2 Weißensee School of Art and Design, Textile- and Surface Design, Germany

Abstract

The research project ADAPTEX pursues the goal of developing adaptive, energy-efficient textile sun shading systems using the smart material Shape Memory Alloy (SMA). Within this approach lies a high potential for novel sun protection systems demanding little energy or even self-sufficiently adapting to external stimuli while reducing operation and maintenance costs and at the same time offering solutions to tackle growing demand for sun and glare protection. A Design Categories Matrix is presented that brings together various involved fields from textile design and façade construction to smart material development. Based on this, two concepts have been further elaborated: ADAPTEX Wave and Mesh. Both incorporate SMA into textile structures but express different design and performance potential by changing the geometry and openness factor of the surface area. For further evaluation, various functional prototypes that scale up from 0.2 x 0.2 m to 1.35 x 2.80 m are developed and reviewed. The buildability and functionality of SMA-driven textile sun shading systems that incorporate requirements from the various involved fields are verified. The feasibility of parallel ADAPTEX Wave and Mesh were assessed in comparison to the performance of state-of-the-art sun shading systems. The technological ideas are subsequently optimised and scaled up in various cycles for follow-up testing in both indoor and outdoor environments.

Keywords

Adaptive sun shading, textile building envelope, smart materials, autarkic operation and control mechanism, Shape Memory Alloy (SMA)

10.7480/jfde.2021.1.5539

1 INTRODUCTION

The United Nations' "Transforming our world: the 2030 Agenda for Sustainable Development" (United Nations General Assembly, 2015) proclaims that there has been a highly increased demand in energy- and resource-efficient building construction. This calls for a new alliance of simplicity and performance in the technology and operation of future building systems.

The building envelope plays a major role in such needed improvements by enabling the use of efficient or even autarkic systems that minimise energy demand by, for example, reducing cooling requirements through efficient sun shading.

ADAPTEX aims to develop such a novel sun shading system. By combining the potentials of lightweight textile construction and the smart material Shape Memory Alloy (SMA), significant reductions in production and material consumption, in transportation and installation, and in operation and dismantling (Barozzi, Lienhard, Zanelli, & Monticelli, 2016) could be achieved.

Shape Memory Alloys (SMA) are metal alloy materials that in the last twenty years have caught the interest of designers and researchers working in the field of adaptive surfaces, due to their shape-changing properties. These materials show solid-state phase transformation through temperature change between martensite and austenite. When heated up, the material is in the high strength austenite state e.g. as shrinkage of a wire, and on cooling, the material changes to the low strength martensite state, moving back into its original state (Josephine, Ruth, & Rebekah, 2020). SMA elements are generally very suitable for construction applications due to their performance, free from wear and maintenance. Moreover SMAs are activated by changes in temperature, allowing an autarkic and adaptive reaction to external stimuli like ambient heat or solar radiation - complemented by decentralised control through electric voltage (smart^3 e.V., 2017). The small size actuator induces force and movement and therefore is able to supersede complex motors and driving mechanisms. However, SMAs are designed for the accuracy and standards of mechanical engineering rather than for architectural façade applications. ADAPTEX closes this gap by integrating SMA into large-scale architectural surfaces using textile technologies (see Fig. 1). Implemented into soft surfaces, SMA initiates changes in geometry thus adjusting parameters like transmission and reflection for shading and enhancing building performance (Denz, 2015).

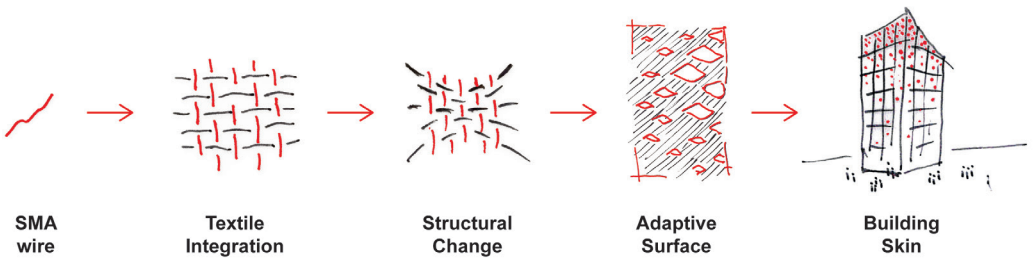

FIG. 1 Conceptual approach ADAPTEX

Although smart materials have been discussed in architectural discourse for many years (Addington & Schodek, 2005; Ritter, 2007; Braun, 2008), so far Smart Textile solutions as envisaged by ADAPTEX have not reached built reality. Smart Materials in combination with textile or membrane structures are often dealt with in the context of responsive / adaptive architecture (Khoo, Salim, & Burry, 2011;

Dewider, Mohamed, & Ashour, 2013), directly influenced by external stimuli or user interaction. Several design studies were developed in which the textile surface is deformed through actuator systems such as SMA. At TU Delft, an adaptive building component using shape memory alloy and shape memory polymer as a composite material to create an exterior layer of fins to reduce wind-loads by changing the façade surface accordingly was investigated (Lieleveld, 2013). More concrete, although still in conceptual/experimental stage, are the Smart Textile Skins using SMA that have been developed. For example, self-sufficient driven courtyard textile shadings such as those used in Seville, Spain, use a shape memory alloy spring as actuator (Callejas Ortega, 2015). In addition, at IAAC in Barcelona, shape memory alloys are used to deform textile surfaces by the external actuator controlling light coming in through stacked textile layers creating a responsive façade solution (Begle, 2013). The most advanced research on Smart Textiles in building construction can be seen in Cherif (2017), but only as a component i.e., as shape memory alloy fibre within concrete reinforcement. Further examples can be found within the smart[3] research network, such as Solar Curtain, flower-like shading units run by SMA (Sigmund, 2016), or Smart Skin, where the usage of SMA as a substitute for a motor in state-of-the-art venetian blinds has been investigated (smart[3] e.V., 2017). However, following the review by Fiorito et al. (2016) it is apparent that SMA is one of the most favourable actuators in research for shape morphing solar shading systems.

This proves that the potential of SMA driven façade systems has not yet been exploited to any great extent. The research by Wærsted (2014) further illustrates how Smart Textiles in general do not yet play any role in the material practise of architects when designing new projects and façades. Simultaneously, complexity in façade design is increasing due to higher expectations and regulations towards environmental, societal, and economic performance requirements (Loonen, Trčka, Cóstola, & Hensen, 2013). ADAPTEX aims at tackling these challenges and developing a Smart Textile Sun Shading feasible for actual façade implementation that can contribute to novel solutions enabling highly efficient building envelopes as defined by Böke, Knaack, and Hemmerling (2018).

2 DEVELOPMENT APPROACH

Due to the interdisciplinary team within the ADAPTEX project, the aim from the beginning was to bring together all relevant requirements to align the knowledge on the topic and develop novel and feasible solutions. In an initial stage, a Design Categories Matrix collecting all necessary data was used to allow for an early design phase – free from major constraints but having the overall requirements in view. These concepts have been reviewed, narrowed down, and grouped into the main typologies. The feasibility of the designs has been continuously checked throughout prototyping, and underlined with a comparison to state-of-the-art systems. During the development, digital tools were used to stay agile and adjust to necessary changes of the concepts during development and for later application, concluding in a high leap of Technology Readiness Level (European Comission, 2014) from TRL 2, formulated technology concept, to TRL 5/6, technology validated/demonstrated in relevant environment, within ADAPTEX. With the help of this research by design approach within ADAPTEX, an interdisciplinary team is able to develop a theoretical research idea (TRL 2) up to relevant size and environment prototypes for performance testing (TRL 5/6), thus aiming at exceeding TRL of former research in the field of Smart Material enhanced adaptive façades as reviewed, for example, by Aelenei et al. (2018).

3 ADAPTEX CONCEPTS

3.1 DESIGN MATRIX

As the basis for the cross-disciplinary development of the intended textile sun shading device, a visual and conceptual *Design Categories Matrix* was developed. As shown in TABLE 1, this comprises the main features and requirements of Shape Memory Alloy technology, building envelope construction, architectural application, and textile design. Among other things, these 22 categories span from *SMA components* such as wire, rod, sheet, spring, or even 3D-printed components, to *Textile Principles* like woven or knitted fabric, mesh, or foil, to general *Façade / Material Requirements* defined as optical properties, fire protection class, or UV resistance. With the help of the Matrix, the partners from various fields could first design conceptual scenarios for SMA-driven textile sun shading solutions, choosing a criterion per category and linking these to each other.

TABLE 1 Design Categories Matrix

FIXED CATEGORIES							FLEXIBLE CATEGORIES										OPTIONAL CATEGORIES				
1. SMA components	2. SMA deformation	3. SMA activation	4. Textile connection/integration	5. Climate regions	6. Façade integration/typology	7. Building/usage type	8. SMA fixing	9. SMA training/programming	10. Reset force	11. Snapping mechanism	12. Textile principle	13. Textile closing mechanism	14. Precision in execution	15. Opening size/movement	16. Sun shading movement	17. Façade construction	18. Gearing	19. SMA circuiting	20. Sun shading control	21. Material requirements	22. Light transmission

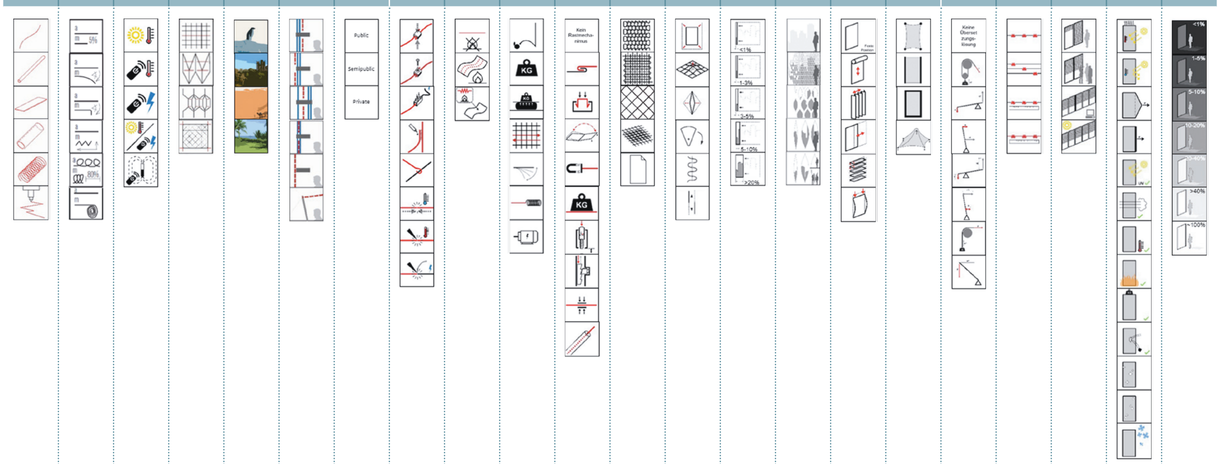

The categories of the Matrix are divided in three main groups: *Fixed Categories*, which have to be chosen first, and solely one chosen per category because of its high influence on the following categories, as well as a high dependency within this group. This is followed by *Flexible Categories* that lead to a more detailed concept, and which first enable visual and physical model-making.

Within this concretisation phase, the *Flexible Categories* might adjust, changing the selected option due to an iterative design process. Lastly, *Optional Categories* have to be reviewed, however, these have only a small impact on the early stage research by design process due to the very precise correlation with execution or even specific real-life project requirements. Within this group, various selections per category, or even none, could be made. These categories become more relevant in the further development, when designs are narrowed down, leading to a more concrete building envelope scope.

Based on these Design Categories, 13 Scenarios for SMA-driven, textile sun shading devices were elaborated, following decision processes in each category incorporating the relationship between the different categories and fields (Denz, Sauer, Waldhör, Schneider, & Vongsingha, 2020). As an example, shown in Figure 2 on Scenario No. 03, the design process is based on the selection of Category values leading to a Scenario plot, for comparison between Scenarios, a Code as well visual representation of the selected Categories is documented. Based on this theoretical concept development, operation and construction sketches, small-scale prototypes, as well as visualisations, were first created. All 13 Scenarios have been developed and formulated according to this scheme for further discussion within the interdisciplinary consortium setting basis for the following development steps (see 3.2 and 3.3).

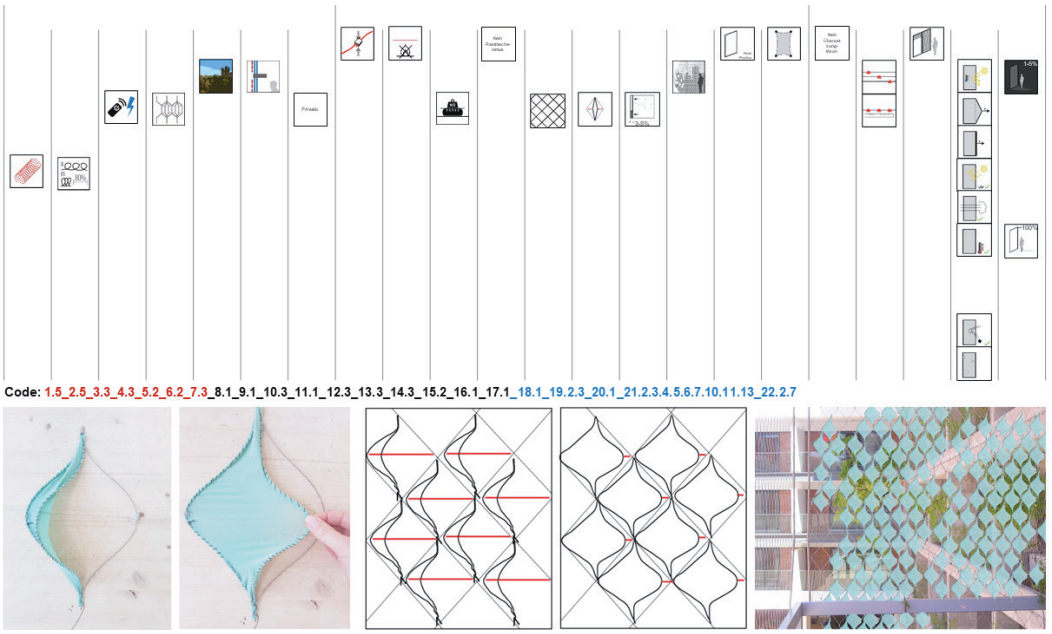

FIG. 2 Scenario No. 03; visual selection of Categories to develop concept (top); Scenario Code according to Categories selection (middle); physical small-scale prototype, sketches of the operation scheme and visualisation (bottom, left to right).

These Scenarios were summarised into three main Typologies (see TABLE 2) based on its application of SMA to focus on the main system properties for further development, thus also leading to a combination of previous scenarios, narrowing down the scope:

— *Pulling:* With this method, SMA is only shortened in a linear direction. The movement can take place along the plane (tangential direction) or perpendicular to the plane (normal direction) of the textile. (Summarising 6 of 13 scenarios).

— *Pushing:* With this method, the surfaces consist of at least 2 layers that move against each other. The overlap of these two layers defines the transparency of the sun protection. (Summarising 4 of 13 scenarios).
— *Rotating:* With this method SMA are moved / deformed by bending force, which causes a rotary movement in the surface. 3-dimensional deformations can be included in this typology. (Summarising 3 of 13 scenarios).

TABLE 2 Scenarios sorted by Typologies

PULLING	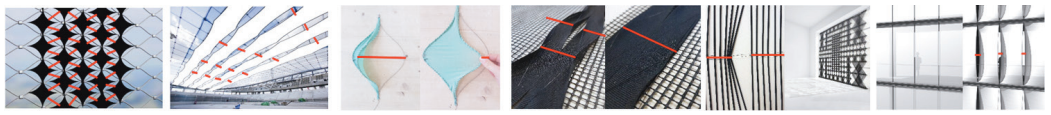
PUSHING	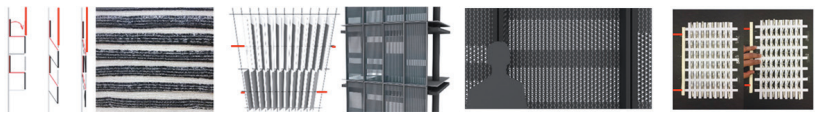
ROTATING	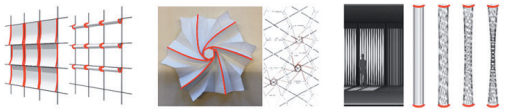

After evaluating these main approaches due to the main feasibility of SMA usage as wire that shrinks/extends in a longitudinal direction, the Rotating category was discarded. This is also directly linked to a higher force, as well as a higher number of cycles that could be undertaken if SMA is not geometrically deformed when activated.

These concepts and design categories and the subsequent decisions within the development process have also been applied and put to the test in various student courses, such as an interdisciplinary workshop on Smart Textile Building Skins at the University of Antwerp (Denz, 2017), or a seminar on textile sun shading at the Weißensee School of Art and Design in Berlin (Sauer et al., 2018).

3.2 ADAPTEX WAVE

Continuing the *Pulling* typology (see 3.1), the system ADAPTEX Wave as a three-dimensional shading device was developed. This concept consists of the following main components (Fig. 3):

— *Textile Band*: A continuous wave-shaped textile band is interwoven with a SMA running through defined points of the textile. Under controlled tension from the shortening of the SMA actuator, the band is deformed by introduced pulling forces at the defined intersection of textile and SMA, resulting in a buckling process, thus moving the edges of two textile bands towards each other, enabling a closing mechanism. This also occurs vice versa, going back into its original shape and stretching the SMA once the SMA is deactivated.

- The textile is specifically designed following three main aspects:
  - Optical properties: High reflection facing outward for optimised sun-protection, currently silver-coloured glass fibre. Low reflection and dark colour for high contrast to enhance the view out and reduce glare in the interior, currently dark blue-coloured glass fibre.
  - Internal stress/stiffness: For a two-way operation, enabling the change from closed to open state, the textile must hold enough internal stress to move back into its original shape and extend the SMA in its deactivated state. Therefore, an exact balance between SMA force and textile stiffness has to be achieved. At the same time, the textile band has to be flexible enough to realise the necessary buckling and induced radius for full closure. In the current prototype, a two-layered glass-fibre laminate is used.
  - Cutting pattern: The wave-like cut of the textile band is optimised to enable a maximum closure/shading once the system is activated and at the same time minimises the necessary length reduction of SMA, which is directly linked to the distance between the fixing point of the textile band and the point at which the SMA passes through the textile. The current design leads to an openness factor of 70 % in its open state versus 0-5 % in its closed state.

- *Shape Memory Alloy*: The SMA, a nickel titanium alloy, is an active component that reacts to temperature change and operates the whole system. Once activated, either by electricity or ambient heat, the SMA shrinks, and once cooled down it is extended again. In the current design, the SMA is activated around a base temperature of 60 - 65 °C while performing a length alteration of up to 5 % and a pulling force of 0.7 N.

- *Sub-Structure*: A main structure to which the textile band is attached as a fixed point to perform geometrical deformation. In the current design, this is performed by a steel-rope net. This not only enables a stiff but at the same time flexible construction but also reduces the material effort as well as thickness to a minimum. This emphasises its overall textile character and reduces the system's impact on the view while in open state.

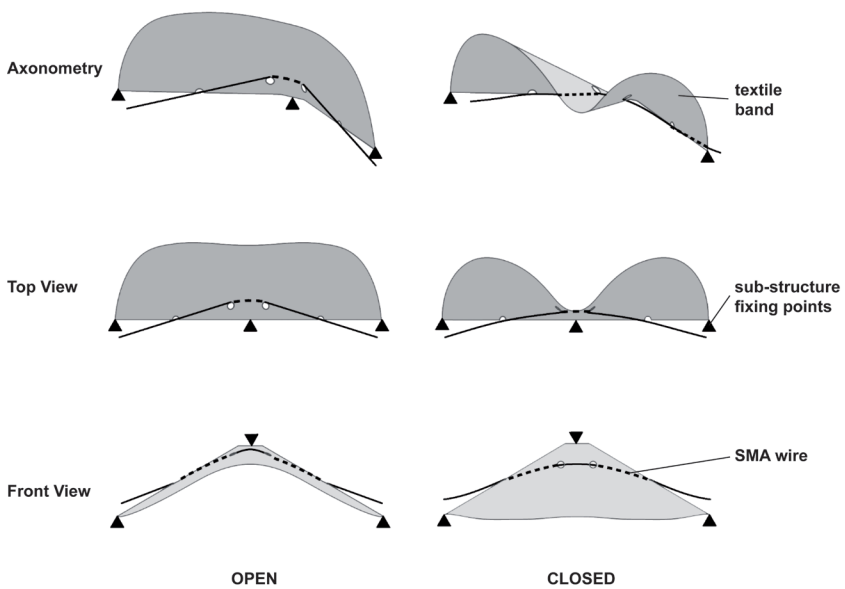

FIG. 3 ADAPTEX Wave Design Principle

Further components to execute the functional Wave system for current prototypes are, among others, a steel frame that holds both the steel-rope net and the SMA, and various small components like screws, eyelets etc. to fix the separate components or enable the threading of the SMA through the textile band. All these components underly a continuous optimisation process aiming for a reduction in material and costs using market available parts.

To develop, optimise, and adjust all these parameters in accordance with input from various partners/components, as well as results from test samples, various tools like Rhino, Grasshopper, Kangaroo, Sofistik, etc. were used (Schneider et al., 2020). An iso-geometric analysis incorporating the textile material values of flexibility, elongation limit, elasticity, etc., was integrated into these computational models. A two-dimensional cutting pattern was generated out of the virtually deformed 3D-model, while calibrating opening angles and fixing parts, thus enabling an iterative design process that led to optimal and feasible solutions as shown in latest Large Scale Demonstrator (Fig. 4.).

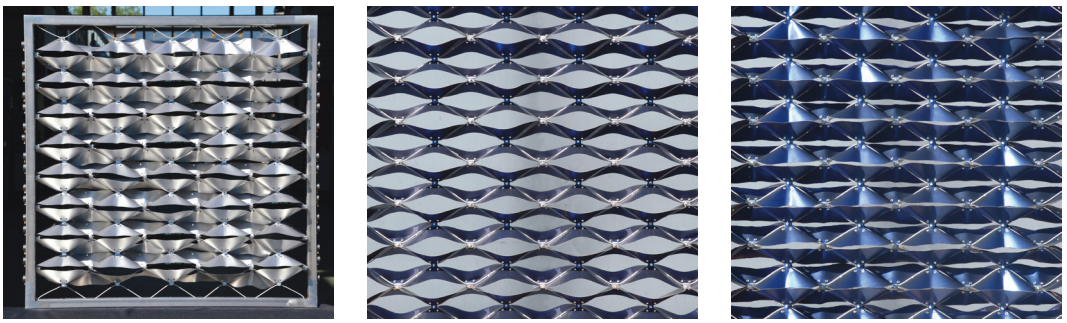

1 2 3

FIG. 4 Demonstrator of ADAPTEX Wave within a constructional frame facing the outer surface (1); close-up of the open state (2), and of the closed state (3) facing the inside surface

3.3 ADAPTEX MESH

As a result of the *Pushing* typology (see 3.1), the system ADAPTEX Mesh as a double (or multiple) layered shading device was developed. This concept consists of the following main components (see Fig. 5):

- *Textile Layers*: Two perforated textile layers move against each other, changing the overall density of the structure in different overlapping states. These textiles are optimised according to the following criteria:
  - Optical/Material Properties: The external, fixed layer aims for high reflectivity to ensure high sun-protection, currently glass fibre mesh, and thus white in colour. The internal, moving layer has a low reflectivity and dark colour for high contrast to enhance the view out and reduce glare in the interior; it is currently dark brown/black in colour, as given by basalt fibre mesh. For the selection of currently used non-woven mesh, the possibility of easy transport, e.g. rolling, as well its stiffness within the final system layout, was taken into consideration.
  - Pattern: A customised pattern of diagonal and vertical fibres to maximise the difference between open and closed state while at the same time minimising the Moiré Effect (Amidror, 2009) has been developed. Currently, the system ranges from an openness factor of

roughly 30 % in its open state to 7 % in its closed state. The pattern can easily be adjusted, e.g. by reducing fibre thickness, or scaled to change these values accordingly.

- Integration of SMA: The SMA is directly integrated into the non-woven mesh during its fabrication process. The design of the pattern specifically gives guidance for the SMA while specific pre-treatment of the SMA prevents a firm connection with the textile fibres, enabling a constant shrinkage of the SMA along the whole distance when activated. The SMA is either fixed at the bottom of the textile layer, or within, depending on the dimensions of the system as well as the necessary length adjustment of the SMA. The weight of the moving textile layer and the moving distance, as well as the force of the SMA, have to be fine-tuned to ensure a full shift from open to closed and back.

- *Shape Memory Alloy*: The SMA, a similar nickel titanium alloy as for Wave, is an active component that reacts to temperature change operates the moving layer. Once activated either by electricity or ambient heat, the SMA shrinks, pulling up the moving textile layer and raising the system density; once it cools down it is extended again, releasing the textile back into the original position imposed by the textile's self-weight. In the current design, the SMA is activated around a base temperature of 60 - 65 °C, while only performing a length alteration of 3 %, lifting a textile of roughly 3.0 kg.

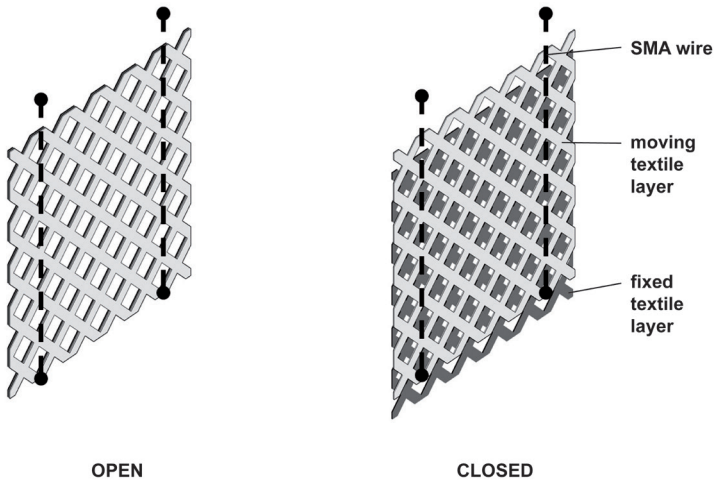

FIG. 5 ADAPTEX Mesh Design Principle

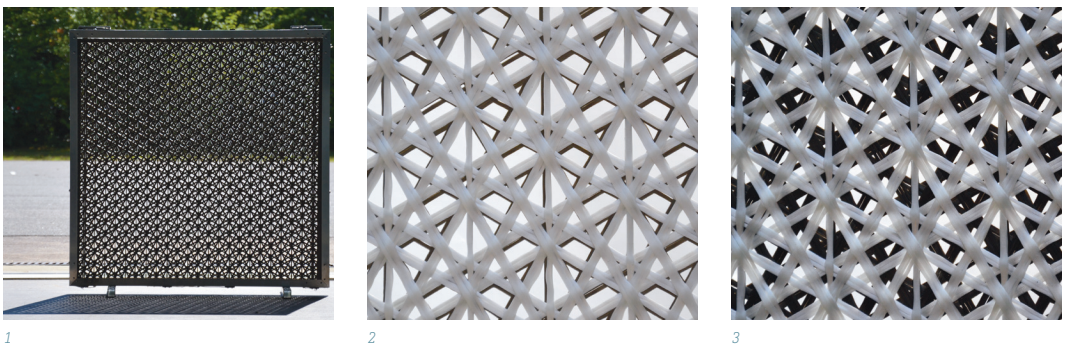

1 2 3

FIG. 6 Demonstrator of ADAPTEX Mesh within the constructional frame (1) facing the inner surface; close-up of open state (2) and close-up of closed state (3) facing the outer surface

To conclude, in the Mesh system a frame structure is used to fix the non-moving outward-facing layer and at the same time to attach the SMA and the inward-facing layer with loose fixings. These fixed and loose points simultaneously ensure the correct positioning of the two layers towards each other: exact overlapping of the same pattern in the open position, defined distance between the layers to prevent or make use of the parallax effect (Waldon & Dyer, 1993) and maximum offset of the pattern towards each other to gain the highest shading values (Fig. 6). To customise the system to project a specific design, performance, and scaling requirements, a parametric script incorporating both textile and architectural demands was developed (Schneider et al., 2020).

4 RESULTS

4.1 FUNCTIONAL PROTOTYPES

Following the development approach (see 2.0) from the first conceptual stage and compiling the Scenarios (see 3.1), moving forward with physical models and prototypes was a crucial part of the research to understand the interplay of textile, SMA, system layout, and geometry. All of these models were created at 1:1 scale, reflecting material and constructional requirements and restrictions. From early-stage geometrical models, *Small Scale Test Samples,* and *Large-Scale Demonstrators* to *Full Scale Prototype,* the main function and operation principles continue. Within ADAPTEX, this is a very feasible approach due to the system design as a textile construction. Consisting of various small-scale components, as shown in 3.2 and 3.3, the scaling up by roughly 100 times from first concept (in average measuring 0.04 sqm) to *Full Scale Prototype* (measuring 3.78 sqm) does not change the core system design. The textile layout uses additional further components, bands, and filaments to enlarge the covered surface – thus also easily integrating the SMA as wire. SMA specifically is very feasible for this scaling up approach due to its customisation potential and strength as well as durability (Habu, 2011). Within ADAPTEX, SMA is adjusted to the various designs and scales solely by choosing appropriate alloys and different wire diameters from market-available products. Working with diameters from 0.1 to 0.4 mm in ADAPTEX, has little to no impact on the design, nor on the construction of Wave and Mesh.

4.1.1 Small Scale Test Samples

Following the two most promising scenarios (see 3.1, 3.2, 3.3), small-scale functional test samples were created to review its feasibility. Both Mesh and Wave test samples, measuring roughly 25 x 25 and 25 x 40 cm, have been run for more than 50 cycles while the SMA was activated by an electrical voltage, as seen in Figure 7.

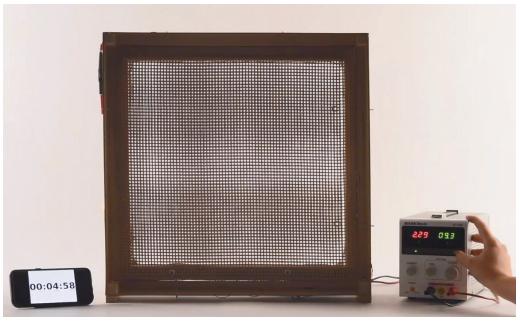

1

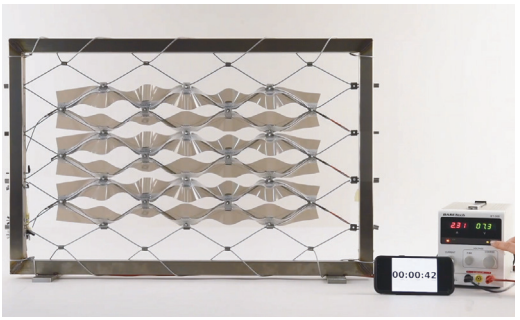

2

FIG. 7 Small-scale functional test samples of ADAPTEX Mesh (1) and ADAPTEX Wave (2).

4.1.2 Large Scale Demonstrator

As already presented in 3.2 (see Fig. 4) and 3.3 (see Fig. 6), functional demonstrators of 1.0 x 1.0 m, including a constructional frame for integration into façade construction, were manufactured. These incorporate a first optimisation loop and have resulted in geometry, material, as well as performance improvement. These demonstrators are already designed following actual façade requirements and can be seen as a clipping of a *Full-Scale Prototype* for further finetuning. The exact sizing was also dependent on the size limitations of the testing setup (see also the following paragraph). This leap from small scale to large scale already shows the potential of further scaling to reach actual façade dimensions and integration. At the same time, these functional demonstrators both run on electricity as well as self-sufficiently on external heat input. However, the current layout of the SMA needs rather high temperatures that are not very common in façade operation.

Apart from providing proof of the viability of further developing both concepts into façade/ architectural usage, these demonstrators are also used to verify its actual sun-protection properties. Both Mesh and Wave are currently undergoing verified indoor testing at the Fraunhofer ISE to measure optical as well as calorimetric performance values under various circumstances, e.g. within a double-skin façade or as an external sun-protection device. The first visual test runs have already verified its architectural design potential, as well as the basic operations of opening and closing the structures as sun-protection (see Fig. 4, Fig 6).

4.1.3 Full Scale Prototype

To prove in-situ feasibility, and review fabrication and operation processes, approaching TRL 6 (technology in relevant environment), two double-skin façade units of 1.35 x 2.80 m are being planned to incorporate both Mesh and Wave. These real-size prototypes will then undergo long term outdoor field tests outside of Berlin and will be presented to relevant stakeholders during fairs and project-related lead-user workshops. These prototypes are based on the construction and design of the *Large Scale Demonstrators*.

For Wave, due to its additive Textile Band design, only a small scaling from 1.0 to 1.35 m in width is necessary. To increase height, this requires solely adding more bands, which doesn't affect the basic design or construction. Only a slight adjustment in the layout of the SMA has to be made to provide sufficient pulling force to operate a longer textile band, and therefore more openings. Fixing and frame construction will be optimised focusing on market-availability of components and meeting higher forces within the system and sub-structure.

For Mesh, an even scaling of the pattern will be undertaken still ensuring the same openness factor for open and closed states. This is driven by an optical and design review, rather than by constructional or functional reasons. Within the *Large Scale Demonstrator,* the pattern of the two layers merged into each other with increasing distance of the viewpoint from the surface. To ensure a visual differentiation between the two states and a clear change in view, the pattern is scaled by a factor of 2. Concerning the fixing and frame construction only small changes for assembly and operation are carried out, without affecting the overall Mesh concept. With the larger size of the unit, and therefore textile layers, higher loads have to be carried by the SMA, thus a stronger SMA is used. However, the positioning and amount of SMA stays the same, as in the previous prototyping stages. For the *Full Scale Prototype,* the SMA can even be run shorter in proportion to the full layer height compared to previous layouts. This is a consequence of the direct relation between percentage shrinkage of the SMA (3 %) to the SMA length to the favourable movement of the two mesh layers towards each other. In this case, the SMA is fixed within the mesh layer using a terminal at the end of the SMA.

4.2 COMPARISON TO STATE-OF-THE-ART

Parallel to the previously described design processes and prototype manufacturing, the first comparisons to state-of-the-art systems (Kuhn, 2017) have been conducted to evaluate basic reasonableness of the ADAPTEX approach to incorporate in next step optimisation processes (Denz et al., 2018) . Simulations on the shading potential of the developed systems compared to standard venetian blinds verified against non-existing shading shows similar results to those shown in Table 3. Although these simulations need to be updated with the outcomes from, for example, Fraunhofer ISE testing (see 4.1), their functionality as sun shading, even in the early design stages, has already been shown, verifying the feasibility of the followed concepts.

Furthermore, quantitative assessment of the scenarios and later developed concepts in comparison with not only standard but also customized and adaptive sun-protection solutions has been conducted. Therefore, properties like *Design Flexibility, Solar Heat Gain, Durability,* or *Costs* have been qualitatively rated from 1 to 5 – 1 for lowest performance, 5 for highest performance, in relation to all reviewed case studies, as well as ADAPTEX Wave and Mesh. The comparison in form of radar charts (Table 4) of ADAPTEX Wave and Mesh to the adaptive sun shading solutions such as those on Al Bahr Towers (Cilento, 2012) or X-LED steel-rope net for second skin façades (Carl Stahl ARC GmbH, 2019) shows similar to better coverage and therefore overall performance.

TABLE 3 Shading/Illuminance simulation with no shading, venetian blind, ADAPTEX Mesh and Wave.

FRANKFURT ORIENTATION: South 21. June (Summer) 12:00 h ROOM SIZE: 5 x 8 x 3.5 m	Without sun-protection	Venetian Blind 45° slats	ADAPTEX Mesh	ADAPTEX Wave
	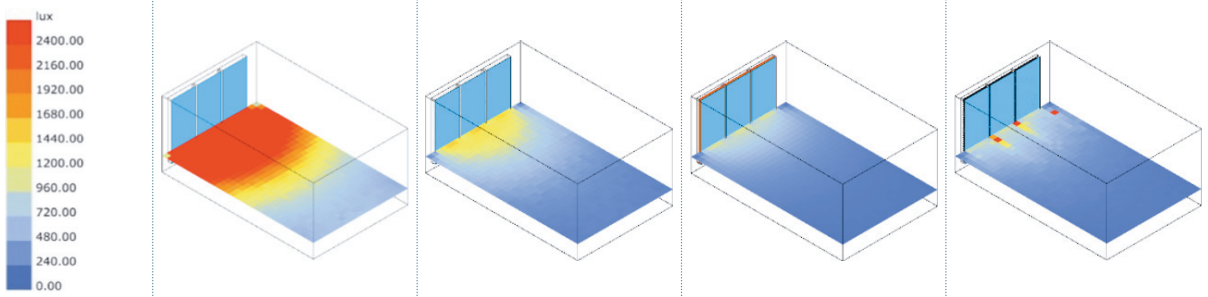			

TABLE 4 Radar chart comparison of ADAPTEX Wave and Mesh to specialized and adaptive facade systems.

ADAPTEX	SPECIALIZED FACADES	ADAPTIVE FACADES
Wave 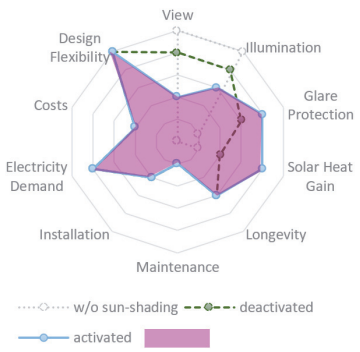	X-LED (steel-rope net) 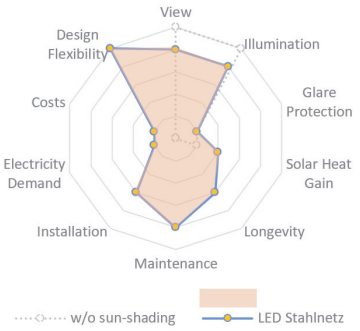	Institute du Monde Arabe, Paris 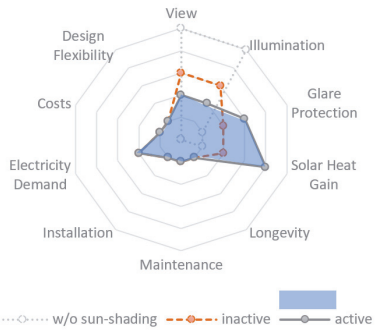
Mesh 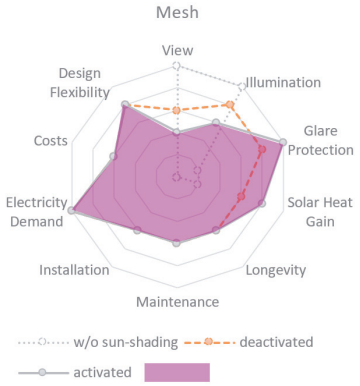	Burj al Arab, Dubai 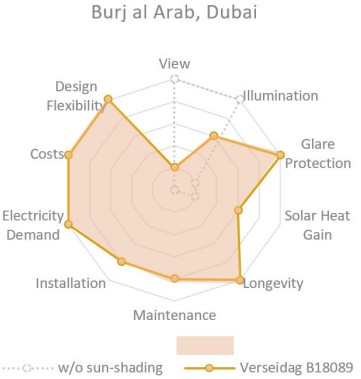	Al Bahr Mashrabiya, Abu Dhabi 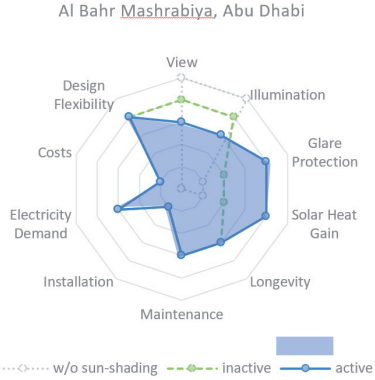

It is worth mentioning that for this comparison both ADAPTEX concepts have been evaluated as electrically driven, which is the worst-case scenario, since with customised SMA these systems can run fully autarkic from any building induced energy source. However, for specific usage cases or building locations, a self-sufficient operation might not be realisable. In that case, the fall-back option would be an electrically-driven ADAPTEX shading system. Within the development, this option has always been investigated in parallel. Therefore, prototypes and testing also made use of electrically induced heat to the SMA, since, within various laboratory or research environments, the naturally appearing solar radiation, and therefore heat, cannot be induced or controlled for reliable evaluation. Still, in general an electrically driven ADAPTEX solution would pursue the initial intent to reduce material input, extend longevity, and reduce energy demand as, for instance, SMAs perform more energy efficiently than state-of-the-art motors (Neugebauer, Drossel, Pagel, Bucht, & Zernecke, 2011). Nevertheless, the overall goal of ADAPTEX is to run SMA self-sufficiently and the various design and development steps always consider this requirement.

5 CONCLUSION

5.1 POTENTIAL

The presented development process within ADAPTEX concluded in two feasible concepts, Mesh and Wave, for Shape Memory Alloy driven textile sun shading solutions. Not only was the basic operation, meaning activation and de-activation of SMA within these textile systems, proven, but various prototypes of different size and detailing, run for several cycles, showed major changes in openness factor (70 to 0 % and 30 to 7 %). Newly developed tools for development, optimisation, and customisation of both concepts enable the following steps for actual façade applications, not only as prototype but as real use cases. Academic exchange undertaken in parallel on the ADAPTEX approach, as well as alignment of Mesh and Wave concepts with realised façade solutions, ensure a high potential for implementation of the concepts into façade construction at a later stage, thus confirming its feasibility.

5.2 FURTHER STEPS

Although these findings already underline the functionality and potential of the ADAPTEX approach, major steps still lie ahead. As mentioned before, the developed prototypes will be used for further testing at indoor and outdoor test facilities, thus providing new insights on the system performances that need to be fed back into the set-up iterative development process as well as assessment tools. Based on this, further optimisation of Mesh and Wave will be undertaken. In addition, the aim to create solely self-sufficient Smart Textile sun shading systems will be focused on. Therefore, a follow-up project, ADAPTEX KLIMA+, is already projected to further investigate the correlation of local climate, ADAPTEX layout, and building skin integration.

FIG. 8 Possible application of ADAPTEX Mesh (top) and Wave (bottom) in open (left) and closed state (right).

Acknowledgements

The authors would like to thank the further project partners of ADAPTEX Fraunhofer IWU, VERSEIDAG-INDUTEX, Carl Stahl ARC, ITP and SGS Ingenieurdienstleistungen as well as the additional support by i-Mesh. The authors gratefully acknowledge the support within the ADAPTEX research project by the smart^3 e.V. and its funding by the German Federal Ministry of Education and Research (BMBF) based on a decision by the German Bundestag.

References

Addington, D. M., & Schodek, D. L. (2005). *Smart materials and new technologies : for the architecture and design professions*. Oxford, USA: Architectural Press.

Aelenei, L., Aelenei, D., Romano, R., Mazzucchelli, E. S., Brzezicki, M., & Rico-Martinez, J. M. (2018). *Case Studies - Adaptive Facade Network*. TU Delft Open.

Amidror, I. (2009). *The Theory of the Moiré Phenomenon*. London: Springer-Verlag. doi:10.1007/978-1-84882-181-1

Barozzi, M., Lienhard, J., Zanelli, A., & Monticelli, C. (2016). The Sustainability of Adaptive Envelopes: Developments of Kinetic Architecture. *Procedia Engineering* (155), 275-284. doi:10.1016/j.proeng.2016.08.029

Begle, M. (2013, June 9). *Advanced Materials – Shape Memory Alloy – Nitinol*. Retrieved from http://www.iaacblog.com/programs/advanced-materials-shape-memory-alloy/

Böke, J., Knaack, U., & Hemmerling, M. (2018, March 26). State-of-the-art of intelligent building envelopes in the context of intelligent technical systems. *Intelligent Buildings International*. doi:10.1080/17508975.2018.1447437

Braun, D. H. (2008). *Bionisch inspirierte Gebäudehüllen. Konzeption einer bionisch inspirierten Gebäudehülle nach dem Vorbild natürlicher Hüllen und Häute (Bionically inspired building envelopes. Conception of a bionically inspired building envelope based on the model of natural envelopes and skins)*. Stuttgart: Universität Stuttgart.

Callejas Ortega, M. A. (2015). *Análisis y estudio metodológico de las aplicaciones de los materiales con memoria de forma y superelasticidad en arquitectura y urbanismo (Analysis and methodological study of the applications of materials with shape memory and superelasticity in architecture and urbanism)*. Seville: Escuela Técnica Superior de Arquitectura, Universidad de Sevilla.

Carl Stahl ARC GmbH. (2019). *X-LED*. Retrieved from https://x-led.de/en/

Cherif, C. (2017). E*ntwicklung von Textilstrukturen mit textiltechnisch integrierten Formgedächtnislegierdrähten zur Umsetzung komplexer Verformungen in Faserkunststoffverbundanwendungen (Development of textile structures with textile-technically integrated shape memory alloy wires for the implementation of complex deformations in fiber plastic composite applications)*. Retrieved from https://forschungsinfo.tu-dresden.de/detail/forschungsprojekt/16051

Cilento, K. (2012). *Al Bahar Towers Responsive Facade / Aedas*. Retrieved from archdaily: https://www.archdaily.com/270592/al-bahar-towers-responsive-facade-aedas

Denz, P. R. (2015, September 22). *Intelligente Gebäudehüllen und Smart Textiles - eine ideale Kombination (Intelligent building envelopes and smart textiles - an ideal combination)*. Retrieved from https://smarttex-netzwerk.de/en/events/199-workshop-on-22-09-2015

Denz, P. R. (2017). Textile Building Skin. New Functionality due to Smart Textiles. In U. Knaack, & U. Pottgiesser (Eds.)., *efnMOBILE 2.0 : Efficient Envelopes* (pp. 94-109). Delft: TU Delft Open. Retrieved from https://facades.ning.com/profiles/blogs/efnmobile-workshop-textile-building-skin

Denz, P.-R., Sauer, C., Boxberger, L., Waldhör, E. F., Schneider, M., & Vongsingha, P. (2018). ADAPTEX. *smart³ Tage*. Berlin.

Denz, P.-R., Sauer, C., Waldhör, E. F., Schneider, M., & Vongsingha, P. (2020). Smart Textile Sun Shading. *15th Conference on Advanced Building Skins*. Bern.

Dewider, K., Mohamed, N., & Ashour, Y. (2013). Living Skins: A New Concept of Self Active Building Envelope Regulating Systems. *SB13 Conference*. Dubai.

European Comission. (2014). *Technology readiness levels*. Retrieved from https://ec.europa.eu/research/participants/data/ref/h2020/wp/2014_2015/annexes/h2020-wp1415-annex-g-trl_en.pdf

Fiorito, F., Sauchelli, M., Arroyo, D., Pesenti, M., Imperadori, M., Masera, G., & Ranzi, G. (2016). Shape Morphing Solar Shadings: a Review. *Renewable and Sustainable Energy Reviews*(55), pp. 863-884. doi:10.1016/j.rser.2015.10.086

Habu, T. (2011). Applications of shape memory alloys (SMAs) in electrical appliances. *In Shape Memory and Superelastic Alloys* (pp. 87-99). Cambridge: Woodhead Publishing.

Josephine, S., Ruth, D., & Rebekah, S. D. (2020). Shape Memory Alloys. In Inamuddin, R. Boddula, M. I. Ahamed, & A. M. Asiri (Eds.). *Alloy Materials and Their Allied Applications,* pp. 213-223. Beverly, MA: Scrivener Publishing LLC. doi:10.1002/9781119654919.ch11

Khoo, C. K., Salim, F., & Burry, J. (2011). Designing Architectural Morphing Skins with Elastic Modular Systems. *International Journal of Architectural Computing*, 4(9).

Kuhn, T. E. (2017). State of the art of advanced solar control devices for buildings. *Solar Energy*. Advance online publication. https://doi.org/10.1016/j.solener.2016.12.044

Lieleveld, C. (2013). *Smart Materials for the Realization of an Adaptive Building Component.* Delft: TU Delft.

Loonen, R. C., Trčka, M., Cóstola, D., & Hensen, J. L. (2013). Climate adaptive building shells: State-of-the-art and future challenges. *Renewable and Sustainable Energy Reviews,* 25, 483-493. doi:10.106/j.rser.2013.04.16

Neugebauer, R., Drossel, W.-G., Pagel, K., Bucht, A., & Zernecke, A. (2011). Design of a controllable shape-memory-actuator with mechanical lock function. *Active and Passive Smart Structures and Integrated Systems*, 11.

Ritter, A. (2007). *Smart materials in architecture, interior architecture and design*. Basel; Berlin et al.: Birkhäuser.

Sauer, C., Waldhör, E. F., Schneider, M., Denz, P.-R., Vongsingha, P., Miodragovic, N., & Brucks, M. (2018). *Shaping Shades.* Retrieved from weißensee kunsthochschule berlin: https://kh-berlin.de/projekt-detail/Project/detail/shaping-shades-2830.html

Schneider, M., Waldhör, E. F., Denz, P.-R., Vongsingha, P., Suwannapruk, N., & Sauer, C. (2020). Adaptive textile façades through the integration of Shape Memory Alloy. *ACADIA 2020 Conference Proceedings*.

Sigmund, B. (2016). Solar Curtain – Sonnenschutz durch Formgedächtniseffekt (Solar Curtain - sun shading through shape memory effect). *DETAIL Research*. Retrieved from https://www.detail.de/artikel/solar-curtain-sonnenschutz-durch-formgedaechtniseffekt-28272/

smart³ e.V. (2017). *Smart Skin : Selbstregulierende Sonnenschutzkomponenten für die Gebäudehülle (Smart Skin: Self-regulating sun protection components for the building envelope)*. Retrieved from http://www.smarthoch3.de/projekte/

United Nations General Assembly. (2015). *Transforming our World: The 2030 Agenda for Sustainable Development. United Nations*.

Wærsted, E. H. (2014). *Textiles in the Material Practice of Architects - Opportunities, Challenges and Ways of Simulating Use*. Lyngby: Technical University of Denmark.

Waldon, S., & Dyer, C. R. (1993). Dynamic Shading, Motion Parallax and Qualitative Shape. *Proceedings IEEE Workshop on Qualitative Vision*, pp. 61-70. doi:10.1109/WQV.1993.262949

A Full Performance Paper House

Rebecca Bach, Alexander Wolf*, Martin Wilfinger, Nihat Kiziltoprak, Ulrich Knaack

* Corresponding author
TU Darmstadt Institute of Structural Mechanics and Design ISM+D, Darmstadt, bach@ismd.tu-darmstadt.de

Abstract

According to the UNHCR, in 2019 there were 70.8 million refugees worldwide. Due to war, catastrophes, and emergency situations a great demand for temporary accommodation has arisen within the last couple of years. The main requirements for these shelters are protection for the inhabitants, easy transportability, and quick construction. In addition, in terms of resource efficiency, the recyclability of the construction materials is of great importance. Paper materials have a high potential for this, due to their strong structure, cost-effective production, and optimised recycling processes.

The following paper presents a case study of a prototype for a temporary paper house that meets the static and technical requirements for a comfortable and hygienic living space by combining different paper materials.

The overall objective of this research was the constructive development of building elements made of paper materials, which meet the requirements for temporary residential use over a period of at least 3 years. The main advantages of using paper materials for this purpose are easy processing, cost-effective production, and a high probability for its sustainable disposal after usage. The main challenges of the material are fire protection and moisture protection, which affect the recyclability, as well as the gluing and joining techniques. An overview of possible solutions for these disadvantages and their applicability will be demonstrated and discussed.

The paper aims to emphasise that simplicity and performance do not need to be diametrically opposed. The envelope, which provides all the functions required of a modern building through its multi-layered structure, represents the performance of this project. Transportation, construction, and joining, on the other hand, were kept as simple as possible in order to make assembly possible even by unskilled workers and under very basic conditions.

The paper is divided into four sections. First, the technical and regulatory requirements for temporary emergency shelters, as well as the decisive characteristics of paper materials are described and analysed. In the second part, the architectural design and the construction typology are defined. The third part focusses on the elaboration and evaluation of building elements with regard to joining technologies, statics, building physics, and production technologies. Finally, the results of the prototype and their transferability are presented and discussed.

Keywords

Paper, construction, building with paper, prototype, emergency shelter, full performance paper house

10.7480/jfde.2021.1.5533

1 INTRODUCTION

In recent years, global crises triggered by natural disasters and wars have led to a steady increase in the number of refugees, now reaching 86.5 million people (UNHCR Global Report, 2019, p. 5). In refugee camps, tents are available on site for shelter, though they are largely unsuitable for a medium to long-term stay. The hygiene situation is also in need of improvement, as often only collective washing places and communal toilets are available (UNHCR Global Report, 2019, p. 207).

One solution to improve the quality of housing is emergency shelters made of paper materials. Paper has been an everyday material for centuries and is used for writing, hygiene applications, packaging, transport, and other purposes. Different types of paper have been developed for all these different purposes. Meanwhile, there are more than 3000 types of paper (Friedrich & Kappen, 2012, p. 4). Paper has the advantages that it is produced cheaply, quickly, and from renewable resources. It is globally available and has highly optimised recycling processes.

As early as the 1990s, Japanese architect Shigeru Ban built the first experimental buildings made of paper materials. These were mainly skeleton constructions, in which cardboard tubes were used for the struts (Latka, 2017, p. 176 ff.). In 2012, the first commercially available paper house, the Wikkelhouse, was introduced in the Netherlands. This project also arose from the intention to create cheap housing for emergency situations within a short time frame. The building consists of a frame construction, which is wrapped in layers of paper materials by a machine (Latka, 2017, p. 233 ff.). Within the framework of the interdisciplinary project BAMP! (**BA**uen **M**it **P**apier (Building with Paper)), several institutes of the TU Darmstadt have been engaged in fundamental research on the use of paper as a building material since 2017 (Kanli et al., 2019; Kiziltoprak et al., 2019).

A wide overview of the topic of building with paper is provided by Dr. Jerzy Latka's dissertation from 2017, which also contains guidelines for the design of emergency accommodation and some prototypes (Latka, 2017, p.293 ff.). Paper as a building material offers the potential to establish a light and cost-effective construction method for temporary buildings. Even after the end of the period of use, unnecessary waste can be avoided as far as possible due to the generally good recyclability of the material.

The following research describes temporary shelters produced from paper materials, which can be built quickly and provide a certain basic level of comfort for their inhabitants. The requirements that have to be fulfilled for emergency accommodation are outlines and an explanation as to how these requirements are met with regard to architecture and construction is given. In addition, the knowledge gained from the prototypes is described and an outlook for future research questions is formulated.

2 TECHNICAL AND REGULATORY REQUIREMENTS

In order to design a paper emergency shelter, it was first necessary to determine the technical and legal requirements for this and to bring them in harmony with the specific characteristics of paper as a material.

The basic research revealed that approximately 86.5 million people worldwide were affected by fleeing and forced displacement. The reasons for this are mainly to be found in disasters, wars,

and political persecution. About half of them are classified as "internally displaced people," whose migration took place within their home countries and often ended in large camps. Another 43 million people have fled to neighbouring countries, or even further away, and need to be taken care of there (UNHCR Global Report, 2019, p. 5).

According to the length of stay in emergency accommodation, a distinction is made between 4 types of accommodation (Latka, 2017, p.308):

- Emergency shelter — as a place to stay for a few days
- Temporary shelter — as a place to stay for a several weeks
- Temporary housing — as a place to stay for a several months to years
- Permanent housing — as a place to stay for years

The need for low-cost and easy-to-erect structures is present in all phases of accommodation. For this purpose, a modular system is designed, whose configurations allow both short-term emergency accommodation and longer-term solutions. Another important criterion is that the developed systems can also be erected by unskilled workers on site. With regard to its properties, the paper house is basically subject to the same requirements as any residential building. These include weather and fire protection, a comfortable indoor climate and sufficient durability. In addition, by using suitable materials, the highest possible degree of recyclability at the end of its useful life should be ensured.

For the temporary accommodation of people in Darmstadt, for example, as a solution in the refugee crisis, the legal requirements for the construction of a building made of paper were examined and clarified in a classic building application procedure with the municipal building administration. In this case, the greatest hurdle is currently the lack of fire protection certificates for the materials used. The results of this enquiry are only applicable within the scope of the Building Regulations of Hessen, Germany, of 2018; in the case of construction in another state or province, the associated applicable regulations have to be applied.

As the decisive characteristics of paper materials are to be considered: Paper is an anisotropic material and can absorb more tensile forces in machine direction than orthogonal to the machine direction. By applying moisture, the hydrogen bonds that bind the cellulose fibres in the paper can be dissolved, thus reducing the mechanical properties by up to 80% (Niskanen et al., 2012: 10).

Due to the fact that they are based on cellulose, paper materials have a capillary-active effect, i.e. they are water-draining. For this reason, it is essential to design the construction of the emergency accommodation in such a way that moisture can diffuse out of the building component and does not precipitate as condensation in the construction. It is precisely these properties that make water ingress a danger to the construction, and which are, on the other hand, beneficial to its later recyclability. By dissolving the fibre bonds in the water bath, it is possible to break down paper materials into their components and give them back into the material cycle.

Paper materials have good thermal insulation properties. The thermal conductivity of paper materials is already comparable with conventional thermal insulation materials without any additional optimisation processes. Recycled cellulose is commercially available as insulation material using the blow-in or pour-in process.

In the event of fire, paper forms a carbon layer depending on its raw density and composition. Due to this carbon layer, paper materials with high raw density show a similar fire behaviour to wood-based materials (Bach, 2020). Sufficient fire protection can be achieved by over-dimensioning load-bearing paper components. By coating or impregnating the material it is also possible to further optimise the building material with regard to its fire behaviour. However, certifications and proof from building authorities still have to be provided.

The following research questions arise from these requirements:

- *What type of modular system enables the combination of all the mentioned types of accommodation?*
- *Which structure is the most suitable for the individual segments to meet the constructional requirements?*
- *How can the connection of the respective segments be solved?*
- *How does the construction of such a system perform in practice?*

3 ARCHITECTURAL DESIGN AND CONSTRUCTION TYPOLOGY

Regarding the architectural design, the emergency shelters reflect the archetype of a house, since the gabled roof is understood almost regardless of culture as a pictographic association of living. In order to match this design approach with the claim to modularity, this form was also applied to the module.

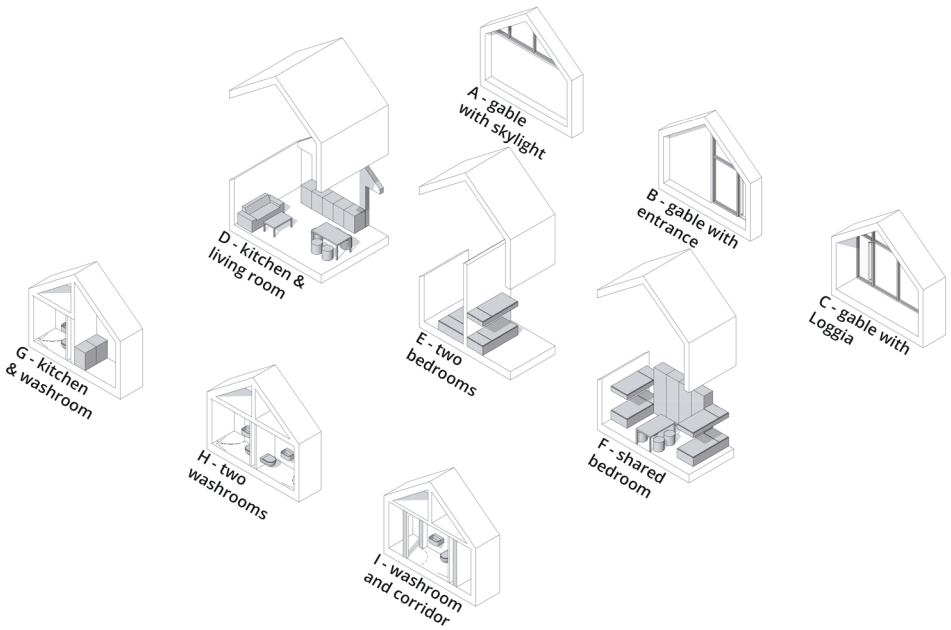

FIG. 1 Module typologies for different types of emergency accommodation depending on number of persons, duration of stay, and level of comfort

The modules are planned with a typical wooden grid dimension of 125 cm and can be combined with each other to form different house sizes. These modules (Fig.1) contain different living functions with reduced space requirements. There are end modules that can be used to close the front sides.

They also contain the windows and the entrance doors to the housing units.The developed system serves the typologies of accommodation (see Chapter 2 - Typologies of accommodation) in a modular way.

The developed systematics range from simple 4-person houses, which serve as emergency shelters for the first few days, to temporary shelters for a few weeks (Fig. 2), to temporary or even permanent housing for months or even years (Fig. 3). Common to all of them is the presence of sanitary units, which should guarantee the best possible hygiene with the greatest possible protection of privacy, especially in larger camp situations.

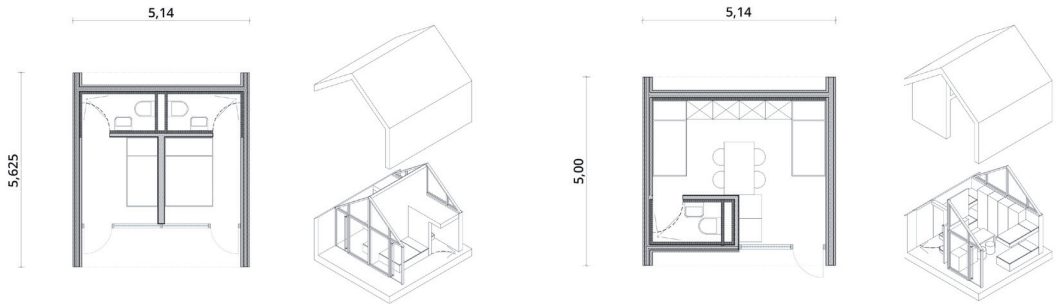

FIG. 2 [left] temporary shelter, [right] emergency shelter

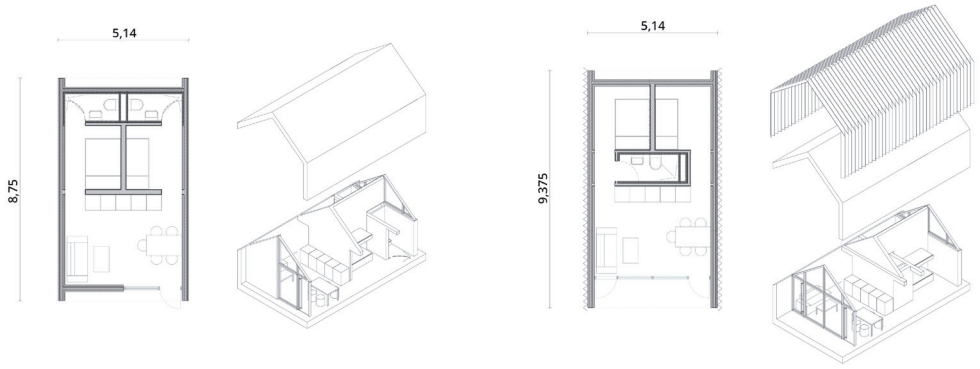

FIG. 3 [left] temporary housing, [right] permanent housing

To prove the constructive feasibility and the quick and easy erection, a demonstrator (Fig. 4) is produced. It has the dimensions of two frame modules and is intended to be used as a proof-of-concept by erecting it in an outdoor area of the TU Darmstadt after completion. Since assembly by unskilled workers is also one of the criteria used to develop the emergency accommodation, the speed at which this can take place will also be investigated.

By committing to a standardised module, it was possible to cover all of the scenarios mentioned in Chapter 2. The alignment of these modules provides sufficient flexibility in the longitudinal direction to meet the needs of long-term residents by providing additional rooms. The results of the design are certainly not to be regarded as exhaustive, since in the 125cm wide grid further spatial uses are conceivable. The question of the system to be used could thus be clarified by applying architectural design methodology.

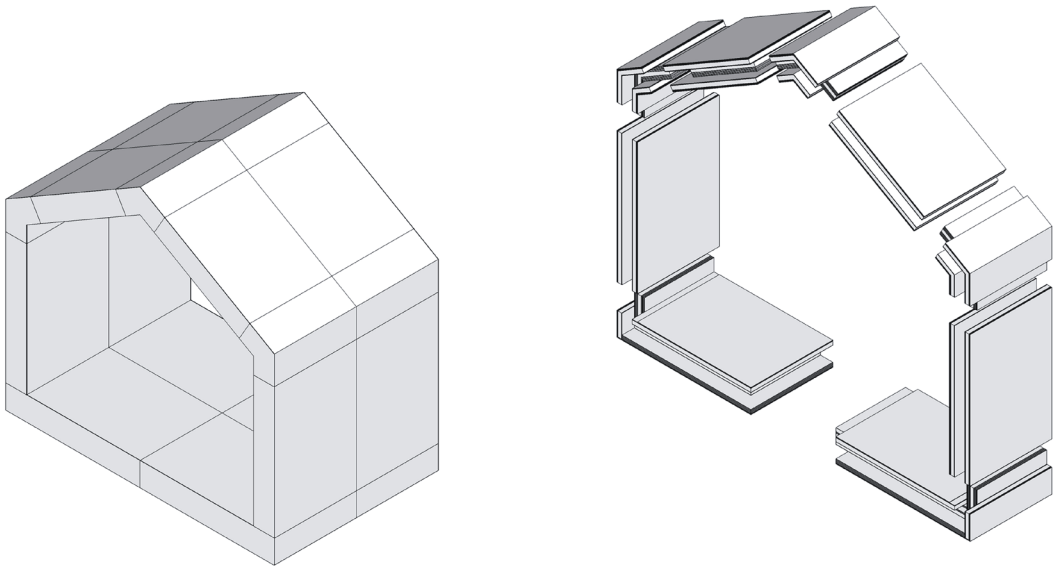

FIG. 4 Construction principle for the demonstrator of the paper emergency shelter

4 ELABORATION AND EVALUATION OF BUILDING ELEMENTS

The construction is a solid paper construction made of prefabricated segments. These are made up of multi-layer laminates with a thickness of 25-30cm, which are combined from cardboard with different specifications. Its production takes place under workshop conditions and the segments are only assembled to the respective frame modules on site. It is planned to equip the emergency shelters on site with a prefabricated wet room containing all the necessary building services installations, which means that piping in the paper construction is not required. Also, the installation of the window and door elements is scheduled only after the construction of the raw paper structure.

The layer structure of the outer walls, which also includes the roof, differs significantly from the layer structure of the floor segments, which is due to the different influences that the respective components are exposed to (Fig. 5). These influences decisively determine the selection and arrangement of the respective layers. The majority of the structure, in terms of the volume used, is made of corrugated cardboard, whose small-cell structure has a good insulating effect.

The layer structure of the wall segments can be divided into 3 areas, the inner and outer protective layer and the core layer in between. While the protective layers protect the structure from environmental influences, the core layer serves primarily to ensure the stability of the structure and is the only one used for the static calculations. It consists of several layers of corrugated and solid board, as well as a core of honeycomb board. The protective layers, which are symmetrically structured, also consist mainly of corrugated cardboard and are covered with phosphorus-impregnated solid cardboard, which has been approved for class B2 fire protection. In the construction of the floor segments, the bending stiffness of the building element and its resistance to rising damp are of particular importance. In contrast to the use of corrugated board, as in the case of the walls, honeycomb board makes up the largest part of the volume of the floor segments. Their cell structure, which is orthogonal to the segment direction, ensures a high degree of compressive rigidity in the thickness direction of the board, whereby the spacing of the cover layers, which is

given by the core, ensures a high degree of flexural rigidity and contributes to the insulating effect of the component. Since no fire protection requirements are placed on the base slab, no B2-boards are used at this point. The focus is on the prevention of moisture damage, which is prevented with the help of a special water-repellent cardboard. This is also done on the inside and outside of the respective segments.

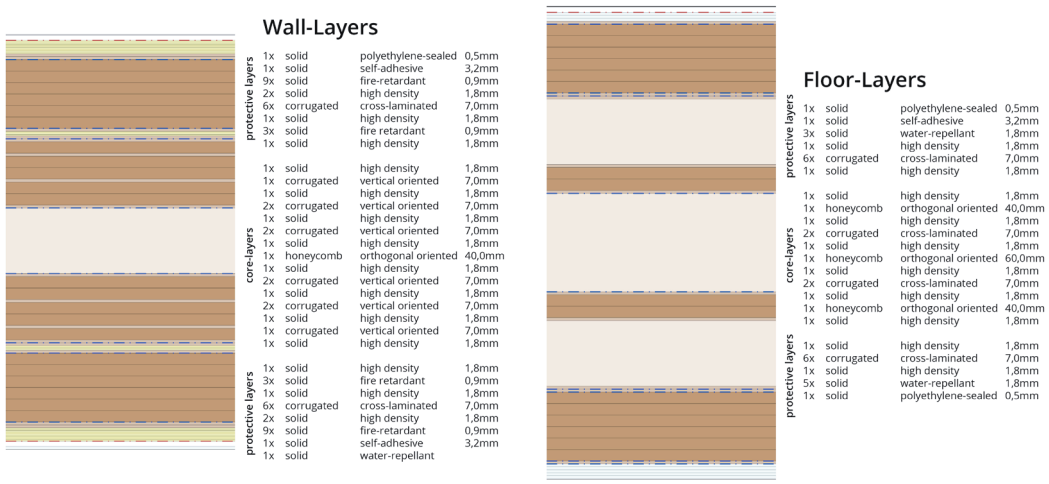

FIG. 5 Layer structure of the wall and floor segments

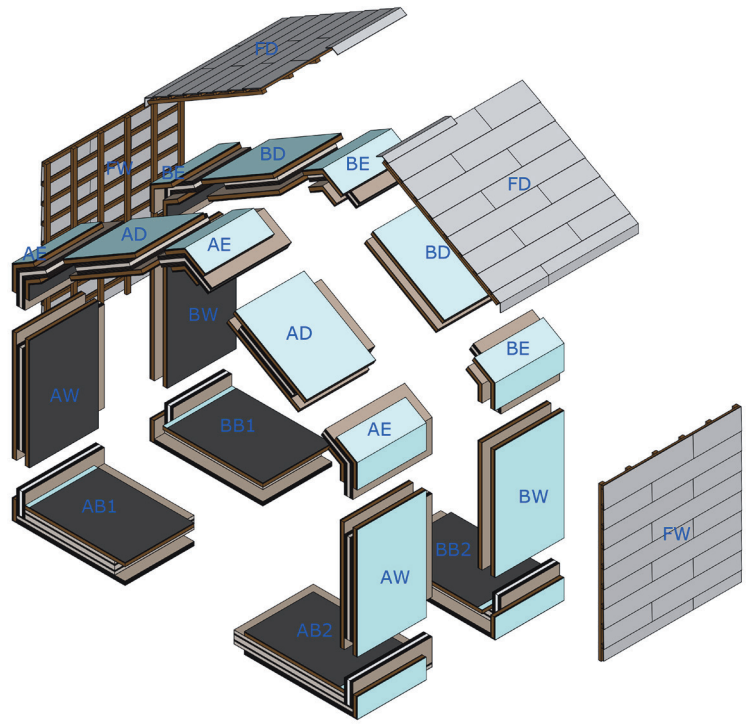

FIG. 6 Exploded view of the demonstrator

As a further protective measure against water, it is also planned to wrap the segments - regardless of their type – in an outer layer of polyethylene-sealed cardboard, also known as beverage packaging. The rain protection thus created is supplemented by a curtain-type ventilated façade made of shingles, which are also made of polyethylene-sealed cardboard (Fig. 6). In this way, an effective rain protection is guaranteed, because even in rainy weather conditions no large amount of water can reach the segments and with subsequent exposure to sunlight the small amount of water that has entered can evaporate again in the space between the segments. The shingles also offer the possibility of replacing single parts without much effort in case of damage.

A challenge in the production process of the modules is the joining by laminating of the individual sheets measuring approx. 1.25 x 2.50 m. Coating the surface with water-based glue leads to a permanent convex deformation of the freshly glued segments, which makes them unusable for further processing. Various attempts to counteract this effect by means of a joining process under pressure, for example with steel weights or wooden planks, failed.

Sufficient pressure has only been achieved with a vacuum pressing process. In this process, an elastic plastic bag is filled with the workpieces, sealed, and then the air is extracted using a vacuum pump. With this process, a surface pressure of up to 100 kN/m^2 can be generated, assuming an ambient pressure of 1 bar and complete evacuation of the plastic bag. Due to the prevalent workshop conditions, a complete evacuation was not achieved, which is why a residual pressure of about 0.3 bar remained in the vacuum bag during production. A surface pressure of approx. 70 kN/m^2 can therefore be assumed. Since the wood glue used initially hardens in the air, it was necessary to find an adhesive that would ensure hardening even under exclusion of air. Two-component adhesives and a few one-component solutions are particularly suitable for this purpose. For the production of the first prototype, a two-component epoxy resin with a processing time of 60 minutes was used, whereby a stable and flat bonding of the layers could be achieved. A disadvantage was that the adhesive had to be applied manually and the laminates had to remain in a vacuum for about 12 hours until the adhesive had completely set. As the epoxy resin was no longer available for the scheduled construction of the demonstrator, a naphtha-based product was found as an alternative which, thanks to its processability by means of spray guns and a hardening time of approximately 30 minutes, allows a more effective production.

The pre-produced segments are joined together using a tongue and groove system (Fig. 6). Here, the core layer takes over the function of the tongue, while the protective layers form the groove. This is ensured by shifting the middle layer by 15cm in both vertical and horizontal alignment. In order to guarantee the sealing at the connections between the individual segments, it is also necessary to fill the grooves with expanding foam sealing tape. In accordance with the hygric requirements for exterior components, it must be ensured that the construction is more impermeable to water vapour diffusion on the room side than to the exterior surface, so that possible water vapour diffusion out of the component is guaranteed.

In order to design the components, it was necessary to match the structural requirements for each component (roof, wall, floor) and the material properties of industrially available paper types. As a result, the functions were prioritised and the paperboards were "sorted" from inside to outside to form a component according to their properties. The tongue and groove connection made it possible to arrange component joints offset from each other and thus minimise weak points. After several tests had determined a suitable adhesive for the laminates, the production of large-format prototypes began.

5 RESULT OF THE PROTOTYPES AND THEIR TRANSFERABILITY

Within the scope of this research, a prototype consisting of two wall segments and a demonstrator consisting of two module frames were produced. In addition, a large number of smaller test specimens were produced to identify the material properties and suitable joining techniques.

The following results were achieved:

— A combination of honeycomb board with a solid board lamination shows high bending resistance and is well suited for the construction of the floor structure. In addition, the high bending resistance is also an advantage for the wall module, as it can counteract buckling.

— Paper materials have good insulating properties and, unlike most other insulating materials, are able to absorb loads. However, this is highly dependent on the structure of the respective semi-finished products. If corrugated board, for example, is aligned vertically, a better load-bearing effect can be achieved than with a horizontal arrangement due to the stiffness of the webs contained in it. However, the vertical arrangement is at the expense of fire protection, as the vertical ducts lead to a chimney effect in the component in the event of a fire.

— The assembly of the components using the tongue and groove system demands additional connecting elements. These should on the one hand counteract the displacement of the elements along the joint and on the other hand prevent the segments from being pulled apart. For this application, connector elements can be used, as they are common in kitchen construction. For this purpose, however, it is necessary to equip the protective layers with a seam of squared wood, since paper materials deform when they are tightened due to their low edge crush resistance.

FIG. 7 The first prototype

Based on the results of these preliminary tests, a first prototype consisting of two wall segments was produced. This prototype was used to verify and demonstrate the assumptions of the preliminary tests as well as the manufacturing technology at a scale of 1:1 (Fig.7). One of the most important parameters to be considered for the production is the enormous amount of time required, since with the exception of the final trimming on the CNC milling machine, all steps for the production of the prototype are done manually.

After the successful production of the prototype, minor adjustments were made to the layer structure and the production process was optimised (Fig. 8). Since a large part of the manufacturing steps are still carried out by hand, the aim was to produce many laminates of the same type in a first step, which are then assembled into segments in the subsequent processes. A detailed assembly plan was also drawn up to enable a structured manufacturing process.

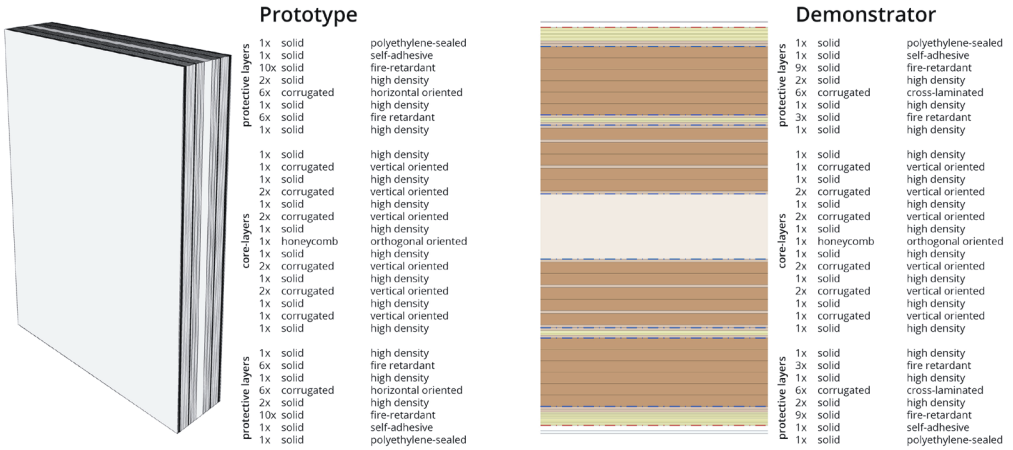

FIG. 8 Comparison of the wall-layers in prototype and demonstrator

Production of the final demonstrator began at the end of July and was completed in mid-September. A total of 18 segments were produced, which were then to be joined together to form two frame modules. In order to make the production of the demonstrator as efficient as possible, a detailed assembly plan was prepared. According to this plan, semi-finished products were initially manufactured, the layer structure of which is repeated in the building. In the next step, these semi-finished products were joined to form the respective layers (core layer and protective layers) of the building elements. These individual parts were trimmed with the help of a CNC milling machine. In the case of the protective layers, the anchor holes for the connectors were also set using the milling machine. These elements were finally assembled to form the floor, wall, roof, and corner segments.

Before the demonstrator was erected, a gravel surface was laid as a substructure and compressed. This serves to ensure the seepage of water and to avoid movements in the subsoil caused by ground frost. Because of the rainy weather, the construction process was carried out under a protective tent. The construction was expected to be sufficiently watertight after the shingle façade had been applied. The construction of the approximately 3.50 x 2.50 x 3.25m sized demonstrator took place within three days and required a team of seven employees.

A layer of polyethylene-impregnated paper was spread over the gravel substructure to protect the components from sharp stones from the ground. Subsequently, an aluminium-sealed vapour barrier membrane was laid on top of this layer, which was later to protect the demonstrator from rising moisture. After laying the floor slabs, the walls were inserted, and the elements were tightened with the connectors. The aluminium-sealed vapour barrier was installed approx. 50cm above the ground at the building elements to serve as a plinth seal.

FIG. 9 Floor and wall modules. Assembly of the roof in the background

FIG. 10 Lifting the roof onto the construction

The assembly of the roof had to take place on the ground, because an overhead assembly of the up to 75kg heavy elements would not have been possible. Afterwards, the roof was lifted with the help of a fork-lift and lowered into the existing construction.

After the supporting structure had been erected, the "expansion" could begin the following day. On the inside, a protective layer of polyethylene-impregnated paper, which was attached to double-sided adhesive solid cardboard, was mounted. On the outside, wooden battens and counter battens were installed to ventilate the façade. The façade shingles made out of polyethylene coated paper were fixed to these battens as the outer protection layer.

The open sides of the gables were closed by a construction of extruded polystyrene sheets, after the front sides of the walls were also protected with a layer of polyethylene-impregnated paper. The U-value of the gable walls corresponds to the U-value of the paper construction. For this reason, a realistic indoor climate can be created to enable further testing and monitoring.

FIG. 11 The finished demonstrator

The demonstrator has been set up at the Lichtwiese campus of the TU Darmstadt. On site, it is to be exposed to real environmental conditions for 3 years in order to be able to make further statements about the usability of the material and the construction method.

During the fabrication and construction of the demonstrator, it was observed that:

- Manual gluing of the elements is very time-consuming and complicates the use of conventional adhesives used in the paper industry, since they were developed for machine applications.
- Trimming the segments on the CNC milling machine has only been possible for planar elements. The six edge-segments had to be cut out manually. Especially regarding the holes for the joints this was a very time-consuming task.

— The individual segments turned out much heavier than expected (see Table 1), which required four or more workers to put them into place. In future, the element weight should not exceed 50kg.

TABLE 1 Weight of the segments

DESCRIPTION		WEIGHT	QUANTITY
AB1	Floor tongue/groove	89,0 kg	1 pc.
AB2	Florr tongue/tongue	95,0 kg	1 pc
AW	Wall tongue	101,1 kg	2 pc.
AD	Roof tongue	74,5 kg	2 pc.
AE	Edge tongue	51,4 kg	3 pc.
BB1	Floor groove/groove	77,0 kg	1 pc.
BB2	Floor groove/tongue	82,0 kg	1 pc.
BW	Wall groove	93,5 kg	2 pc.
BD	Roof groove	68,5 kg	2 pc.
BE	Edge groove	46,0 kg	3 pc.
FW+FD	Shingles	105,0 kg	all
total		1.415,4 kg	

In summary, it can be said that the construction of the demonstrator required an unexpectedly large number of volunteers due to the high segment weights. However, with the exception of the forklift, the assembly was able to be carried out with simple hand tools. About 1/3 of the construction team consisted of employees who had already carried out the prefabrication of the segments. Due to the simplicity of the system the construction method was quickly explained to the remaining 2/3 of the workers.

6 CONCLUSION AND OUTLOOK

The developed system meets the essential requirements for temporary accommodation. With the construction of the demonstrator as proof of concept, it has been proven that the production of segment components from paper materials is possible and feasible. The assumptions made with regard to the durability of the construction will only be further investigated in the course of the demonstrator's three-year service life.

The knowledge gained during the design and manufacture of the demonstrator can be used as the basis for further solid paper constructions. Results on the durability of the construction under real environmental conditions can only be researched in situ.

In the medium term the construction of a habitable prototype is imaginable. The developed module variants by no means exhaustively reflect all possibilities in which the buildings can be used. Other floor plans and application scenarios are conceivable, such as the further development of the segment system into a kind of construction kit for paper houses.

A more in-depth scientific investigation is required, especially with regard to fire protection and adhesive technology. Since there is no available information on the fire behaviour of the construction method used, it is essential to research this before constructing an habitable building. With regard to the bonding technology, it is first necessary to investigate what a more suitable adhesive could look like. The epoxy or naphtha-based adhesives used in the tests prevent the building from being recycled at the end of its lifespan and should, from an ecological point of view, urgently be replaced. After researching a suitable adhesive, the question of what the industrial production of the segments could look like has to be answered. Gluing and subsequent pressing by hand cannot be assumed to be cost-effective and only cutting the segments by means of a CNC milling machine appears to be efficient. Once these questions have been clarified, it would be imaginable to produce the system in larger quantities and ship it to places where temporary accommodation is urgently needed as part of crisis and development aid.

Acknowledgements

Special gratitude is due to Dr. Jerzy Latka, who contributed actively to this project as a guest scientist at the TU Darmstadt, and to the student assistants, without whom the manual production of the prototypes would largely not have been possible. The research project was supported and funded by the research initiative ZukunftBau of the Bundesinstitut für Bau-, Stadt- und Raumforschung and the following industrial partners: KATZ GmbH & Co. KG, SWAP (Sachsen) GmbH Verbundwerkstoffe, Yamaton Paper GmbH, Eurowell GmbH & Co. KG, Transsolar Energietechnik GmbH,imagine computation GmbH, Unger-Diffutherm GmbH, Ingenieurbüro Langner GmbH, Easy to trade GmbH, Papier- und Kartonfabrik Varel GmbH & Co.KG.

References

Bach, R. (2021). *Papier Fassaden - Entwicklung konstruktiver Prinzipien für Fassaden aus Papierwerkstoffen mit Fokus auf Brandschutz, Wärmedämmung, Feuchteschutz und ökologische Eigenschaften (Translation) (Paper facades - development of constructive principles for facades made from paper materials with a focus on fire protection, thermal insulation, moisture protection and ecological properties).* (Doctoral Dissertation. RWTH Aachen). (expected release: 2021)

Friedrich, S. & Kappen, J. (2012). *LWF aktuell 89/2012.* Freising: Bay. Landesanstalt für Wald und Forstwirtschaft und für das Zentrum Wald-Forst-Holz Weihenstephan.(Freising: Bavarian State Institute for Forestry and the Center for Forestry Weihenstephan) https://www.lwf.bayern.de/service/publikationen/lwf_aktuell/012307/index.php

Kanli, E., Bach, R., Götzinger, R., Kiziltoprak, N., Knaack, U., Schabel, S., & Schneider, J. (2019). Case study: development and evaluation methods for bio-based construction realized with paper-based building materials. In *3rd International Conference on Bio-Based Building Materials (ICBBM).* Belfast, United Kingdom

Kiziltoprak, N., Kanli, E., Schneider, J., Knaack, U., Bach, R. (2019). Load capacity testing method for non-conventional nodes joining linear structural paper components. In *International Conference on Structures and Architecture, 2019,* Lisbon, Portugal.

Latka, J. (2017). Paper in architecture. *Architecture and the Built Environment.* https://journals.open.tudelft.nl/abe/issue/view/547

Niskanen, K., Berglund, L., Carlsson L., Coffin, D. Gustafsson, P., Hägglund, R., Kulachenko, A., Mäkelä, P., Nygards, M., Östlund, S., & Uesaka, T. (2012). *Mechanics of Paper Products*. Walter de Gruyter GmbH

UNHCR The UN Refugee Agency (2019). UNHCR Global Report. *UNHCR.* https://www.unhcr.org/globalreport2019/ (24.08.2020)

Skin Metrics

The Wicked Problem of Façade System Assessment

Keith Boswell[1*], Stéphane Hoffman[2], Stephen Selkowitz[3], Mic Patterson[4]

* Corresponding author
1 Skidmore, Owings & Merrill, keith.boswell@som.com
2 Morrison Hershfiel
3 Lawrence Berkeley National Laboratory
4 Façade Tectonics Institute

Abstract

Building façades are key to the building systems integration necessary to realise critical health, carbon, resilience, and sustainability goals in buildings and urban habitats. In addition, façade system design and delivery may be the most rapidly developing building technology, with novel materials, assemblies and techniques introduced in the marketplace frequently. However, these developments are occurring in the long-running absence of an appropriate framework for façade system performance evaluation. There has been no general convergence on the assessment criteria nor, for the most part, on the metrics to accompany those criteria. The convergence of myriad and often competing variables that characterise the building façade mark the development of a comprehensive integrative assessment framework as a wicked problem, The lack of such a framework inhibits meaningful development and adoption of innovative façade technology, leaving aesthetic considerations to drive application and compromising the evolution of performative system behaviour. It prohibits a meaningful comparison between façade systems, or of new techniques with prior applications. Adoption of new façade technology is constrained as designers, building owners, and, most importantly, authorities with jurisdiction at the level of city government are unable to accurately value its performative contribution to occupants, to a building project, or to the urban environment.

Very early efforts and thinking in the development of a comprehensive Integrative Façade Assessment Framework by the Façade Metrics Working Group of the Façade Tectonics Institute are documented here. A preliminary review of existing façade system metrics and assessment strategies reveals they are fragmented, too narrowly focused, and lack the comprehensive integration to provide an accurate evaluation. With a strong focus on energy performance in new buildings, deep and vital considerations like retrofit and renovation strategies, passive survivability, durability and service life, and resilience are often neglected entirely. We outline some new directions that begin to address these gaps and suggest a data-rich, visual framework and knowledge-sharing platform to advance progress with enhanced metrics and façade systems evaluation and comparison.

Keywords

Façades, building skin, curtainwall, building envelope, façade performance metrics, façade performance, sustainable façade systems, building resilience

10.7480/jfde.2021.1.5538

1 INTRODUCTION

The built environment plays an increasingly important role in all aspects of our personal lives and impacts our collective future. In addition to the obvious function of providing shelter, housing, work, and institutional functions, the built environment has two less obvious but perhaps even more potent impacts on our lives. The building industry and our existing building stock has 1) a major impact on energy use and thus carbon emissions and 2) a direct impact on our health, wellbeing, and productivity, as we spend 90% of our time indoors. Globally we are still struggling to understand and clarify the nature of these challenges, to formulate goals and targets to address these problems and then to create comprehensive and aggressive programmes to solve them. These must ideally be implemented and executed in an unprecedented rapid time frame of just 10-30 years in order to address the threats posed by the climate crisis. Success requires that the overall performance of our new and existing building stock be dramatically improved so that the associated carbon impacts can be reduced at a scale never-before seen.

Innovation and rapid change in the building industry at this scale has always been a challenge and is only achievable if there are well defined performance goals and clear metrics to measure progress in the direction of their attainment. In order to tease apart and explore some of the underlying issues and challenges, we focus in this paper on the subset of those performance challenges that relate to the building façade system. Myriad building performance considerations converge, and often conflict, at the building skin, casting the façade system in a pivotal role in the larger performance context of buildings and urban habitat. Complex social and economic relationships combine with the technical considerations to form wicked problems (Rittel & Webber, 1973).

Current metrics and metric sets are inadequate to provide for the comparative evaluation of complex façade systems (Avesani, 2019; Bianco et al. 2018; Dave, 2012). We are directly concerned with performance across the building lifecycle with a time frame that can extend to 100+ years. Performance will be defined by a series of metrics that help define a system of measurement, which includes performance indicators with associated scales or benchmarks. For example, a common metric for an office building might be energy use intensity, EUI, expressed as kWh/m^2. Metrics are frequently, but not solely, based on quantitative descriptors of performance and there is generally a scale with explicit or implied rankings that can be quantitative or qualitative in nature.

Our goal is not to invent new metrics, but to identify and assemble the best existing metrics into a holistic framework that facilitates façade system evaluation. After a discussion of the broad challenges of organising building skin metrics, we demonstrate that challenge in the further exploration of two different metric sets: façade thermal performance and daylight performance. As this project develops beyond the scope of this paper, we also intend to confront the holes in the framework where conventional metrics do not yet exist and their very formulation is a challenge, e.g., adaptive capacity (Patterson, 2017, p.136), reclamation potential (Hartwell & Overend, 2020), biophilic considerations (Browning, Ryan, & Clancy, 2014), and more.

Applied to enclosure system design and delivery, building skin metrics must be organised, presented, tracked, and updated in a manner that is supportive of decision-making, not only in design and execution but across the building lifecycle. Central to this project is the intent to organise, structure, and communicate a complex set of façade process metrics across the whole-building lifecycle in a graphic and accessible format so as to encourage engagement, understanding, refinement, and enhanced decision making. We conclude with a preliminary template for the visual presentation of

an individual case. Additional output forms of comparative data between cases are suggested and briefly discussed, as are additional future opportunities, barriers, and limitations.

2 FAÇADE METRICS: MEASURES OF THE BUILDING SKIN

Even a short-list of performance factors for which we need metrics, focused on the building skin or directly connected to it, becomes a long list (Table 1).

TABLE 1 Sample performance attribute sets requiring façade metrics

SCALE	PERFORMANCE CONSIDERATION
Occupant	View
	Thermal, visual, acoustical comfort
	Productivity
	Health, wellness
	Daylight and ventilation
	User control
Facade	Properties: – thermal/optical – condensation – air flow/ventilation/ infiltration – acoustical – structural – moisture
	Embodied energy/carbon; LCA
	Power generation
	System: framing, glazing, thermal bridging, interfaces, vapor, condensation
	Shading integration
	Sensors, controls and interfaces
	Durability, adaptability, maintenance
	Cost
Building	Daylighting integration with electric lighting
	Annual energy/carbon behavior – overall and façade related
	Embodied energy/carbon; LCA
	Electric load, shape/peak – overall and façade related
	Power generation
	Smart controls infrastructure
	Operating cost
City/Neighborhood	Urban shadows
	Heat island effects – façade related
	External reflections – glare, energetic, visual
	Aesthetic – integration with urban fabric

This disaggregation of performance factors and related metrics can be further expanded in terms of the physical construction of the façade into a "nested" series of other physical, operational, or time-based lifecycle constructs. In the physical world of size and scale we address metrics across 8 orders of magnitude, from the level of coatings on glass (~ 10^{-6}m) to a full curtain wall (~100m).

In the temporal realm we also consider metrics across 8 orders of magnitude, from the scale of seconds, e.g. wind gusts, to durability over 100 years. As illustrative examples we show a hierarchy of system complexity and scale below, with typical sample associated metrics (Table 2).

TABLE 2 Hierarchy of metrics across system complexity and scale

FAÇADE ELEMENT	METRIC
Coated glass	Tv, emissivity
Insulating glazing unit, IGU	Tv, SHGC, U_{cog}
Curtainwall element	U, wind load resistance
External automated blind	SHGC vs blind position, BSDF

Virtually no building skin is homogeneous and metric values may change as the scale and boundaries change. The U-value, or rate of thermal heat transfer, will have an initial value for the centre of glass of an IGU, a different value for the full IGU including edges, a different U for the IGU in the framing system and finally yet another effective U for the as-built system in the wall. From the standpoint of an evaluation framework, at some point we need to consider all of these discrete metrics; the challenge is to know which metrics are critical or most applicable for each element and at each stage in the building life cycle.

2.1 WHAT TO MEASURE

Do we care what the centre-of-glass U-factor is for the glass if the U-factor for the façade assembly meets intended performance goals? What opportunities are there to simplify our evaluation framework, e.g., by focusing on high-level and holistic metrics in as-built systems?

Metrics cover a wide range of performance domains. Relevant metrics for the building skin include energy/thermal and optical parameters, acoustics, structural, lighting, durability, and so on (Table 1). While many are intrinsic to the device or system some will be dependent on the specific application, for example the U of a glazing assembly will change as the tilt changes from horizontal to vertical, and the visible transmittance will change as the angle of incidence of sunlight changes. The exposure of the façade assembly in the building is certainly relevant contextual information and integral to some of the desired metrics.

Some building façade metrics are nearly universally referenced and will be utilised in virtually all projects. Others are unique to building type, e.g. hospitals, or geography, e.g. earthquake resistance, or climate, e.g. freeze protection.

While a vast body of building skin metrics have existed for years and evolve only slowly over time, emerging new performance concerns and, in some cases, new products with new performance characteristics have driven the invention, development, and refinement of new metrics to help assess these new performance concerns. For example, coatings on glass can now generate electric power, so new metrics are needed to quantify that performance. Conventional PV systems have their own performance metrics; can these be used for power-generating façades or are new metrics needed? Developing concerns with the behaviour of buildings during periods of electrical grid failure, whether the result of extreme climate impacts or other causes, have given rise to the concept of

passive survivability, requiring new metrics to evaluate and compare performance. For example, in the case of very hot, sunny climates the ability of the building envelope to withstand and/or delay the rise of life-threatening internal temperatures with no functional HVAC is now a design concern with associated metrics. In brutally cold climates the thermal integrity of the building envelope can be measured and compared with a "time-to-freeze" metric; the time it takes for interior temperature to drop below freezing without power.

The values of metrics related to materials and assemblies in the as-built systems may change as they age through the building operations cycle due to forces like exposure to sunlight and other natural processes of wear and degradation, e.g. pressure cycling over time may cause argon glass leaking from a window which will raise the U. Metrics that track deterioration of the service condition of a façade system can inform facility management and ownership of a looming need for repair or renovation while becoming an important measure of comparative durability. Determining targets, standards, or baselines for some of these important performance metrics, like durability, can be a challenge in itself, e.g., there are widely divergent opinions on how long a building or façade system should last (Patterson, 2017, p.150).

Most metrics can be expressed in quantitative terms, but others may be subjective, or lack agreed upon scales or benchmarks, such as view from a window. The growing importance of occupant wellness and productivity considerations to building owners and designers has given rise to questions of what constitutes an adequate view, and a resurgence in research to define new and better metrics to characterise and quantify views from windows. Biophilic considerations similarly produce a new array of metrics intersecting with the façade system as the interface between the building interior and the world of nature outdoors.

Some metrics are intrinsic to the materials and their application and others may be highly dependent on the specific manufacturer. For example, the visible transmittance of 6mm low iron glass will be similar across most suppliers, but the embodied carbon in that glass may vary widely depending upon the source of the glass. Metrics like embodied energy or carbon depend not only on the manufacturing process and location but also on transport from source to component manufacture to system integration to building site. These complex cradle-to-grave or cradle-to-cradle assessments fall under the broader term of Life Cycle Assessment (LCA). Entire new, and often complex, rating systems have been developed in recent years to quantify not just embodied carbon metrics but a wide range of comprehensive environmental impact metrics for many building components for their full cradle-to-cradle life cycle. The initial focus was on structural materials, but this has expanded to envelope components and systems as well. While some data elements may be relatively generic, e.g. energy/kg for glass manufacture, the overall environmental impact can be highly dependent on differences in operational practices between manufacturers and in supply chain logistics.

Some key performance parameters are well known in the façade industry and have not changed dramatically over time, while other commonly referenced metrics have evolved rapidly over the last decade in response to multiple drivers such as: the need for new and more robust performance data for decision making, new underlying research that supports accurate and verifiable results, and new tools and design processes that allow more complex metrics to be calculated or extracted from other data processing. Many of these are applicable to most projects and in fact may be referenced by international, national, and state building codes, as well as by voluntary rating systems such as LEED or BREEAM.

We briefly highlight two important examples of trends in the field of building skin metrics. The first example involves the development of a new metric, TEDI, that helps directly distinguish and quantify the impact of the building skin on overall building energy performance. The ability to quantify envelope impacts separately from overall building EUI metrics is crucial to enabling the next generation of high-performance façade system solutions. The second is the refinement and development of a series of new daylighting metrics to quantify and rank the daylight performance of buildings as impacted by the design of the building skin. These metrics involve design parameters interior to the skin, as well as site and climate parameters. And they relate not only to building performance but to the health, comfort, and productivity of occupants.

3 BETTER BUILDINGS THROUGH BETTER METRICS

Façade system metrics provide the gauge by which performance is evaluated and systems compared, and the measure of the contribution of these systems to the overall performance of buildings and urban habitat. Business management guru, Peter Drucker, is famously quoted as saying, "If you can't measure it, you can't improve it."

3.1 WHY BETTER METRICS MATTER

Metrics that fail to properly account for the contribution of the façade system stifle innovation and lead to persistence of the status quo. This in turn can result in stagnation of façade system development while other building systems embedded in conventional practices continue to evolve. As relative performance gaps widen, it becomes increasingly difficult to reform these entrenched practices.

One key example of this in the façade industry is the role the enclosure plays in the overall thermal performance of buildings. It is widely acknowledged that as-built digital energy models of buildings are rarely accurate. The gap between as-simulated designs and as-built building performance has been known for some time and has been attributed to many factors including inaccurate simulation, inaccurate simulation inputs, poor construction, value-engineering post-simulation, sub-optimal building operation and user impacts.

One way to significantly advance the adoption of new façade technologies is to acknowledge the need to provide a better accounting of how they impact overall building thermal performance. The traditional "parallel path" approach to modelling the façade system is still common in current whole-building energy simulation. This approach evaluates different elements of the façade in isolation and ignores the impact of the interface between systems (wall and fenestration, opaque wall panels and structure, fenestration and structure, spandrel and transparent elements, etc.).

Furthermore, the persistence of 2D thermal simulations of complex 3D façade systems, such as spandrel panels, tends to overestimate the performance of current systems making it harder to justify new, better-performing technology based on energy savings alone. If, based on these simplified simulations, we are led to believe current technologies provide a performance of R-15 (0.9 $m^2 \cdot K/W$) or better, there is limited value in going to technologies that could deliver R-30 (5.3 $m^2 \cdot K/W$) performance. However, if we acknowledge that current construction may only deliver an effective performance of R-5 (0.9 $m^2 \cdot K/W$) and new practices or technologies can increase this to an

effective R10 or R15 (1.8-2.6 $m^2 \cdot K/W$) then the payback period on this investment becomes much more appealing. This concept was demonstrated by Norris et al. (2015) in a paper comparing the thermal performance of spandrel assemblies using 2D and 3D simulations in comparison with guarded hot box testing.

To achieve this more stringent approach to accounting for the effective 3D performance of façades in whole building energy modelling, the concept of point and linear transmittances at interfaces outlined in the *ASHRAE 1365RP* (Roppel & Marif, 2011) needs to be incorporated. Better simulation tools and practices are needed to provide accurate analysis of system level performance; While the clear field performance of windows and simple wall panels may be reasonably accurately estimated in current 2D simulations, the report demonstrated that large thermal losses can occur at the interfaces/connection points to the building and between façade elements (e.g., panel attachments, through spandrel panels) that can only be accurately assessed with 3D simulations. The development of the *Building Envelope Thermal Bridging Guide* (Morrison Hershfield, 2020) in British Columbia and its further development this past decade has provided the industry with a wealth of information on the effective clear field performance of a wide range of enclosure assemblies based on 3D thermal simulations, including the impact of thermal bridging at the interface between them in terms of linear transmittance. Resources like this make it easy for practitioners to achieve greater accuracy of façade system performance in whole-building energy simulations. The 2020 Energy Conservation Code of New York City (ECCNYC) is moving in this direction by requiring design teams to provide a tabular analysis of thermal bridges and related linear transmittance values. In the absence of these changes, current practices are akin to modelling a HVAC system and not accounting for duct losses.

3.2 EUI VS. TEDI

Comparisons of whole building EUI metrics is a typical starting point for comparing building performance, but it should be a starting point, not an end point, in understanding and improving building performance. While incorporating the result of more realistic simulations that accurately reflect the impact of thermal bridging in whole-building energy simulations is a first step, it will still not be enough to significantly move the industry forward. The current reliance on the Energy Use Intensity (EUI) metric in whole building simulation also tends to under-value the impact of the façade. When this metric is used to compare the energy impact of other, often unrelated, systems, it diminishes the impact of the façade. Therefore, the performance of the façade needs to be evaluated on the basis of new metrics such as Thermal Energy Demand Intensity (TEDI) rather than the traditional EUI.

TEDI is a metric that represents the annual heating load per floor area of a building. This is the amount of heat needed to offset the heat loss through the building envelope and condition the ventilation air. TEDI is derived from energy simulations where any parameter that impacts the heating load is captured by TEDI, including exterior surface area, thermal transmittance of building envelope components, airtightness, solar radiation, internal gains, heat recovery, and ventilation. The TEDI concept has been applied by the Passive House Institute to focus the industry on minimising heating loads, reducing the dependence on large and complex mechanical systems and increasing occupant comfort in buildings. Codes like the British Columbia Step Code and the latest Toronto Green Standard have already implemented TEDI as a key metric in building performance. The concept of TEDI is outlined in further detail in the recent publication in British Columbia of the *Guide to Low Thermal Energy Demand for Large Buildings* (Morrison Hershfield, 2018).

Taken together, the concept of the TEDI metric coupled with the adoption of accurate 3D thermal simulations of façade systems and the additional heat loss at key interfaces in energy simulations has the potential to focus industry awareness on the key role façade systems have in building performance and spur the development and adoption of new technologies that can further improve the performance of façades.

3.3 DAYLIGHTING METRICS

For decades the key global metric for daylighting design in buildings was daylight factor (DF), the ratio of horizontal illuminance at an indoor location divided by the outdoor global illuminance under an overcast sky. This was implicitly a metric that was used to measure daylight adequacy, developed in the UK where skies were characteristically overcast. If DF was 2% or greater the daylight was deemed to be adequate at that location in the room. DF is not necessarily an indicator of good design; it is not sensitive to climate or orientation and provides mostly an insight into typical or minimal interior illuminance levels at the point for which it was calculated. It had the advantage that it could be quantified rapidly using simple available graphical tools that could be overlayed on plans and elevations of a room design in an era of slide rules and hand calculators.

If we fast forward to 2020, designers now refer to a whole series of new daylight metrics that are climate-based and time-based (CBDM, climate based daylight modelling), account for exterior obstructions, explicitly address direct solar effects with any type of glazing or shading (operable or fixed), report traditional horizontal or vertical illuminance values as well as view-based luminance maps. The time-based analyses provide detailed statistical data for averages, distributions, extremes, and more. While these can be enabling in the exploration of novel performance attributes, they can also be confusing, given the complexity of the input and output data. Not only are there new metrics to assess daylight performance but these new metrics are associated with new tools, workflows, and optical databases for products that allow these metrics to be determined rapidly and accurately, assuming the input data for the glazing and shading products is available and accurate, and assuming the 3-D geometry and surface properties of the rooms are properly represented. The availability of these core computational engines supports a whole new series of tools and workflows to optimise multicriteria assessments of daylight designs, where multiple, often conflicting, metrics must be considered. For example, maximising one metric, lighting energy savings based on work-plane daylight availability, can be achieved with large glass area and minimal shading, but may produce intolerable glare, as well as large cooling loads and thermal discomfort. Use of electrochromic glass or automated blinds may optimise glare metrics but lower the daylight energy savings metric.

A short-list of daylight related metrics in use today is included in Table 3. In some cases these are complementary, in others they may be duplicative and even give contradictory design insights and guidance, which is why this topic is of keen research interest and practical importance.

A more detailed discussion of these evolving design and operational metrics for daylighting is beyond the scope of this paper, but current state of the art as it has evolved over the last 20 years can be reviewed in a selection of recent research papers which address metrics as well as process issues (Dubois, 2003; Reinhart, Mardaljevic, & Rogers, 2006; Mardaljevic, Heschong, & Lee, 2009; Mardaljevic, Andersen, Roy, & Christoffersen, 2012; Van Den Wymelenberg & Inanici, 2014; 2015; Carlucci, Causone, De Rosa, & Pagliano, 2015; Galatioto, 2016; Ko, Schiavon, Brager, & Levitt, 2018; Beltran, 2020; Shafavi et al., 2020)

TABLE 3 Common daylight metrics

METRIC
Workplane illuminance; Illuminance uniformity
Surface luminance; Luminance ratios
Daylight Factor, DF
Useful Daylight Illuminance, UDI
Spatial Daylight Autonomy, sDA
Daylight Glare Index, DGI
Discomfort Glare Probability, DGP
Annual Sunlight Exposure, ASE

4 KNOWLEDGE-SHARING: HOW TO BEST CONVEY BUILDING FAÇADE INFORMATION

Metrics out of context are meaningless. Communicating façade system information, to be informative, is an inherently holistic undertaking and a challenge for many of the reasons discussed above. The façade system links multiple scales of material/product, assembly, system, building and site, and key information from these various domains are necessary context for project documentation. The complexities of the metrics themselves have been extensively discussed previously. At the primary scale of documentation—the façade system itself—large buildings frequently involve multiple wall types, each with its own performance measures and sometimes involving varying metrics. Finally, façade system documentation must include communication of visual, design, and other descriptive information in addition to the performance criteria. The availability of a façade documentation resource consisting of graphics, details, criteria, metrics, and measures could provide a valuable industry resource and inform future façade system design and delivery.

As part of this façade metrics project, we propose to develop a robust, fully searchable database of projects with comprehensive information and data on their façade systems. A compendium framework is suggested here that is intended to be independent of façade scale or type, searchable, and consistent in format. Information on individual projects, as well as comparative assessment between projects, will be accessible. Multivariate search capability will accommodate refined research parameters, e.g., all curtainwall wall types incorporating smart glass in San Francisco and Seattle completed between 2012 and 2016, or e.g., all commercial projects in high seismic zones internationally incorporating adaptive exterior shading. The intent is to promote informed façade system assessment and development, and, ultimately, to accelerate the evolution of advanced, high-performance façade technology.

A simple preliminary draft framework for organising, compiling, comparing, and presenting façades is represented in Table 4 and is keyed to Figures 1-6, which follow the table. The figures represent a single case of web pages that will be built from database output forms as required to fully represent individual projects. These forms will likely link to sub forms, e.g., an output form used as a template for a unique wall type, multiple cases of which can be linked to an individual project case, as well as to outside data and information sources.

TABLE 4 Preliminary organization of façade system cases by section, and keyed to following Figures 1-6.

SEE FIG. (FOLLOWING)	SECTION REPRESENTED	PROPOSED CONTENT
Fig. 1	Project Description / Splash Page	Overview and context
Fig. 2	Architect's Pages – building plan, elevation, section and 3d depiction of façade system	Building and façade system design
Fig. 3, 4	Façade system description- façade system facts	Façade performance–principles and application
Fig. 5	Façade performance narrative	Description of performance attributes
	Performance criteria graphic	Metric graphic representation (in development)
Fig. 6	Performance criteria and metrics	Qualified metric values for project

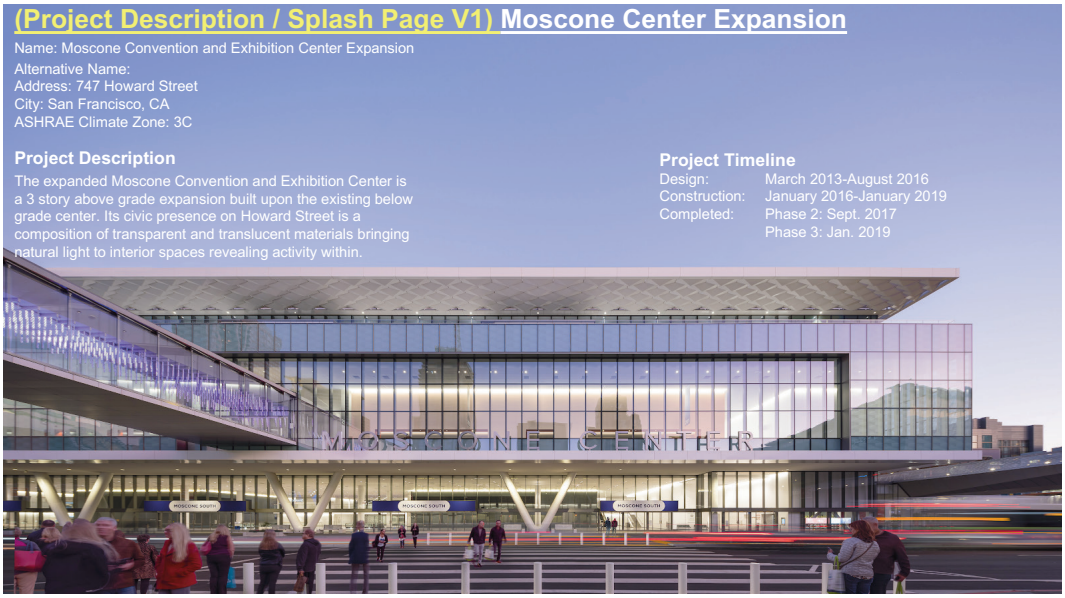

FIG. 1 Splash Page – Contextual introduction: overview image of building featuring the façade system(s), with project general facts/description/timeline

(Architects Page V1) Moscone Center Expansion

Architect's Description

1) Visuals: Plans, Sections, Elevations
2) Architect's façade design brief (visual and performance): Provide highly transparent and translucent facades that engage the city's cultural hub surroundings to areas of internal circulation creating an extension of the community. Provide high performance, energy efficient, low embodied carbon, and seismic resistant facades that address local climate and internal building functions.

Companies Involved

Owner: Department of Public Works City of San Francisco
Architect: Skidmore, Owings, & Merrill LLP San Francisco, CA
Contractor: Webcor Builders San Francisco, CA
Enclosure Contractor: Enclos San Ramon, CA

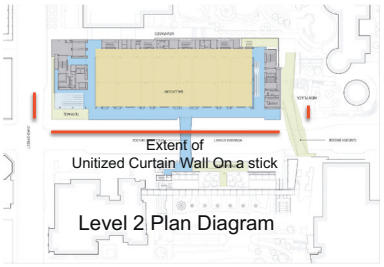

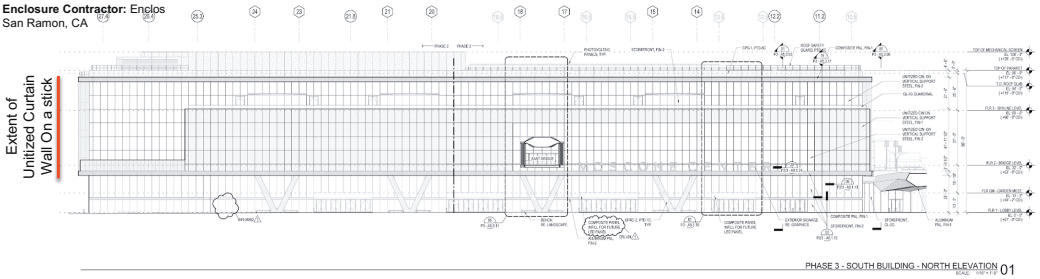

FIG. 2 Architects Page – Description of façade system visual and performance design objectives

(Facade System Description V1) Moscone Center

Façade Narrative

Façade Details of note:

Unitized Aluminum and Glass Curtain Wall on a Stick
Description: Custom extruded unitized aluminum frames with insulated low-e coated glass and custom pattern frit with structural silicone attaching the glass to the aluminum frames. Unitized frames are "hard-stacked" (one unit on top of the unit below) for the height of the enclosure for gravity support and laterally supported by custom aluminum anchors integrated into the interior reveal profile attached to architectural exposed steel tube sticks.

Read More

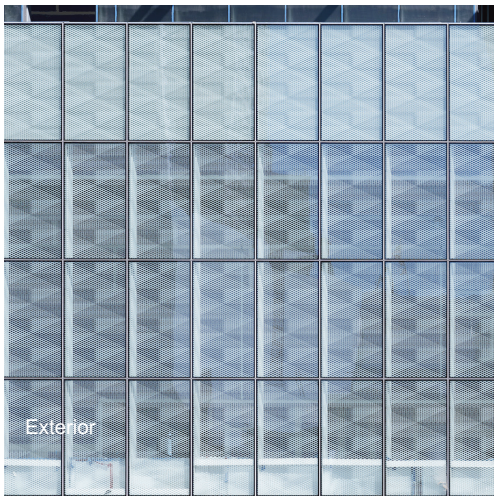

FIG. 3 Façade System Description – Exterior and Interior image illustrate the façade system design

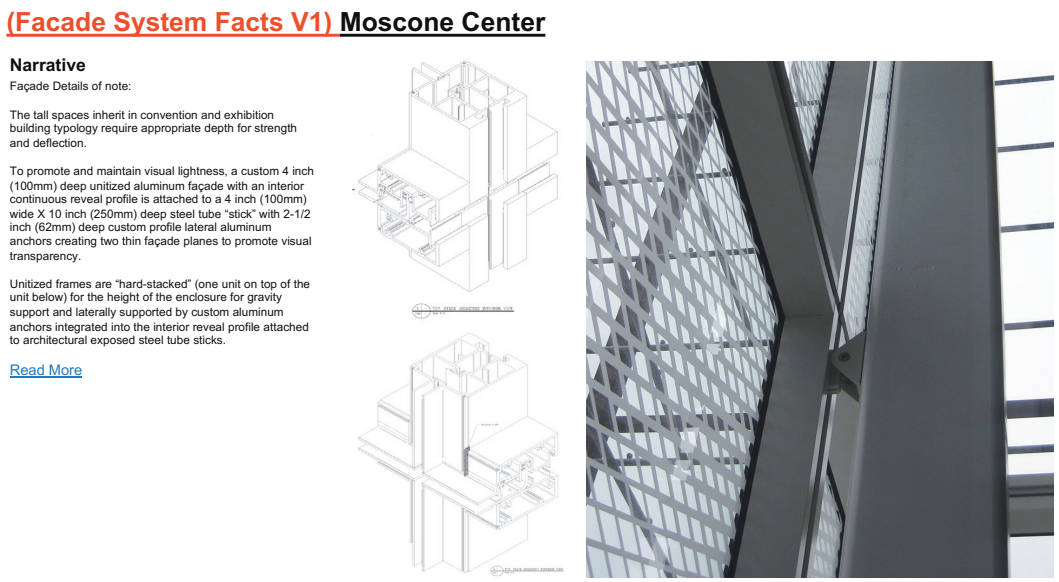

FIG. 4 Façade System Facts - Interior reveal frame profile houses custom designed lateral anchors providing visual separation from steel stick supports creating 2 thin and distinct façade planes.

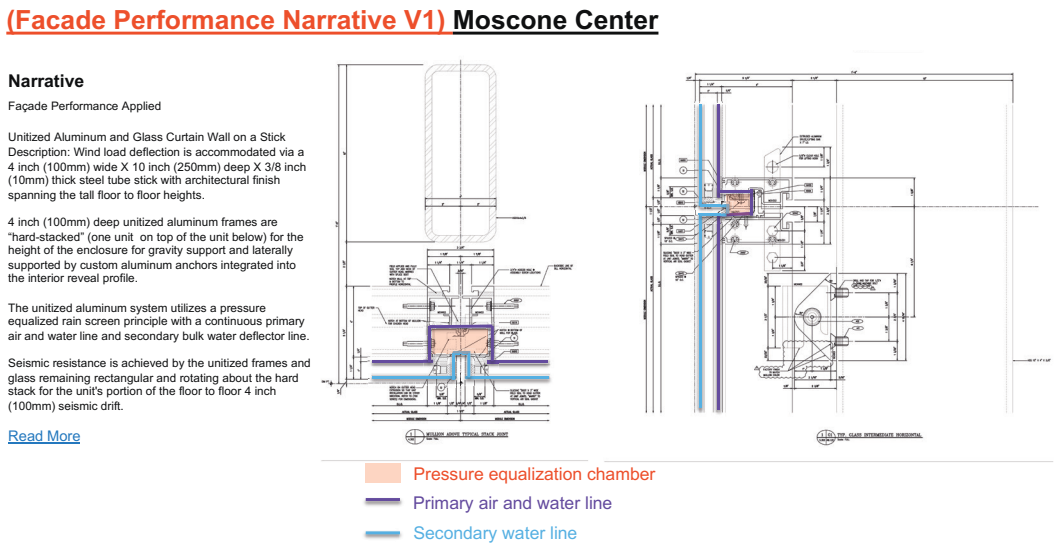

FIG. 5 Façade Performance Narrative – Unitised aluminium frames utilise a pressure equalised rain screen principle. Deflection control is achieved via a steel tube stick. Seismic drift is accommodated via each unit remaining rectangular and rotating about the hard stack joint.

These images are intended to represent a particular case. Comprehensive data fields incorporated into the database will be used as relevant to an individual project. The following Figure 6 is intended only to represent a possible template for displaying key performance metrics and data. It is not intended to represent the full spectrum of relevant metrics; this will be a component of future work.

(Facade Metrics) Moscone Center Expansion

Performance Criteria	Description	Standard	Achieved Metric	Comments
Air Infiltration	Assembly Whole Building	ASTM E283 / E2357 .06 CFM/sqft ASTM E779	.01 CFM/sqft achieved	Lab Tested
Water Infiltration	Static Dynamic	ASTM E331 AAMA 501.1	No infiltration	Tested
Vapour Diffusion		ASTM E96	NA	
Thermal (Vision)	U- Value	ASTM C1199 NFRC 101	.29 (hr X sqft X F.	Calculated
Thermal (Vision)	SHGC	NFRC 201	.34	Calculated
Thermal (Opaque)		ASHRAE 1365 ASTM C1363	NA	Calculated
Thermal (Weighted)			NA	Calculated
Structural (Wind)	Static	ASTM E330	18 psf	Tested
Structural (Seismic)	Interstory Drift	UBC and AAMA 501.4 (AAMA 501.6 - DYNAMIC)	3-3/16 inches	Tested
Building Structure	Deflection (Vertical Displacement)	AAMA 501.7	2 inches	Tested
Fire Resistance		UBC NFPA 285 CAN/ULC S134	Non-combustible	
Visual Transmission		NFRC 202		
UV Transmission		ASTM E903		
Daylighting				
Acoustics	STC/OITC	ASTM E90 / E1425 / E1332	NA	
Durability		CSA S478		
Service Life				
Operational Carbon				
Life Cycle Assessment		ISO 14040 / 14044		
Embodied Carbon				
Occupant Comfort		ASHRAE 55		
Occupant Health		ASTM E3182		

FIG. 6 Façade Metrics – A compendium of performance metrics and standards with applicable results for façade.

With respect to performance criteria the knowledge-sharing platform must identify:

1. the metric (and method of measure)
2. relevant code, standard or baseline values
3. the project specific measure(s)

5 LIMITATIONS, BARRIERS, AND FUTURE WORK

A quick look to the future.

5.1 LIMITATIONS

The potential limitations of the initiative proposed here are threefold and significant. The efficacy of such a system will depend upon its:

1. quality, in terms of the adequacy and accuracy of metrics,
2. clarity, how well it communicates, and
3. ease of use: the functionality of an inherently complex system is a challenge.

5.2 BARRIERS

There are two primary barriers to the system as proposed. The first is with respect to its implementation, specifically, the financial and human resources required for the initial database development, including the database structure, coding, and input and output form design, and those required for the ongoing maintenance and administration: data gathering, vetting, and input. Should the system become efficacious, some level of technical support may be required.

The second predominant barrier will be in populating the database with projects and detailed project data. One challenge here is that of culture; the culture of the building industry is not notable for its practices of sharing information. Especially in litigious societies like the United States, owners are often reluctant to share detailed project information for fear of potential liabilities, e.g. a particular building may be revealed to be a poor performer compared with buildings of a similar type and location. Construction contracts in the U.S. typically come packaged with an egregious non-disclosure agreement that prevents contractors from sharing any data on the project. This has had the unfortunate consequence of effectively severing important feedback loops that allow building practices to evolve over time in response to past experience. A related challenge has to do with the protection of intellectual property and know-how; companies, and sometimes individuals, are concerned about losing competitive advantage if they share core practices and techniques.

The Façade Tectonics Institute has strategies in place intended to overcome these barriers. The Institute is a non-profit member organisation that pursues collaborative education and research initiatives (including funding) and promotes "a neutral platform for knowledge-sharing" as a core mission strategy, and has experienced some success in encouraging a higher level of information exchange among its broad-based constituency.

5.3 FUTURE WORK

This initiative is in its early conceptual stage, so there is an abundance of work to be done just in realising the vision as described herein, as discussed in the previous section with respect to needed human and financial resources.

The larger potential for this proposed initiative is open-ended and high, and suggestive of many possibilities. While not discussed, a database system as described here could be usefully used to capture other building façade related information, e.g. delivery strategy and supply chain management detail. The supply chain management of increasingly complex façade programmes is one of the biggest challenges in the building industry today.

A database of the suggested project data can easily be envisioned as the foundation for a number of other initiatives related to the building façade system. Examples include a façade rating system (e.g. a point-based system similar to LEED but focused solely on the building skin), a guideline or best practices document for high-performance façade system design and/or delivery, design or procurement guideline documents for various types of façade wall types (e.g. framed glass curtainwall, window wall, storefront, precast, masonry, fire-rated, etc.), guideline documents for

the use of various materials and assemblies in the building façade (e.g. fibre-reinforced panels, glass-fibre-reinforced concrete panels, terracotta panels, etc.), and so on. Descriptions, details, vendors, images, and performance characteristics could all be drawn directly from the database.

The database as envisioned here would act as a powerful data-rich resource for research by both academics and practitioners.

6 SUMMARY

Very early efforts and thinking in the development of a comprehensive Integrative Façade Assessment Framework by the Façade Metrics Working Group of the Façade Tectonics Institute are documented here. The literature on metrics related to various façade system attributes is extensive and has yet to be thoroughly researched as part of this effort. Much of the literature tends to be reductive in nature, looking at specific performance attributes in isolation. This is important and has its place, and some will doubtlessly provide relevant metrics, but few of these works address the integrated framework sought here.

Building an assessment framework for building and façade system ecology, deciding what is important to measure and how to measure it, is an inherently wicked problem in that solutions are ultimately rooted in issues of resilience and sustainability that transcend technical boundaries and form complex relationships in social and economic domains. Developing an integrated assessment framework will require a paradigm change in the way we think about buildings and their façade systems.

We made the decision to publish these early efforts as a form of outreach to solicit input from the global building façade community, which largely shares the recognition of the façade system as the lynchpin to achieving resilience, occupant comfort and sustainability goals in the building sector. We strongly encourage you to reach out to us with your comments, criticisms, and suggestions. This is a significant undertaking, and we need all the help and support we can get, ranging from peer-review to research and implementation; if you are so inclined, or if you just want to follow progress, let us know. We do plan to provide periodic progress updates reporting on further research and development. At some point these will be available on the Façade Tectonics website http://www.façadetectonics.org/metrics. In the meantime, please reach this group at metrics@façadetectonics.org

Acknowledgements

The authors would like to acknowledge and thank the Façade Tectonics Institute for its support in this effort and for hosting the Institute's Façade Metrics Working Group.

References

Avesani, S., Babich, F.& Papaiz, L. (2019). *M3. 5: Report on the key performance indicators*. Facecamp.

Bianco, L., Cascone, Y., Avesani, S., Vullo, P., Bejat, T., Koenders, S., Loonen, R. C. G. M., Goia, F., Serra, V., & Favoino, F. (2018). Towards new metrics for the characterisation of the dynamic performance of adaptive façade systems. *Journal of Façade Design and Engineering,* (S.l.), v. 6, n. 3, p. 175-196, oct. 2018. ISSN 2213-3038.

Beltran, L. & Liu, D. (2020). Evaluation of Dynamic Daylight Metrics based on Weather, Location, Orientation and Daylight Availability, *Passive Low Energy Architecture 2020*

Browning, W., Ryan, C., & Clancy, J.(2014). *14 Patterns of biophilic design: Improving health & well-being in the built environment.* New York City: Terrapin Bright Green. Retrieved from http://www.terrapinbrightgreen.com/wp-content/uploads/2014/04/14-Patterns-of-Biophilic-Design-Terrapin-2014e.pdf

Carlucci, S., Causone, F., De Rosa, F., & Pagliano, L. (2015). A Review of indices for assessing visual comfort with a view to their use in optimization processes to support building integrated design. *Renewable and Sustainable Energy Reviews* 47, 1016-1033

Dave, S. H. (2012). *Comprehensive performance metrics for Complex Fenestration Systems using a relative approach.* (Master's Dissertation), Massachusetts Institute of Technology.

Dubois, M-C. (2003). Shading devices and daylight quality: an evaluation based on simple performance indicators. *Lighting Res. Technol.*, 35.1, 61-76

Galatioto, A., & Beccali, M. (2016). Aspects and Issues of daylighting assessment: A review study. *Renewable and Sustainable Energy Reviews* 66, 852-860

Hartwell, R., & Overend, M. (2020). End-of-life challenges in façade design: A disassembly framework for assessing the environmental reclamation potential of façade systems. *Proceedings of the Façade Tectonics Institute 2020 World Congress, 19 August 2020*. Retrieved from https://www.façadetectonics.org/papers/end-of-life-challenges-in-façade-design

Ko, W.H., Schiavon, S., Brager, G., & Levitt, B. (2018). Ventilation, Thermal and Luminous Autonomy Metrics for an Integrated Design Process. *Building and Environment,* Vol 145, 153-165.

Mardaljevic, J. Heschong, L., & Lee, E. (2009). Daylight metrics and energy savings, *Lighting Research and Technology, 41(3),* 261-283.

Mardaljevic, J. Andersen, M. Roy, N., & Christoffersen, J. (2012). Daylighting Metrics: Is There a Relation Between Useful Daylight Illuminance and Daylight Glare Probability? *First Building Simulation and Optimization Conference*, IBPSA England

Morrison Hershfield. (2020). *Building envelope thermal bridging guide, version 1.4*. BC Housing Research Centre.

Morrison Hershfield. (2018). *Guide to low thermal energy demand for large buildings*. BC Housing Research Centre.

Norris, N., Carbary, L.D., Yee, S., Roppel, P., & Ciantar, P. (2015). The reality of quantifying curtain wall spandrel thermal performance: 2D, 3D and hotbox testing. B*EST 4 Proceedings, National Institute for Building Science.*

Patterson, M. *R. (2017). Skin fit and retrofit: Challenging the sustainability of curtainwall practice in tall buildings* (Doctoral Dissertation). Retrieved from http://digitallibrary.usc.edu/cdm/compoundobject/collection/p15799coll40/id/457628/rec/16

Reinhart, C.F., Mardaljevic, J., & Rogers, Z. (2006). Dynamic Daylight Performance Metrics for Sustainable Building Design, *Leukos,* 3.1, 1-25.

Rittel, H. W. J. & Webber, M. M. (1973). Dilemmas in a general theory of planning. *Policy Sciences 4, 155-169*. Amsterdam: Elsevier Scientific.

Roppel, P., Lawton, M., & Norris, N. (2012) ASHRAE research report 1365: Thermal performance of envelope details for mid & high-rise buildings. *American Society of Heating, Refrigerating and Air-Conditioning Engineers, Inc*

Shafavi, N.S., Tahsildoost, M., & Zomorodian, Z. S. (2020). Investigation of illuminance-based metrics in predicting occupants' visual comfort (case study: Architectural design studios), Solar Energy, 197, 111-125

Van Den Wymelenberg, K., & Inanici, M. (2015). Evaluating a New Suite of Luminance-Based Design Metrics for Predicting Human Visual Comfort in Offices with Daylight. *Leukos,* 12:3, 113-138

Van Den Wymelenberg, K., & Inanici, M. (2014). A Critical Investigation of Common Lighting Design Metrics for Predicting Human Visual Comfort in Offices with Daylight. *Leukos*, 10:3, 145-164

PAOSS

Pneumatically Actuated Origami Sun Shading

Christina Eisenbarth[1], Walter Haase[1], Yves Klett[2], Lucio Blandini[1,3], Werner Sobek[1,3]

* Corresponding author
1 ILEK Institute for Lightweight Structures and Conceptual Design, Faculty 2: Civil and Environmental Engineering, University of Stuttgart, Germany, christina.eisenbarth@ilek.uni-stuttgart.de
2 IFB Institute of Aircraft Design, Faculty 6: Aerospace Engineering and Geodesy, University of Stuttgart, Germany
3 Werner Sobek AG, Stuttgart, Germany

Abstract

This paper describes the development of an innovative, material- and energy-efficient façade concept: a pneumatically actuated Origami sun shading system - abbreviated "PAOSS" - which combines the aesthetic and material-immanent qualities of textile materials with the functional aspects of a controlled and targeted light transmission regulation by means of integrated active pneumatic components (Fig. 1). Due to the possibility of reducing a given surface to a minimal form, textile-based folding structures are highly suitable for selective sun and glare protection systems, in order to optimise energy consumption and increase user comfort. For astrophysical purposes, the American space agency (NASA) developed an Origami folding geometry called "Starshade," which is characterised by a particularly high difference between its closed and open state. Inspired by NASA's "Starshade," an adaptive, pneumatically actuated sun and glare protection system was designed and developed to be embedded in the cavity of pneumatically supported multi-layer ETFE cushion façades. By implementing active components, one can obtain a targeted, partial, or full-surface regulation of light and radiation transmission as well as the back-reflection properties of the façade. Within the scope of the research project "Adaptive Membrane Façades" funded by the research initiative Zukunft Bau, the PAOSS will be prototypically built at a scale of 1:1 and implemented on one storey of the demonstration high-rise building of the Collaborative Research Centre 1244 entitled "Adaptive Skins and Structures for the Built Environment of Tomorrow." The goal is the system validation and the monitoring of its reliability and efficiency, especially in terms of building physics and daylight performance under real weather conditions.

Keywords

Adaptivity, textile, pneumatic cushion, sun shading, glare protection, origami folding, façade

10.7480/jfde.2021.1.5535

1 INTRODUCTION

Nowadays, several solutions are available to provide active sun and glare protection: the majority of these systems use mechanically or electronically operated actuation technologies, being highly sensitive to defects, material deterioration, system failures, and obsolescence. Moreover, they are characterised by a higher resource consumption in terms of the embodied material and the required operating energy. Thus, the challenge is to develop solutions, that combine high performance and low technological requirements with a minimum of energy and material use. (Meagher, 2014)

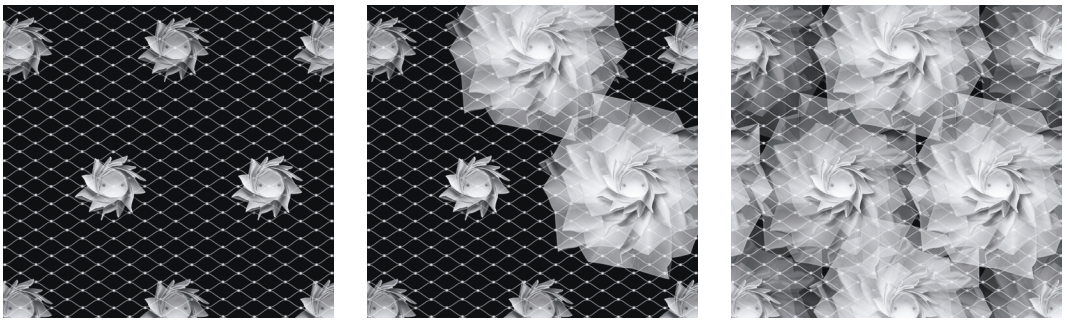

FIG. 1 PAOSS in closed state (left), in partially actuated state as selective glare protection (middle), and in open state as full sun protection (right). Copyright by ILEK / Visualisation by Christina Eisenbarth

The purpose of PAOSS is to combine an efficient kinetic sun and glare protection geometry with a lightweight textile high performance material by using a simple, resilient, and low energy actuation mechanism. The development takes place in an iterative process of design research and evaluation, that is briefly introduced in the following paragraph.

In a first step, the basic folding geometry of the system (NASA`s "Starshade" Origami folding) has been optimised in terms of efficiency and applicability as sun and glare protection in the façade cavity. In a second step, the spectral transmittance, absorption, and reflection properties of conventional textile sun protection materials were analysed and, based on the photo spectrometric measurements, the most suitable material was identified. In a further step, manufacturing methods for producing the folding geometry, that are applicable to different textile-based materials, have been investigated. Furthermore, concepts to integrate the pneumatic actuators as well as the synergistically optimised implementation of the PAOSS elements in an overpressure-stabilised ETFE façade system by using the existing air infrastructure have been examined. Future research will focus on the prototypical realisation of the PAOSS at a scale of 1:1 under real weather conditions in order to evaluate their functionality and durability.

1.1 SUN AND GLARE PROTECTION

Office and residential buildings are becoming more and more transparent, whereas current climatic developments require planners to move in the opposite direction, towards protecting our interiors from the rising global temperatures and from overheating caused by high solar radiation input. (Blandini, 2020; Blandini & Grasmug, 2018)

Particularly in dense urban areas, a significant temperature increase due to the urban heat island effect is noted. Therefore, it is important to provide an efficient sun and glare protection system with a low energy demand for activation. The large-area glass façades transmit incoming solar radiation and lead to a high cooling demand. This has to be compensated by oversized technical building equipment leading to higher heat stresses on the exterior environment. Suitable sun shading and glare protection systems are urgently needed in order to reduce the demand of energy required for interior conditioning and lighting, thus ensuring the users' need for sufficient daylight and visual contact to the outside. This has to be achieved with a minimum amount of material, mass, and CO_2 together with maximum aesthetic and design flexibility (Magli, Lodi, Lombroso, Muscio & Teggi, 2015).

In this context, it is essential to clearly distinguish the terms *sun protection* and *glare protection* from each other. The characteristic function of a sun protection is to shield high solar radiation from the building. A basic distinction is made according to the position of the sun protection system in the interior, the exterior, or in the façade cavity. While external systems are the most effective in terms of reducing solar transmission and heat transfer, they are also vulnerable to weather influences such as wind loads. On the other hand, interior systems are protected from climate influences, whereas the passage of solar radiation through the façade is always larger, resulting in a greater heating up of the interior. In this project we focus on the application in the façade cavity. (Knaack et al., 2018)

The term *glare* is understood as a disturbance of visual perception, which emanates from a too bright light source within the field of view. According to this definition, glare is caused by differences in brightness. The reason for this phenomenon is the adaptation of the eye. The perception from high to low luminance needs a certain amount of time, making it impossible to achieve perfect visual performance in the short-term. Nevertheless, a sufficient amount of daylight and visibility to the outside world is still required, which in particular favours the development of adaptive, selective sun and glare protection systems. (Haas-Arndt & Ranft, 2007; Hammer & Wambsganß, 2020; Knaack et al., 2018)

1.2 TEXTILE- AND FOIL-BASED MATERIALS

Compared to conventional façade materials, textiles and foils combine a particular lightness and flexibility with a clear design language, that predestines them to be used in dynamic façade systems. Textile fabrics create a unique aesthetic effect, that distinguishes them from other façade materials due to their haptic qualities, their translucency, their micro-structured surfaces, as well as their immense variety of colours, patterns, and structures. They therefore expand the visual design spectrum of the building envelope at the micro, meso, and macro scale. Notwithstanding the diversity of design options and techniques offered by textile materials, their scope of application in architecture has so far only been used to a limited extent. Consequently, target for the future will be "to leave the goal of wrinkle-free prestressed monochrome skin and to give textile building back the quality it has lost: that of a fabric." (Blaser, 1999)

Their minimal weight per unit area and their high mechanical strength open up a previously unexploited potential for their application in resource-efficient architecture. In this field, they offer both a ground-breaking expansion of the functional spectrum of the outer shell as well as a significant weight reduction of new and existing buildings. Considerable economic and ecological advantages can result in a fully multi-layer, textile- and foil-based enveloping system of flexible high-performance materials framed in a profile system, thereby creating an outer thermal building envelope, that fulfils all the requirements of a façade. (Haase et al., 2011a; Haase et al., 2011b)

1.3 ADAPTIVITY OF THE BUILDING SKIN

A very interesting way of designing textile building envelopes is the combination of aesthetic and functional qualities with the potential of varying the façade properties by implementing active components. Conventional façades due to their constant building physics and design characteristics can react only to a small extent to climatically varying outside conditions or changing user requirements.

Thus, the aim of our research is to develop adaptive building envelope systems whose properties are variable in terms of light transmission, energy reflection, and external appearance. The term *adaptivity* is here understood as the implementation of sensors and actuators which, in combination with an automated control unit, allow to react on differing environmental situations or user requirements in order to provide automatically or in a user-controlled manner the optimum interior and exterior conditions. The synthesis of an appealing design with the functionality of an adaptive adjustment enriches the architectural qualities of textile building envelopes. (Knaack, Klein, Bilow, & Auer, 2007; Sobek, Haase & Teuffel, 2000)

Due to the high individualisation degree of textile façades, a precise adaptability to strongly fluctuating requirements can be achieved by implementing active components, thus resulting in a significant increase of user comfort and a reduction of energy consumption. This allows to create new design elements, that emphasise the material-immanent properties of the textile, such as the soft, the folded, and the supple, by simultaneously integrating various functions, like a precise and systematic control of the daylight transmission values of the façade for example. (Zapala, 2018).

The Institute for Lightweight Structures and Conceptual Design (ILEK) is a pioneer in the field of textile construction, and has worked out, within the scope of various research projects (Haase et al., 2011a; Haase et al., 2011b; Bäumer, Haase, Mielert, Ocanto, & Schmid, 2012), the fundamental principles on the physical building measurement as well as ground-breaking research results on the design and construction of textile- and foil-based skins. In the following, the development of a textile-based, energy- and resource-efficient façade component for targeted sun and glare protection (PAOSS) is presented in detail.

2 PNEUMATICALLY ACTUATED ORIGAMI SUN SHADING

Conventional folding systems are opened by tensile forces acting on the periphery, but making it necessary to install additional cable structures on the façade. Investigations at the ILEK have demonstrated their opening and closing mechanism by the action of centrifugal forces (Sobek, Morgan & Bogdan, 2004). For this purpose, the folding structure is mounted on a centrally positioned electric motor, which generates the necessary centrifugal forces when rotated.

Meanwhile, this approach has been further developed towards a radial system, that can be opened and closed by one central activation source, only requiring a small amount of energy input into the system once, while creating two stable states by implementing active pneumatic components. The logic is similar to the one used in an air whistle. Through air pressure, the Origami elements unfold, while the restoring mechanism of the system is provided by an integrated spiral spring whose force causes the refolding.

During the day, the unfolded, opened structures reflect the irradiated solar energy and prevent the interior from overheating by a partial or full-surface regulation of light and radiation transmission. Individually activated single elements offer a targeted, selective glare protection, while at the same time ensuring the required daylight supply. In case of a clear night the heat radiation to the cold night sky and thus the cooling down of the building can also be influenced by these elements.

2.1 ORIGAMI GEOMETRY OPTIMISATION

The above-described pneumatically actuated sun and glare protection system is based on the Origami folding geometry "Starshade," developed by the Origami artist R. Lang for astrophysical purposes of the American space agency (NASA). The original "Starshade" is applied to shade the brighter and thus glaring starlight during the exploration of unknown exoplanets in space. The transportation and positioning of the immense "Starshade" shading and glare protection elements in space requires a maximum compactness of their geometry in the folded state with a maximum reduction of their dead load as well. In this context, the Japanese Origami folding art was used to develop a space-saving, efficient, and lightweight system design, covering a surface of around 34 m diameter, which is characterised by a particularly high difference between its closed and open state. (Arya et al., 2017; Sigel et al., 2014)

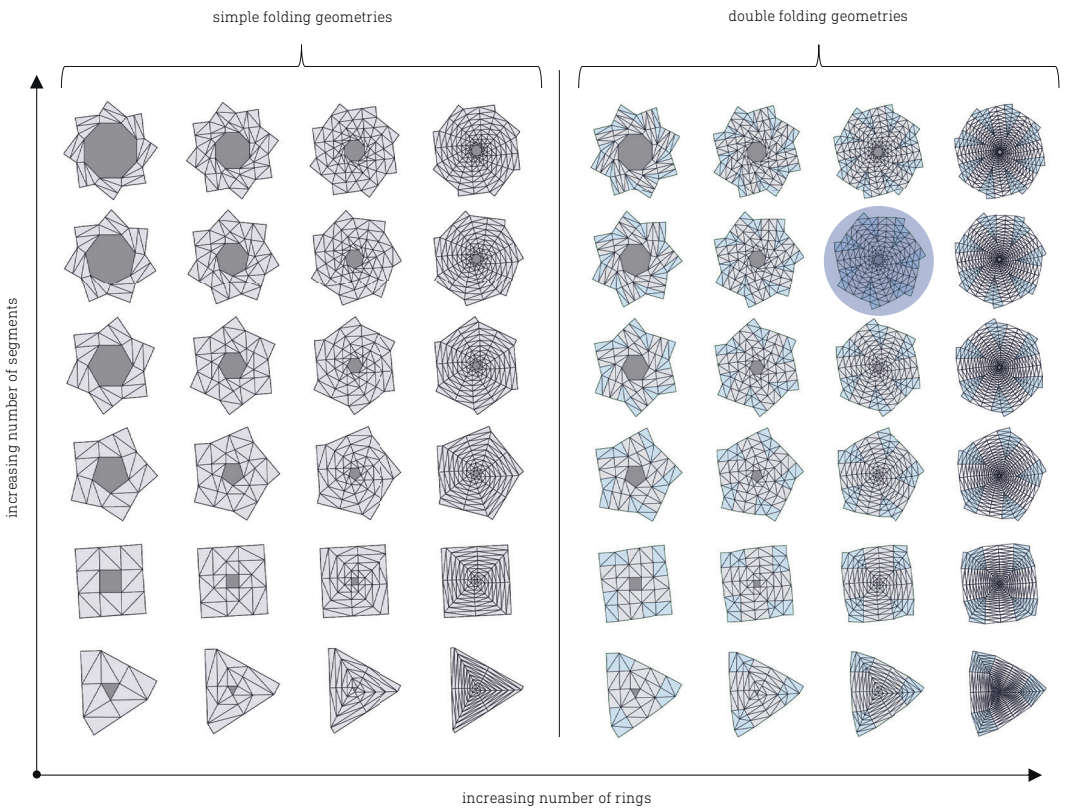

FIG. 2 Connotation of simple and double folding geometries. Copyright by ILEK

In order to be applied in the façade cavity of an ETFE cushion, the basic geometry of the "Starshade" has to be optimised in terms of the specific parameters of a minimum component depth with a maximum surface area difference between the closed and the open state, while at the same time reducing the complexity of the system as much as possible.

For this purpose, simple as well as double-shaped folding geometries were analysed in order to identify the most efficient folding geometry. The three main characteristics of a radial folding shape are: the folding type, the number of segments, and the number of rings. Fig. 2 represents variations of different folding geometries, obtained by varying these parameters at a constant outer radius of 50 cm.

An increasing number of segments leads to an expansion of the inner radius, while reducing its depth. Thus, an increasing number of rings causes a reduction of the inner radius, while expanding its depth. In order to keep better control of the rising complexity, the maximum was limited to eight inner rings. Double folding geometries are characterised by downfolded peaks (marked in blue) achieving a reduction of the structures depth and thus are identified to be more efficient in terms of a maximum surface area difference between closed and open state.

Respecting the restriction of a maximal component depth of 100 mm to provide the applicability of the PAOSS elements in all types of façade cavities, the most suitable folding geometry according to the parameters above is specified. With a structure height of 94.5 mm, an inner radius of 91.8 mm, and a difference of 0.613 m^2 between its open and closed state along with the outer radius of 50 cm, the folding geometry marked in the connotation (Fig. 2) above fulfils all the specific requirements. The resulting maximum switching difference of the system is approximately 82%.

2.2 MATERIAL ANALYSIS

The application of textiles and foils in the building façade depends on their UV resistance as well as on their sufficient fire protection quality. According to DIN 4102, at least B1 level (flame resistance) is required. In order to provide enough natural daylight illumination of the room even in a shaded state, the translucence of the shading material in terms of light transmission value may vary between 0 % and 40 %, depending on the type and thickness of the material (Zapala, 2018). Textile materials can be classified in the following three main categories: non-woven fabrics, woven fabrics, and knitted fabrics. (Sobek & Speth, 1993)

FIG. 3 Tyvek Material. Copyright by ILEK

FIG. 4 Airtex Super FR Material. Copyright by ILEK

The first prototypes of the PAOSS elements were made of perforated and folded Tyvek (Fig. 3), a flame-resistant, high-density polyethylene (PE) nonwoven fabric from DuPont de Nemours (Luxembourg) with a surface related weight of 120 g/m^2. After a few folding and unfolding cycles, the material tends to wrinkle as a result of the pneumatic actuation, which significantly interfere with the opening and closing mechanism of the structure.

In this context, paper-like Origami materials are not compatible with the pneumatic actuation of the system, since this method requires a textile material with a typical softness and flexibility. Further material analyses therefore concentrate on flexible, textile woven fabrics, in particular on technical composite textiles from PES with various coating techniques to guarantee the material-specific requirements as well as a low bending stiffness for their implementation in radial folding structures. Table 1 contains a selection of appropriate materials with their specific technical properties.

TABLE 1 Sun Shading Material Analysis (Bender, 2020)




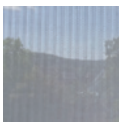



NO SUN SHADING	VALMEX TF 400 F1	SOLTIS HARMONY 88	SUNWORKER	TEMPOTEST STARSCREEN	TWILIGHT METAL	AIRTEX SUPER FR	FIREMASTER
Material	PES	PES	PES/PVC	PES	PES/PAC	PES	PES/MAC
Coating	Vinyl		PVC	PTFE	Metal	PUR	Resin
Weight [g/m^2]	420	360	300	220	350	275	400
Thickness [mm]	0,77	0,45	0,42	0,52	0,5	0,35	0,6
Openness factor [%]	34	8	6	3,5	1,4	0	0
MEASURED SOLAR TRANSMISSION, REFLECTION AND ABSORPTION DATA (WAVE SPECTRUM 300 NM TO 2500 NM)							
T_{SOL} [%]	44,17	27,16	25,08	39,48	7,66	16,95	15,13
R_{SOL} [%]	51,75	67,14	68,56	54,32	42,08	74,65	71,91
A_{SOL} [%]	4,07	5,70	6,36	6,20	50,26	8,40	12,96
MEASURED VISIBLE TRANSMISSION, REFLECTION AND ABSORPTION DATA (WAVE SPECTRUM 380 NM TO 780 NM)							
T_{VIS} [%]	43,85	25,09	23,90	41,16	4,14	15,59	13,17
R_{VIS} [%]	51,50	73,62	76,19	57,72	37,68	82,95	78,44
A_{VIS} [%]	4,64	1,29	-	1,12	58,19	1,46	8,39

The pictures in Table 1 thereby give an impression of the visual appearance of the examined textiles. With an increasing openness factor, the transparency and the visual relation of the user to the exterior accordingly rises. A zero-openness factor implies a translucency of the material, which is sufficient in particular for selective sun and glare protection systems allowing a targeted view to the outside. In particular, a higher openness factor of the textile implies a lower degree of efficiency in terms of sun and glare protection. A lower material thickness leads to an advantageous, higher compactness of the structure in a folded state as well as to a maximum surface related weight reduction.

The evaluation of the material properties in the solar and visible range of radiation is a significant parameter for the selection of sun and glare protection materials. According to DIN EN 14500, the spectral radiation behaviour of textiles is measured by means of a spectrometer with an integrating sphere ("Ulbricht sphere"), whereas a distinction is made between the three following spectral parameters: reflectance (R_{SOL}, R_{VIS}), transmittance (T_{SOL}, T_{VIS}), and absorbance (A_{SOL}, A_{VIS}). For this purpose, empirical measurements were carried out in the photo spectral measuring device of the institute. Since the spectral data of textiles are influenced by the colour of the material, the textile samples have all been tested in the same colour (white), with the exception of the textile Twilight Metal, which is only available in silver. (DIN EN 410, 2011; DIN EN 14500, 2018)

The measurements were carried out both on the spectrum visible to humans within a wavelength range of 380 nm to 780 nm (VIS), considering the spectral brightness sensitivity $V(\lambda)$ as well as on a frequency range of 300 nm to 2500 nm (SOL), including the relative spectral radiation distribution S_λ according to DIN EN 410 Table 2. The frequency range includes the UV-B range from 280 nm to 315 nm, the UV-A range from 315 nm to 380 nm, the visible spectrum from 380 nm to 780 nm, and parts of the short-wave IR range from 780 nm to 2500 nm. The generated measuring data are listed in Table 1.

For a sun and glare protection system, the reflection coefficient should be as high as possible whilst the absorption coefficient should be as low as possible, in order to prevent heat radiation to the interior. Other advantages include a low visual transmittance T_{VIS}. To ensure sufficient daylight, while avoiding glare, an average value for T_{VIS} is recommended by $T_{VIS} \approx 10 – 15$ %.

Based on the photometric evaluation of the transmission, reflection and absorption properties of the appropriate textile materials via photo spectrometer, while also taking into account other parameters such as material thickness, surface related weight, UV-, and fire-resistance, the most suitable fabric was selected.

With a thickness of 0.35 mm, the polyester based and thermoplastic polyurethane coated Airtex Super FR (Fig. 4) is the thinnest, and with a weight per area of 275 g/m^2, one of the most lightweight among the above considered materials. Its surface structure is woven matt, whilst the fabric is UV-resistant and weatherproof. The textile has no openness factor and thus appears translucent. In addition, it is resistant to temperatures between -25 °C and +70 °C. According to the accomplished investigations, Airtex Super FR is identified to be the most suitable for the implementation in the PAOSS structures.

2.3 KINEMATIC FOLDING TECHNOLOGY

Depending on the respective material-immanent properties, in particular the material stiffness, appropriate digital and industrial manufacturing methods for a selective and specific functionalisation of the textile structure in order to generate the articulation effect were analysed. Dynamic folding elements are required to have both stiff properties in their planes and flexible qualities in the folding hinges.

Fig. 5 shows the investigated subtractive, additive, and mechanical/thermal methods. Subtractive methods include the abrasion of material in the folding hinges to achieve more flexibility. Additive methods foresee the application of thin layers to increase a local stiffness to a thin textile with low form stability, while adding no additional layers at the hinges to allow for the articulation.

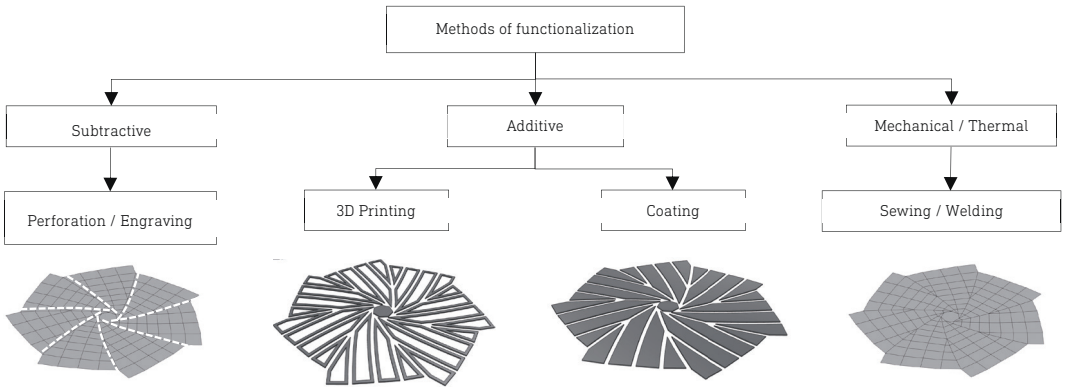

FIG. 5 Manufacturing methods to functionalise a textile folding structure in order to generate an articulation effect. Copyright by ILEK.

Mechanical or thermal processes, meanwhile, attempt to create a shape memory in the structure without applying or removing any material. Within experimental investigations, subtractive methods with a perforation or engraving of the hinges as well as additive textile 3D-printing or coating methods to precisely define the textile's stiffness were carried out. Additionally, the application of mechanical or thermal methods, such as sewing or welding, has been evaluated.

Subtractive methods such as thermal cutting techniques (laser or plasma cutting) prevent fraying edges by fusing the textile cuts, but often cause black or brown discolouration on the cut edges due to oxidation of the material. Mechanical techniques (cutting, plotting, water jet cutting, or punching) offer higher precision without edge finishing. Subtractive manufacturing methods are more suitable for stiffer materials. (Fahrenwaldt, Schuler, & Twrdek, 2014; Gries Veit, & Wulfhors, 2014; Lütke, Klotzbach, Wetzig, & Beyer, 2009; Machova et al., 2011)

The additive methods require a high flexibility and softness of the textile. Particularly for additive techniques, it is important to ensure the traceability of all individual components into the material cycle. This is why it is recommended to use additive skeletal structures via FDM (Fused Deposition Modelling), made of thermoplastic polymer, that can be applied in layers onto polyester materials, for example, and bond with the textile without impairing its recycling properties (Fig. 6). The biggest challenge in this context is the adhesion to the textile, making double-sided printing a viable option. (Deleersnyder & Ruys, 2015)

Partial coatings, applied in several layers at one or both sides of the material, prevent the angular twisting of threads in the woven fabric, thus generating a partial membrane stiffness. Besides this reinforcement, it is furthermore possible to obtain high-performance material properties such as heat resistance by means of additives and auxiliary ingredients. (Gries & Klopp, 2007)

Thermal and mechanical methods are appropriate for producing the articulation effect, as they provide the mountain and valley folds with an additional orientating shape memory (Fig. 7) in comparison to subtractive or additive manufacturing methods. Their succesful experimental validation was achieved for the textiles Airtex Super FR, Soltis Harmony 88, Sunworker, Firemaster. Preconditions for the thermal transformation of a polymer are thermoplastic material properties.

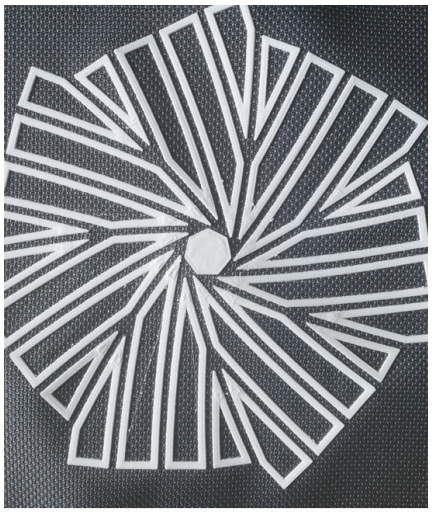

FIG. 6 3D-printed skeletal polymer structure on polyester fabric. Copyright by ILEK

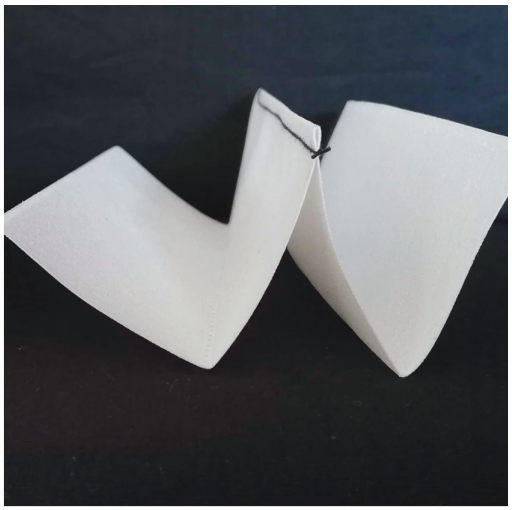

FIG. 7 Shape memory effect by sewing. Copyright by ILEK

Applying high-frequency radiation, heat, or electrical impulses, the molecules oscillate and, by means of mechanical pressure, are joined together at the folding edge to a water- and airtight weld seam. Sewn joints can be subsequently tightened up by welding or by injecting a coating to achieve an airtight lamination respecting all requirements for a clear material separability. The use of digital, automated production methods in general enables the folding structures to be produced with high precision in a fast and cost-effective way.

2.4 ACTUATION STRATEGY

The opening and closing mechanism (Fig. 8) of the PAOSS elements is carried out by special pneumatic actuators, that generate a deployment of the system via air pressure. An integrated spiral spring - without air pressure - provides the resetting effect of the system to its original state, similar to an air whistle. (Eisenbarth, Haase, & Sobek, 2019)

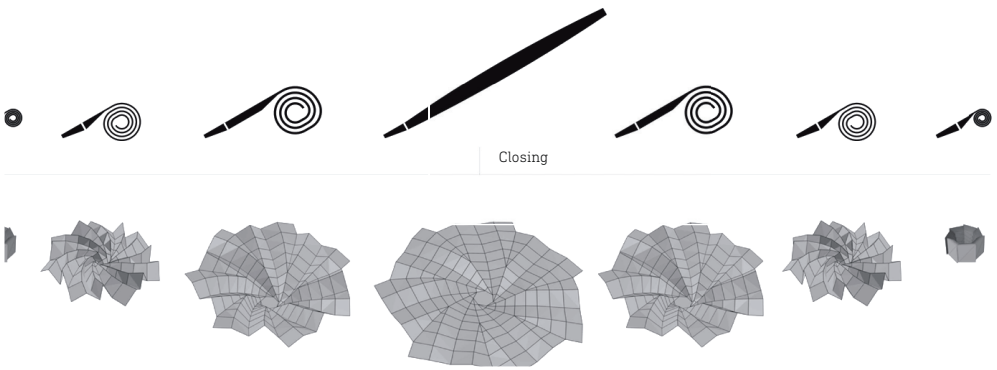

FIG. 8 Opening and closing mechanism. Copyright by ILEK

For the integration of the pneumatic actuators, additive and integral methods were investigated. The first prototypes of the pneumatic actuators were integrated additively (Fig. 9). For this purpose, the hermetically laminated one-piece woven pneumatic actuators by Jacquard weaving technology are fitted with the spiral spring inside and fixed to the PAOSS elements by thermal or mechanical joining techniques such as sewing, welding etc. at the back of the folding structure. The maximum number of additively applied actuators is limited by the connectivity of the air supply ducts.

From an aesthetic, functional, and economic point of view, the integral implementation of the actuators is of particular interest. In this way, considerably more actuators can be integrated to achieve a more homogeneous air distribution at equal manufacturing costs. Therefore, on the inside, the fabric has to be partially coated for airtightness and then laminated together to create airtight cushions.

FIG. 9 Additively joined pneumatic actuators.
Copyright by ILEK

FIG. 10 Connection joint for PAOSS elements.
Copyright by ILEK

The supply is provided from the centre of the folding structure, wherefrom the air can be distributed to an unlimited number of segments. To integrate the spiral spring, a special channel is necessary in which the spring can be inserted and fixed. In order to connect the folding structures to the pneumatic lines and to enable air supply, special 3D-printed connection elements (Fig. 10) were developed, which can be used to fix the elements to the substructure e.g. to a steel cable net.

Table 2 shows the evolution from the first prototype to the final product in terms of folding geometry optimisation as well as material analysis and selection under consideration of the investigated kinematic folding technologies and actuation strategies.

The PAOSS are automatically controlled by detecting illuminance and glare in the room they are intended to shade. In case the light intensity increases or decreases to a defined level, the control unit transmits this information to selectively open or close the air supply of the individual actuators via adjustable valves to ensure sufficient daylight provision and to provide glare protection by individually adjusting single PAOSS. Manual control of the system by the building user is achieved for individual adjustment of the comfort requirements.

The prototypical implementation and development of the integral method for integrating the pneumatic actuators will be the subject of ongoing research activities in the context of the PAOSS structures and will therefore not be discussed further in this paper.

TABLE 2 Evolution of PAOSS

	FIRST PROTOTYPE	LAST PROTOTYPE
Depth [mm]	185	94,5
Difference open-closed [m^2]	0,422	0,613
Material	Tyvek	Airtex Super FR
Actuation	additive	integral

3 FUTURE OUTLOOK

The PAOSS elements are designed to be implemented as sun and glare protection in the façade cavity of a conventional glass double façade or in overpressure-stabilised ETFE cushion constructions. Focusing on maximum savings of material, mass, CO_2, and energy, their implementation in ETFE cushion constructions leads to synergies in the use of the pre-existing air-compressing infrastructure.

A prototypical realisation and application (Fig. 11, Fig. 12) is planned within the research projects described below: an ETFE cushion construction will be designed to be easily implemented in the standard profile system ETFE_THERM+ provided by RAICO. Here, the air supply is invisible, being integrated in the post and rail system. In order to generate an easy mounting and demounting of the PAOSS elements, a modular insert based on the RAICO profile system is developed, comprising a substructure to attach the individual elements together with the appropriate air supply hoses via the specially developed connection joints shown in Fig. 10. The substructure does not interfere with the light transmission or the visual connection out of the building, thus transparent glass grid constructions or filigree, prestressed cable net structures are suitable.

Within the scope of the project "Development of Adaptive Membrane Façade Modules," funded by the research initiative Zukunft Bau of the German Federal Institute for Research on Building, Urban Affairs, and Spatial Development (BBSR), prototypes of the above described PAOSS elements will be investigated in terms of building physics and daylight performance as well as detailed from a technical-constructive point of view. Aim of the BBSR project is an integrative and comprehensive development of adaptive, modular, textile- or foil-based, multi-layered and multi-functional façade

systems with envelope and profile, which considerably expand the façade functionalities as well as the design possibilities of the outer skin. The development includes the realisation of transparent, translucent, and opaque façade solutions at the site of the demonstrator high-rise building of the CRC 1244, where the resulting systems will be extensively monitored.

Considering the limited availability of natural resources, the Collaborative Research Centre 1244 (CRC 1244) at the University of Stuttgart, entitled "Adaptive Skins and Structures for the Built Environment of Tomorrow," outlines ways to minimise the use of material, resources, and energy with a maximum increase in user comfort by investigating the potential and applicability of adaptive building skins and structures. Within the CRC 1244, funded by the German Research Foundation (DFG), the world's first adaptive high-rise building (Fig. 12) is being constructed on the University Campus Stuttgart-Vaihingen (Weidner et al., 2018). The building is equipped with an extensive measuring infrastructure in the interior and exterior, thus serving as a platform for the investigation and demonstration of innovative adaptive building envelopes in order to verify their long-term suitability, reliability, and efficiency under real weather conditions at a scale of 1:1. In this context, the demonstrator high-rise building is predestined for the first prototypical implementation, evaluation, and validation of the PAOSS system in the above mentioned overpressure-stabilised ETFE cushion construction.

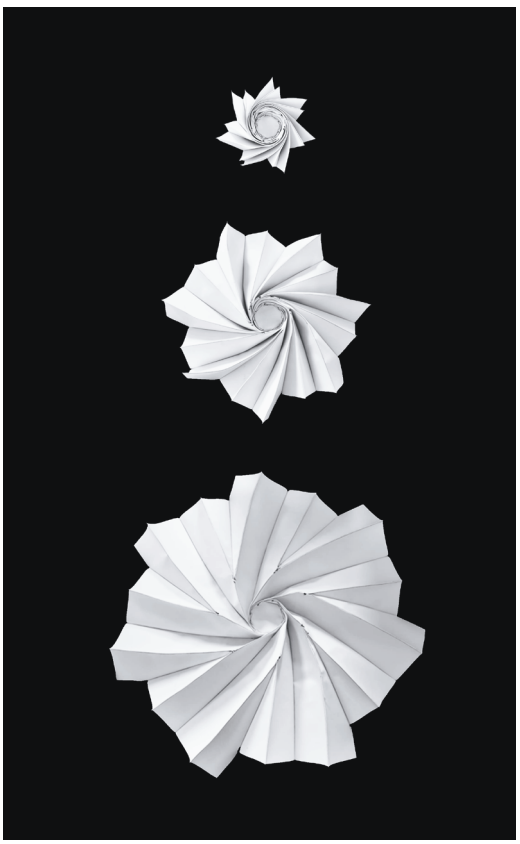

FIG. 11 Deployment of the PAOSS elements from a compact state (above) to an opened state (below). Copyright by ILEK

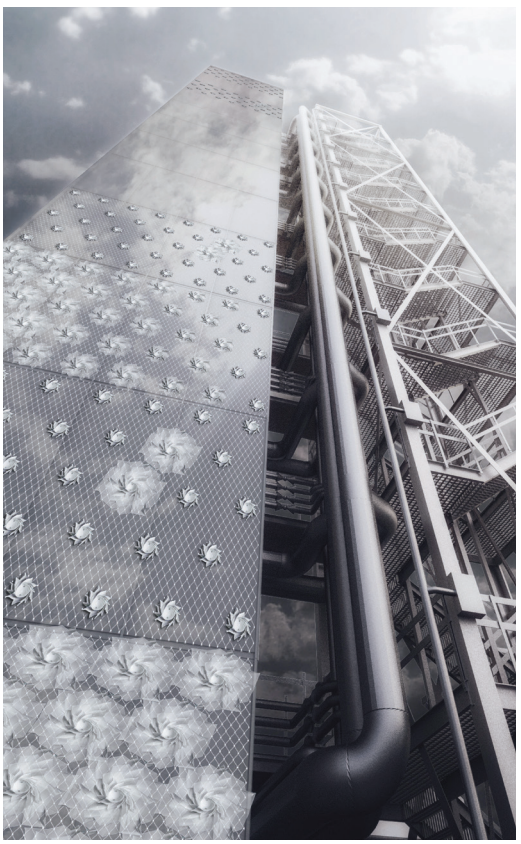

FIG. 12 Visualisation of the demonstrator high-rise building with adaptive membrane façades. Copyright by ILEK

4 CONCLUSIONS

In the context of the increasing transparency of our buildings and rising outdoor temperatures, notably in our cities, the importance of adaptive sun and glare protection systems has been clearly identified. The target is to achieve a selective or full-surface regulation of light and radiation properties in the building envelope in order to protect the interior from overheating without interfering with daylight supply. Therefore, a new lightweight, textile, pneumatically actuated, adaptive sun and glare protection system based on Origami folding has been developed. Applied in the façade cavity of ETFE cushion constructions, synergies of the pre-existing air infrastructure can be used for economical savings.

The geometry based on NASA`s "Starshade" Origami folding has been optimised in terms of a minimum complexity, a minimum component depth, and a maximum surface area difference between its closed and open state resulting in a maximum switching difference of 82%. Based on photometric measurements a UV- and fire-resistant, translucent, polyester-based, textile fabric with thermoplastic polyurethane coating could have been identified, that has a low weight per unit area of only 120 g/m^2. Among the conventionally available and suitable materials this textile offers the highest reflection coefficient in solar and visible range of radiation (R_{SOL} = 74,65 %, R_{VIS} = 82,95 %), a low absorption coefficient (A_{SOL} = 8.40%, A_{VIS} = 1,46 %), and an optimal visual transmittance of approximately T_{VIS} ~ 15 %. Subtractive, additive, and thermal-mechanical manufacturing methods for the functionalisation of the textile, e.g. to generate the articulation effect, were investigated. For thermoplastic polymer-based materials, welded or sewn, air-tightened seams are the most suitable, due to the resulting orientating shape memory effect of the mountain and valley folds.

This paper focuses on the integration of a simple, resilient, and low energy actuation mechanism as an alternative approach to the vast number of conventional adaptive solar and glare protection systems. Linked to the use of high-tech components, these are characterised by high complexity and susceptibility to defects, system failures, and obsolescence. Meanwhile, the use of simple, conventionally established actuation mechanisms such as the transfer of the functional mechanism of an air whistle into a new context opens up a low-cost and durable actuation method. Compared to the conventional electro-mechanically actuated systems, the implementation of pneumatic actuators to open the PAOSS in combination with an integrated spiral spring system to re-close offers an aesthetically and energetically optimised solution. Only a small amount of energy is required to be put into the system for the deployment, thus creating two stable states as well as a very smooth and elegant opening movement.

A further increase of the prefabrication level to a serial production, including the use of simple assembling techniques without any inseparable connections, leads to a modular system design, which due to the exchangeability, recyclability, and returnability of all system components into the material cycle, is lucrative in economic as well as ecological terms.

Acknowledgements

The authors are very grateful for the financial support provided by the research initiative Zukunft Bau of the German Federal Institute for Research on Building, Urban Affairs, and Spatial Development (BBSR) and the German Research Foundation (DFG). For their generous support concerning the development of adaptive, textile- and foil-based building envelopes, the authors cordially thank the following industrial and business cooperation partners:
Carl Stahl Süd GmbH, Dr. Zwissler Holding AG, Eschler Textil GmbH, Essedea GmbH & Co. KG, Global Safety Textiles GmbH, Groz Beckert KG, Heimbach GmbH, Low & Bonar GmbH, Mattes & Ammann GmbH & Co. KG, Novavert GmbH & Co. KG, Nowofol Kunststoffprodukte GmbH & Co. KG, Pervormance International GmbH, Raico Bautechnik GmbH, Roma-Strickstoff-Fabrik Rolf Mayer GmbH & Co. KG, Vector Foiltec GmbH, Versaidag Indutex GmbH, Wicona - Hydro Building Systems Germany GmbH

References

Arya, M., Warwick, S., Webb, D., Lisman, D., Shaklan, S., Bradford, S., Steeves, J., Hilgemann, E., Trease, B., Thomson, M., Freebury, G., McGown, J., & Gull, J. (2017). Starshade mechanical design for the Habitable Exoplanet imaging mission concept (HabEx), *Proceedings Vol. 10400, Techniques and Instrumentation for Detection of Exoplanets VIII, SPIE Optical Engineering + Applications*, 2017, San Diego.

Bäumer, R., Haase, W., Mielert, F., Ocanto, L., & Schmid, F. (2012). *Entwicklung leichter Profile und Bauteile aus faserverstärkten Kunststoffen für Anwendungen in der textilen Gebäudehülle und der Fenstertechnik (PROFAKU) (Development of lightweight, fiber-reinforced polymer-based profiles and components for applications in textile building envelopes and window technology).* Research Report, Fraunhofer-IRB-Verl., Stuttgart.

Bender, A.-L. (2020). *Weiterentwicklung und Optimierung einer adaptiven, textilbasierten Faltstruktur zum selektiven Sonnen- und Blendschutz (Further development and optimisation of an adaptive, textile based folding structure for selective sun and glare protection).* Master Thesis, Universität Stuttgart

Blandini, L. (2020). Glasfassaden: Neue Herausforderungen und Entwicklungsmöglichkeiten im 21. Jahrhundert (Glass façades: New challenges and development opportunities in the 21st century). *Glasbau,* Ernst & Sohn, p. 93–101.

Blandini, L., & Grasmug, W. (2018). The search for dematerialised building envelopes – the role of glass and steel. *Steel Construction*, 11, p. 140–145.

Blaser, W. (1999). Werner Sobek, art of engineering. *Ingenieur-Kunst,* Birkhäuser.

Deleersnyder, K., & Ruys, L. (2015). 3D-Druck auf Textilien (3D printing on textiles). *Textilplus*, 07/08, p. 23–25.

DIN EN 410. (2011). *Glas im Bauwesen - Bestimmung der lichttechnischen und strahlungsphysikalischen Kenngrößen von Verglasungen (Glass in the construction sector - Determination of photometric and radiophysical parameters of glazings).*

DIN EN 14500. (2018). *Abschlüsse - Thermischer und visueller Komfort - Prüf- und Berechnungsverfahren (Terminations - Thermal and visual comfort - Methods for testing and calculation).*

Eisenbarth, C., Haase, W., & Sobek, W. (2019). Adaptive membrane façades. *14th International Conference on Advanced Building Skins,* Bern.

Fahrenwaldt, H. J., Schuler, V., & Twrdek, J. (2014). Thermisches Trennen (Thermal separation). *Praxiswissen Schweißtechnik: Werkstoffe, Prozesse, Fertigung*. Springer Vieweg, Wiesbaden, p. 241–263.

Gries, T., & Klopp, K. (2007). *Füge- und Oberflächentechnologien für Textilien: Verfahren und Anwendungen (Joining and surface technologies for textiles: methods and applications).* Springer-Verlag Berlin Heidelberg.

Gries, T., Veit, D., & Wulfhorst, B. (2014). *Textile Fertigungsverfahren: eine Einführung (Textile manufacturing processes: an introduction).* Carl Hanser, München.

Haas-Arndt, D., & Ranft, F. (2007). *Tageslichttechnik in Gebäuden (Daylighting technology in buildings).* Müller (C.F.), Heidelberg.

Haase, W., Klaus, T., Knubben, E., Mielert, F., Neuhäuser, S., Schmid, F., & Sobek, W. (2011a). *Adaptive mehrlagige textile Gebäudehüllen: mit Anl. 1. Recherchebericht: Beispiele zur konstruktiven Ausführung mehrlagiger gedämmter Membranbauwerke; Anl. 2. Dokumentation: Simulationstool für mehrlagige Aufbauten (Adaptive multi-layer textile building envelopes: with annex 1. research report: examples for the structural design of multi-layer insulated membrane structures; annex 2. documentation: simulation tool for multi-layer structures).* Research Report, Fraunhofer-IRB-Verl., Stuttgart.

Haase, W., Klaus, T., Schmid, F., Schmidt, T., Sedlbauer, K., Sobek, W., & Synold, M. (2011b). Adaptive textile und folienbasierte Gebäudehüllen (Adaptive textile and film-based building envelopes). *Bautechnik*, 88(2), p. 69–75.

Hammer, R., & Wambsganß, M. (2020). *Planen mit Tageslicht - Grundlagen für die Praxis (Planning with daylight - basics for practical use).* Springer Vieweg, Wiesbaden.

Knaack, U., Klein, T., Bilow, M., & Auer, T. (2007). *Fassaden - Prinzipien der Konstruktion (Façades - principles of construction).* Birkhäuser.

Knaack, U., Koenders, E., Alexandrakis, E., Bewersdorff, D., Haake, I., Hickert, S., & Mankel, C. (2018). *Bauphysik der Fassade - Prinzipien der Konstruktion (Building physics of the façade - principles of construction)*, Birkhäuser, p. 135.

Lütke, M., Klotzbach, A., Wetzig, A., & Beyer, E. (2009). Laserschneiden von Faserverbundwerkstoffen (Laser cutting of fiber composites). *Laser Technik Journal, 6*, p. 23–26.

Machova, K., Zschetzsche, J., Füssel, U., Friedrich, C., Riedel, M., Schuster, H., & Rückert, R. (2011). Innovatives Schneiden technischer Textilien mittels Plasmastrahl (Innovative cutting of technical textiles by means of plasma jet). *Schweissen und Schneiden, 63*(10), p. 599–603.

Magli, S., Lodi, C., Lombroso, L., Muscio A., & Teggi S. (2015). Analysis of the urban heat island effects on building energy consumption. *International Journal of Energy and Environmental Engineering, 6*(1), p. 91–99.

Meagher, M. (2014). Responsive Architecture and the Problem of Obsolescence. *Archnet-IJAR International Journal of Architectural Research, 8*(3), p. 95–104.

Sigel, D., Trease, B. P., Thomson, M. W., Webb, D. R., Willis, P., & Lisman, P. D. (2014). Application of Origami in Starshade Spacecraft Blanket Design. *ASME 2014 Design Engineering Technical Conferences and Computers and Information in Engineering Conference (DETC)*.

Sobek, W., Morgan, C. L., Bogdan, I. (2004). Poetry—Rotating umbrellas. *Show me the future: Engineering and design by Werner Sobek*, p. 50–51.

Sobek, W., Haase, W., & Teuffel, P. (2000). Adaptive Systeme (Adaptive Systems). *Stahlbau*, 69, p. 544–555.

Sobek, W., Speth, M. (1993). Von der Faser zum Gewebe. Textile Werkstoffe im Bauwesen (From fiber to fabric. Textile materials in the building industry). *db Deutsche Bauzeitung, 127,* p. 74–81.

Weidner, S., Kelleter, C., Sternberg, P., Haase, W., Geiger, F., Burghardt, T., Honold, C., Wagner, J., Böhm, M., Bischoff, M., Sawodny, O., & Binz, H. (2018). The implementation of adaptive elements into an experimental high-rise building. *Steel Construction, 11*(2), p. 109–117.

Zapala, E. (2018). *Faltstrukturen in der textilen Gebäudehülle: Eine Erweiterung tradierter Entwurfsgrundlagen unter Berücksichtigung schall- und lichttechnischer Aspekte (Folded Structures in the Textile Building Envelope: An Extension of Traditional Design Principles Considering Sound and Light Engineering Aspects)*. Dissertation, Universität Stuttgart.